A Newton solution for the harmonic analysis of power systems with multiple non-linear devices

Graeme N. Bathurst

A thesis presented for the degree of
Doctor of Philosophy
in
Electrical and Electronic Engineering
at the
University of Canterbury,
Christchurch, New Zealand.

February 1999

ABSTRACT

This thesis describes a new algorithm for the harmonic analysis of power systems. Existing non-linear models are incorporated into a structure that allows very general configurations that are linked by linear ac and dc systems. A three phase loadflow is included at the power frequency and the steady-state is solved iteratively using a real-valued, positive frequency, full Newton technique. This structure allows electrical and non-electrical variables to be solved simultaneously. The resultant process is fast, robust and shows excellent comparison with time domain simulation.

The harmonic characteristics of large power conversion installations such as HVdc and high-pulse LVdc are investigated. The effects of system operation on the harmonic transfer through an HVdc link are investigated using the multiple run feature of the algorithm. Also, the representation of bipolar HVdc links is investigated and justifications for accurate dc system representation shown.

The harmonic domain converter has been generalised, and a representation of the zigzag transformer developed. Using this the effects of outage conditions of a high-pulse installation are modelled, and a proposal is given for the minimisation of low order harmonic generation during this condition.

Finally, a fast numerical technique for the accurate calculation of non-linear device impedances is described. This is used in conjunction with simplified converter models to assess the impact of the converter on the linear ac system impedance. A comparison is made between the different methods of harmonic analysis and a quantitative assessment of their accuracy given.

ACKNOWLEDGEMENTS

The completion of this thesis marks the end of a significant era for myself, one that been an amazing blend of happiness, stress and learning.

For the last part of this period I would like to thank my supervisors Dr Neville Watson and Professor Jos Arrillaga for their support and guidance. Also to Dr Alan Wood for patiently rescuing me from some of the *interesting* results that computers have given me. A special thanks must go to Dr Bruce Smith, I would not be finishing now if it was not for your sagacious advice and encouragement throughout my studies. I would also like to acknowledge the financial support I received from Transpower NZ (Ltd), the University of Canterbury Doctoral Scholarship and the Royal Society of New Zealand.

To all my colleagues here at school, various friends and other associates, a huge thank-you for all the discussions, tramping, climbing and mountain biking that has kept me sane over the past three years; Dr Bruce Smith, Dr Simon Todd, Dr Wade Enright, Dr Tom Keppler, Prof. Bob Yacamini, Dave Hume, Chris Osauskas, Hamish Laird, Hamish Avery, Chris Gadd, Andrew Ward, Lisa Winthrop, Cindy Baker, Gillian Rodgers, Derrick Westendra, Nigel Tavendale, John Row, Elwyn Smith, Anna, Adrian and Cairn. Thanks also goes out to the remainder of the academic and technical staff that makes up this departmental family. RDU and "trip odyssey" should also not be forgotten for helping me through those long hours of late night coding.

Finally to Sonja, for your continued love and support and for continually dragging me away from this place, thanks heaps.

This thesis was brought to you by Unix (care of Achenar, Heka, Jabbah, Hydra, Lupus, Lepus and Spica; not forgetting the retired Vega and Shogun), good ol' Fortran 77, Matlab™, PSCAD, LaTeX , the number 2.71828182845905, and vast quantities of the letter C.

CONTENTS

LIST OF FIGURES

LIST OF TABLES

GLOSSARY

Abbreviations

ABCD	A matrix form of representing the HVdc converter
CIGRE	Conference Internationale de Grandes Reseaux Electriques
CSC	Current Sourced Converter
D	Delta transformer connection
DA	Direct Analysis
DNA	Direct Norton Analysis
IHA	Iterative Harmonic Analysis
EMF	Electro Magneto Force
EMTDC	ElectroMagnetic Transient Direct Current
FAST	An accelerated time domain simulation technique
FFT	Fast Fourier Transform
FPI	Fixed Point Iteration (Gauss-Seidel)
HPF	Harmonic power flow
HVdc	High Voltage direct current
IEEE	Institute of Electrical and Electronic Engineers
GIC	Geomagnetic Induced Current
LSI	Lower South Island of New Zealand test system
LVdc	Low Voltage direct current
NIT	Number of Iterations
OLTC	On-Load Tap-Changer
pu	per-unit
PCC	Point of Common Coupling
PI	Proportional-Integral controller
PPF	Positive sequence power flow
PQ	Loadflow constraint where the real and reactive power are specified
PSCAD	Power System Computer Aided Design - graphical interface for EMTDC
PV	Loadflow constraint where the real power and voltage magnitude are specified
RL	Resistance and Inductance network
SCR	Short Circuit Ratio
SVC	Static Var Compensator

STATCOM	Static Compensator
TCR	Thyristor Controlled Reactor
TCSC	Thyristor Controlled Series Capacitor
UMEC	Unified Magnetic Equivalent Circuit
VSC	Voltage Sourced Converter
Y	Star transformer connection
Yg	Star-ground transformer connection
Yz	Star transformer connection with neutral earthing impedance z
Y12M	LU Linear equation solver in Fortran
3PF	Three phase power flow
(n-1)	mode of operation where one unit is out of service
(n-2)	mode of operation where two units are out of service

General notation

In the following, X and W are generic variables. Frequent use is made of other variables for local explanations, but these are explained in the immediate context.

$[X]$	matrix form of X
$Real\{X\}$, X_r	Real part of X
$Imag\{X\}$, X_i	Imaginary part of X
X^T	matrix transposition
X^*	Conjugate of X
$\|X\|$, $\angle X$	magnitude, angle of X
ΔX	Change in X
$F(X)$	Single variable mismatch equation
$W \otimes X$	W convolved with X in the frequency domain
$X_{B/E/O}$	Phase, beginning/ending/not involved in, the commutation
$X_{a/b/c}$	Phase $a/b/c$ quantity
$X_{pri/sec}$	primary/secondary transformer quantity
X_{prim}	primitive transformer quantity
$\exp^X$	exponential of X
$\frac{\partial X}{\partial W}$	partial derivative of X with respect to W
$X'/''/'''$	used to differentiate between different quantities
$W = f(X)$	W is a function of X
X_+	Positive frequency phasor or positive sequence frequency depending on context
X_-	Negative frequency phasor or negative sequence frequency depending on context
X_0	Zero sequence frequency or dc term depending on context
$X_{ac/dc}$	ac/dc system harmonic quantity
$X_{d/q}$	d/q-axis quantity
X_{node}	nodal quantity

$X(t)$, $X(k)$	time, frequency domain quantity
Y, Z	admittance, impedance
V, I	voltage, current

Symbols

a_{pri}	Transformer primary tap ratio
a_{sec}	Transformer secondary tap ratio
c_k	partial derivative term
$[C]$	Transformer connectivity matrix
G_t	dc current transducer gain
I_{comm},I_c	Commutation current sample
I_d	dc current harmonics
I_{ds}	dc current set-point for an HVdc link
I_{dm}	dc current margin for an HVdc link
I_N	Norton current injection
I_{nl_i}	Non-linear device current vector at iteration i
$I_{re-eval}$	Harmonic currents calculated with the re-evaluation method
j, i	$\sqrt{-1}$
J_i	Jacobian matrix at iteration i
h, k	h^{th} or k^{th} harmonic
L_{ac}	dc system inductance
L_{dc}	dc system inductance
M_i	Mismatch vector at iteration i
nb	number of busbars
nh	number of harmonics in solution set
n_1	zigzag ratio of primary voltage to total secondary voltage
n_2	zigzag ratio of secondary winding 1 voltage to total secondary voltage
n_3	zigzag ratio of secondary winding 2 voltage to total secondary voltage
P_{comm_I}	transfer from dc current to commutation current sample I_{comm}
P_{comm_V}	transfer from ac voltage to commutation current sample I_{comm}
P_{volt_I}	transfer from dc current to dc voltage sample V_{volt}
P_{volt_V}	transfer from ac voltage to dc voltage sample V_{volt}
$radius$	Radius of tensor impedance from the centroid
R_{dc}	dc system resistance
R_{eq}	Equivalent commutation circuit resistance
R_s	Bridge resistance
R_T	Transformer resistance
S_T	Nett transformer power base
S_2	Zigzag transformer winding 2 power base

S_3	Zigzag transformer winding 3 power base
T	sequence to phase transform
T_D	Transformer current transfer matrix
T_t	dc current transducer time constant
V_d	dc voltage harmonics
V_{node_i}	Nodal voltage vector at iteration i
ΔV_{node_i}	Nodal voltage vector update at iteration i
V_{volt}, V_v	dc voltage samples
X''	salient pole generator sub-transient reactance
X_{eq}	Equivalent commutation circuit reactance
X_T	Transformer reactance
Y_c	Shunt admittance at the common busbar of parallel installations
Y_D	Transformer reduced shunt admittance
Y_N	Norton admittance
Y_{sys}	Nodal admittance matrix of the system
Z_{centre}	Complex impedance centroid of tensor impedance
Z_e	neutral earthing impedance for HVdc links
z_{xx}	Real-valued tensor impedance co-efficient
α	average firing angle
α_{ripple}	Firing order ripple
β_p	p^{th} equi-distant firing pulse
δ	salient pole generator rotor angle
δ_p	p^{th} commutation voltage zero-crossing
γ	extinction angle
ϕ	salient pole generator power factor
ϕ_p	p^{th} end of commutation instant
λ_i	rate of solution convergence
μ	average commutation duration
ψ	Fourier co-efficient of rectangular sampling function
ψ	salient pole generator flux linkage
σ	zigzag transformer phase shift
θ	salient pole generator rotor angle referred to d-axis
θ_p	p^{th} firing instant

Chapter 1

INTRODUCTION

1.1 GENERAL

With the increased de-regulation of the power markets world-wide, the needs of the consumers are becoming more and more important. Power quality, particularly harmonic distortion, is a growing concern of consumers and power utilities due to the increasing number of power conversion devices at both transmission and industrial levels.

To the ordinary consumer, harmonics are normally only noticeable as annoying buzzing, telecommunication interference, or small appliance malfunction. However, they have a major indirect effect resulting from their impact on power system operation. Harmonics within power systems result in increased heating in system components which results in a shortening of their expected lifespan. They can also result in the malfunction of system protection, inaccurate powerflow metering and faults due to insulation breakdown. There are also instances where excessive harmonic levels have resulted in HVdc installations shutting down due to control malfunctions.

The majority of new converter installations will require filtering banks to minimise their impact and existing filtered installations may need to be upgraded. For example, it wasn't until 1983 that the 480MW 48-pulse Aluminium Smelter at Tiwai, New Zealand had to install harmonic filters, some 10 years after its initial commissioning. However, to design systems with adequate harmonic power quality, simulation tools are required that can quickly and accurately perform multiple system contingency studies to determine the harmonic profiles at Points of Common Coupling (PCC).

1.2 THESIS OBJECTIVES

Power system harmonic analysis is not a new topic. A considerable amount of time and effort has been spent analysing the various components that form a power system so that appropriate harmonic models can be developed. This thesis itself relies heavily on material developed at the University of Canterbury over the past 20 years of work. The key objective was to provide a working framework that combines all the important

aspects of steady-state harmonic analysis. These include the linear network components through to sub-transmission levels, and the main non-linear harmonic generating plants and their controls.

As the power system is continually changing, its modelling requires multiple snapshots of fixed operating points. To simplify the engineer's task, the initial system specifications should attempt to reflect the state of the physical system as closely as possible. For this specification, a three phase loadflow should be included and any harmonically affected controls on large system components, with as few simplifications as possible.

Once an algorithm such as this is achieved, the secondary objective can then be pursued. This is to investigate the various simplified methods of harmonic analysis that are commonly used within industry. By comparing the results, from both system impedance studies and harmonic penetration techniques, with those of a fully inclusive harmonic program, a critical assessment of the commonly used methods can be made.

1.3 THESIS OUTLINE

Chapter 2 contains a brief review of harmonic modelling and outlines the specifications for a general harmonic solution algorithm. This includes the classification of the various system components that make up a power system and are important to harmonic generation and propagation.

Chapter 3 describes the modelling of linear and non-linear system components. It covers the modelling of a 6-pulse converter in detail, specifically to improve the transformer representation, and expressions are shown for a zigzag connected transformer. The modelling of salient pole generators is briefly described, as well as the modelling of the linear components. Finally the potential inclusion of other non-linear components is discussed.

Chapter 4 details the formulation and structure of the harmonic solution algorithm. It deals with the solution formulation, initialisation and some considerations with validating the input data.

Chapter 5 discusses the main modelling aspects of HVdc transmission, and then describes of the mechanisms important to the harmonic generation and transfer of HVdc links.

Chapter 6 analyses multi-pulse installations using zigzag transformers. It looks at the characteristics of a parallel connected dc system under a variety of non-ideal operating conditions. Also, an interesting proposal is made for reducing the nominal pulse number of these installations during outage contingencies.

Chapter 7 describes a method for the accurate calculation of the converter impedance by means of a fast numerical technique. It then compares the effect of alternative modelling techniques to assess the effect of the converter impedance.

Chapter 8 provides a critical assessment of power system harmonic analysis by comparing the results of different representations of the harmonic power system. The interaction between non-linear devices is discussed and a comparison made between the direct penetration and full IHA solution. Finally an indicator is proposed to decide on the need for a full IHA solution.

Chapter 9 contains several conclusions of the work and suggests some direction for further research work in this area including the possible extension to non-integer harmonics (interharmonics).

Chapter 2

A REVIEW AND SPECIFICATIONS FOR GENERAL HARMONIC SOLUTIONS

2.1 INTRODUCTION

Power system harmonics come from a variety of sources, the dominant ones within transmission networks being large power converters such as those used for HVdc links and large industrial processes. The harmonics generated by these devices can be divided into three categories:

- integer harmonics; are integer multiples of the power frequency.
- interharmonics; period and integer multiples of some base frequency, they normally result from cross-modulation of the integer harmonics of two systems with different power frequencies.
- non-integer harmonics; are the frequencies that do not fit either of the above two categories. They are not integer multiples of a base frequency and may not even be periodic.

The last two categories usually come from back-to-back HVdc links (periodic), cyclo-converters (periodic) and arc-furnaces (non-periodic) which are significantly harder to model properly. At present the work is concentrated on integer based harmonics as this is where the majority of concern is. However with the large motor drives and asynchronous HVdc links becoming more prevalent it is becoming important to take into consideration the non-integer and interharmonic based frequencies. Non-periodic frequencies pose a special problem as they cannot usually be analysed by traditional Fourier means; the use of wavelet theory has been proposed to analyse these waveshapes.

The large power converters produce mainly characteristic harmonics which are present during operation under ideal conditions and most of the early work revolved around these harmonics. Classical equations have been derived to obtain average firing angles, commutation durations, dc side voltages and harmonic magnitudes [Kimbark 1971]

[Arrillaga 1983]. However few of the harmonic problems reported occur under ideal system operation, and so this form of analysis is very limited for harmonic purposes.

The linearity of synchronous machines and power transformers is very dependant upon their power-flow operating point. Both of these devices can normally be approximated as passive harmonic impedances, but these harmonic impedances often change with the system operating point.

Transmission asymmetries lead to a negative sequence fundamental component in the terminal busbar voltages and due to the frequency coupling behaviour of converters, this will lead to the generation of non-characteristic harmonics. Thus the ac transmission system must be represented in three-phase so that these effects be fully represented. Also with increased public resistance to new transmission lines being built, the need for shared ac-dc right-of-ways will increase. The mutual coupling between these lines will result in both non-characteristic harmonic generation and converter transformer saturation problems. There are various solutions that minimise these effects, but analysis programs are required to accurately represent the systems.

2.2 EXISTING HARMONIC ANALYSIS METHODS

Harmonic analysis methods can be fitted into three categories; time domain, direct frequency domain and iterative techniques.

2.2.1 Time domain methods

Time domain modelling typically involves the numerical integration of system differential equations. Various methods are available for the creation of these differential equations and their integration [Dommel 1969] [Woodford *et al.* 1983]. Time domain representation is the most extensively used method for power system modelling. Although its primary function is for dynamic analysis, it is often used for steady-state analysis due to users familiarity with it. Harmonic analysis with a time domain package involves simulation to the steady-state and then the use of the Fourier transform. Due to the combination of both long (inductances and capacitances) and short (device switching times) time constants within a system, small time steps and long simulation times are required for accurate steady-states. Due to this computational expense, methods for accelerating convergence to steady-state using boundary problem analysis have been developed [Aprille and Trick 1972].

A significant problem is the time domain modelling of the frequency dependency of transmission lines, but a variety of methods have been developed which provide a reasonably accurate representation [Manitoba HVdc Research Centre 1988]. Other methods use RLC branches calculated by numerical analysis to provide simple equivalents of large networks [Watson 1987].

A time domain modelling does have the advantage that the same system developed for transient studies can be used for harmonics, a further advantage is the accurate representation of control systems. This is, however, due to the fact that time domain simulation has been around longer than frequency domain approaches. Modern frequency domain tools can also give good representation of realistic controllers.

2.2.2 Direct frequency domain methods

Most commercial harmonic analysis packages use a direct frequency domain analysis using either single or three phase representation [Densem *et al.* 1984]. The analysis consists of performing a loadflow to determine the system operating conditions and then calculating harmonic injections using simplified non-linear models. Then using the following nodal equation the system harmonic voltages are solved directly.

$$I_{node} = Y_{sys} V_{node} \tag{2.1}$$

This form of analysis is well suited to audio-frequency ripple control studies, where the injected frequencies are non-integer and of low magnitude. However, it does not permit the incorporation of the effect of harmonic voltages on the non-linear devices or the transfer of harmonics across HVdc links.

To maintain simplicity a variety of linearised converter models have been developed for analysing harmonic interaction with control systems [Dickmander *et al.* 1994] [Wood and Arrillaga 1995] and for the transfer of harmonics across dc links [Sadek *et al.* 1992] [Hu and Yacamini 1993]. However, the accuracy of these methods is limited by the approximations made within the device linearisations and the use of fixed operating points.

2.2.3 Iterative Harmonic Analysis

When a non-linear device injects a harmonic current into a non-infinite linear ac system busbar, a harmonic voltage of that same frequency is produced. If the non-linear device is sensitive to harmonic voltages, the injected harmonic current will change. This then requires an iterative solution to solve the system for accurate harmonic information. The following is a review of techniques that have been used for Iterative Harmonic Analysis (IHA) since its conception. A more exhaustive review of the HVdc converter modelling can be found in [Smith *et al.* 1998].

Basic iterative techniques

Two basic iterative methods are used in power system IHA; Fixed Point Iteration (Gauss-Seidel) and the Newton method. The simplest and previously most predom-

inant iterative technique has been the Fixed Point Iteration. The current injections of a non-linear device (I_{nl_i}) are calculated from the system nodal voltages (V_{node_i}). Then using these currents and the system admittance matrix (Y_{sys}), new nodal voltages ($V_{node_{i+1}}$) are calculated which are then used to re-calculate the non-linear device current injections. This iterative method is shown as follows:

$$I_{nl_i} = f(V_{node_i}) \tag{2.2}$$

$$V_{node_{i+1}} = [Y_{sys}]^{-1} I_{nl_i} \tag{2.3}$$

This method has been reported to have poor convergence for highly distorted or resonant systems [Callaghan 1989]. Better convergence has been obtained by using the Newton method for adjusting the solution variables. A mismatch function is calculated which compares the non-linear device harmonic currents (I_{nl_i}) with the nodal currents (I_{node_i}) calculated from the nodal voltages (V_{node_i}). This mismatch function is then used in conjunction with the system Jacobian (a matrix of partial derivatives) to calculate adjustments to the nodal voltages (ΔV_{node_i}). As the solution progresses, the mismatch function (M_i) is driven to zero by the Jacobian (J_i) and convergence is obtained. This is as follows:

$$I_{nl_i} = f(V_{node_i}) \tag{2.4}$$

$$I_{node_i} = Y_{sys} V_{node_i} \tag{2.5}$$

$$M_i = J_i \Delta V_{node_i} \tag{2.6}$$

$$V_{node_{i+1}} = V_{node_i} - \Delta V_{node_i} \tag{2.7}$$

This method does require a system Jacobian though which can be difficult to obtain, depending upon the style of non-linear device modelling.

Non-linear device representations

The representation of non-linear devices does differ between the reported models in the literature. Three key representations are used, as shown in Figure 2.1. The first and simplest is the ideal current source to which harmonic voltages have no effect. It is very simple to develop a model in this fashion as no linearised information is required. However it will degrade solution convergence in an iterative scheme or accuracy in a direct solution. An improvement on this approach is the method of Norton Equivalents, which linearises the non-linear device around its operating point to obtain a Norton impedance. The calculated current injections are adjusted to account for any harmonic voltage so that the nett nodal injection remains the same. This is shown as follows:

$$I_{nl_i} = f(V_{node_i}) \tag{2.8}$$

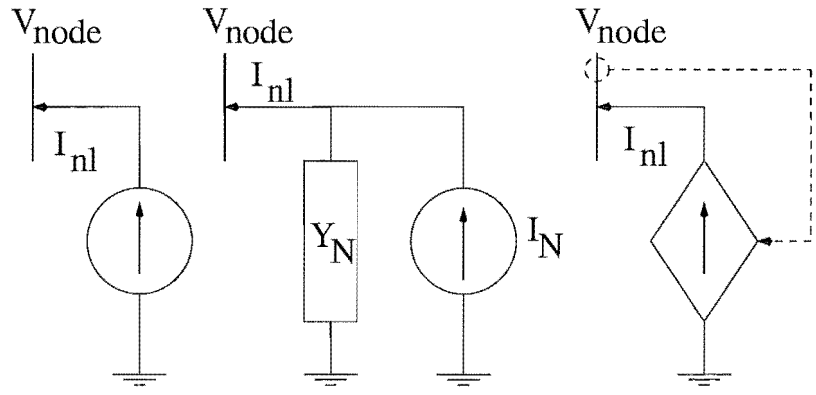

(a) Ideal current source (b) Norton equivalent (c) Dependent current source

Figure 2.1 Different non-linear device representations

$$Y_N = \frac{\Delta I_{nl_i}}{\Delta V_{node_i}} \tag{2.9}$$

$$I_N = (I_{nl_i}) - Y_N V_{node_i} \tag{2.10}$$

$$M_i = Y_{sys} V_{node_i} + (Y_N V_{node_i} + I_N) \tag{2.11}$$

$$\frac{\partial M_i}{\partial V_{node_i}} = (Y_{sys} + Y_N) \tag{2.12}$$

Another approach, from the nodal analysis point of view, is the use of a dependent current source. The nodal injections are then exactly those calculated by the non-linear model and the linearisation is included only in the solution Jacobian, if used.

$$I_{nl_i} = f(V_{node_i}) \tag{2.13}$$

$$M_i = Y_{sys} V_{node_i} + I_{nl_i} \tag{2.14}$$

$$\frac{\partial M_i}{\partial V_{node_i}} = \left(Y_{sys} + \frac{\partial I_{nl_i}}{\partial V_{node_i}} \right) \tag{2.15}$$

$$\frac{\partial I_{nl_i}}{\partial V_{node_i}} \equiv Y_N \tag{2.16}$$

The method of Norton equivalents will improve the convergence of fixed point iterations as the linearisation is inherent within the nodal analysis. However, if a Newton style solution is being used then the two latter approaches are mathematically identical. Here, there is no gain with a Norton representation and the nodal analysis must represent frequency coupling instead of just being linear.

Harmonic solution format

A problem with the representation of non-linear devices is the phase dependency inherent within their linearisations [Acha 1988] [Smith 1996]. The linearisation of this phase dependency using complex numbers requires the complex conjugate notation [Semlyen *et al.* 1987] of Equation 2.17 which uses positive and negative frequency phasors.

$$\begin{bmatrix} \Delta I_+ \\ \Delta I_- \end{bmatrix} = \begin{bmatrix} Y_1 & Y_2 \\ Y_1^* & Y_2^* \end{bmatrix} \begin{bmatrix} \Delta V_+ \\ \Delta V_- \end{bmatrix} \tag{2.17}$$

where $I_{-f} = I_{+f}^*$ for a real valued waveform [Press *et al.* 1992]. This can also be represented by using real-valued positive frequency phasors.

$$\Delta I_+ = Y_1 \Delta V_+ + Y_2 \Delta V_+^* \tag{2.18}$$

Decomposing this into real and imaginary positive frequency components yields:

$$(I_r + jI_i) = (Y_{1r} + jY_{1i})(V_r + jV_i) + (Y_{2r} + jY_{2i})(V_r - jV_i) \tag{2.19}$$

$$I_r = (Y_{1r}V_r - Y_{1i}V_i) + (Y_{2r}V_r + Y_{2i}V_i) \tag{2.20}$$

$$I_i = (Y_{1r}V_i + Y_{1i}V_r) + (-Y_{2r}V_i + Y_{2i}V_r) \tag{2.21}$$

which in matrix form is:

$$\begin{bmatrix} I_r \\ I_i \end{bmatrix} = \left(\begin{bmatrix} Y_{1r} & -Y_{1i} \\ Y_{2i} & Y_{2r} \end{bmatrix} + \begin{bmatrix} Y_{2r} & Y_{2i} \\ Y_{2i} & -Y_{2r} \end{bmatrix} \right) \begin{bmatrix} V_r \\ V_i \end{bmatrix} \tag{2.22}$$

Both of the above methods provide the same representation of linear phase dependency. Approximately the same amount of storage and computation is required for the linearised admittance of the non-linear devices, though the complex conjugate method requires twice as much computation for the linear systems.

The complex conjugate notation creates difficulties when incorporating real valued variables such as control or other non-electrical variables. Also, the linearisation of a loadflow becomes approximate and significantly more difficult in complex form [Nguyen 1997]. The inclusion of the DC term of ac systems can also cause numerical problems.

It should be considered though that the complex conjugate method was used for the representation of magnitude dependent magnetic non-linearities described by the function:

$$y = f(x) \tag{2.23}$$

The linearised admittance or Jacobian of such a function is a Toepliz matrix and all the elements can be obtained from a single FFT of the time domain current derivative [Acha 1988].

$$\begin{bmatrix} I_{-2} \\ I_{-1} \\ I_0 \\ I_1 \\ I_2 \end{bmatrix} = \begin{bmatrix} c_0 & c_1 & c_2 & c_3 & c_4 \\ c_{-1} & c_0 & c_1 & c_2 & c_3 \\ c_{-2} & c_{-1} & c_0 & c_1 & c_2 \\ c_{-3} & c_{-2} & c_{-1} & c_0 & c_1 \\ c_{-4} & c_{-3} & c_{-2} & c_{-1} & c_0 \end{bmatrix} \begin{bmatrix} V_{-2} \\ V_{-1} \\ V_0 \\ V_1 \\ V_2 \end{bmatrix} \tag{2.24}$$

The same Fourier coefficients can be used to construct the real-valued positive frequency Jacobian. By observing the structure of Equation 2.17 and remembering that $c_{-k} = c_k^*$, the complex admittances Y_1 and Y_2 can be obtained in terms of c_k.

$$Y_1(h,k) = c_{(|h+k|)} \quad , \quad Y_2(h,k) = c^*_{(|h-k|)} \tag{2.25}$$

for I_h and V_k. The Jacobian term is then constructed using Equation 2.22.

The resultant Jacobian though is no longer Toepliz and is also non-symmetric. While this representation is not as elegant as the complex conjugate approach, it correctly represents the linearisation of the non-linear device and allows a more general overall solution.

A brief history of IHA

The first occurrence of an Iterative Harmonic Analysis within the literature was a method developed for harmonic analysis of HVdc [Reeve and Baron 1971] using a three phase fixed point iteration. The next major development was by Heydt [1982] with a single phase unified Newton algorithm. It incorporated a positive sequence loadflow at the fundamental frequency and coupling between harmonics. Some form of power flow control was also included. A key limitation with single phase analysis is that it neglects system imbalance. An imbalanced fundamental voltage will cause a 6-pulse converter to generate non-characteristic harmonics, predominantly the third in positive sequence. The accurate prediction of these non-characteristic harmonics is important for system design and hence the need for three phase representation.

Since then there has been a substantial level of development of the three-phase fixed point iteration approaches [Yacamini and de Oliveira 1980] [Eggleston 1985]. Callaghan [1989] showed that improved convergence could be obtained by the use of matched reactance pairs which shifted high reactance levels into the converter commutation circuit and out of the ac system. This served to increase the convergence strength of the global solution by effectively decreasing the terminal voltage harmonic distortion. However, multiple iteration stages were required for representation of the load-

flow, ac, and dc harmonic systems [Callaghan and Arrillaga 1989]. Another reference [Arrillaga *et al.* 1987] showed, by comparison with time domain simulation, that the divergence of an IHA solution did not indicate a harmonic instability as previously suggested [Reeve and Baron 1971] [Yacamini and de Oliveira 1980].

As the simple matched reactance pair could not cancel ac system parallel resonances, it has been suggested that matched impedance pairs be used for further convergence improvement [Carbone *et al.* 1992] [Carpinelli *et al.* 1994]. This complicates the non-linear device analysis significantly and so time domain simulation is often used for the actual harmonic transfer calculations.

An unbalanced three phase Newton solution, termed the Harmonic Domain, was developed by Acha [Acha 1988] for the harmonic representation of single phase banks of non-linear transformers. This method used Norton Equivalents and a complex conjugate formulation, and was subsequently extended for transformer generator interactions, three limb non-linear transformers and a TCR model [Medina and Arrillaga 1994] [Arrillaga *et al.* 1995] [Lisboa 1996] [Rico *et al.* 1996]. However, due to the complex variable formulation, the inclusion of control and loadflow specifications is difficult and a double iterative scheme was used for the fundamental frequency loadflow adjustment [Lisboa 1996].

Xu *et al.* [1991b] also used Norton Equivalents to improve the convergence of the fixed point or Gauss-Seidel iterations. A three phase loadflow using a Newton method was included at the fundamental but the harmonic voltages were updated using a decoupled fixed point approach. Control was also implemented but in a further decoupled iteration [Xu *et al.* 1991a] [Xu *et al.* 1994].

A better approach was formulated by Mayordomo and Valcárcel [1993] which used three sequential full Newton solutions; three phase loadflow, IHA and control. A number of useful industrial level non-linear device models have been developed for both iterative and direct solution methods [Mayordomo *et al.* 1997] [Asensi *et al.* 1998].

There is however a difficulty in separating the three phase loadflow and the full harmonic interaction. For the full Newton solution to be maintained, the non-linear devices must be properly linearised within the loadflow to avoid convergence difficulties [Smith and Arrillaga 1998]. The same is true for linearising the loadflow so that the fundamental can be included within the iterative harmonic solution. This is more difficult due to the non-linear PV and PQ constraints of the loadflow busbars which are not trivial to linearise. This complexity can be simply avoided by combining them both into the same solution. While the unified solution initially appears to be more complicated, it can be minimised through intelligent programming [Bathurst *et al.* 1998a].

A modified form of the Harmonic Domain extended the representation to a 12-pulse HVdc rectifier which incorporated control interaction using a real-valued positive frequency analysis [Smith *et al.* 1996]. This approach allowed the simultaneous

solution of electrical and non-electrical quantities, such as control and switching instances. An extension to this was made by Dinh [1998] for the representation of a unit connected HVdc rectifier configuration which was validated against real measurements [Dinh *et al.* 1997]. Since then this representation has been extended to allow full representation of multiple interconnected non-linear devices and a variety of control configurations. This method is described in detail in the following chapters.

2.3 ALGORITHM SPECIFICATIONS

In order to develop an algorithm for detailed harmonic analysis, a specification must be created for the important aspects of harmonic modelling within power systems. The specifications should detail the possible device and network configurations, operating point definitions and incorporate all important mechanisms of harmonic generation. It is difficult to determine exactly what is important within a complex problem such as this and so an initial loose specification is made to observe these effects and their importance quantified.

2.3.1 Non-linear harmonic components

Active sources

Components such as large ac-dc converters and saturated transformers couple between frequencies and are generally non-linear with operating point. They can be either shunt devices or link ac and/or dc busbars. The busbar(s) that they are connected to are represented in full harmonic form within the solution. Generally the non-linear devices require a control variable as well.

Passive sources

To approximate small non-linear devices or background harmonic levels, passive harmonic sources can be specified. These can be either current or voltage sources and are held constant during the full harmonic solution. Simplified non-linear device models can be used to minimise the effort required to calculate these constant injections. These would be active at the power frequency during the loadflow solution but the resultant harmonic injections would be constant.

2.3.2 Power frequency loadflow components

The majority of power system loads and generators are operated within their linear regions. Their operating point specifications are normally in terms of loadflow conditions of power and voltage magnitude. A three phase loadflow should represent specify the operating point in these terms to minimise the effort required for the simulation. At

harmonic frequencies, the linear components are represented by equivalent impedances which are calculated from pre-determined equations based upon some basic load or generator information. It is important that the connection of these loads (star-ground, delta, etc) is properly represented as this will have a significant impact on the zero-sequence and inter-phase impedances.

2.3.3 Passive system components

The significant part of the system representation is in the form of passive components that are not affected by the loadflow operating point. They are represented within the solution as shunt impedances or equivalent π-models. These can be generally calculated in any particular method and couple between phases and busbars, but not frequencies. For simplicity the transformers and filters have their impedances calculated internally using pre-specified equations while the transmission line data is supplied externally.

Transformers and filters can be affected by system conditions if certain external control equations are specified. An automatic tap changer will affect the transformer impedance and a reactive power controller may switch out a filter bank. In these cases, the harmonic impedance of the system will change and so such control actions are only performed during an initial loadflow to minimise computational effort.

2.3.4 Operating point controllers

System controls are an important part of the operating point specification. These can be either simple controls that are used to govern the power generated by the slack busbar or more complex ones that modulate converter firing angles from measured dc currents. The modelling of these controls should be as realistic as possible so as to simplify effort in system representation.

2.3.5 System solution

Using the linearity of the transmission network at harmonic frequencies, the system can be reduced so that only the non-linear busbars are present. However, the three-phase loadflow is maintained in full at the power frequency as this is non-linear due to the power and voltage specifications. A real-valued unified solution structure is used to allow for the sometimes significant frequency coupling of the non-linear devices. This also simplifies the inclusion of system controllers which are real-valued and often dependent upon multiple solution variables. As the solution of the combined power system model is reasonably non-linear, a good iterative technique is required. The Newton method has been chosen as in the past it has shown good convergence potential, provided a reasonable initialisation is provided.

2.3.6 Multiple run capability

Power systems are rarely in a true steady-state due to the continually changing nature of their loading. However by taking multiple operating point snapshots, a set of simulations can be performed which reflect the typical harmonic behaviour. The logical extension to this is to provide operating points for the entire day or week so that a harmonic profile of the system can be obtained. For this to be realistically feasible, the solution algorithm must be able to automatically process the multiple operating points and calculate the profiles with as little user interaction as possible. For a complex solution structure, care must be taken so as to minimise the overall computation that load changing requires.

For a system loading change, the harmonic system reduction will be required. However, if the generation schedule is changed, the harmonic impedances do not change and so the reduction is not required to be renewed. Likewise for a change in a controller's setpoint for a non-linear device. A multiple run feature within a program should be intelligent enough to determine how much of the full solution algorithm is required to be performed for a given system.

Chapter 3

HARMONIC MODELLING OF POWER SYSTEM COMPONENTS

3.1 INTRODUCTION

Non-linear devices can be defined as system components that cause coupling between frequencies, have operating points that respond significantly to harmonics and have harmonic impedances that can not be easily pre-determined. A requirement of an algorithm for the modelling of power systems containing non-linear components is that such devices appear as dependant sources within the linear systems they are connected to. This chapter will illustrate a methodology for formulating non-linear devices into this framework.

Section 3.2 details a method for modelling the six pulse current sourced converter/transformer unit. The Harmonic Domain HVdc rectifier model developed by Smith [1996] is generalised and extended to include the modelling of zig-zag transformers, inverters, un-controlled rectifiers and then a formulation for the multi-limb converter transformer. The converter is represented in the algorithm as an ac-dc series non-linear component.

The next section briefly describes the inclusion of a salient pole synchronous machine, as developed by Dinh [1998], as an ac shunt non-linear component. Finally there is a brief discussion on the harmonic modelling of linear system components and on the inclusion of other commonly used non-linear devices.

3.2 6-PULSE CONVERTER BY CONVOLUTION

The convolution method was originally developed by Smith [1996] for a 12-pulse HVdc rectifier under constant current control with star-g/star and star-g/delta transformers. The analytical approach was slightly different for the two transformer/converter units due mainly to the sequence of their development. A general approach is presented here that allows for most transformer configurations, and fits within the solution framework (Figure 3.1). The solution structure is also different from Smith's in that the switching

angles are solved explicitly given the terminal conditions of the converter, instead of implicitly within the main solution. The main system Jacobian has also been modified to maintain the full Newton structure by linearising the effect of modulation of the switching instants.

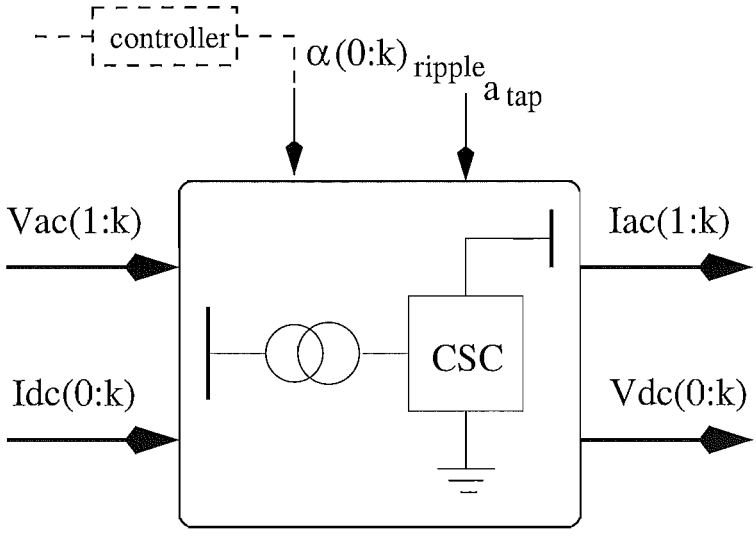

Figure 3.1 New representation of the converter unit for inclusion within a general harmonic algorithm

3.2.1 Generalised form of the converter

The 6-pulse converter model is formulated assuming that the dc current is continuous and that, within each 6-pulse bridge, there are no simultaneous commutations. For most large converter units this is normal in steady-state operation; there are however, instances where the dc current is not continuous or there are simultaneous commutations. These are usually during transient events or machine startups [CIGRE 14.07 1992] and so the analysis of the harmonic content during these periods is not particularly meaningful.

In this mode of operation, the bridge has 12 distinct periods of conduction, six of these involve two-device conductions and the other six are three-device conductions. Using nodal analysis for each of the 12 circuits, equations can be written to define steady-state waveshapes which are valid during these periods of conduction. The switching instants of the converter are solved explicitly and then used to determine the spectra of the bandlimited rectangular sampling functions. These sampling functions are convolved with the sample waveshapes to select the period of validity of each of the samples. The resultant spectra of the convolutions for the 12 sample periods are then combined to yield the transferred quantity, i.e. the dc voltage or the phase currents on the converter side of the transformer. The primary phase currents of the converter transformer are then obtained via the transformer transfer matrix.

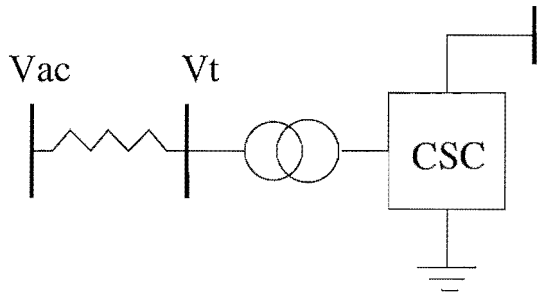

Figure 3.2 Inclusion of commutation resistance within ac system.

To represent the nodal analysis of the twelve periods as steady-state waveshapes, any resistance within the conduction circuit must be removed. The resistance is placed between the busbar terminal voltage and the solution commutating voltage. Using a small Gauss-Seidel step, the solution commutation voltage can be obtained from the busbar terminal voltage using the phase currents from the previous iteration. While deviating slightly from a true Newton method, the solution convergence is not significantly affected in most realistic situations.

If the commutation circuit resistance is large, the Gauss-Seidel step may result in solution divergence. This problem can avoided by including a ficticious busbar, as shown in Figure 3.2. The commutation circuit is then purely inductive and the solution is full Newton, which results in dramatically improved convergence.

Analytic expressions for the harmonic transfers have been formed for a standard 6-pulse bridge with the anode grounded and the dc current defined to be leaving the cathode busbar. The voltage generated from anode to cathode is negative when the average firing angle is greater than 90^o and positive when less than 90^o. For a basic HVdc link, the inverter operates with the average firing angle greater than 90^o, but has a positive voltage due to the bridge orientation. To avoid further analytic expressions a new variable, *orient*, is used to account for the bridge orientation in the bipolar link model (Figure 3.3).

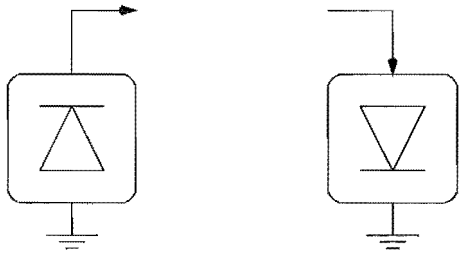

Figure 3.3 HVdc converter bridge representation

3.2.2 General formulation of the samples

The equivalent circuit of Figure 3.4(a) is used to represent the transformer within the converter model. As explained above, any resistance within the circuit must be removed so that the steady-state samples can be written. In this model, the transformer is assumed linear; if saturation is to be included it will appear as an independent primary shunt term. Tap changers are assumed to be equal on all phases but the phase resistance and reactances can be different. If any converter bridge resistance is to be modelled, it must be balanced so that it can be moved to between the system and the primary terminals of the transformer.

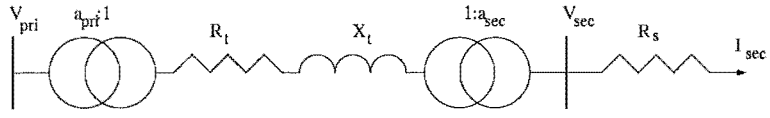

(a) Equivalent transformer

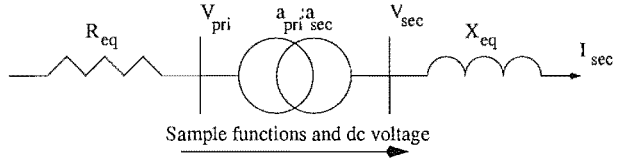

(b) Transformer representation for steady-state transfers

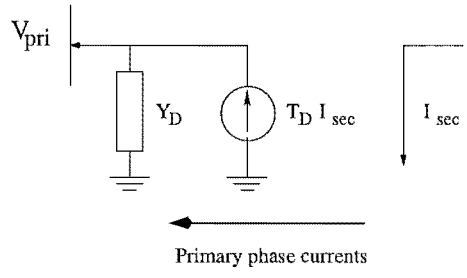

(c) Transformer representation for primary phase currents

Figure 3.4 Converter transformer representation

The equivalent circuits of Figures 3.4(b) and 3.4(c) are obtained by referring the resistance to the primary side and the reactance to the secondary side. The equivalent resistances and reactances are given by Equations 3.1 and 3.2.

$$X_{eq} = a_{sec}^2 X_T \tag{3.1}$$

$$R_{eq} = a_{pri}^2 R_T + \left(\frac{a_{pri}}{a_{sec}}\right)^2 R_s \tag{3.2}$$

Figure 3.5 illustrates the equivalent commutation circuit for a star-g/star transformer. Simple nodal analysis is then used to obtain analytic expressions for the samples, using the secondary phase current substitutions given by Equation 3.3. For this switching period, the following notation is used for the phase beginning commutation, the phase endding commutation, and the other phase not directly involved in the commutation by; $B = a$, $E = c$ and $O = b$ respectively.

$$\begin{bmatrix} I_B & I_O & I_E \end{bmatrix} = \begin{cases} \begin{bmatrix} I_{dk} & -I_{dk} & 0 \end{bmatrix} , & \text{Normal (2 devices)} \\ \begin{bmatrix} I_{comm} & -I_{dk} & I_{dk} - I_{comm} \end{bmatrix} , & \text{Commutation (3 devices)} \end{cases} \tag{3.3}$$

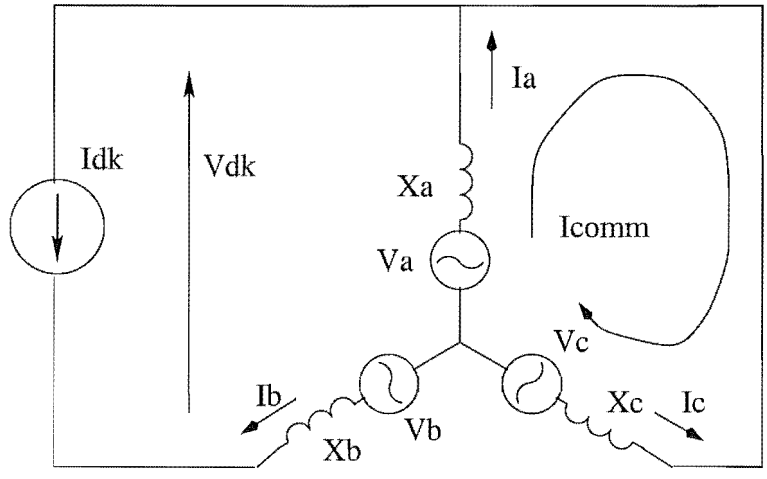

Figure 3.5 Commutation circuit for nodal analysis.

The voltage drops around the commutation loop are summed to zero i.e.

$$0 = V_B - V_E \text{ , solve for commutation current samples } (I_{comm}) \tag{3.4}$$

The commutation current sample can then be formed as a function of the terminal ac voltage and dc current harmonics.

$$[I_{comm}] = [P_{comm\_V}] \begin{bmatrix} V_B \\ V_E \\ V_O \end{bmatrix} + [P_{comm\_I}] [I_d] \tag{3.5}$$

As the commutation current is zero when the device turns on (θ), the dc component of the commutation current is defined as:

$$I_{comm}(0) = Imag \left\{ \sum_{k=1}^{nh} I_{comm}(k) \exp^{jk\theta} \right\} \tag{3.6}$$

Similarly the dc voltage can be expressed as the difference between the two conducting phases.

$$V_{volt} = V_B - V_O \text{ , solve for the dc voltage samples } (V_{volt}) \tag{3.7}$$

During a commutation, the expression previously derived for the commutation current is substituted in so that the dc voltage samples are expressed as functions of the terminal voltage and dc current harmonics.

$$[V_{volt}] = [P_{volt\_V}] \begin{bmatrix} V_B \\ V_E \\ V_O \end{bmatrix} + [P_{volt\_I}] [I_d] \tag{3.8}$$

The transfer matrices for the Yg-Y and Yg-D transformer types, as derived by Smith [1996], are shown in Appendix A.

3.2.3 Derivation of samples for a zigzag transformer

Harmonic cancellation related to 12-pulse operation can be achieved by using star-star and star-delta transformers due to the thirty degree phase shift inherent within the star-delta transformer; however for higher pulse operation, special phase shifting transformers are required.

The required voltage phase shift is achieved by dividing the secondary windings into two parts and connecting pairs of windings from different phases in series, as shown by the phasor representation in Figure 3.6. This connection, referred to as a zig-zag connection, can then provide any required phase shift by changing the relative ratios of the two secondary windings. The ratios required can be obtained from the phasor diagram in Figure 3.6 and are shown in Equation 3.9 [Yacamini and de Oliveira 1980].

$$n_1 = \frac{|V_{pri}|}{|V_{sec}|} \quad , \quad n_2 = \frac{2n_1}{\sqrt{3}} \sin(\tfrac{\pi}{3} - \sigma) \quad , \quad n_3 = \frac{2n_1}{\sqrt{3}} \sin(\sigma) \tag{3.9}$$

$$\begin{aligned} S_2 &= \tfrac{n_2 S_T}{(n_2+n_3)} \quad , \quad S_3 = \tfrac{n_3 S_T}{(n_2+n_3)} \\ V_2 &= n_2 V_{pri} \quad , \quad V_3 = n_3 V_{pri} \end{aligned} \tag{3.10}$$

The transfers that are shown below are for a positive phase angle shift. Similar transfers can be obtained for a negative phase angle shift by changing the phase connections of the secondary windings.

For simplicity, the zig-zag transformer is specified as a single unit, even though it is modelled as six separate single phase transformers. The analysis assumes an ideal zig-zag transformer where there is no magnetic coupling between phases, no saturation, and each phase is specified as a single leakage reactance. The leakage reactances of each

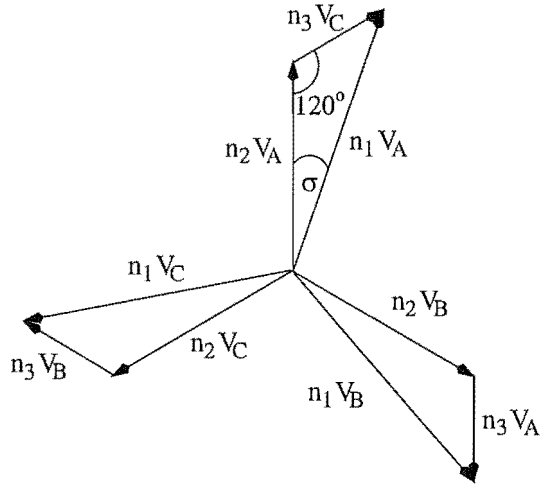

Figure 3.6 Phasor representation of zig-zag winding for a positive shift.

of the two transformers forming the zigzag winding are scaled to reflect the different power sharing between them. This can be done via a power base transform from the scaled power bases.

$$X_n = X_T \left(\frac{S_n}{S_T} \right) \tag{3.11}$$

(3.12)

The leakage reactances of the two single phase transformers are:

$$X_2 = \frac{X_T}{n_2(n_2 + n_3)} \tag{3.13}$$

$$X_3 = \frac{X_T}{n_3(n_2 + n_3)} \tag{3.14}$$

As required for the calculation of the samples, these have been referred to the secondary side of the zigzag transformer.

The equivalent circuit used in the calculation of the samples for the zigzag transformer is shown in Figure 3.7. It is drawn for period 1, where phase C is commutating to phase A on the positive dc rail.

Table 3.1 Definition of switching period types

Type=+1	Commutation on the positive rail from phases B to E with phase O on.
Type=0	Normal conduction between phases B and O with E off.
Type=-1	Commutation on the negative rail from phases B to E with phase O on.

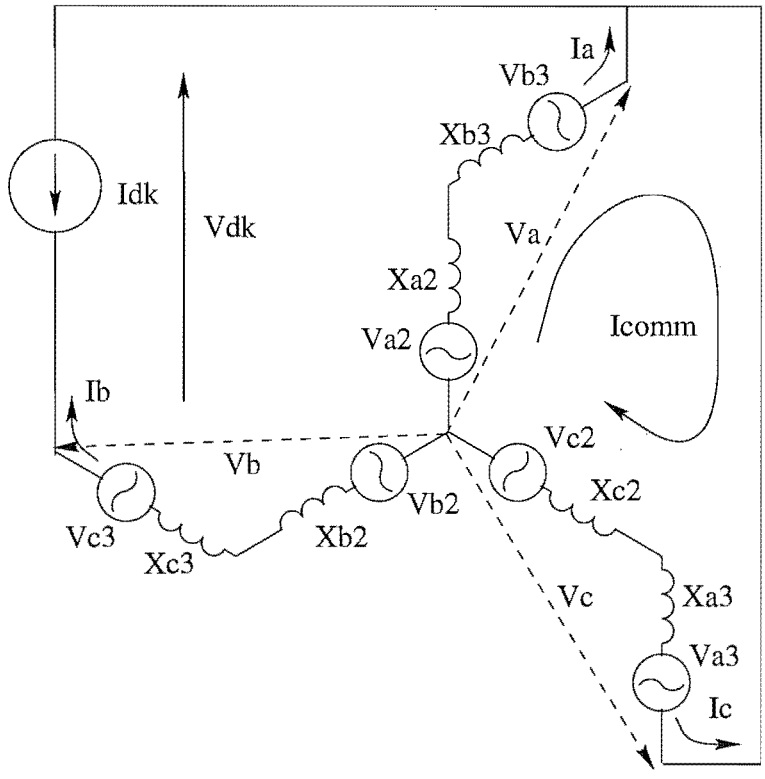

Figure 3.7 Equivalent commutation circuit for a zigzag transformer for period 1.

Table 3.2 Switching pattern for 6-pulse converter.

Type	+1	0	-1	0	+1	0	-1	0	+1	0	-1	0
B	a	a	c	a	b	b	a	b	c	c	b	c
E	c	c	b	b	a	a	c	c	b	b	a	a
O	b	b	a	c	c	c	b	a	a	a	c	b

Calculation of the commutation current samples

Using the expression given in Equation 3.4, analysis of the circuit in Figure 3.7 results in Equation 3.15.

$$\begin{aligned} 0 &= [(n_2 V_a - jki_a X_{a2}) - (n_3 V_b + jki_a X_{b3})] \\ &- [(n_2 V_c - jki_c X_{c2}) - (n_3 V_a + jki_c X_{a3})] \end{aligned} \tag{3.15}$$

The appropriate current expressions in Equation 3.3 are substituted in and the commutating current solved for. This provides the following expression for the commutating current sample:

$$I_{comm} = \frac{(n_2 + n_3)V_a - n_2 V_c - n_3 V_b + jk(X_{c2} + X_{a3})I_d}{jk(X_{a2} + X_{b3} + X_{c2} + X_{a3})} \tag{3.16}$$

Using the switching pattern given in Table 3.2 the following general expression can

be written: (The ± refers to whether the commutation is on the positive or dc negative rail)

$$[P_{comm\_V}] = \pm \begin{bmatrix} (n_2+n_3)/(jk(X_B+X_E)) \\ -n_3/(jk(X_B+X_E)) \\ -n_2/(jk(X_B+X_E)) \end{bmatrix} \tag{3.17}$$

$$[P_{comm\_I}] = \begin{bmatrix} X_E/(X_B+X_E) \end{bmatrix} \tag{3.18}$$

The storage requirements can be minimised by observing that some of the samples are not frequency dependent and, where frequency dependency does occur, the frequency term can be removed. Thus the following expression for the commutation current samples can be formed:

$$I_{comm_k} = \left(\frac{1}{jk}\right)[P_{comm\_V}] \begin{bmatrix} V_{ak} \\ V_{bk} \\ V_{ck} \end{bmatrix} + [P_{comm\_I}]\, I_{dk} \tag{3.19}$$

Calculation of the dc voltage samples

Using the expression in Equation 3.7, the dc voltage sample is derived for period 1 where there is a commutation on the positive rail from phase C to phase A. The voltage sample from the positive rail to the negative rail (phase A to phase B) is shown in Equation 3.20.

$$\begin{aligned} V_{volt} &= [(n_2V_a - jki_aX_{a2}) - (n_3V_c + jki_aX_{c3})] \\ &- [(n_2V_b - jki_bX_{b2}) - (n_3V_a + jki_bX_{a3})] \end{aligned} \tag{3.20}$$

The phase currents from Equation 3.3 and the commutation current sample from 3.16 are substituted into Equation 3.20. Then, using Table 3.2, the general expressions of Equations 3.21 and 3.22 can be obtained. The ± refers to whether the commutation that resulted in this condition was on the positive or negative dc rail.

$$[P_{volt\_V}] = \pm \begin{bmatrix} (n_2+n_3) - (n_2X_B)/(X_B+X_E) \\ -n_2 - (n_3X_B)/(X_B+X_E) \\ -n_3 + ((n_2+n_3)X_B)/(X_B+X_E) \end{bmatrix} \tag{3.21}$$

$$[P_{volt\_I}] = \begin{bmatrix} -jk(X_O + (X_BX_E)/(X_B+X_E)) \end{bmatrix} \tag{3.22}$$

The normal conduction of period 2 has only two switches in operation. This sample is derived where phase A is conducting on the positive rail, and phase B on the negative rail with phase C off. The nodal equation for this sample is the same as Equation 3.20 except that the secondary phase currents are for a normal conduction as given by

Equation 3.3. Using Table 3.2 again, the following general expressions are obtained:

$$[P_{volt\_V}] = \pm \begin{bmatrix} n_2 + n_3 \\ -n_2 \\ -n_3 \end{bmatrix} \tag{3.23}$$

$$[P_{volt\_I}] = \begin{bmatrix} -jk(X_B + X_E) \end{bmatrix} \tag{3.24}$$

The storage requirements can again be minimised by observing that some of the samples are not frequency dependent and, where frequency dependency does occur, the frequency term can be removed. Thus the following expression for the voltage samples can be formed, where the P_{volt} arrays are only real valued and constant for all frequencies.

$$V_{volt_k} = [P_{volt\_V}] \begin{bmatrix} V_{Bk} \\ V_{Ek} \\ V_{Ok} \end{bmatrix} - jk\,[P_{volt\_I}]\,I_{dk} \tag{3.25}$$

Transformer transfer matrix

The transformer transfer matrix is used to calculate the primary phase currents from the secondary currents. As the converter bridge has no path for zero-sequence, the transfer to the primary can be expressed in terms of only two secondary currents.

$$I_A = n_2 I_a - n_3 I_c \tag{3.26}$$

$$I_B = n_2 I_b - n_3 I_a \tag{3.27}$$

$$I_C = n_2 I_c - n_3 I_b \tag{3.28}$$

as $I_c = -(I_a + I_b)$, then:

$$[T_D] = \begin{bmatrix} n2 + n3 & n3 \\ -n3 & n2 \\ -n2 & -n2 - n3 \end{bmatrix} \tag{3.29}$$

This completes the analysis required for the modelling of a star-g/zigzag transformer which consists of six electrically connected single phase transformers. If the mutual coupling through the magnetic core of a multi-limb transformer is to be modelled, then the analysis needs to be further generalised to eliminate the increasingly complex nodal analysis. This is done in the next section.

3.2.4 Derivation of samples for a three phase transformer

To simplify the formulation of the converter analysis most frequency domain modelling of the converter transformer assumes that it is a bank of three single phase linear transformers. This is a reasonable assumption as in practice, a significant number of the transformer banks are actually single phase for both economic and for redundancy reasons. However, in the case where a multi-phase transformer is actually present, the representation of the converter transformer as a bank of single phase transformers will result in inaccurate harmonic responses due to magnetic flux coupling within the transformer core [Enright 1996]. If this form of response is to be investigated, then a method of including these mutual couplings must be created.

Assuming that the leakages and mutual couplings are the same for the three phases, the primitive matrix for a basic three limb transformer is given as below [Arrillaga *et al.* 1983].

$$\left[\begin{array}{c} I_1 \\ I_2 \\ I_3 \\ \hline I_4 \\ I_5 \\ I_6 \end{array}\right] = \left[\begin{array}{ccc|ccc} y_p & y'_m & y'_m & -y_m & y''_m & y''_m \\ y'_m & y_p & y'_m & y''_m & -y_m & y''_m \\ y'_m & y'_m & y_p & y''_m & y''_m & -y_m \\ \hline -y_m & y''_m & y''_m & y_s & y'''_m & y'''_m \\ y''_m & -y_m & y''_m & y'''_m & y_s & y'''_m \\ y''_m & y''_m & -y_m & y'''_m & y'''_m & y_s \end{array}\right] \left[\begin{array}{c} V_1 \\ V_2 \\ V_3 \\ \hline V_4 \\ V_5 \\ V_6 \end{array}\right] \tag{3.30}$$

The primitive quantities are related to the nodal quantities by a connection matrix which depends upon the electrical connection of the windings. As equation 3.33 shows, these can be used to form the nodal admittance matrix from the primitive matrix for a given transformer connection.

$$[V_{prim}] = [C]^T[V_{node}] \tag{3.31}$$

$$[I_{node}] = [C][I_{prim}] \tag{3.32}$$

$$[Y_{node}] = [C][Y_{prim}][C]^T \tag{3.33}$$

For a star-g/star the connection matrix, $[C]^T$, is:

$$\left[\begin{array}{c} V_1 \\ V_2 \\ V_3 \\ \hline V_4 \\ V_5 \\ V_6 \end{array}\right] = \left[\begin{array}{ccc|ccc|c} 1 & 0 & 0 & 0 & 0 & 0 & 0 \\ 0 & 1 & 0 & 0 & 0 & 0 & 0 \\ 0 & 0 & 1 & 0 & 0 & 0 & 0 \\ \hline 0 & 0 & 0 & 1 & 0 & 0 & -1 \\ 0 & 0 & 0 & 0 & 1 & 0 & -1 \\ 0 & 0 & 0 & 0 & 0 & 1 & -1 \end{array}\right] \left[\begin{array}{c} V_A \\ V_B \\ V_C \\ \hline V_a \\ V_b \\ V_c \\ \hline V_n \end{array}\right] \tag{3.34}$$

A Kron reduction is used to eliminate the neutral node from the un-grounded star connection [Lisboa 1996]. The phase nodes are taken as the reduced variable set and the neutral node as the variable to be eliminated.

$$\left[\begin{array}{c} I_{nodes} \\ \hline I_{neutral} \end{array}\right] = \left[\begin{array}{c|c} A & B \\ \hline C & D \end{array}\right] \left[\begin{array}{c} V_{nodes} \\ \hline V_{neutral} \end{array}\right] \tag{3.35}$$

Where the reduced admittance matrix is of the form:

$$[I_{nodes}] = [A - BD^{-1}C]\,[V_{nodes}] \tag{3.36}$$

Following this method the admittance matrix for the star-g/star transformer is:

$$\frac{1}{3}\left[\begin{array}{ccc|ccc} 2(y_s-y_m''') & -(y_s-y_m''') & -(y_s-y_m''') & -2(y_s-y_m''') & (y_s-y_m''') & (y_s-y_m''') \\ -(y_s-y_m''') & 2(y_s-y_m''') & -(y_s-y_m''') & (y_s-y_m''') & -2(y_s-y_m''') & (y_s-y_m''') \\ -(y_s-y_m''') & -(y_s-y_m''') & 2(y_s-y_m''') & (y_s-y_m''') & (y_s-y_m''') & -2(y_s-y_m''') \\ \hline -2(y_s-y_m''') & (y_s-y_m''') & (y_s-y_m''') & 2(y_s-y_m''') & -(y_s-y_m''') & -(y_s-y_m''') \\ (y_s-y_m''') & -2(y_s-y_m''') & (y_s-y_m''') & -(y_s-y_m''') & 2(y_s-y_m''') & -(y_s-y_m''') \\ (y_s-y_m''') & (y_s-y_m''') & -2(y_s-y_m''') & -(y_s-y_m''') & -(y_s-y_m''') & 2(y_s-y_m''') \end{array}\right] \tag{3.37}$$

The electrical equivalent circuit for this is very complicated and a manual nodal analysis, as previously shown, would be prohibitive. Similarly for a star-g/delta, the nodal admittance matrix is:

$$\left[\begin{array}{ccc|ccc} y_p & y_m' & y_m' & -\frac{(y_m+y_m'')}{\sqrt{3}} & \frac{(y_m+y_m'')}{\sqrt{3}} & 0 \\ y_m' & y_p & y_m' & 0 & -\frac{(y_m+y_m'')}{\sqrt{3}} & \frac{(y_m+y_m'')}{\sqrt{3}} \\ y_m' & y_m' & y_p & \frac{(y_m+y_m'')}{\sqrt{3}} & 0 & -\frac{(y_m+y_m'')}{\sqrt{3}} \\ \hline -\frac{(y_m+y_m'')}{\sqrt{3}} & 0 & \frac{(y_m+y_m'')}{\sqrt{3}} & \frac{2(y_s-y_m''')}{3} & -\frac{(y_s-y_m''')}{3} & -\frac{(y_s-y_m''')}{3} \\ \frac{(y_m+y_m'')}{\sqrt{3}} & -\frac{(y_m+y_m'')}{\sqrt{3}} & 0 & -\frac{(y_s-y_m''')}{3} & \frac{2(y_s-y_m''')}{3} & -\frac{(y_s-y_m''')}{3} \\ 0 & \frac{(y_m+y_m'')}{\sqrt{3}} & -\frac{(y_m+y_m'')}{\sqrt{3}} & -\frac{(y_s-y_m''')}{3} & -\frac{(y_s-y_m''')}{3} & \frac{2(y_s-y_m''')}{3} \end{array}\right] \tag{3.38}$$

For a bank of single phase transformers where there is no coupling between the magnetic circuits, the mutual coupling terms, y_m', y_m'' and y_m''' are all zero. The matrix then simplifies down to those given in Section 3.4. However, if there is coupling between the magnetic circuits, these terms should be included.

The problem with representation of the multi-limb transformer in this manner relates to the actual calculation or measurement of the mutual coupling terms. In practice, it is very difficult to measure some of these terms.

A recently developed time domain modelling technique [Enright 1996], referred to as the Unified Magnetic Equivalent Circuit (UMEC), represents the saturation and flux distribution through the multi-limb transformer core specified from detailed core measurements, or a *per-unit* core based on the name plate leakage reactance. Using the UMEC method a linearised admittance matrix can be calculated that accurately

represents the transformer during its unsaturated operation. This admittance matrix can then be used to form the dc voltage samples and commutation current samples for harmonic analysis. An example of a multi-limb transformer is given in Appendix A as a coupled inductance matrix.

The linearised admittance matrix is only valid for un-saturated conditions, and so a different formulation must be used if a saturated condition is required. The transformer nodal admittance is written in general matrix form as follows:

$$\left[\begin{array}{c} I_{pri} \\ \hline I_{sec} \end{array}\right] = \left[\begin{array}{c|c} A & B \\ \hline C & D \end{array}\right] \left[\begin{array}{c} V_{pri} \\ \hline V_{sec} \end{array}\right] \tag{3.39}$$

The secondary side voltages are solved for in terms of the primary voltages and the secondary phase currents, i.e.

$$[V_{sec}] = [D]^{-1}\left([I_{sec}] - [C]\,[V_{pri}]\right) \tag{3.40}$$

These are then used to obtain the expressions for the commutation currents and the dc voltages during the different periods of conduction. Generally for a converter transformer, the secondary winding uses either an un-grounded star or delta connection. This will result in the D matrix being non-invertible as the system is over-determined, i.e. there is no path for zero sequence current. This restriction can be over-come by removing one of the secondary currents from the above equation. This results in the following equation which can be solved:

$$\left[\begin{array}{c} V_B \\ V_E \end{array}\right] = \left[\begin{array}{cc} D_{BB} & D_{BE} \\ D_{EB} & D_{EE} \end{array}\right]^{-1} \left(\left[\begin{array}{c} I_B \\ I_E \end{array}\right] - \left[\begin{array}{ccc} c_{Ba} & c_{Bb} & c_{Bc} \\ c_{Ea} & c_{Eb} & c_{Ec} \end{array}\right] \left[\begin{array}{c} V_A \\ V_B \\ V_C \end{array}\right] \right) \tag{3.41}$$

The analytic expressions for the general transfer matrices are obtained by the same analysis as given in Section 3.2.2. Equations 3.3, 3.4 3.7 are repeated here for clarity, i.e.

$$\begin{aligned} 0 &= V_B - V_E \text{ , solve for commutation current samples } (I_{comm}) \\ V_{volt} &= V_B - V_O \text{ , solve for the dc voltage samples } (V_{volt}) \end{aligned}$$

$$\left[\begin{array}{ccc} I_B & I_O & I_E \end{array}\right] = \left\{ \begin{array}{ll} \left[\begin{array}{ccc} I_{dk} & -I_{dk} & 0 \end{array}\right] & \text{, Normal (2 devices)} \\ \left[\begin{array}{ccc} I_{comm} & -I_{dk} & I_{dk} - I_{comm} \end{array}\right] & \text{, Commutation (3 devices)} \end{array} \right.$$

Once the appropriate currents are substituted in, expressions for the dc voltage or

commutation current can easily be obtained.

$$V_{volt} = \begin{bmatrix} p_{Bo} & p_{Ob} \end{bmatrix} \left(\begin{bmatrix} I_B \\ I_O \end{bmatrix} - \begin{bmatrix} c_{Ba} & c_{Bb} & c_{Bc} \\ c_{Oa} & c_{Ob} & c_{Oc} \end{bmatrix} \begin{bmatrix} V_A \\ V_B \\ V_C \end{bmatrix} \right) \tag{3.42}$$

$$I_{comm} = \frac{1}{p_{Be} - p_{Eb}} \left(\begin{bmatrix} p_{Be} & p_{Eb} \end{bmatrix} \begin{bmatrix} c_{Ba} & c_{Bb} & c_{Bc} \\ c_{Ea} & c_{Eb} & c_{Ec} \end{bmatrix} \begin{bmatrix} V_A \\ V_B \\ V_C \end{bmatrix} - p_{(E)} I_d \right) \tag{3.43}$$

where,

$$\begin{bmatrix} p_{Be} & p_{Eb} \end{bmatrix} = \begin{bmatrix} di_{BB} & di_{BE} \end{bmatrix} - \begin{bmatrix} di_{EB} & di_{EE} \end{bmatrix} \tag{3.44}$$

$$\begin{bmatrix} p_{Bo} & p_{Ob} \end{bmatrix} = \begin{bmatrix} di_{BB} & di_{BO} \end{bmatrix} - \begin{bmatrix} di_{OB} & di_{OO} \end{bmatrix} \tag{3.45}$$

After the secondary currents have been obtained, they are referred back through the transformer to the primary side. This is done using Equation 3.46, where again, only two of the secondary phases are required to define the three phase primary currents.

$$[I_{pri}] = \left([A] - [B][D]^{-1}[C]\right)[V_{pri}] - [B][D]^{-1}[I_{sec}] \tag{3.46}$$

Appendix A shows that simple matrix manipulations result in identical expressions for the samples derived from direct nodal analysis for a star-g/delta transformer when using single phase transformers.

A problem that arises is the removal of resistance from the conduction circuits. Previously with the single phase banks where there was no magnetic coupling between the phases, it was possible to shift any transformer or thyristor resistance to between the primary terminals and the ac system. However, with the increased circuit complexity, this may no longer be possible. Approximations can be made though to obtain a combined resistance as before which, while not ideal, may be satisfactory.

Extension to multi-winding transformers

For a three-phase three-winding transformer connected in zigzag, the analysis is the same except that the secondary phase voltages are built up from four voltages rather than two. Thus, the nodal admittance is represented by a 9 by 9 matrix rather than a 6 by 6 matrix.

$$P = \left([D]^{-1}_{(B_2,1:4)} - [D]^{-1}_{(B_3,1:4)}\right) - \left([D]^{-1}_{(E_2,1:4)} - [D]^{-1}_{(E_3,1:4)}\right) \tag{3.47}$$

Another common occurrence is the single phase multi-winding transformer used in multiple converter applications. The problem now is that the individual converters can no longer be considered in isolation and so the formulation becomes more complicated. For the standard analysis described above to be valid, the commutation angle must be smaller than 30^0 to avoid simultaneous commutations between the two bridges. This is normally the case to minimise dc voltage depression and VAr consumption. To represent simultaneous commutations, new periods of conduction would have to be derived.

3.2.5 Switching instant calculations

As the converter action is defined by its switching instants, accurate determination of these is important in order to accurately represent its operation [Wood 1993]. The switching instants (angles) required by the converter depend upon the control strategy used. Table 3.3 illustrates this for the five different converter categories.

Table 3.3 Converter switching instants required for the solution

type	firing	end of comm.	extinction
un-controlled rectifier	✓	✓	
equi-distant rectifier		✓	
modulated rectifier	✓	✓	
equi-distant inverter		✓	✓
modulated inverter	✓	✓	✓

The definition of these angles consist of multiple frequencies, therefore an iterative root finding method is required. Previously the converter angles were solved as part of the main solution. However, divergence of one of these angles resulted in the failure of the entire solution. As the angles are simply functions of the terminal conditions and of the average firing angle, they can be solved for explicitly. Using a combination of the Newton-Raphson method, which is fast but not globally convergent, and a slower globally convergent strategy a robust solution can be obtained. The Newton-Raphson method is formulated as shown below:

$$\theta_{(i+1)} = \theta_i - \frac{F(\theta_i)}{\left(\frac{dF(\theta_i)}{d\theta_i}\right)} \tag{3.48}$$

The size of the mismatch $F(\theta_i)$ is monitored and if either it, or the number of iterations, exceed specified thresholds then divergence is assumed to have occurred. When this is the case, for example under severe harmonic distortion, a bounded stepping method is used which is guaranteed to converge if a solution is present within the specified bounds. While the stepping method of Equation 3.49 is slow compared to the Newton approach, full solution convergence can be maintained where not previously

possible. The iterative stepping method is as shown as below where the zero-crossing function must be negative to the left of the root.

$$\begin{aligned}&\text{IF } F(\theta_i + \Delta\theta) < \text{tolerance THEN}\\ &\theta_{(i+1)} = \theta_i + \Delta\theta\\ &\text{ELSE}\\ &\Delta\theta = \tfrac{1}{2}\Delta\theta\\ &\text{END IF}\end{aligned} \tag{3.49}$$

The framework allows for any globally or bounded convergent method to be used, the method shown above is just a simple method used for illustration.

Firing angles

When modelling an uncontrolled rectifier such as a diode bridge, the angle of device turn on is defined by the positive going commutation zero-crossing. This is found from the intersection of the commutation voltage sample and the preceding normal conduction voltage sample. This intersection, as shown in Figure 3.8, is described by the following mismatch equation. There are six firing angles per converter and 12 dc voltage samples, the expressions $(2p-1)$ and $(2p-2)$ are used to show which of the voltage samples form the zero-crossing.

$$F_{\theta_p} = Imag\left\{\sum_{k=1}^{nh}(V_{volt}(2p-1)_k - V_{volt}(2p-2)_k)\exp^{jk\theta_p}\right\} = 0 \text{ , p=1:6} \tag{3.50}$$

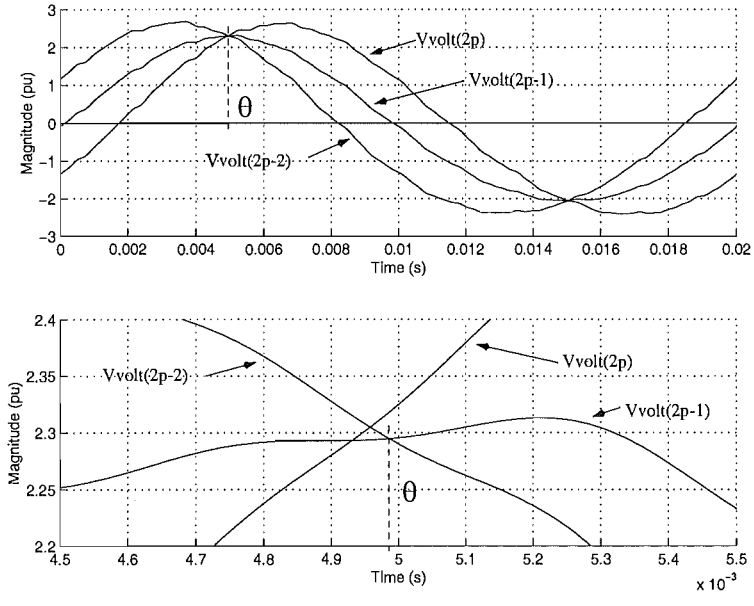

Figure 3.8 Definition of the device firing instant for an uncontrolled bridge.

For a controlled converter, the switching devices are turned on by a specified firing order. These firing angles are obtained by comparing a specified firing order (α_{ripple}) with a pulse train (β) from an equidistant pulse generator.

$$F_{\theta_p} = Imag\left\{ j\left(\alpha_{ripple}(0) + \beta_p - \theta_p\right) + \sum_{k=1}^{nh} \alpha_{ripple}(k) \exp^{jk\theta_p} \right\} \tag{3.51}$$

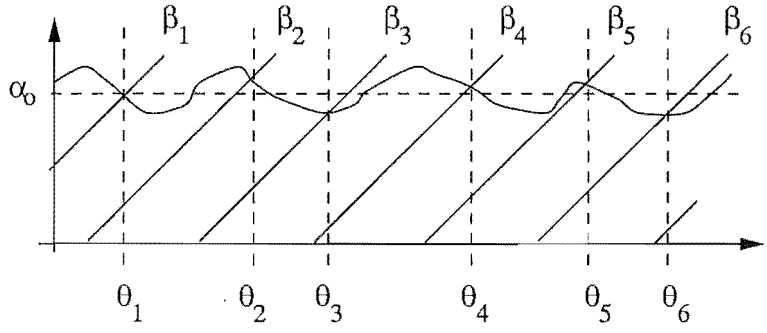

Figure 3.9 Calculation of the device turn on's for a controlled bridge.

For most steady-state analysis, the Phase Locked Oscillator (PLO) and pulse generator can be assumed to be ideal and make no contribution to the modulation of the converter firings. However if such a case is required, the calculation of the firing angles can be modified to include ripple in the pulse train. As the firing order ripple is dependent upon the controller type and measured quantity, the converter model takes this as an input and has the controller defined separately.

End of commutation angles

The majority of high power converters use devices that are naturally commutated such as diodes and thyristors. With converters such as these, end of commutation is defined as the instant when the commutation current, in the switch that has just turned on, is the same as the dc current at that instant. This coincides with the instant that the other switch involved in the commutation, turns off. The mismatch defining this instant, as shown in Figure 3.10, is defined by Equation 3.52. The dc component D in Equation 3.53 is used to offset the commutation current sample so that the commutation current is zero at the instant of firing. This corresponds to the dc component of the switching transient.

$$F_{\phi_p} = (Id_0 - D) + Imag\left\{ \sum_{k=1}^{nh} \left(Id_k - I_{comm}(p)_k\right) \exp^{jk\phi_p} \right\} = 0 \text{ , p=1:6} \tag{3.52}$$

$$D = Imag\left\{ \sum_{k=1}^{nh} I_{comm}(p)_k \exp^{jk\theta_p} \right\} \tag{3.53}$$

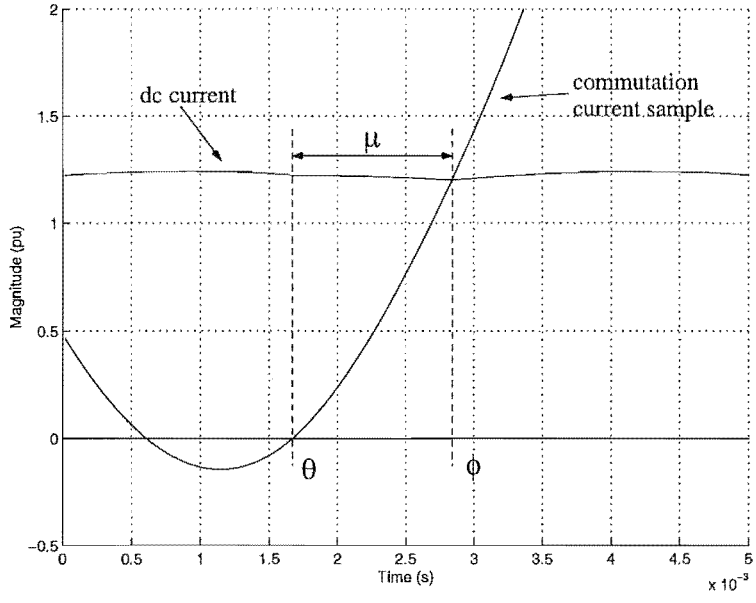

Figure 3.10 Instant defining the end of commutation.

When the switching devices in a converter can be forced off, such as GTO's, the turn off angles are defined by the controller and so will be calculated in much the same way as the controlled firing angles.

Extinction angles

When a bridge is under inverter operation, the firing instant must ensure sufficient time for successful commutation. In order that this can be achieved during solution, it is necessary to calculate the extinction angle. This is the angle from the end of commutation to the last possible point of commutation; the instant where the commutating voltage goes negative.

The last point of commutation is defined by the intersection of the present commutation voltage sample and the next normal conduction voltage sample (Figure 3.11). The mismatch is similar to the earlier zero-crossing firing mismatch:

$$F_{\delta_p} = Imag\left\{\sum_{k=1}^{nh}(V_{volt}(2p-1)_k - V_{volt}(2p)_k)\exp^{jk\delta_p}\right\} = 0 \text{ , p=1:6} \qquad (3.54)$$

3.2.6 Harmonic transfer through the converter

The convolution process works on the basis that the transferred waveshape can accurately be represented as piecewise linear. A steady-state waveshape is derived so that between two bounds it will accurately represent the segment of the full waveshape. This waveshape is then multiplied by a rectangular pulse train of magnitude one which bounds the period of validity. The resultant waveshape is the contribution

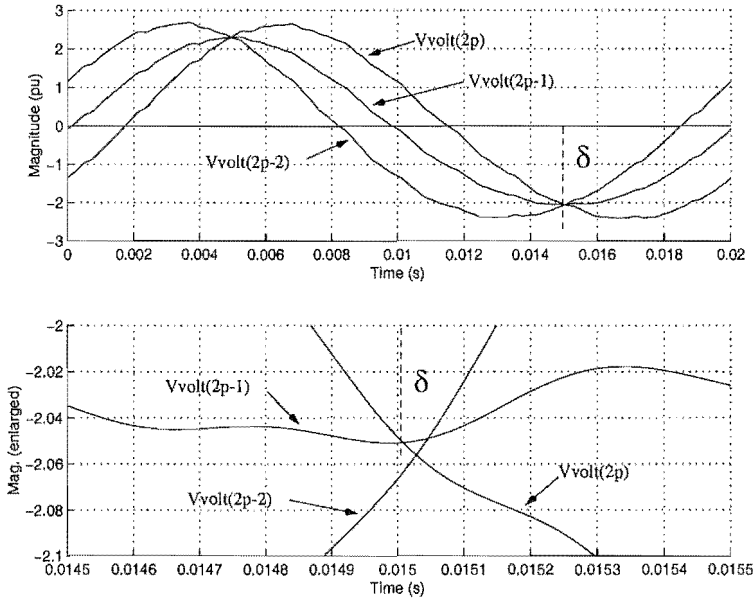

Figure 3.11 Instant defining last point for a successful commutation.

of the sample waveshape to the total piecewise waveshape. By adding this component to the remainder of the other sampled waveshapes, the total piecewise waveshape is constructed.

As the frequency domain convolution is the dual of the time domain multiplication, it is possible to duplicate the multiplication process in the frequency domain. Only the first nh harmonics of the piecewise waveshape are wanted and therefore the sample waveshape and rectangular sampling pulse can be bandlimited to nh and $2nh$ harmonic components respectively [Smith *et al.* 1996].

For a converter, the sampling function period is solely defined by the switching angles relating to that period. For a commutation period, the first angle a is the device turn on, the second b is the device turn off. For a normal conduction period, the first angle a is the last device turn off and the second b, the next device turn on. Thus by simple Fourier analysis of the rectangular pulse train, the following analytic expressions can be obtained for the harmonic components.

$$\psi_0 = \begin{cases} j\frac{(b-a)}{2\pi} & b > a \\ j\left(1.0 - \frac{(a-b)}{2\pi}\right) & a \leq b \end{cases} \tag{3.55}$$

$$\psi_k = \frac{1}{k\pi}(\exp^{jka} - \exp^{jkb})^* \ , \ k > 0 \tag{3.56}$$

The requirement of negative frequency harmonics is avoided by use of the conjugation operator. While this makes the convolution non-analytic, it is still easy to obtain partial derivatives of the convolution as the solution is represented in terms of real and imaginary components instead of complex. Using peak valued complex phasors,

the convolution process is described by the following expression, where F is a generic sample.

$$(F \otimes \psi)_k = \frac{j}{2}\left[-2F_0\psi_0 + \sum_{m=0}^{nh} F_m\psi_m^*\right], \; k = 0 \tag{3.57}$$

$$(F \otimes \psi)_k = \frac{j}{2}\left[\sum_{m=0}^{nh}(F_m\psi_{(m+k)}^*)^* - \sum_{m=0}^{k} F_m\psi_{(k-m)} + \sum_{m=k}^{nh} F_m\psi_{(m-k)}^*\right], \; k > 0 \tag{3.58}$$

Calculation of the dc voltage

The dc voltage of a 6-pulse converter is built up from the twelve voltage samples convolved with the twelve respective sampling functions. One such convolution is shown, using a time domain representation, in Figure 3.12 along with the total dc voltage.

$$V_d = \sum_{p=1}^{12} V_{volt_p} \otimes \psi_p \tag{3.59}$$

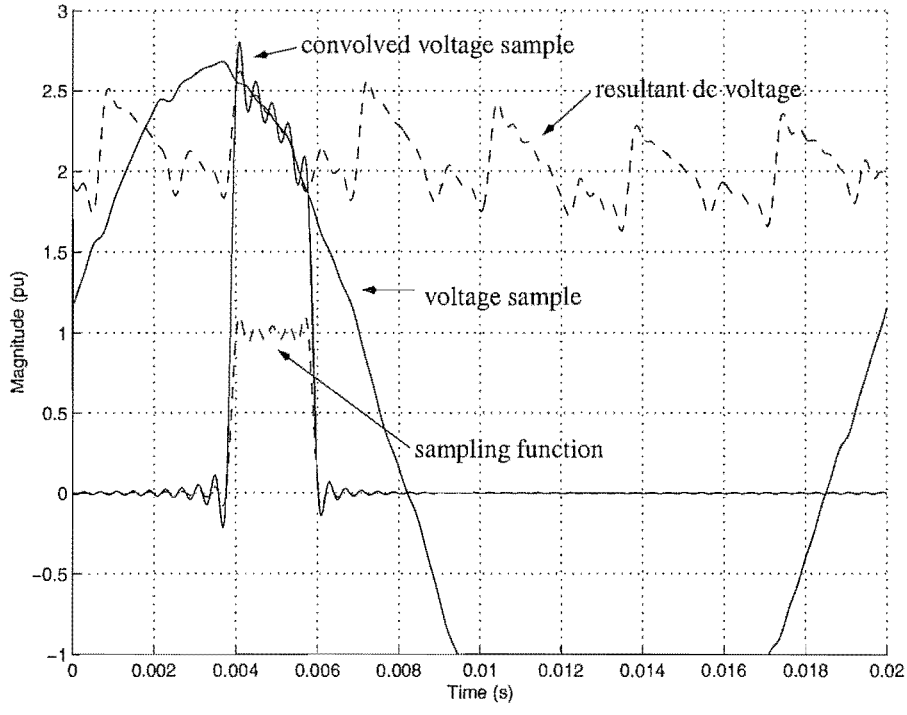

Figure 3.12 Convolution of one period for the dc voltage.

Calculation of the ac phase currents

Each secondary phase current is built up from 4 commutation current samples and eight dc current samples. For this a maximum of 36 convolutions would be required if nothing else was done. However, by some simple re-arranging and knowledge of the symmetry of the converter, the 36 convolutions can be reduced to 8.

Using the linearity of the convolution, the eight rectangular sampling functions convolved with the dc current can be combined into one compound sampling function (Figure 3.13). This reduces 24 of the convolutions to only 3. Also, as the six commutation currents all occur during the same periods in each phase, only 6 convolutions are required instead of 12. This allows the secondary phase currents to be written as below where only 9 convolutions are required.

$$\begin{aligned} I_a &= I_d \otimes (\psi_2 + \psi_3 + \psi_4 + \psi_5 - \psi_8 - \psi_9 - \psi_{10} - \psi_{11}) \\ &\quad + Ic_1 \otimes \psi_1 - Ic_3 \otimes \psi_5 + Ic_4 \otimes \psi_7 - Ic_6 \otimes \psi_{11} \end{aligned} \tag{3.60}$$

$$\begin{aligned} I_b &= I_d \otimes (\psi_6 + \psi_7 + \psi_8 + \psi_9 - \psi_{12} - \psi_1 - \psi_2 - \psi_3) \\ &\quad - Ic_2 \otimes \psi_3 + Ic_3 \otimes \psi_5 - Ic_5 \otimes \psi_9 + Ic_6 \otimes \psi_{11} \end{aligned} \tag{3.61}$$

$$\begin{aligned} I_c &= I_d \otimes (\psi_{10} + \psi_{11} + \psi_{12} + \psi_1 - \psi_4 - \psi_5 - \psi_6 - \psi_7) \\ &\quad - Ic_1 \otimes \psi_1 + Ic_2 \otimes \psi_3 - Ic_4 \otimes \psi_7 + Ic_5 \otimes \psi_9 \end{aligned} \tag{3.62}$$

As there is no path for zero sequence current into the converter bridge, calculation of only two secondary phase currents is required, which further reduces the number of convolutions by one.

$$I_c = -I_a - I_b \tag{3.63}$$

Thus only eight convolutions are required to obtain the secondary ac phase currents for the converter bridge. The three primary phase currents are then obtained by using the transformer transfer matrix and combining this with current from the shunt at the primary terminals. This shunt is only present when the magnetising branch or a delta winding are present [Smith 1996].

$$\begin{bmatrix} I_A \\ I_B \\ I_C \end{bmatrix} = [T_D] \begin{bmatrix} I_a \\ I_b \end{bmatrix} + [Y_D] \begin{bmatrix} V_A \\ V_B \\ V_C \end{bmatrix} \tag{3.64}$$

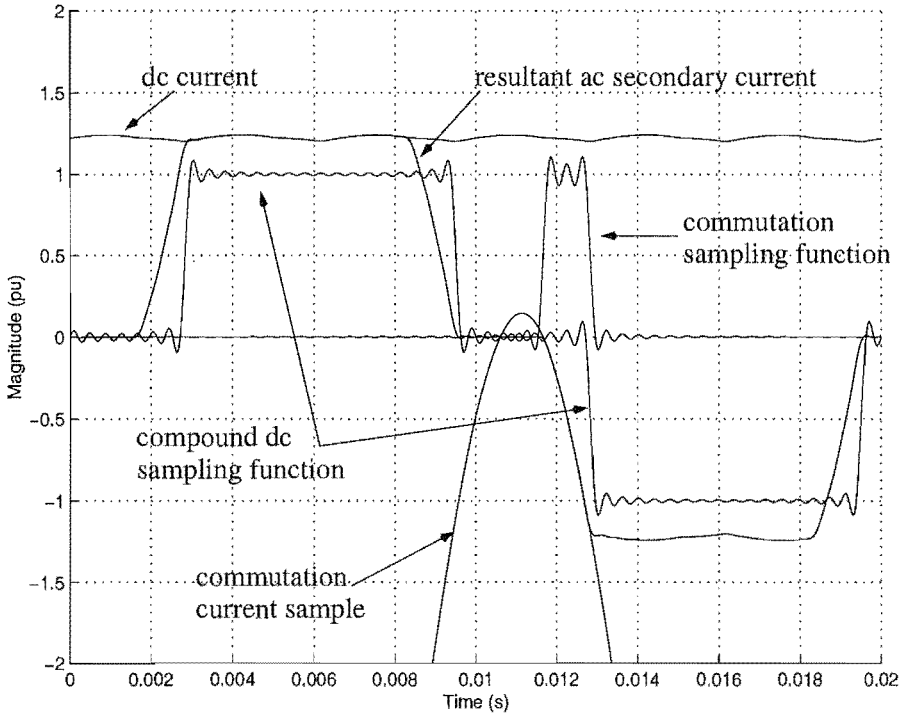

Figure 3.13 Convolution of forming the secondary phase currents.

3.2.7 Jacobian for ABCD formulation

The original formulation of the HVdc rectifier by Smith [1996] included the switching angles as variables within the main Newton solution. The inclusion of these within the solution made it full Newton and consequently their linearised effect gave excellent convergence characteristics. The solution Jacobian for a 12-pulse rectifier under current control was of the form as shown below:

$$
\begin{array}{|c|}\hline M_{V_{ac}} \\ \hline M_{V_{dc}} \\ \hline M_{\phi} \\ \hline M_{\theta} \\ \hline M_{Id_0} \\ \hline \end{array}
=
\begin{array}{|ccccc|}\hline \frac{\partial M_{V_{ac}}}{\partial V_{ac}} & \frac{\partial M_{V_{ac}}}{\partial I_{dc}} & - & \frac{\partial M_{V_{ac}}}{\partial \theta} & - \\ \hline \frac{\partial M_{V_{dc}}}{\partial V_{ac}} & \frac{\partial M_{V_{dc}}}{\partial I_{dc}} & \frac{\partial M_{V_{dc}}}{\partial \phi} & \frac{\partial M_{V_{dc}}}{\partial \theta} & - \\ \hline \frac{\partial M_{\phi}}{\partial V_{ac}} & \frac{\partial M_{\phi}}{\partial I_{dc}} & \frac{\partial M_{\phi}}{\partial \phi} & \frac{\partial M_{\phi}}{\partial \theta} & - \\ \hline - & \frac{\partial M_{\theta}}{\partial I_{dc}} & - & \frac{\partial M_{\theta}}{\partial \theta} & \frac{\partial M_{\theta}}{\partial \alpha_0} \\ \hline \frac{\partial M_{Id_0}}{\partial V_{ac}} & \frac{\partial M_{Id_0}}{\partial I_{dc}} & \frac{\partial M_{Id_0}}{\partial \phi} & \frac{\partial M_{Id_0}}{\partial \theta} & - \\ \hline \end{array}
*
\begin{array}{|c|}\hline V_{ac} \\ \hline I_{dc} \\ \hline \phi \\ \hline \theta \\ \hline \alpha_0 \\ \hline \end{array}
\qquad (3.65)
$$

As the calculation of the converter switching angles can be specified solely from the solution variables, the converter can be represented in an ABCD parameter form. The use of ABCD parameters with respect to converter modelling was proposed by [Larsen *et al.* 1989a] where an HVdc rectifier was represented by a matrix linking the ac current and dc voltage harmonics to the ac voltage and dc current harmonics. Using this approach, the interface of the converter with the solution contains only electrical variables and the control strategy used. Such a form will significantly increase the modularity of the converter as the switching angles are hidden from the main solution.

To remove the switching angles as variables from the main solution, while their effect is implicitly included, the electrical block of the system Jacobian has to be modified. The Jacobian structure for the same converter, represented in ABCD form, is shown below in Equation 3.66. It should also be noted that the ac mismatches are now current mismatches, which simplifies the Jacobian formation. Moreover, with the switching angles included within the solution, the ac phase currents and dc voltages now have a direct dependence upon the average firing angle α_0.

$$\begin{bmatrix} M_{I_{ac}} \\ M_{V_{dc}} \\ M_{Id_0} \end{bmatrix} = \begin{bmatrix} \frac{\partial M_{I_{ac}}}{\partial V_{ac}} & \frac{\partial M_{I_{ac}}}{\partial I_{dc}} & \frac{\partial M_{I_{ac}}}{\partial \alpha_0} \\ \frac{\partial M_{V_{dc}}}{\partial V_{ac}} & \frac{\partial M_{V_{dc}}}{\partial I_{dc}} & \frac{\partial M_{V_{dc}}}{\partial \alpha_0} \\ \frac{\partial M_{Id_0}}{\partial V_{ac}} & \frac{\partial M_{Id_0}}{\partial I_{dc}} & \frac{\partial M_{Id_0}}{\partial \alpha_0} \end{bmatrix} * \begin{bmatrix} V_{ac} \\ I_{dc} \\ \alpha_0 \end{bmatrix} \tag{3.66}$$

The calculation of the individual blocks of the ABCD Jacobian are slightly more complicated than before because there are more terms involved. However, as will be shown, the modularity of the converter minimises the effort required to obtain the analytical expressions.

The dependency of the phase currents on the solution variables is shown in Figure 3.14. The solution variables are on the right and contribute to the phase currents through the blocks as shown. For example, the firing instances (θ) are determined by the average firing angle (α_0), the ac voltage harmonics (V_{ac}) and the dc current harmonics (I_{dc}). The firing instances then effect the end of commutation instances, the commutation current samples and the sampling functions. The ac phase currents themselves are each built up from four commutation current samples and the dc current which are convolved with their respective sampling functions. Equations 3.67 and 3.69

show that by moving through Figure 3.14 from left to right, the expressions for the dependence of I_{ac} on the solution variables can be obtained.

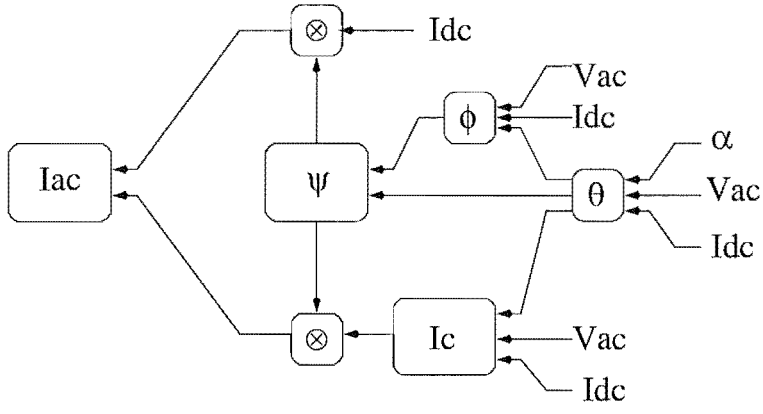

Figure 3.14 Dependency of converter phase currents upon solution variables.

$$\frac{\partial I_{ac}}{\partial V_{ac}} = \frac{\partial I_c}{\partial V_{ac}} \otimes \psi + I_c \otimes \frac{\partial \psi}{\partial \theta}\frac{\partial \theta}{\partial V_{ac}} + I_c \otimes \frac{\partial \psi}{\partial \phi}\left(\frac{\partial \phi}{\partial V_{ac}} + \frac{\partial \phi}{\partial \theta}\frac{\partial \theta}{\partial V_{ac}}\right) + I_{dc} \otimes \frac{\partial \psi}{\partial \theta}\frac{\partial \theta}{\partial V_{ac}} + I_{dc} \otimes \frac{\partial \psi}{\partial \phi}\left(\frac{\partial \phi}{\partial V_{ac}} + \frac{\partial \phi}{\partial \theta}\frac{\partial \theta}{\partial V_{ac}}\right) \tag{3.67}$$

$$\frac{\partial I_{ac}}{\partial I_{dc}} = \frac{\partial I_c}{\partial I_{dc}} \otimes \psi + I_c \otimes \frac{\partial \psi}{\partial \theta}\frac{\partial \theta}{\partial I_{dc}} + I_c \otimes \frac{\partial \psi}{\partial \phi}\left(\frac{\partial \phi}{\partial I_{dc}} + \frac{\partial \phi}{\partial \theta}\frac{\partial \theta}{\partial I_{dc}}\right) + \frac{\partial I_{dc}}{\partial I_{dc}} \otimes \psi + I_{dc} \otimes \frac{\partial \psi}{\partial \theta}\frac{\partial \theta}{\partial I_{dc}} + I_{dc} \otimes \frac{\partial \psi}{\partial \phi}\left(\frac{\partial \phi}{\partial I_{dc}} + \frac{\partial \phi}{\partial \theta}\frac{\partial \theta}{\partial I_{dc}}\right) \tag{3.68}$$

$$\frac{\partial I_{ac}}{\partial \alpha_0} = I_c \otimes \frac{\partial \psi}{\partial \theta}\frac{\partial \theta}{\partial \alpha_0} + I_c \otimes \frac{\partial \psi}{\partial \phi}\frac{\partial \phi}{\partial \theta}\frac{\partial \theta}{\partial \alpha_0} + I_{dc} \otimes \frac{\partial \psi}{\partial \theta}\frac{\partial \theta}{\partial \alpha_0} + I_{dc} \otimes \frac{\partial \psi}{\partial \phi}\frac{\partial \phi}{\partial \theta}\frac{\partial \theta}{\partial \alpha_0} \tag{3.69}$$

A similar process is followed for the dc voltage, which is built up from convolution of twelve voltage samples with twelve rectangular sampling functions. As Figure 3.15 shows, two main contributions form the actual derivative. The first is the direct effect which is the effect of the solution variables on the voltage samples. The second is the effect of the solution variables on the switching instants, which in turn affect the sampling functions and hence the transfer to the dc voltage. For the dc voltage mismatch, the Jacobian elements are as follows:

$$\frac{\partial V_{dc}}{\partial V_{ac}} = \frac{\partial V_v}{\partial V_{ac}} \otimes \psi + V_v \otimes \frac{\partial \psi}{\partial \theta}\frac{\partial \theta}{\partial V_{ac}} + V_v \otimes \frac{\partial \psi}{\partial \phi}\left(\frac{\partial \phi}{\partial V_{ac}} + \frac{\partial \phi}{\partial \theta}\frac{\partial \theta}{\partial V_{ac}}\right) \tag{3.70}$$

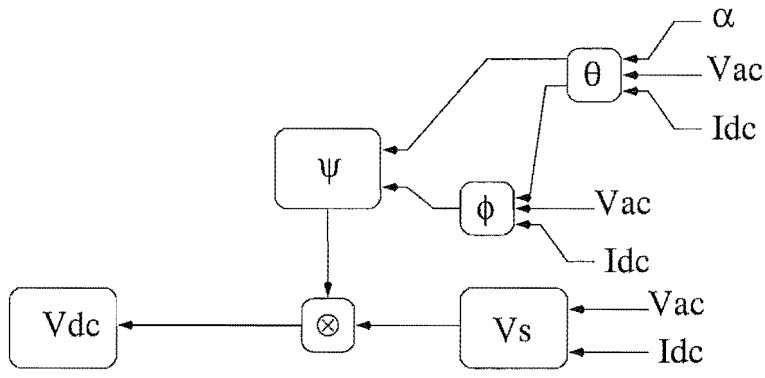

Figure 3.15 Dependency of converter dc voltage upon solution variables.

$$\frac{\partial V_{dc}}{\partial I_{dc}} = \frac{\partial V_v}{\partial I_{dc}} \otimes \psi + V_v \otimes \frac{\partial \psi}{\partial \theta}\frac{\partial \theta}{\partial I_{dc}} + V_v \otimes \frac{\partial \psi}{\partial \phi}\left(\frac{\partial \phi}{\partial I_{dc}} + \frac{\partial \phi}{\partial \theta}\frac{\partial \theta}{\partial I_{dc}}\right) \tag{3.71}$$

$$\frac{\partial V_{dc}}{\partial \alpha_0} = V_v \otimes \frac{\partial \psi}{\partial \theta}\frac{\partial \theta}{\partial \alpha_0} + V_v \otimes \frac{\partial \psi}{\partial \phi}\frac{\partial \phi}{\partial \theta}\frac{\partial \theta}{\partial \alpha_0} \tag{3.72}$$

A number of simplifications can be made in the analytical representation. For example with reference to the transfer to ac current, the effect of firing angle modulation on the dc current transfer is nil, as the dc current sampling function is defined solely by end of commutation angles. Also, for a current controlled rectifier, the term $\frac{\partial \theta}{\partial V_{ac}} = 0$ as the firing angles are only modulated by measured dc current. The various partial derivative terms shown above are derived in Appendix C.

As the Jacobian only needs to be approximate, only the dominant terms really need to be calculated. As the converter Jacobian blocks have a determinable structure, the significant terms can be pre-determined and consequently only these calculated. This should reduce the amount of computation by approximately a factor of two.

The derivation of the last row of the Jacobian depends on the converter control strategy and will be discussed in Chapter 4.

3.2.8 Positive sequence representation

The first stage in the harmonic solution is a positive sequence loadflow. In this case, the system is assumed to be initially perfectly symmetric and the detailed analysis shown above is not required. The converter is represented by classical equations for the dc voltage and ac phase currents [Arrillaga 1983]. This loadflow formulation allows the control equations and general system format to remain the same except that, in the positive sequence loadflow the average firing angle is relative to the fundamental voltage zero-crossing, not the ac system angle reference. The equations shown here are for a converter operating as a rectifier and some slight modifications are required for inverter operation.

Given the terminal positive sequence ac voltage, average dc current and average firing angle; the commutation duration can be calculated from:

$$\mu = \cos^{-1}\left(\cos(\alpha) - \frac{\sqrt{2}X_T I_d}{\sqrt{3}|V_+|}\right) - \alpha \tag{3.73}$$

and the average dc voltage and ac phase current can be calculated as follows:

$$V_{dc} = \frac{3}{\pi}\left(a\sqrt{6}|V_+|\cos(\alpha) - X_T I_d\right) \tag{3.74}$$

$$|I_{ac}| = \frac{a\sqrt{6}\sqrt{n1^2 + n2^2}}{\pi d} I_d \tag{3.75}$$

$$\angle I_{ac} = \tan^{-1}\left(\frac{Imag(V_+)}{Real(V_+)}\right) + \tan^{-1}\left(\frac{-n2}{n1}\right) \tag{3.76}$$

where,

$$n_1 = \cos(2\alpha) - \cos(2\alpha + 2\mu)) \tag{3.77}$$

$$n_2 = 2\mu + \sin(2\alpha) - \sin(2\alpha + 2\mu)) \tag{3.78}$$

$$d = 4(\cos(\alpha) - cos(\alpha + \mu)) \tag{3.79}$$

3.3 SALIENT POLE SYNCHRONOUS MACHINE

The following is a summary of the Harmonic Domain model of the salient pole synchronous machine as developed by Dinh [1998]. That model was used in a unit connection configuration which meant the fundamental terminal voltage positive sequence was specified and removed from the solution. With this approach, the internal EMF was not represented and so the rotor angle had to be calculated via a Gauss-Seidel step. A further Gauss step was needed to represent saturation. By not including the internal EMF, the representation of the generator was limited to a few simple configurations.

Although the impedance calculations that follow are as described Dinh's thesis, the representation of the generator has been changed to a more versatile form.

3.3.1 Rotor angle calculation

In the original formulation with the internal EMF not represented, a complicated method was required to obtain the rotor angle from the specified positive sequence fundamental terminal voltage. By some trigonometry using Figure 3.17, the expression below can be formed which requires both the terminal voltage and phase currents.

$$\delta = \tan^{-1}\left(\frac{|I_+|\left(X_q\cos\phi - R_a\sin\phi\right)}{|V_+| + |I_+|\left(X_q\sin\phi + R_a\cos\phi\right)}\right) \tag{3.80}$$

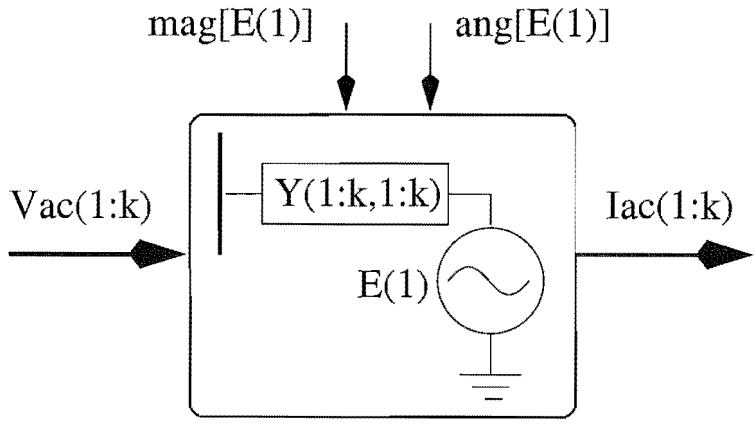

Figure 3.16 Representation of the salient pole generator unit

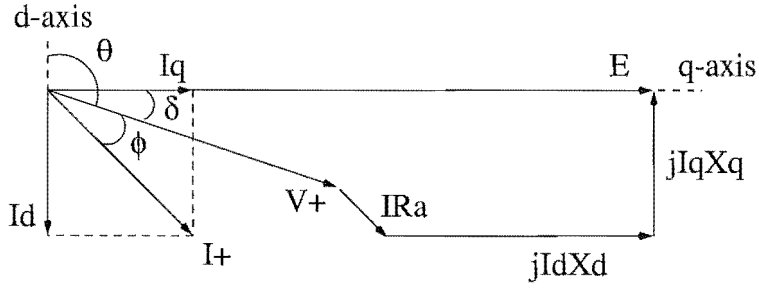

Figure 3.17 Phasor diagram for calculation of the rotor angle of an unsaturated salient pole synchronous generator operating at a lagging power factor [Dinh 1998]

However, with the magnitude and phase angle of the internal EMF known, the rotor angle can be calculated simply from:

$$\delta = \angle E - \angle V_+ \tag{3.81}$$

3.3.2 Harmonic impedance

Once the rotor angle is known, the analytical expressions for the frequency coupling impedance of a salient pole synchronous machine can be formed. This is achieved by applying current injections to Park's equations using the dq transform and then calculating the voltages due to both the current and the flux change.

The derivation of the current injection vector in the dq frame of reference is achieved using the following transform:

$$\begin{bmatrix} i_d(t) \\ i_q(t) \\ i_0(t) \end{bmatrix} = \frac{2}{3} \begin{bmatrix} \cos(\theta) & \cos(\theta - 2\pi/3) & \cos(\theta + 2\pi/3) \\ -\sin(\theta) & -\sin(\theta - 2\pi/3) & -\sin(\theta + 2\pi/3) \\ \frac{1}{2} & \frac{1}{2} & \frac{1}{2} \end{bmatrix} \begin{bmatrix} i_a(t) \\ i_b(t) \\ i_c(t) \end{bmatrix} \tag{3.82}$$

with $\theta = wt + \pi/2 + \delta$.

It is assumed that the rotor excitation circuit produces only dc and that no other harmonics are produced within the rotor.

Then using Park's flux linkages, the dq flux vector is first obtained and then transformed back into phase components using the dq to abc transform, i.e.

$$\begin{bmatrix} \psi_a(t) \\ \psi_b(t) \\ \psi_c(t) \end{bmatrix} = \begin{bmatrix} \cos(\theta) & -\sin(\theta) & 1 \\ \cos(\theta - 2\pi/3) & -\sin(\theta - 2\pi/3) & 1 \\ \cos(\theta + 2\pi/3) & -\sin(\theta + 2\pi/3) & 1 \end{bmatrix} \begin{bmatrix} L''_d i_d(t) \\ L''_q i_q(t) \\ 0 \end{bmatrix} \tag{3.83}$$

The phase voltages that result from the applied sequence current are then obtained by using the following differential equations:

$$v_a(t) = R_a i_a(t) + \frac{d\psi_a(t)}{dt} \tag{3.84}$$

$$v_b(t) = R_b i_b(t) + \frac{d\psi_b(t)}{dt} \tag{3.85}$$

$$v_c(t) = R_c i_c(t) + \frac{d\psi_c(t)}{dt} \tag{3.86}$$

By limiting the solution to the steady-state, the differential equations can be transformed into frequency expressions, which allow the following impedances to be derived.

Negative Sequence Harmonic Impedance

The voltage generated from the negative sequence injection consists of two harmonic components. One is of the same frequency and sequence as the applied current injection. The other is of frequency $(k+2)$ and positive sequence where the applied current was k and negative sequence. By following the above process algebraically, the following impedances can be obtained which provides the negative sequence current response.

$$Z_{(-k,-k)} = R_a + jk\left(\frac{X''_d + X''_q}{2}\right) \tag{3.87}$$

$$Z_{(+(k+2),-k)} = j(k+2)\left(\frac{X''_d - X''_q}{2}\right)\exp^{j(2\delta+\pi/2)} \tag{3.88}$$

Positive Sequence Harmonic Impedance

Similarly for a positive sequence injection where $k > 1$, the impedance is:

$$Z_{(+k,+k)} = R_a + jk\left(\frac{X''_d + X''_q}{2}\right) \tag{3.89}$$

$$Z_{(-(k+2),+k)} = j(k-2)\left(\frac{X''_d - X''_q}{2}\right)\exp^{j(-2\delta+\pi/2)} \tag{3.90}$$

Zero Sequence Harmonic Impedance

As there is no coupling to the zero-sequence during steady-state conditions for a balanced generator, the zero-sequence impedance is approximated by:

$$Z_{(0k,0k)} \simeq R_{01} + jkX_{01} \tag{3.91}$$

3.3.3 Cross-coupling admittance matrix

For the harmonic solution the generator is represented as a frequency coupling harmonic admittance. This is obtained by inverting the already calculated impedance matrix as shown in Figure 3.18 for the first 7 harmonics.

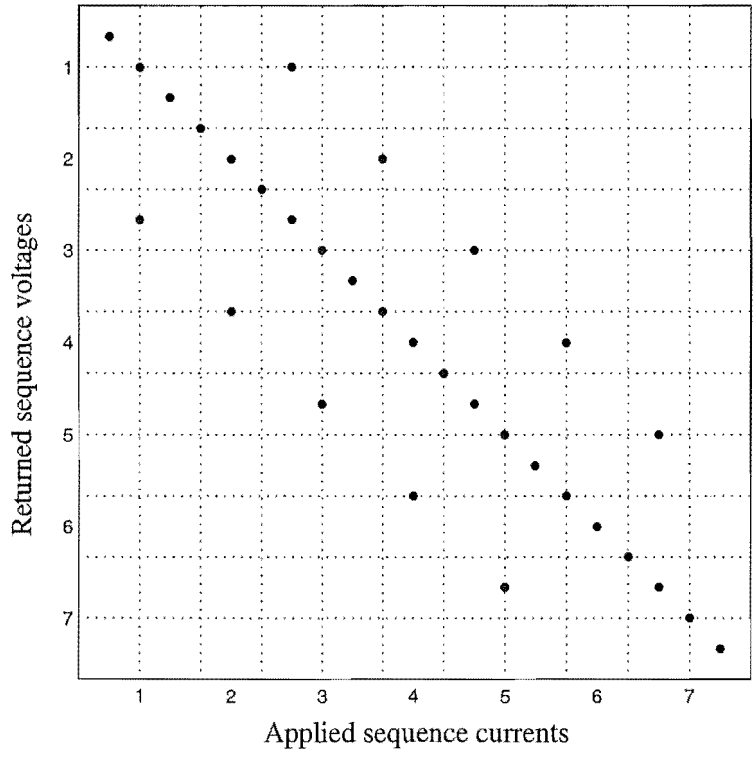

Figure 3.18 Frequency coupling impedance of a salient pole generator.

The inversion can be simplified due to the structure of the coupled matrix. The admittance matrix retains the same sparse structure and so each of the element types can be inverted individually:

$$Y_{(+k,+k)} = Z_{(-k,-k)}D \tag{3.92}$$

$$Y_{(-k,-k)} = Z_{(+k,+k)}D \tag{3.93}$$

$$Y_{(+k,-(k-2))} = -Z_{(-k,+(k+2))}D \tag{3.94}$$

$$Y_{(-k,+(k+2))} = -Z_{(+k,-(k-2))}D \tag{3.95}$$

$$Y_{0k,0k} = \frac{1}{Z_{0k,0k}} \tag{3.96}$$

where D is the determinant of this block given by:

$$D = \frac{1}{\left(Z_{(+k,+k)}Z_{(-k,-k)} - Z_{(+k,-(k-2))}Z_{(-k,+(k+2))}\right)} \tag{3.97}$$

By inverting the impedance matrix in this fashion, the computational effort is smaller than with a general sparse method. Due to the admittance representation of the generator, the Jacobian block is simply the cross-coupling harmonic admittance matrix (except for the positive sequence fundamental).

3.3.4 Positive sequence fundamental current

The positive sequence fundamental current is calculated differently from the harmonic currents as it is rotating in phase with the rotor. Consequently it has a large reactance, i.e. the synchronous reactance, X_d and X_q, for the d and q axes respectively. Unlike the harmonic self impedances, for a salient pole machine, the positive sequence fundamental impedance is dependent on the rotor angle and power factor of the current drawn. Using the phasor diagram as drawn in Figure 3.17, the following vector expression can be derived:

$$E = V_+ + I_+R_a + jI_dX_d + jI_qX_q \tag{3.98}$$

As $I_+ = I_r + jI_i = I_d + I_q$, the above expression can be decomposed into rectangular components and written in matrix form as shown below.

$$\begin{bmatrix} Real\{E - V_+\} \\ Imag\{E - V_+\} \end{bmatrix} = \begin{bmatrix} R_a & -X_q \\ X_d & R_a \end{bmatrix} \begin{bmatrix} Real\{I_+\} \\ Imag\{I_+\} \end{bmatrix} \tag{3.99}$$

Thus for a salient pole synchronous machine $I_d \neq I_q$ and so the synchronous impedance requires a tensor representation as shown above rather than a complex number. This is inherently correct as the effect of saliency is that the generator presents an impedance that changes with load power-factor. As the positive sequence current is required, the tensor impedance is inverted to an admittance. This allows the current to be calculated directly from the voltage differential created by the internal EMF and the terminal voltage.

$$\begin{bmatrix} Real\{I_+\} \\ Imag\{I_+\} \end{bmatrix} = \frac{1}{(R_aR_a + X_dX_q)} \begin{bmatrix} R_a & X_q \\ -X_d & R_a \end{bmatrix} \begin{bmatrix} Real\{E - V_+\} \\ Imag\{E - V_+\} \end{bmatrix} \tag{3.100}$$

3.4 HARMONIC MODELLING OF LINEAR SYSTEM COMPONENTS

Most system components are operated well within their unsaturated zone and so it is not unreasonable to model them as linear. When a component is known to be in saturation then a full harmonic model with saturation may be required. As full device representation is computationally expensive, this should only be used when deemed necessary. The three main types of linear components are: shunt elements, π-model elements and constant harmonic sources as Thevenin or Norton equivalents.

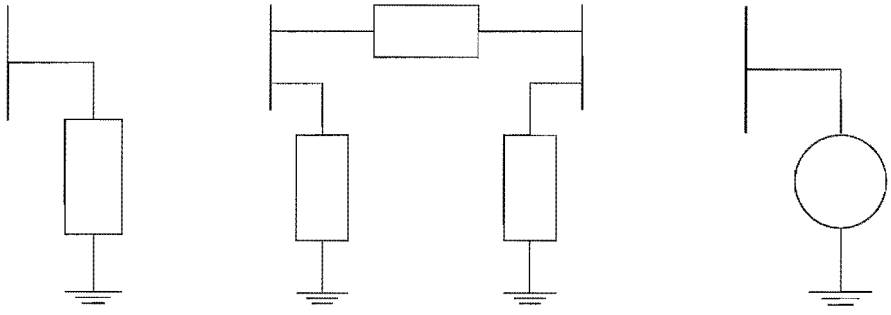

(a) Shunt element. (b) π-model element. (c) Harmonic source.

3.4.1 Shunt elements

PQ specified loads

For most AC system loads, little information is available as to their frequency profile, and also their internal state is changing continually there is therefore little point in attempting to model them in great detail. Normally only the fundamental real and reactive powers are specified in the loadflow. The harmonic admittances are then calculated using these values, the positive sequence voltage, and simple RL networks [Densem 1983] based upon some assumptions on the load composition. As the loads can be specified in a variety of configurations, the harmonic impedances should be also represented likewise. This is important as a delta or star-ungrounded load connection has no path for zero-sequence currents and so will have a different harmonic response than that of a star-ground connection.

Generators

A variety of simplifications have been made which, for the general system operation, should not be significant. The generators are assumed to have no saliency which eliminates sequence and frequency coupling. This allows the generator to be assumed to be balanced and so a simple frequency dependant model is all that is required. A variety

of models are used to calculate the harmonic admittance based usually around the negative sequence impedance [Densem 1983].

Filters and admittance specified loads

There are two ways of representing a linear shunt load, either as a pre-calculated system admittance in the main data file or as a pre-specified RLC network. A pre-calculated admittance is a simple version of a transmission line where there is only one bus and a shunt element. The RLC parameters for the filters are stored after being loaded and the frequency terms are calculated as required. The filters can be unbalanced and connected in star-grounded, star-ungrounded, or delta.

3.4.2 π-model elements

Transmission lines

The transmission lines are the backbone of a network and generally have a dominant effect in the response of a large system. The lines themselves are represented within the system as a π-model connecting two or more busbars. The data is pre-calculated and stored as a π-model for each frequency in a datafile. The mutual coupling between phases is full represented as well as mutual coupling between parallel circuits either on the same tower or sharing the same right-of-way. While the data-files can be formed by any means, typically they are created from the physical geometry of the lines, metal properties, skin and long-line effects.

$$Y_{transmission\_line} = \left[\begin{array}{c|c} \frac{1}{Z_{series}} + \frac{Y_{shunt}}{2} & \frac{-1}{Z_{series}} \\ \hline \frac{-1}{Z_{series}} & \frac{1}{Z_{series}} + \frac{Y_{shunt}}{2} \end{array}\right] \tag{3.101}$$

System Transformers

The transformers are generally efficient and have very low magnetising currents. They are assumed to be in single phase banks or the mutual coupling between phases is assumed insignificant. This allows simplification of the transformer to a simple series RL component. While the three single phase transformers are assumed to be balanced, simple modifications will allow unbalanced representations. Again there are a wide variety of models used to calculate the series impedance at harmonic frequencies based upon name-plate information [Densem 1983].

The transformer is a series device connecting n system busbars and so the admittance matrix consists of n 3x3 admittance sub-blocks similar to a transmission line. These admittance blocks are scaled by the primary and secondary tap changer positions and so will have to be modified prior to their addition to the system admittance

matrix. A two winding transformer admittance with off-nominal tap settings, where α is the primary tap setting and β is the secondary tap setting, is written as follows.

$$Y_{transformer} = \left[\begin{array}{c|c} \frac{1}{\alpha^2}A & \frac{1}{\alpha\beta}B \\ \hline \frac{1}{\alpha\beta}C & \frac{1}{\beta^2}D \end{array}\right] \tag{3.102}$$

where the element blocks A, B, C, D depend upon the transformer type as shown by Table 3.4 [Arrillaga *et al.* 1983], for both basic transformers and the inclusion of neutral point earthing impedances. More complex transformers such as auto-wound units and zig-zag transformers can also be included within this framework.

Table 3.4 Representation of different transformer connections

Connection	A	B, C^T	D
Yg-Yg	Y_i	$-Y_i$	Y_i
Yg-Y	$\frac{1}{3}Y_{ii}$	$-\frac{1}{3}Y_{ii}$	$\frac{1}{3}Y_{ii}$
Yg-D	Y_i	$\frac{1}{\sqrt{3}}Y_{iii}$	$\frac{1}{3}Y_{ii}$
Y-Y	$\frac{1}{3}Y_{ii}$	$-\frac{1}{3}Y_{ii}$	$\frac{1}{3}Y_{ii}$
Y-D	$\frac{1}{3}Y_{ii}$	$\frac{1}{\sqrt{3}}Y_{iii}$	$\frac{1}{3}Y_{ii}$
D-D	$\frac{1}{3}Y_{ii}$	$-\frac{1}{3}Y_{ii}$	$\frac{1}{3}Y_{ii}$
Yg-Yz	Y_{iv}	$-Y_{iv}$	Y_{iv}
Yz-D	Y_{iv}	$\frac{1}{\sqrt{3}}Y_{iii}$	$\frac{1}{3}Y_{ii}$

$$Y_i = \begin{bmatrix} y_t & 0 & 0 \\ 0 & y_t & 0 \\ 0 & 0 & y_t \end{bmatrix}, \quad Y_{ii} = \begin{bmatrix} 2y_t & -y_t & -y_t \\ -y_t & 2y_t & -y_t \\ -y_t & -y_t & 2y_t \end{bmatrix}, \quad Y_{iii} = \begin{bmatrix} -y_t & y_t & 0 \\ 0 & -y_t & y_t \\ y_t & 0 & -y_t \end{bmatrix}$$

$$Y_{iv} = \begin{bmatrix} y_t - c_n & -c_n & -c_n \\ -c_n & y_t - c_n & -c_n \\ -c_n & -c_n & y_t - c_n \end{bmatrix}, \quad c_n = \frac{y_t^2}{(y_n + 3y_t)} \tag{3.103}$$

On-load tap changers (OLTC) are used to control a particular busbar voltage by adjusting their tap-ratio and hence their impedance. If a tapchanging transformer is present in the system, its control should be included within the loadflow model as well. The tap changer is assumed to be linear and be on either the primary or secondary winding. As it is used only for powerflow control, the OLTC is assumed to be non-responsive to harmonics, i.e. it is only present during the loadflow solution.

3.4.3 Constant harmonic sources

Often it is necessary to represent the background harmonic distortion or the presence of small harmonic sources as a constant injection. This is allowed for by means of

constant voltage or current sources that can be placed anywhere within the ac or dc systems. For modelling simplicity there are two exceptions to this; harmonic voltage sources cannot be placed on a non-linear device ac busbar and harmonic current sources cannot be placed on a non-linear device dc busbar.

Care must be taken when specifying harmonic injection sources, as their relative phase angles may result in incorrect harmonic current flows [IEEE Taskforce 1996]. It is for this reason as well as to simplify the analysis process, that simplified versions of non-linear devices are used. A simplified model will be essentially the same as the full representation at the power frequency during the initialisation loadflow stages. After the three phase loadflow has converged, the harmonic injection currents or voltages are calculated and these are entered into the system as constant harmonic injections. The system is reduced and these newly calculated injections are transformed to local busbar injections.

For the case of the 6-pulse converter, it is relatively straight forward to formulate the simplified expressions when calculating the ac current harmonics assuming only distorted power frequency voltage and smooth dc current. Likewise from the dc side allowing for dc ripple but assuming a pre-determined ac terminal voltage. This allows simple equivalents to be formed so that full control action can be implemented without the need for a full harmonic model. A logical extension to this approach is to allow for the inclusion of Thevenin and Norton impedances to improve the harmonic representation.

3.5 INCLUSION OF OTHER NON-LINEAR COMPONENTS

The framework shown here should allow for the modelling of the majority of linear and non-linear devices commonly found in power systems. Two different non-linear device models have been shown in the previous sections that illustrate the non-linear device interface to the main iterative solution.

The calculation of the harmonics through the non-linear devices can be either direct or iterative. A particular device may be simpler to represent by a FAST technique [Aprille and Trick 1972] using the solution variables as constant ac and dc sources. This local solution would be iterated to convergence and the resultant harmonic transfers past through to the main solution.

A variety of simplified ac-dc converter models [Xu *et al.* 1994] [Asensi *et al.* 1998] exist in the literature. These, along with the various TCR [Rico *et al.* 1996] and SVC models [Xu *et al.* 1991a], can be incorporated relatively simply into this structure provided that care is taken to assess their relative solution accuracy.

The development of models for the various STATCOM devices being promoted is likely to be simpler than the conventional devices. This is because they use forced turn

Full ac-dc converter	ac-port, dc-port + control
Simple converter	ac-port or dc-port + control
Salient pole generator	ac-port + control
Non-linear transformer	n*ac-port + control
Thyristor Controlled Reactor	ac-port + control
Static Var Compensator	ac-port + control
Thyristor Controlled Series Capacitor	ac-port, ac-port, + control
STATic COMpensator	ac-port, dc-port + control

Table 3.5 Non-linear device interface requirements

off devices with well defined switching instances. Their complexity comes from circuit configurations and the control strategy used to generate the switching signals.

A number of non-linear harmonic transformer models have also been developed [Acha 1988] [Lisboa 1996], some specifically for a Newton solution IHA program. Incorporation of these should be relatively straightforward with the major complexity arising from the conversion from a complex conjugate style solution to the real-valued positive frequency approach.

Finally, as mentioned in the future work section, it is possible to extend the converter transformer modelling to include three-pulse representation and series compensation.

Chapter 4

A GENERAL HARMONIC SOLUTION ALGORITHM

4.1 INTRODUCTION

This chapter describes an algorithm to represent the interconnections that are prevalent in a modern transmission system. Figure 4.1 shows the basic structure of the iterative solution, which contains four main components. These are the system nodal analysis, the non-linear device harmonic transfers, the system mismatches and Jacobian formation, and the linear equation solution. The selected iterative process is a unified Newton solution chosen due to its excellent convergence and relatively straight forward formulation. A source of complexity is the formation of the system Jacobian used within the convergence process; it will be shown however, this can be simplified.

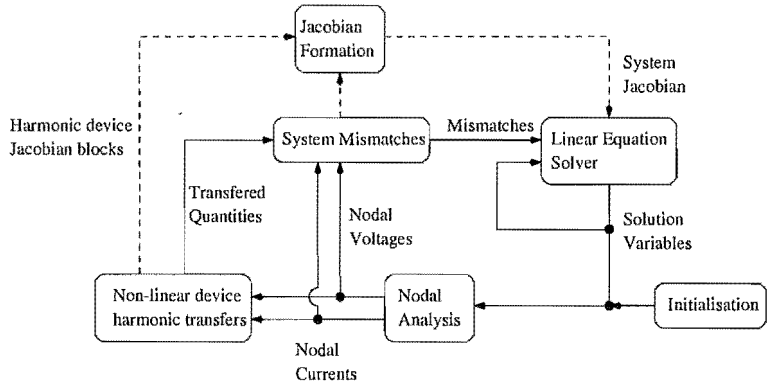

Figure 4.1 Block diagram of the iterative solution process.

An important aspect with regards to the iterative process is the number of elements that the system Jacobian contains, as the speed of solution is proportional to the sparsity of the Jacobian. Fast efficient solutions being the primary aim, it is desirable that the nodal analysis of a given system be streamlined to match the solution variables and minimise the contribution of elements to the Jacobian.

A significant number of simulation problems stem from input data errors rather than actual system complexity. Other problems arise from simplifications made when converting the physical system into an equivalent modelled system. An important

requirement of the algorithm is to minimise the effort required in locating or identifying such difficulties.

4.2 SOLUTION OF THE NON-LINEAR SYSTEM

4.2.1 Iterative scheme

Previous work [Acha 1988] [Smith 1996] has shown the Newton method to be a satisfactory solution technique for non-linear systems that show rapid robust convergence. With reference to Equation 4.1, the system is written as a set of mismatch equations $M(X_i)$ where X_i are the solution variables. The solution variables are updated by ΔX_i at each iteration using a Jacobian of partial derivatives J_i. This Jacobian of partial derivatives can be obtained by either numerical calculation or analytic formation. To minimise computational effort, it is desirable that an analytic Jacobian be formed, especially when mismatch calculation is computationally intensive. The iterative method is continued until the mismatch equations are deemed sufficiently close to zero and convergence is declared.

$$\begin{aligned} M(X_i) &= J_i \Delta X_i \\ X_{i+1} &= X_i + \Delta X_i \end{aligned} \tag{4.1}$$

The Newton method exhibits super-linear convergence as the variable set nears a solution. However, the more non-linear the problem, the closer the initial starting point must be to the solution for convergence. Thus, a sensible choice of solution variables is important to obtain good initialisation easily.

A different iterative scheme has been suggested for the solution of the non-linear problem [Nhut-Quang 1998] which did not require a Jacobian and was claimed to be globally convergent within specified bounds. This is Broyden's method and is formulated as follows:

$$B_{i+1}^{-1} = B_i^{-1} + \frac{\left(\delta x_i - B_i^{-1}\delta F_i\right) \otimes \delta x_i B_i^{-1}}{\delta x_i B_i^{-1} \delta F_i} \tag{4.2}$$

$$\delta x_i = -B_i^{-1}\delta F_i \tag{4.3}$$

There are however problems with the application of the above method to the harmonic solution. First, while no Jacobian as such is required for the iterative scheme, the method effectively builds its own numerically (B), starting from an estimate. The better the initial estimate, the fewer iterations are required. However, the number of iterations required can be significantly larger than that of an equivalent Newton method. Also, most references to this method are for a full technique and a sparse

approach has not yet been found. While it is often acceptable to start simply with the identity matrix, and then allow N updates to produce a reasonable approximation to the Jacobian [Press *et al.* 1992]; It is preferred to spend the first N function evaluations on a finite-difference approximation to initialise B. A numerically calculated Jacobian will take a significant amount of time to calculate for even a single converter system, far longer than the entire solution time of a Newton method utilising an analytic Jacobian.

4.2.2 Data error checking

The formation of a large test system can be arduous; there will be small problems with the system data, transmission lines overlooked, or setpoints that haven't been properly specified. There are a number of approaches that can be used to assist in locating such problems.

A simple but very effective data check is to locate isolated busbars and islanded networks. Using the system admittance of the positive sequence loadflow, a check for linkages can be easily made due to the row-ordered structure of the storage scheme. If a busbar has no off-diagonal elements then it is isolated and a warning can be produced. This approach can be easily extended as follows to ensure that all busbars are linked back to a slack busbar.

For a well designed ac transmission system, it can be expected that the admittance matrix of the power frequency is reasonably well conditioned. It is possible then to check for isolated subsystems by applying a 1.0 pu voltage to the slack busbar terminal, the connected busbars will then have non-zero voltages. As not every busbar has a direct connection to the slack busbar, a simple nodal current calculation will not provide the required information. The slack busbar is re-ordered first in the positive sequence admittance matrix so that the structure is as shown in Equation 4.4.

$$\left[\begin{array}{c} I_{slack} \\ \hline I_{other} \end{array}\right] = \left[\begin{array}{c|c} A & B \\ \hline C & D \end{array}\right] \left[\begin{array}{c} V_{slack} \\ \hline V_{other} \end{array}\right] \tag{4.4}$$

The system is assumed to be completely unloaded so that $I_{other} = 0$ which allows the simple expression of $DV_{other} = -CV_{slack}$ to be formed. By setting $V_{slack} = 1.0$, and using a linear equation solver, the voltages V_{other} can be obtained. Any busbar connected directly or indirectly to the slack busbar will have a non-zero voltage and so can be assigned to that ac system. This is done for all slack busbars if there are multiple independent ac systems. When this has been completed, any busbars which are still unassigned a system number are electrically isolated from any slack busbar and so they belong to isolated ac sub-systems. This approach is also used to automatically assign system numbers to all the busbars.

The only problem with this method is that a busbar can be specified but still have

a zero admittance block. The result will be zero rows and columns in the D matrix, which will cause the linear solution to fail. This problem can be picked up simply by checking the diagonal elements prior to the test.

Convergence of an unloaded system is generally very rapid and robust as the nodal voltages and currents are generally very close to their initialised quantities. By using a scaling factor on all the system loads and generation, the system can be slowly moved towards the fully loaded system. Using this approach, problems within the system formation become more apparent, thus allowing them to be found and corrected. Also for systems nearing voltage collapse, the Newton update can be slowed by a specified factor, so that a solution can be assisted and the problem located.

4.2.3 System initialisation

The full harmonic solution is reasonably non-linear therefore for efficient solution using a Newton method, a good initialisation is required. As each iteration of the full harmonic solution is computationally intensive, obtaining a good initialisation is worthwhile for fast and reliable convergence.

The initialisation is performed in two stages, the first using a positive sequence loadflow with the control variables fully included. This formulation is very robust and fast but also has the advantage of allowing quick assessment of the operating point. This results in a vastly simpler initialisation stage than the previous approaches of using classical equations and flat voltage profiles. Upon convergence, this stage initialises the main solution which is first restricted to the power frequency only. This is effectively a three-phase loadflow with full imbalance and the non-linear harmonic models represented. All the non-linear models initialise their internal variables at this point which for a HVdc converter are the switching instances.

The three-phase loadflow solution is run through to convergence and for a nearly balanced system very few iterations are required. Upon convergence, the solution is expanded to include the specified number of harmonics. For most systems, once the fundamental solution has been obtained, the harmonic solution converges quickly and reliably. Divergence, when observed to occur, seems to have been due to highly distorted systems.

The positive sequence loadflow generally starts from a flat voltage profile of 1.0 per-unit. Only in special cases is a more specific initialisation of the terminal voltage required due to multiple loadflow solutions. One such case is a star-delta transformer connecting a weak transmission system to a PQ load. In this case a low voltage solution is converged to rather than the true nominal voltage solution. This problem can be usually over come by initially phase-shifting the voltage at the PQ busbar by the transformer phase shift angle. If multiple transformer phase shifts exist within the network between the slack bus angle reference and the PQ loads, a simple method

such as this may not be sufficient. The appropriate phase shift information can be easily obtained during the check for isolated subsystems. As the system is unloaded, the 1.0pu voltage at the slack busbar will result in voltages throughout the connected system at approximately the correct phase shifts. These phase shifts can then be used for initialising the positive sequence loadflow and this results in improved convergence.

Another method suggested for loadflow initialisation [Xu *et al.* 1991b] linearises the loadflow by removing the PV and PQ constraints. Then by a direct solution of the system, an approximation to the voltage profile can be obtained.

4.2.4 Multiple loadflow solutions

During the development of the loadflows it was noticed that multiple solutions occurred at system busbars, usually at PQ specified busbars. This is in some part due to the quadratic nature of a PQ specified bus where the nodal current due to the specified power is proportional to the square of the nodal voltage. It has been shown that the multiple solutions at a PQ specified busbar in a three-phase loadflow are due to the zero-sequence blocking of a star-g/star or star-g/delta transformer. The formulation was shown algebraically and numerically to have two roots, one with a zero-sequence voltage close to zero and the other with a zero-sequence voltage close to 1.0 pu. The former is the correct solution as the other can only occur due to the simplifications made with the system modelling. To avoid converging upon the latter root either the bus is initialised to 1.1 pu positive sequence or a small zero-sequence shunt is placed at the busbar [Smith and Arrillaga 1997]. A check for this occurrence can be made by calculating the zero-sequence shunt admittance of the self blocks at each PQ busbar. If the admittance is less than approximately 1.0 pu then it is likely that the multiple solution will cause convergence problems.

A similar problem with multiple solutions occurred during the positive sequence loadflow with PQ busbars connected on the low voltage side of a transformer. It was also noticed that the multiple solution only occurred at busbars connected to a weak part of a transmission network. The multiple solution was noticed as the converged solution had abnormally large reactive power flows due to the particular busbar having a near zero voltage. If the solution busbar was initialised to either 1.1 pu or an appropriate phase shift was applied, then the solution converged to more sensible values.

The positive sequence loadflow was observed to converge onto the low voltage solution when the ratio of the transformer series element to the high voltage shunt element was approximately less than 2. If this was the case, usually only with the star-g/delta transformer, then the busbar voltage required specific initialisation. This was either in the form of making the voltage slightly greater than 1.0 pu or adding a 30 degree phase shift.

4.2.5 Minimising computation effort

Given the above initialisation, the solution convergence is quite robust. A significant amount of the solution time is involved with the formation and decomposition of the solution Jacobian to obtain the variable updates. The linear equation solver, Y12M [NEUJW@vm.uni-c.dk], can perform multiple right-hand sides as it stores the decomposed matrix. As the majority of the time is to do with the decomposition, while the backsubstitution is relatively fast, it is desirable to minimise the number of Jacobian updates.

By not updating the Jacobian continually, the method is no longer true Newton as the solution is non-linear. However, this is generally a good approximation and does not affect solution convergence significantly. While a few more iterations are generally required, the time required for these is considerably less than the time required to calculate and decompose a new Jacobian.

In order to determine when an update should be made, the rate of convergence is calculated. When this rate drops below a user specified level, the Jacobian is recalculated and decomposed. The following equation defines the measure of convergence, a good convergence is typically above 0.8, although satisfactory convergence is anything above 0.5.

$$\lambda_i = 1.0 - \frac{\sum M_i}{\sum M_{(i-1)}} \tag{4.5}$$

Another aspect to the speed of solution is the number of elements within the Jacobian. As the Jacobian does not have to be exact, simplifications can be made by specifying a tolerance level and thus eliminating many of the smaller terms. As the tolerance level is increased, the number of elements decreases (Ele) and the speed increases, but so too do the number of iterations (NIT). However, as the tolerance level increases, more significant terms are removed and convergence starts to decrease and divergence can occur.

The test system used was the full CIGRE HVdc link, as shown in Appendix B, run on a Sun SPARC-5 for 50 harmonics. The Jacobian matrices were calculated only once for all but the last two solutions, where four harmonic Jacobian updates were required. 3PF refers to the power frequency only solution and HPF refers to the full harmonic solution.

As can be seen from Table 4.1, there is an optimum tolerance range between 0.05 and 0.3 that provide the fastest solutions. However, this range is dependent upon the particular system being modelled. A good tolerance level can usually be found very quickly.

Table 4.1 Effect of the Jacobian tolerance on solution convergence

Tolerance	NIT 3PF	NIT HPF	Ele 3PF	Ele HPF	CPU time
0.000001	2	6	166	104978	16.44
0.000010	2	6	165	104883	16.48
0.000100	2	6	165	103797	17.70
0.001000	2	6	159	94309	13.45
0.010000	2	6	145	53722	12.84
0.050000	3	7	141	20745	6.23
0.100000	3	8	130	12412	5.86
0.200000	4	12	114	8016	6.04
0.300000	4	12	103	6444	5.74
0.400000	6	28	96	5893	8.80
0.500000	7	29	88	5248	17.31
0.600000	8	28	85	4374	16.92

4.3 SYSTEM DATABASE REQUIREMENTS

An important part of the solution of a large interconnected system is the ability to link all the system data together. This is particularly so for a method which forms an analytic Jacobian as part of the solution.

The following sections discuss main areas of linking that the development of this algorithm has highlighted as significant. Such linking is important so that new models and mismatches can be added simply for a fast and efficient solution.

4.3.1 System component linking

For the linking of the system components (loads, generators and non-linear devices), it is assumed that the system busbars are the common element. Given the busbar name or number the following information can be immediately obtained; the mismatch type, number of phases and whether the busbar solution is in phase or sequence components. If the busbar is a harmonic busbar, a link points to the first non-linear device. The general storage block for this non-linear device has another link that points to the next non-linear device at the busbar if one exists. This is required for every busbar that the non-linear devices are attached to. If it is an ordinary loadflow busbar, the same link points to the load or generator attached instead; it is possible to have a load on the same busbar as a generator or non-linear device. This allows the easy calculation of the system mismatches and placement of blocks when forming the analytic Jacobian.

For the calculation of the non-linear device harmonic quantities, each device requires a link to the busbar numbers that it is connected to. The busbar number then points to the full nodal voltage or current array to obtain the information required. The control variables of the device are stored in local arrays which may or may not be updated during the Newton solution updates of system controls. This allows the control

parameters of a device to be specified in the initialisation and consequently fixed during the solution. The harmonic output of the non-linear devices is stored into global arrays which are referenced by the non-linear device number. The large frequency coupling Jacobian blocks are also stored in global arrays using a sparse row-ordered format for efficient addition [Pissanetsky 1984]. This decouples the non-linear device calculation blocks from the rest of the solution process.

4.3.2 Solution variable and admittance linking

The system matrix is formed for all frequencies and stored using a general dynamic sparse technique as it is typically less than 5% full. A dynamic technique is used initially as this allows efficient addition of branches during the matrix formation. The shunt blocks of each busbar are stored in pre-specified placements so that a busbar number referenced pointer array can be used to retrieve or modify these terms. This is particularly important for the formation of the analytic Jacobian blocks. The rest of the matrix terms are store sequentially as they are added.

An optimised search routine is used to find all the elements relating to a specific harmonic set and then indexed separately using a *row-indexed sparse storage* scheme [Press *et al.* 1992]. This form is optimised for multiplication of a square sparse matrix by a column vector, as in the case of the nodal analysis. The search routine also forms mapping arrays to link the reduced solution variables, with the global full harmonic voltage and current arrays. This methodology serves a major part in decoupling the system components from the nodal analysis and solution method.

4.3.3 Solution control linking

Providing a general framework for the linking of controllers to a general system is difficult due to the large variety of different controller configurations. Linking arrays are formed with the control variables referenced to specific busbars. The components that they control and the resultant control action are predetermined, i.e. one type of HVdc current controller controls all converters attached to the specified dc busbar. A general storage array is used for any parameters specific to the particular controller.

For the Jacobian formation, the controllers are often interconnected due to their operation, and it is very difficult to anticipate every eventuality. A method for minimising these problems with a hybrid Jacobian formation is given in Section 4.7.

4.4 NODAL ANALYSIS OF THE LINEAR SYSTEM

Due to the linear nature of the various elements which form the ac transmission system, a frequency independent admittance matrix can be used for its representation. An admittance matrix is much simpler to form and modify than its impedance alternative.

The addition of a new branch to an admittance matrix simply requires an addition to the elements concerned, whereas with the impedance form, it requires modification of the entire matrix.

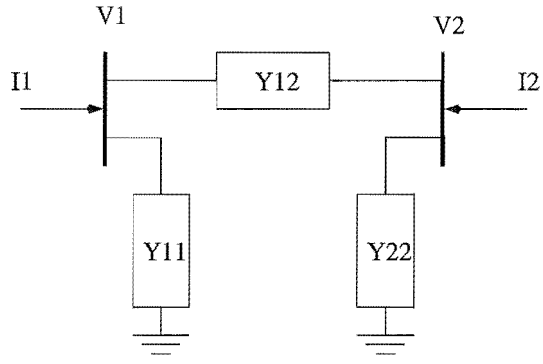

Figure 4.2 Diagram of two busbar network.

Consider a simple two busbar system such as Figure 4.2. Using the convention that all currents leaving a node sum to zero, the two nodal current injections can be written, i.e.

$$\begin{aligned} I_1 &= Y_{11}V_1 + Y_{12}(V_1 - V_2) \\ I_2 &= Y_{22}V_2 + Y_{12}(V_2 - V_1) \end{aligned} \tag{4.6}$$

These equations are then placed into the matrix form of:

$$\begin{bmatrix} I_1 \\ I_2 \end{bmatrix} = \begin{bmatrix} Y_{11} + Y_{12} & -Y_{12} \\ -Y_{12} & Y_{12} + Y_{22} \end{bmatrix} \begin{bmatrix} V_1 \\ V_2 \end{bmatrix} \tag{4.7}$$

The equivalent impedance representation of Figure 4.2 is shown by Equation 4.8 where $Z_{nm} = 1/Y_{nm}$.

$$\begin{bmatrix} V_1 \\ V_2 \end{bmatrix} = \begin{bmatrix} \frac{Z_{12}+Z_{22}}{Z_{22}(Z_{11}+Z_{12}+Z_{22})} & \frac{1}{Z_{11}+Z_{12}+Z_{22}} \\ \frac{1}{Z_{11}+Z_{12}+Z_{22}} & \frac{Z_{11}+Z_{12}}{Z_{11}(Z_{11}+Z_{12}+Z_{22})} \end{bmatrix} \begin{bmatrix} I_1 \\ I_2 \end{bmatrix} \tag{4.8}$$

The greater complexity of forming the system using the impedance matrix is obvious. Moreover the system voltages are more often known or specified than the branch currents and so the admittance formation is also preferable from the analysis viewpoint.

To use this approach though, the system must be non-singular. Basically, the system must have a reference to ground in the form of a shunt so that the nodal voltages are not floating. For ac systems this is rarely a problem, however for special dc systems, such as back to back HVdc links and high current parallel converter installations, care must be taken to avoid this situation.

In nodal analysis, each node involves two quantities, the nodal voltage, and the

nett injected current. One of these quantities is specified and then multiplied by the system matrix to calculate the unknown quantity. This process can be streamlined in the total solution process by using the Newton solution variables as the specified quantities. As will be shown in the next sections, the nodal quantities to be used as solution variables depend somewhat upon the amount of initialisation required for the Newton solution.

4.4.1 Representation of the ac system

Generally, the nodal voltages within an ac system are significantly less distorted than the nodal currents, it is therefore sensible to use these as solution variables. The majority of components are represented in phase components, and since the data is specified in phase components, the nodal quantities are normally represented as rectangular phase components.

The modelling of some non-linear devices however, is best suited to sequence component analysis [Smith 1996] as their block contributions to the system Jacobian contain significantly fewer elements. So that the solution variables can be represented in sequence components, the elements of the admittance matrix that link to a sequence components busbar are transformed. This is performed during the admittance matrix formation and thus only has to be performed once, instead of every iteration. Equation 4.9 represents the admittance matrix as represented within the data files in phase components.

$$\begin{bmatrix} I_n \\ I_m \end{bmatrix} = \begin{bmatrix} Y_{nn} & Y_{nm} \\ Y_{mn} & Y_{mm} \end{bmatrix} \begin{bmatrix} V_n \\ V_m \end{bmatrix} \tag{4.9}$$

If V_n and I_n are in sequence components, denoted by $V_n^{'}$ and $I_n^{'}$, then the admittance matrix is required to be a hybrid of phase and sequence components. This is achieved by transforming the full phase to phase matrix in the following manner.

$$\begin{bmatrix} I_n^{'} \\ I_m \end{bmatrix} = \left[\begin{array}{c|c} T^{-1}Y_{nn}T & T^{-1}Y_{nm} \\ \hline Y_{mn}T & Y_{mm} \end{array}\right] \begin{bmatrix} V_n^{'} \\ V_m \end{bmatrix} \tag{4.10}$$

where,

$$T = \begin{bmatrix} 1 & 1 & 1 \\ a^2 & a & 1 \\ a & a^2 & 1 \end{bmatrix} \quad , \quad a = \exp^{\frac{j2\pi}{3}} \tag{4.11}$$

such that,

$$[V_{phase}] = [T]\,[V_{sequence}] \tag{4.12}$$

The resultant effect of this transformation is that the solution variables can be used directly in the nodal analysis. The admittance matrix though is now no longer symmetric and so a system reduction must use the entire matrix, not just the upper or lower triangle.

Multiple ac systems

The only special requirement for the representation of multiple ac systems is that each ac system requires a slack busbar which provides the angle references within the solution.

Nodal analysis for the positive sequence loadflow

The nodal analysis is a critical part of a loadflow and so an equivalent positive sequence power frequency admittance matrix must be formed. This matrix is formed at the same time as the main three phase full frequency matrix. The power frequency component of each system element is transformed to sequence components and then reduced to its positive sequence component.

$$\left[\begin{array}{c} I_+ \\ \hline I_- \\ I_0 \end{array}\right] = \left[\begin{array}{c|cc} Y_{++} & Y_{+-} & Y_{+0} \\ \hline Y_{-+} & Y_{--} & Y_{-0} \\ Y_{0+} & Y_{0-} & Y_{00} \end{array}\right] \left[\begin{array}{c} V_+ \\ \hline V_- \\ V_0 \end{array}\right] \tag{4.13}$$

$$[Y_{++}] = \left[\begin{array}{cc} Y_{+-} & Y_{+0} \end{array}\right] \left[\begin{array}{cc} Y_{--} & Y_{-0} \\ Y_{0-} & Y_{00} \end{array}\right]^{-1} \left[\begin{array}{c} Y_{-+} \\ Y_{0+} \end{array}\right] \tag{4.14}$$

For transformers with delta or un-grounded star windings, this reduction cannot be performed numerically as the admittance matrix is singular. However, analytic expressions can be written for the positive sequence [Arrillaga *et al.* 1983]. These are shown below for an ordinary star-g/star and a star-g/delta transformers. The 30^o degree phase shift inherent in the star-g/delta transformer is maintained by the complex mutual coupling terms.

$$\left[\begin{array}{c} I_{1+} \\ I_{2+} \end{array}\right] = \left[\begin{array}{cc} Y_t & -Y_t \\ -Y_t & Y_t \end{array}\right] \left[\begin{array}{c} V_{1+} \\ V_{2+} \end{array}\right], \text{ star-g/star-g} \tag{4.15}$$

$$\left[\begin{array}{c} I_{1+} \\ I_{2+} \end{array}\right] = \left[\begin{array}{cc} Y_t & -Y_t \exp^{j\frac{\pi}{6}} \\ -Y_t \exp^{-j\frac{\pi}{6}} & Y_t \end{array}\right] \left[\begin{array}{c} V_{1+} \\ V_{2+} \end{array}\right], \text{ star-g/delta} \tag{4.16}$$

where Y_t is the specified transformer leakage admittance.

4.4.2 Representation of the dc system

During system formation, the dc system is assumed to be a single phase version of the ac system. While the admittance representation makes system formation simple, it is not necessarily the most satisfactory for modelling all types of dc systems. Thus, a greater variety of dc system configurations is required due to significant differences within the devices attached and to obtain the most suitable solution variables.

The different types of dc system representation are less of a problem than for an ac network. Generally a network will not consist of both Voltage Sourced Converters (VSC) and Current Sourced Converters (CSC) which simplifies the formulation. These dc system types are generally decoupled from one another and so can be considered independently. Different configurations can be developed which ideally suit the devices being modelled. If such a system did exist, then this would be a special case and so a configuration can be developed to suit.

Average dc component of the dc systems

For dc systems where there are more than two dc busbars, the dc current can be dependant upon the dc voltages applied to the busbars and not just the injected currents. The formulation allows for the representation of constant current and voltage sources within the dc networks. However for a full Newton solution, the dc current of a device must either be pre-specified or a solution variable.

Modelling of general CSC systems

When modelling current sourced converters (CSC) such as those for HVdc installations, the dc current harmonics are used as solution variables as these are the least distorted. Consequently, these will require less initialisation than, for example, the dc voltage harmonics. Also, as the current harmonics are used for the current and voltage transfers of the device, derivation of the analytic expressions required for the analytic Jacobian, is much simpler.

To use the solution variables directly within the nodal analysis, the dc system needs to be inverted from admittance to impedance. As the dc system is single phase and contains minimal busbar linkages, the inversion can be performed with little difficulty.

$$\left[\begin{array}{c} I_{ac} \\ \hline V_{dc} \end{array}\right] = \left[\begin{array}{c|c} Y_{ac} & 0 \\ \hline 0 & Z_{dc} \end{array}\right] \left[\begin{array}{c} V_{ac} \\ \hline I_{dc} \end{array}\right] \tag{4.17}$$

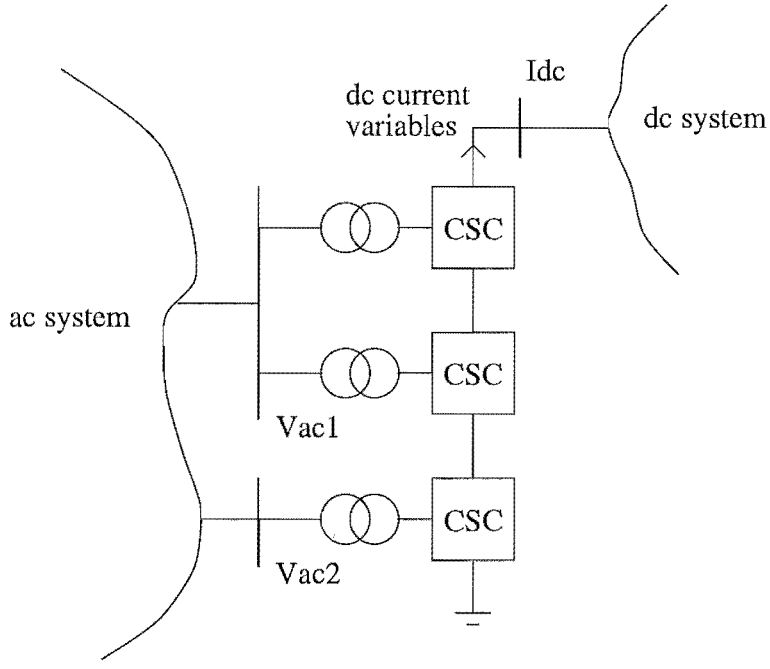

Figure 4.3 series connection of devices for dc current busbar.

Modelling of general VSC systems

If voltage sourced converters (VSC) are used, such as those for some dc motor drives and STATCOM devices, then an inversion is not required as the voltage harmonics will be more suitable for solution variables. As described earlier, this will also make the analytic Jacobian derivation simpler as the transfers will be dependent on the solution variables, not on the result of the nodal analysis.

$$\left[\begin{array}{c} I_{ac} \\ \hline I_{dc} \end{array}\right] = \left[\begin{array}{c|c} Y_{ac} & 0 \\ \hline 0 & Y_{dc} \end{array}\right] \left[\begin{array}{c} V_{ac} \\ \hline V_{dc} \end{array}\right] \tag{4.18}$$

Modelling of singular dc system CSC installations

A different approach is required for modelling installations such Aluminium smelters where several current sourced converters are connected in parallel to a common busbar through very low impedance linkages (Figure 4.5).

When such a system is modelled with an ideal current source ($Y_c = 0$ in Equation 4.19), the dc system is singular and so inversion is impossible. To solve this system, a shunt term is required at one of the busbars, the common busbar for example. However, as the linking impedances are very small, the large shunt term used commonly for numerical purposes dominates the solution, leading to erroneous results [Bathurst *et al.* 1998b]. To avoid the poor conditioning of the system admittance matrix, the shunt term needs to become non-trivial, therefore distorting the solution.

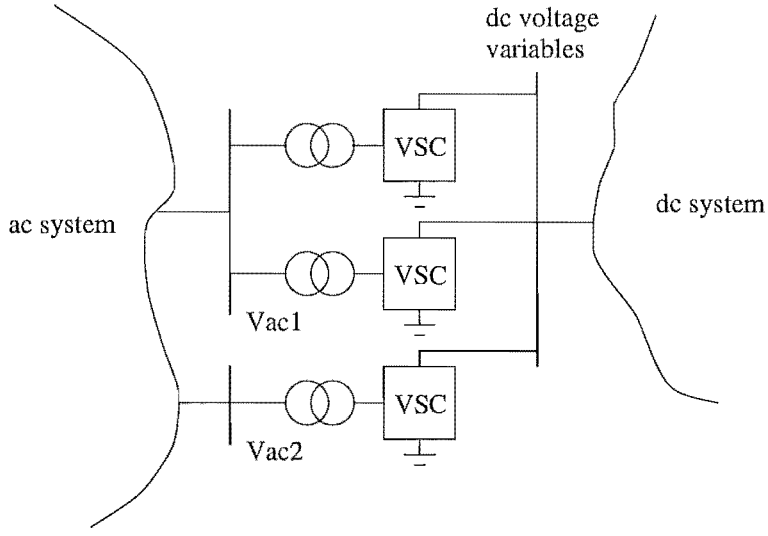

Figure 4.4 parallel connection of devices for dc voltage busbar.

The ideal current source means that the dc harmonic system is over-determined. That is, the current flowing out of the n^{th} dc busbar is the negative sum of the other dc busbars and so only $n-1$ busbar currents are required for full system knowledge. To avoid this numerical problem the n^{th} dc busbar is specified as a dc voltage busbar where the dc voltage harmonics are solution variables. This requires some matrix manipulation as the dc inversion is now a hybrid inversion, but the main system reduction can be performed normally. The dc current harmonics at the n^{th} converter are then calculated by the nodal analysis of the system.

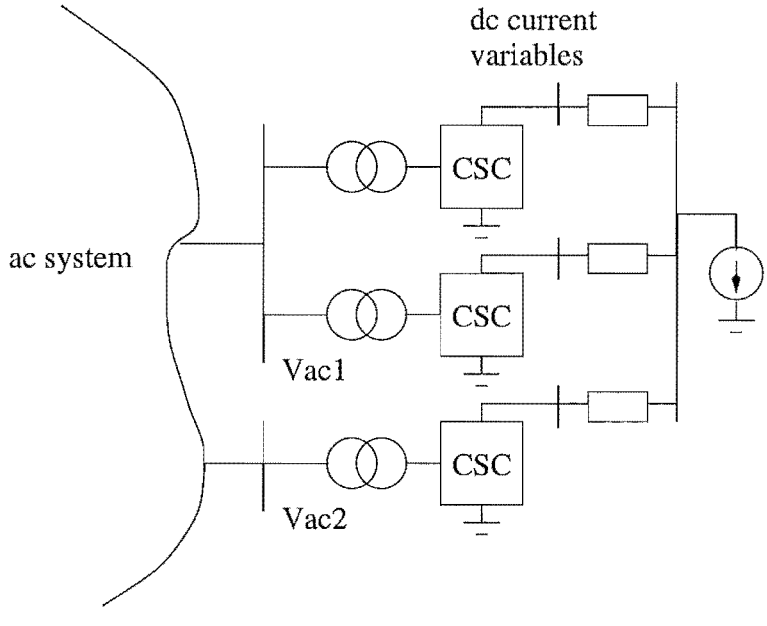

Figure 4.5 Parallel connection of current sourced devices.

The dc system will have been formed as an admittance matrix, which will be of

the form of Equation 4.19 for a system similar to Figure 4.5.

$$\begin{bmatrix} I_1 \\ I_2 \\ I_3 \\ I_4 \\ I_c \end{bmatrix} = \begin{bmatrix} y_1 & 0 & 0 & 0 & -y_1 \\ 0 & y_2 & 0 & 0 & -y_2 \\ 0 & 0 & y_3 & 0 & -y_3 \\ 0 & 0 & 0 & y_4 & -y_4 \\ -y_1 & -y_2 & -y_3 & -y_4 & y_t \end{bmatrix} \begin{bmatrix} V_1 \\ V_2 \\ V_3 \\ V_4 \\ V_c \end{bmatrix} \tag{4.19}$$

where $y_t = y_1 + y_2 + y_3 + y_4 + y_c$.

The busbars are next re-ordered, the subscript m denoting the majority of the dc busbars while subscript n refers to the dc busbar which is chosen as the voltage busbar, and c is the common busbar.

$$\left[\begin{array}{c} I_m \\ I_c \\ \hline I_n \end{array}\right] = \left[\begin{array}{c|c} A & B \\ \hline C & D \end{array}\right] \left[\begin{array}{c} V_m \\ V_c \\ \hline V_n \end{array}\right] \tag{4.20}$$

by re-arranging V_n and I_n, a partial inversion results.

$$\left[\begin{array}{c} I_m \\ I_c \\ \hline V_n \end{array}\right] = \left[\begin{array}{c|c} A - BD^{-1}C & BD^{-1} \\ \hline -D^{-1}C & D^{-1} \end{array}\right] \left[\begin{array}{c} V_m \\ V_c \\ \hline I_n \end{array}\right] \tag{4.21}$$

The full dc system is inverted using the general dc system inversion and the common busbar is eliminated during the general system reduction. Other than the re-arrangement of the dc system, no special storage or one-off routines are required for the analysis of singular systems. The n^{th} dc busbar mismatch remains as voltage mismatches, which does result in a more complex Jacobian than for ordinary CSC busbars, but not substantially so.

4.4.3 Mutual coupling between ac and dc systems

Normally the ac and dc power systems can be assumed to be coupled only through the switching action of devices such as HVdc converters. However, linear coupling can occur by means of mutual coupling between transmission circuits. This would be the case if ac and dc transmission lines were parallel for any distance or for example, if they shared the same right of way. If this mutual coupling occured then any harmonics on one system would couple through to the other system. For the characteristic harmonics of a standard HVdc link this would result in even harmonics on the ac system and odd harmonics on the dc system.

This could be a significant problem as a power frequency component on the dc side of an HVdc converter results in dc on the secondary side of the converter transformer.

This dc component can cause the transformer to saturate, thus generating more non-characteristic harmonics which can worsen this phenomenom causing an instability. Such a case is referred to as a core saturation instability [Chen *et al.* 1996].

In order to model such a configuration, the mutual coupling between ac and dc transmission systems must be represented. The transmission line modelling can be achieved simply by specifying the system to have n lines where one or two of those are the dc conductors. The admittance matrix is then formed normally except that now there are elements coupling ac busbars to dc busbars.

$$\begin{bmatrix} I_{ac} \\ I_{dc} \end{bmatrix} = \left[\begin{array}{c|c} Y_{ac} & Y_{ac2dc} \\ \hline Y_{dc2ac} & Y_{dc} \end{array}\right] \begin{bmatrix} I_{ac} \\ I_{dc} \end{bmatrix} \tag{4.22}$$

As mentioned earlier, the dc system needs to be inverted so that the HVdc configuration can be represented simply. However, due to the coupling in the ac admittance matrix, the dc system is no longer decoupled and so the inversion cannot be performed independently.

$$\begin{bmatrix} I_{ac} \\ V_{dc} \end{bmatrix} = \left[\begin{array}{c|c} Y_{ac} - Y_{ac2dc}Y_{dc}^{-1}Y_{dc2ac} & Y_{ac2dc}Y_{dc}^{-1} \\ \hline Y_{dc}^{-1}Y_{dc2ac} & Y_{dc}^{-1} \end{array}\right] \begin{bmatrix} V_{ac} \\ I_{dc} \end{bmatrix} \tag{4.23}$$

Normally the dc system inversion can be performed simply and quickly as the systems generally only consist of a few busbars and are single phase. If mutual coupling is modelled between the ac and dc systems then this inversion affects the entire system admittance matrix. While the use of sparsity techniques can reduce the computational effect required for this operation, it will still be intensive and discretion should be used. At present the routine for this inversion has not been implemented but allowance has been made for this enhancement. It may also be desirable to perform the dc system inversion after the general system reduction, to minimise the computational effort required for the matrix manipulation.

4.4.4 Inclusion of HVdc earthing networks

Normally, the bipole is run in balanced operation with the dc current in each pole balanced so that minimal dc current exists in the earth return path. Any small difference either in operating point or pole impedances will result in different harmonic conditions in each of the poles and hence imbalance between the poles, the residual current will then flow through the earthing path. As the earthing conductors have a finite impedance, this imbalance will result in a harmonic voltage building up at the neutral point. In order to represent the effect of this, the earthing conductor must be represented. Also, if a converter model is developed to investigate the generation of three-pulse harmonics due to stray capacitance, then the inclusion of the

neutral and earthing paths is essential for accurate simulation [Larsen *et al.* 1989b] [Shore *et al.* 1989].

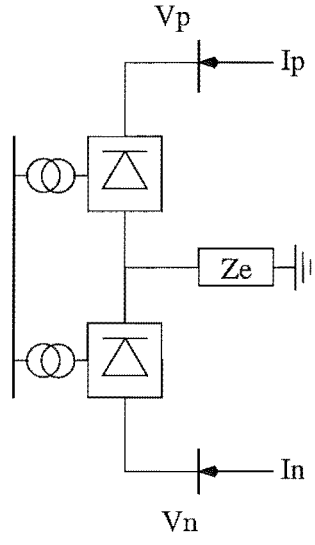

Figure 4.6 Diagram of the earthing network

The dc terminal voltages (Vp and Vn) from Figure 4.6, can be expressed as follows:

$$\begin{aligned} V_p &= V_{c1} + (I_p + I_n)Z_e \\ V_n &= V_{c2} + (I_p + I_n)Z_e \end{aligned} \tag{4.24}$$

The system mismatches for the dc voltage busbars are then:

$$\begin{aligned} M_{V_p} &= V_{c1} + (I_p + I_n)Z_e - [I_{dc}][Z_{dc}] \\ M_{V_n} &= V_{c2} + (I_p + I_n)Z_e - [I_{dc}][Z_{dc}] \end{aligned} \tag{4.25}$$

This can be rewritten as for the original formulation by including the effect of the earthing impedance with the rest of the dc system as a series impedance contribution.

$$\begin{bmatrix} M_{V_1} \\ M_{V_2} \end{bmatrix} = \begin{bmatrix} V_{c1} \\ V_{c2} \end{bmatrix} - \left(\begin{bmatrix} Z_{11} & Z_{12} \\ Z_{21} & Z_{22} \end{bmatrix} - \begin{bmatrix} Z_e & Z_e \\ Z_e & Z_e \end{bmatrix} \right) \begin{bmatrix} I_1 \\ I_2 \end{bmatrix} \tag{4.26}$$

This approach as shown below does not require the use of new system variables or solution formulation. The solution simplicity is maintained and the complexity is moved to the post-processing of the system data as described by Equation 4.24.

4.4.5 Transmission system analysis

For a fast and efficient solution of a non-linear problem, as many linear nodes as possible should be eliminated. The loadflow busbars are only non-linear at the power frequency,

and so for the remainder of the represented frequencies these can be reduced to an equivalent impedance linking the non-linear busbars. For example, the system shown in Figure 4.7 contains nine busbars, three of these have non-linear devices attached to them, two are passive harmonic current sources, and one passive harmonic voltage source. There are also two loadflow PV generators and four ordinary PQ specified loads. As the loadflow is non-linear at the power frequency, all of the busbars are maintained as shown by Figure 4.8(a). However, for the remainder of the frequencies that are represented, the linear parts of the system are reduced to the equivalent three busbar system shown in Figure 4.8(b). The remote passive injections are fully accounted for by the constant current injections at the three harmonic busbars. This formulation is shown by the following analysis, first for an ac system and then extended to a general ac-dc system.

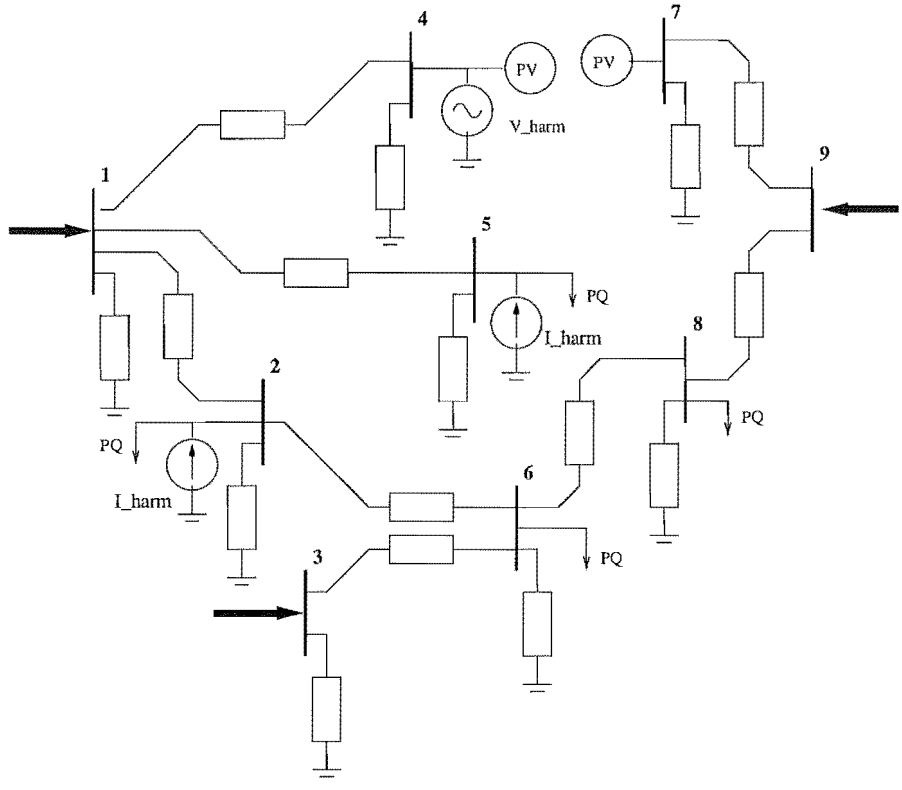

Figure 4.7 Full representation of a generic system.

The busbars of the modelled harmonic system are categorised as either linear or non-linear. The non-linear busbars have non-linear devices attached to them such that, they will couple different frequencies and actively respond to/or generate harmonics. The linear busbars on the other hand will not couple different frequencies or respond actively to harmonics.

The linear busbars are of two different types, one of them is used if there is a harmonic voltage source within the system, and therefore specifies the nodal voltage. Such a busbar will appear as a direct short to ground for harmonics other than the

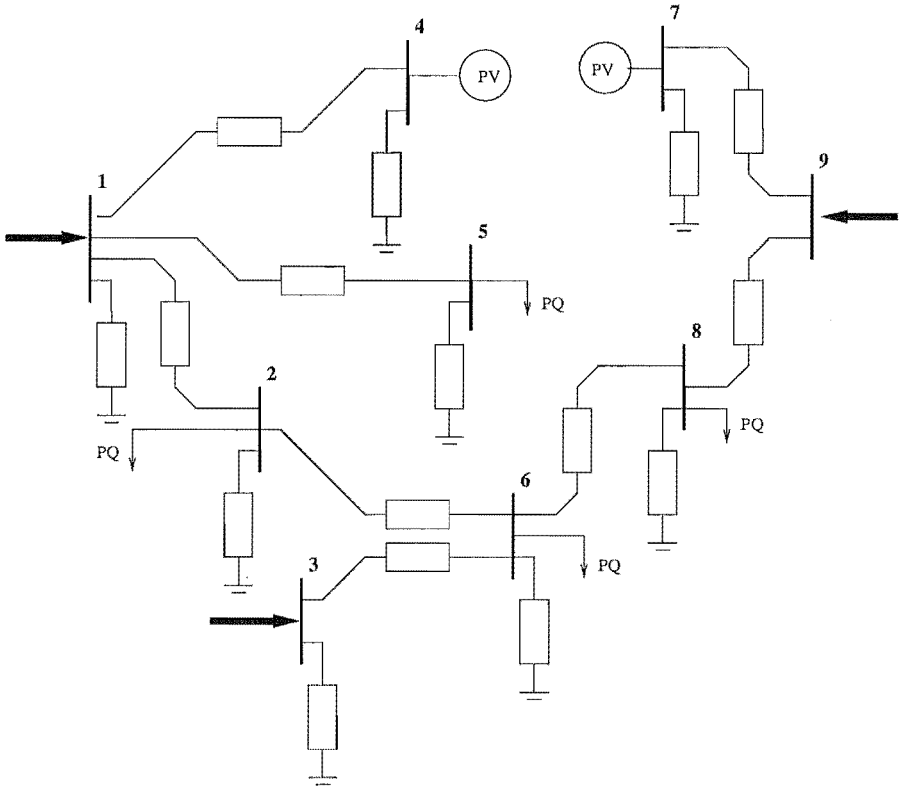

(a) loadflow system.

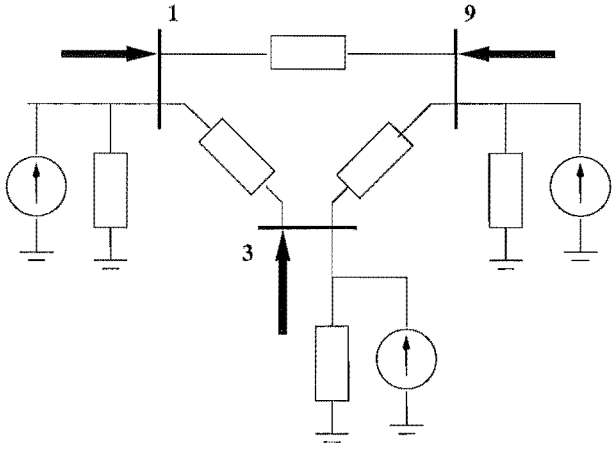

(b) harmonic system.

specified one and thus any shunt term, such as that at busbar 4, will be ignored. The second type is needed where a harmonic injection into a busbar is specified. This is most commonly used for representation of background harmonic noise, such as that from domestic or general industrial consumers.

These constant sources are an important part of accurate harmonic modelling and are included in the reduced harmonic system as equivalent shunt sources at the non-linear busbars. Unless otherwise specified, the ac system busbar is a harmonic injection busbar with a zero injection.

Basic analysis for an ac system

The nodal quantities of the busbar types as specified in the previous section are defined as follows:

$V_{nl} \in$ ac voltage for non-linear busbars
$I_{nl} \in$ ac current for non-linear busbars
$V_{vs} \in$ ac voltage for linear node specified busbars
$I_{vs} \in$ ac current for linear node specified busbars
$V_{is} \in$ ac voltage for linear injection specified busbars
$I_{is} \in$ ac voltage for linear injection specified busbars

The variables in bold are the quantities in which the nodal analysis is defined, so that the non-linear current injections must be obtained in terms of these.

$$\left[\begin{array}{c} I_{nl} \\ \hline \mathbf{I_{is}} \\ I_{vs} \end{array}\right] = \left[\begin{array}{c|cc} A & B & C \\ \hline D & E & F \\ G & H & J \end{array}\right] \left[\begin{array}{c} \mathbf{V_{nl}} \\ \hline V_{is} \\ \mathbf{V_{vs}} \end{array}\right] \tag{4.27}$$

The constant harmonic voltage and harmonic current sources reduce to constant injections, N_{inject}, at the non-linear busbars. This is compatible with the non-linear device modelling which represents the non-linear devices as dependent current sources within the ac system. The nodal analysis for the non-power frequencies post-reduction is then:

$$[I_{nl}] = [A - BE^{-1}D]\,[V_{nl}] + [N_{inject}] \tag{4.28}$$

where the constant ac current and dc voltage injections at each busbar are equal to:

$$[N_{inject}] = [C - BE^{-1}F]\,[V_{vs}] + [BE^{-1}]\,[I_{is}] \tag{4.29}$$

The E matrix represents the majority of the linear part of the power system being

reduced, which despite its sparsity is still very large even for moderate systems. To avoid inversion, a sparse linear solver is used to solve the equation $Ex = D$ for x, where x is a column of the product $E^{-1}D$. This process is more accurate and requires less operations, than a direct inversion and matrix multiplication [Press *et al.* 1992]. The reduction is only performed once to set up the sparse reduced hybrid system matrix for the full harmonic solution. As the system admittance matrix is linear, the system reduction and harmonic penetrations can be performed for each harmonic independently, thus minimising memory requirements.

When the final solution has been obtained, the harmonic components at the reduced busbars can be calculated using harmonic penetration from the non-linear device busbars. This is performed sequentially using Equations 4.30 and 4.31, the nodal voltages at current injection busbars are calculated, then these results are used to calculate the branch/nodal currents at the voltage source busbars.

$$\left[V_{is} \right] = \left[E \right]^{-1} \left(\left[I_{is} \right] - \left[D \mid F \right] \left[\frac{V_{nl}}{V_{vs}} \right] \right) \tag{4.30}$$

$$\left[I_{vs} \right] = \left[G \mid H \mid J \right] \left[\frac{V_{nl}}{\frac{V_{is}}{V_{vs}}} \right] \tag{4.31}$$

The inversion of the large linear system matrix is again avoided using the linear solver as described above. As mentioned before, the Y12M linear solver package stores the decomposed matrix so that multiple right-hand sides can be solved. The decomposed E matrix can be stored from the main reduction and re-used in the harmonic penetration. This procedure minimises duplication of calculations, but requires significant extra storage as the reduction and penetrations are at this stage performed for each frequency independently.

Extension to general systems

As the systems being modelled contain ac and dc components, possibly with mutual coupling between them, the harmonic representation shown above must be generalised to suit the hybrid systems.

The busbar type definitions need to be changed slightly to account for the differences in representation of the ac and dc systems. The main problem arises when a dc system is represented in impedance form (Z-type). The specified variables on the left and right hand sides of the nodal equation are inter-changed and the dc system becomes the dual of the ac system. Basically, a dc voltage source is handled in the same fashion as an ac current source and a dc current source like an ac voltage source. If a dc admittance represented system (Y-type) is used, the formulation is the same

as for an ac system. It is assumed that the nodal matrix has already been formed as described in the earlier sections using the following definitions.

$$W_{nl} \in \begin{cases} \text{Currents calculated for non-linear ac and Y-type dc busbars} \\ \text{Voltages calculated for non-linear Z-type dc busbars} \end{cases}$$

$$X_{nl} \in \begin{cases} \text{Voltage variables for non-linear ac busbars and Y-type dc busbars} \\ \text{Current variables for non-linear Z-type dc busbars} \end{cases}$$

$$W_{is} \in \begin{cases} \text{Specified currents for linear current injection ac and Y-type dc busbars} \\ \text{Specified voltages for linear voltage sourced Z-type dc busbars} \end{cases}$$

$$X_{is} \in \begin{cases} \text{Calculated voltages for linear current injection ac and Y-type dc busbars} \\ \text{Calculated currents for linear voltage sourced Z-type dc busbars} \end{cases}$$

$$W_{vs} \in \begin{cases} \text{Specified voltages for linear voltage sourced ac and Y-type dc busbars} \\ \text{Specified currents for linear current injection Z-type dc busbars} \end{cases}$$

$$X_{vs} \in \begin{cases} \text{Calculated currents for linear voltage sourced ac and Y-type dc busbars} \\ \text{Calculated voltages for linear current injection Z-type dc busbars} \end{cases}$$

An identical analysis to that in the previous section can be derived, i.e.

$$\left[\begin{array}{c} W_{nl} \\ \hline \mathbf{W_{is}} \\ W_{vs} \end{array}\right] = \left[\begin{array}{c|cc} A & B & C \\ \hline D & E & F \\ G & H & J \end{array}\right] \left[\begin{array}{c} \mathbf{X_{nl}} \\ \hline X_{is} \\ \mathbf{X_{vs}} \end{array}\right] \tag{4.32}$$

$$[W_{nl}] = [A - BE^{-1}D]\,[X_{nl}] + [N_{inject}] \tag{4.33}$$

The constant ac current and dc voltage injections at each busbar can be expressed as:

$$[N_{inject}] = [C - BE^{-1}F]\,[X_{vs}] + [BE^{-1}]\,[W_{is}] \tag{4.34}$$

The linear nodal voltages and currents can then be determined as follows:

$$\left[\ X_{is}\ \right] = \left[\ E\ \right]^{-1} \left(\left[\ W_{is}\ \right] - \left[\ D \,\middle|\, C\ \right] \left[\begin{array}{c} X_{nl} \\ \hline X_{vs} \end{array}\right] \right) \tag{4.35}$$

$$\left[\ W_{vs}\ \right] = \left[\ G \,\middle|\, H \,\middle|\, J\ \right] \left[\begin{array}{c} X_{nl} \\ \hline X_{is} \\ \hline X_{vs} \end{array}\right] \tag{4.36}$$

Optimised reduction for multiple runs

When a system busbar has it's power frequency loading information changed, the harmonic impedance of that busbar will also change. This then requires the full harmonic system to be re-reduced to account for the new loading. When multiple loading scenarios are being performed on large systems, a large amount of the total solution time will be spent on the system reduction.

For this case, the system reduction can be split into two parts. As within a loadflow, a significant amount of the busbars representing the transmission system do not have loads attached to them, and consequently will not change with system operating point. The linear busbars would be ordered, such that the busbars that change with operating point are ordered first. The first reduction reduces the system down to the non-linear busbars and load changing linear busbars. For every operating point change after this, the reduction is simply to eliminate the load changing linear busbars instead of all of the linear busbars. This should reduce the nett amount of computation required for the loading study.

4.4.6 Per unit system used

The use of a standard per-unit system in the algorithm's calculations minimises internal complexity and potential matrix conditioning problems. However, the control and other operating point specifications can be in either real or per-unit depending upon the user's personal preferences.

Within traditional ac-dc loadflows [Arrillaga *et al.* 1983], the dc system voltage base is defined in terms of the converter transformer secondary side voltage base. This choice is very limiting for general analysis as the dc system modelling requires knowledge of the converters to define the system voltage bases; unlike the ac systems where the elements are independent. The problem especially arises with long distance HVdc links where the secondary side voltage bases of the rectifier and inverter transformers are different to account for nominal operating conditions. A traditional voltage base system results in different dc voltage bases at each end of the transmission line and this will result in incorrect simulation results.

To avoid such problems and allow for elemental independence, a base conversion is required between the converters and the dc transmission lines. The generated per-unit voltage will be transformed from the internal converter voltage base to the external transmission line voltage base. A similar scaling is performed in reverse for the dc current harmonics.

4.5 SYSTEM MISMATCHES FOR NEWTON SOLUTION

Sections 4.5.1 to 4.5.3 describe the system mismatches relevant to the three phase loadflow and its related harmonics. As the solution is framed in terms of real-valued rectangular co-ordinates, the representation of a three phase ac busbar requires six variables and six independent mismatch equations per frequency. Section 4.5.4 describes the simplified version of the system where it is just represented by the positive sequence or balanced conditions.

4.5.1 Load Mismatches

A number of three phase load configurations are possible, each giving a different power frequency response. A simple example of this is the difference between a star-ground connected load and a star-ungrounded connected load. An imbalance in the former may produce zero-sequence current while the second configuration has no path for such current. Thus as configurations such as these exist, it is important to allow for them in the loadflow models. Three examples of mismatches which model these are discussed next.

Star-grounded PQ specified load

This is the simplest form of load modelling with the power in each phase specified in real and reactive quantities from phase to ground. Each phase is effectively independent and so the complex power can exist in all sequences.

$$\begin{aligned} M_{P_a} &= P_a + Real\{V_a I_a^*\} \\ M_{Q_a} &= Q_a + Imag\{V_a I_a^*\} \\ M_{P_b} &= P_b + Real\{V_b I_b^*\} \\ M_{Q_b} &= Q_b + Imag\{V_b I_b^*\} \\ M_{P_c} &= P_c + Real\{V_c I_c^*\} \\ M_{Q_c} &= Q_c + Imag\{V_c I_c^*\} \end{aligned} \tag{4.37}$$

Star-ungrounded PQ specified load

For a star-ungrounded load connection, there is no path for zero-sequence and so the sum of the phase currents should be zero. As the star point voltage now will be non-zero for an imbalanced loading, the phase powers of the first two phases are defined by the phase current and the difference between the nodal voltage and the star-point

voltage.

$$\begin{aligned}
M_{P_{an}} &= P_{an} + Real\left\{\left(V_a - \left(V_c + \tfrac{P_c + jQ_c}{I_c^*}\right)\right) I_a^*\right\} \\
M_{Q_{an}} &= Q_{an} + Imag\left\{\left(V_a - \left(V_c + \tfrac{P_c + jQ_c}{I_c^*}\right)\right) I_a^*\right\} \\
M_{P_{bn}} &= P_{bn} + Real\left\{\left(V_b - \left(V_c + \tfrac{P_c + jQ_c}{I_c^*}\right)\right) I_b^*\right\} \\
M_{Q_{bn}} &= Q_{bn} + Imag\left\{\left(V_b - \left(V_c + \tfrac{P_c + jQ_c}{I_c^*}\right)\right) I_b^*\right\} \\
M_{R0} &= Real\left\{I_a + I_b + I_c\right\} \\
M_{I0} &= Imag\left\{I_a + I_b + I_c\right\}
\end{aligned} \tag{4.38}$$

Delta connected PQ specified load

Again for a delta connected load there is no path for zero-sequence, so the current into the third phase is the negative sum of the current into the other two phases. Simple nodal analysis leads to the following equations:

$$\begin{aligned}
M_{P_{ab}} &= P_{ab} + Real\left\{(V_a - V_b)\left(I_a + \left(\tfrac{P_{ca} + jQ_{ca}}{V_a - V_c}\right)^*\right)^*\right\} \\
M_{Q_{ab}} &= Q_{ab} + Imag\left\{(V_a - V_b)\left(I_a + \left(\tfrac{P_{ca} + jQ_{ca}}{V_a - V_c}\right)^*\right)^*\right\} \\
M_{P_{bc}} &= P_{bc} + Real\left\{(V_b - V_c)\left(I_b + \left(\tfrac{P_{ab} + jQ_{ab}}{V_b - V_a}\right)^*\right)^*\right\} \\
M_{Q_{bc}} &= Q_{bc} + Imag\left\{(V_b - V_c)\left(I_b + \left(\tfrac{P_{ab} + jQ_{ab}}{V_b - V_a}\right)^*\right)^*\right\} \\
M_{R0} &= Real\left\{I_a + I_b + I_c\right\} \\
M_{I0} &= Imag\left\{I_a + I_b + I_c\right\}
\end{aligned} \tag{4.39}$$

4.5.2 Generation mismatches

Two different methods can be used to specify a generating source within the loadflow. In the first model the generator is specified by positive sequence real power and positive sequence power frequency voltage. It also requires two sequence shunts to account for any negative and zero sequence currents resulting from power frequency distortion at the terminal busbar. If the generator is chosen as the system slack bus, the specified power is simply governed externally as a separate control variable. This helps to generalise the formation of the Jacobian by minimising the information requirements.

In the second type of generation source is represented as an ideal three phase voltage source which can be specified in terms of phase or sequence components. This is useful for modelling hypothetical systems or if a Thevenin equivalent of a real system is used. There should be only one voltage source represented within a given ac system, as the voltage is exactly specified and it has the action of a slack bus generator.

Star connected PV specified generator with sequence shunts

The linear physical generator is represented within the three phase loadflow by the following equation set.

$$\begin{aligned} M_{P_+} &= P_{set} - Real\{V_+(I_+ + Iload_+)^*\} \\ M_{V^2} &= V_{set}^2 - Real\{V_+V_+^*\} \\ M_{Rn} &= Real\{I_- + V_-Ygen_- + Iload_-\} \\ M_{In} &= Imag\{I_- + V_-Ygen_- + Iload_-\} \\ M_{R0} &= Real\{I_0 + V_0Ygen_0 + Iload_0\} \\ M_{I0} &= Imag\{I_0 + V_0Ygen_0 + Iload_0\} \end{aligned} \tag{4.40}$$

where the local load at the generation busbar is:

$$Iload = \left(\frac{P + jQ}{V_{ph}}\right)^* \tag{4.41}$$

The first two equations define the generator's controlled positive sequence set point, while the remaining four describe its response to negative and zero sequence voltages. The positive sequence voltage magnitude constraint is written as the voltage squared to avoid the use of a square-root. This simplifies the calculation of the analytic Jacobian terms while leaving the solution convergence the same. As the generator reactive power is unconstrained with this representation, the reactive power of the local load is effectively ignored during the solution and is only added during post-processing of the results.

Three phase specified voltage source

This case is represented by the following equation set:

$$\begin{aligned} M_{Ra} &= Real\{Vset_a - V_a\} \\ M_{Ia} &= Imag\{Vset_a - V_a\} \\ M_{Rb} &= Real\{Vset_b - V_b\} \\ M_{Ib} &= Imag\{Vset_b - V_b\} \\ M_{Rc} &= Real\{Vset_c - V_c\} \\ M_{Ic} &= Imag\{Vset_c - V_c\} \end{aligned} \tag{4.42}$$

A busbar can have its three phase nodal voltage specified exactly in either phase or sequence components. The voltage source can be imbalanced simply by specifying the phase or sequence magnitudes and angles. This source generates completely unconstrained real and reactive power and so any local load will be ignored during the solution.

4.5.3 Harmonic busbar mismatches

As the non-linear devices provide frequency coupling, their Jacobian contributions will generally involve significant blocks. It is thus desirable to form the mismatches at these busbars in such a way as to minimise the complexity of the calculations.

ac busbar mismatches

Smith [1996] solved the converter interaction with a shunt equivalent of the ac system by means of voltage mismatches, which required the Jacobian blocks to be scaled by the ac side impedance. This means that a parallel resonance will scale rows of the Jacobian possibly causing ill-conditioning problems, although this was not a significant problem for a single 12-pulse HVdc rectifier. However, with multiple non-linear devices connected through an ac network, the system inversion will be large and parallel resonances will result in more Jacobian elements as the impedance at each harmonic affects the entire row.

$$M_{[V_c]_k} = \sum_{n=1}^{nb} [Z_{cn}]_k [I_n]_k - [V_{nl}]_k \tag{4.43}$$

A simpler method is the use of current mismatch equations at the ac busbars. In this case multiple devices can be simply connected to the same bus by summing their current contributions with the current calculated from the nodal analysis. The Jacobian block is then a transfer from ac voltage to ac currents and any busbar coupling blocks are simply the diagonal reduced system admittance.

$$M_{[I_c]_k} = \sum_{n=1}^{nb} [Y_{cn}]_k [V_n]_k - \sum [I_{nl}]_k \tag{4.44}$$

As the HVdc converter is characterised by sequence conversions between frequencies, the converter is more efficiently solved in sequence components, even though the transfer formulation is in phase components. This is because the Jacobian can be formed with substantially fewer elements which leads to a faster decomposition and general solution. For this, the ac mismatch equations need to be transformed to sequence components after being calculated.

At the power frequency, the current contribution of any local load is combined with the non-linear device currents. For the harmonic frequencies, the shunt contribution is combined with the ac system admittance.

dc busbar mismatches

The dc system busbars use a similar philosophy, but due to different device configurations, can have either voltage or current mismatches. For example, the standard current sourced converters such as those used in HVdc and LVdc installations, will use the dc current components as variables as these are generally the least distorted. Also, to simplify the Jacobian block calculations, they will use voltage mismatches. These are the difference between the sum of the dc voltages of the devices in series and the nodal voltage calculated from the solution harmonic currents.

$$M_{[V_c]_k} = \sum_{n=1}^{nb} [Z_{cn}]_k [I_n]_k - [V_{nl}]_k \tag{4.45}$$

For voltage sourced converters such as those used in some dc motor drives and STATCOM's, the device inputs should be the dc voltage harmonics. Also as these are going to be the least distorted, it makes sense to use them as the Newton variables. Again, in order to simplify the Jacobian block calculation, current mismatches should also be used, this is the dual of the voltage mismatches. Here the devices are in parallel and their dc currents are combined and then subtracted from the current calculated by nodal analysis.

$$M_{[I_c]_k} = \sum_{n=1}^{nb} [Y_{cn}]_k [V_n]_k - \sum [I_{nl}]_k \tag{4.46}$$

4.5.4 Positive sequence loadflow mismatches

The positive sequence loadflow is a simplified version of the three-phase loadflow and is used here as an initialisation stage. The formulation is such that a simplified analysis can be used while maintaining approximately the same operating point. As only two variables are used to define each busbar, only two mismatch equations are required.

Load busbars

As the various PQ load configurations have effectively the same positive sequence response, they can all be presented by the following positive sequence power mismatch equations:

$$\begin{aligned} M_{P_+} &= \tfrac{1}{3}(P_a + aP_b + a^2P_c) + Real\left\{V_+ I_+^*\right\} \\ M_{Q_+} &= \tfrac{1}{3}(Q_a + aQ_b + a^2Q_c) + Imag\left\{V_+ I_+^*\right\} \end{aligned} \tag{4.47}$$

Generation busbars

Again, as only the positive sequence components are required, the generation sources are also easily simplified by removing any negative or zero sequence parts, i.e.

$$\begin{aligned} M_{P_+} &= P_{set} - Real\left\{V_+ I_+^*\right\} \\ M_{V^2} &= V_{set}^2 - Real\left\{V_+ V_+^*\right\} \end{aligned} \tag{4.48}$$

The voltage source mismatches become:

$$\begin{aligned} M_{R+} &= Real\left\{V_{set_+} - V_+\right\} \\ M_{I+} &= Imag\left\{V_{set_+} - V_+\right\} \end{aligned} \tag{4.49}$$

Non-linear device busbars

For the non-linear device representation, a few changes need to be made. As the dc power transfer in the dc system are the dc components, the dc busbars are not required in the positive sequence solution. The dc power transfer itself is governed by specified control equations. With reference to the ac system representation, as balanced conditions are assumed, simplified mismatch equations can be used, i.e.

$$M_{[I_+]_k} = \sum_{n=1}^{nb} [Y_+]\,[V_+] - \sum [I_+] \tag{4.50}$$

4.6 REPRESENTATION OF SYSTEM CONTROLS

Inclusion of a control variable within the unified solution is a powerful method for obtaining the steady-state value of an otherwise difficult control state. The inclusion of control variables within the main solution has already been implemented in single and three phase [Arrillaga *et al.* 1983] ac-dc loadflow solutions.

An example is the control equation used for the slack bus generator. The control variable is the generator positive sequence power setpoint and the control constraint is the specification of the terminal voltage angle. The control mismatch compares the busbar voltage angle with the specified angle. There is no direct coupling between the generated power and the terminal voltage angle and it is thus a non-linear problem to calculate the required slack power. However, by including the control equation, such a constraint can be easily met.

Another example is the average firing angle of the converter. Classical theory can calculate this angle only under ideal operating conditions. However, with multiple generation sources, transmission and loading asymmetry and dc current distortion, any existing analytic expression will only be an approximation. By introducing the average firing angle as a solution variable, the Jacobian will adjust the solution variables such that the specified condition is met.

The specification of controllers is left open so that there can be a great variety to suit the conditions to be represented. The main limitation of the modelling of controllers is in the formation of the analytic expressions for the solution Jacobian. To minimise the complexity of forming these expressions, the mismatch equations should be written in terms of easily obtainable system parameters. Often there is sufficient similarity between the control equations of the devices such that general Jacobian blocks can be formed which simplifies the inclusion of new controllers.

4.6.1 Base operating point only

Some controllers are used to provide a single variable which is then used as the control setpoint. These constitute the simplest forms of control and are probably the most widely used. The mismatch equations can either use power frequencies only or derive their mismatch from the full harmonic spectrum, while only controlling a single variable. Table 4.2 below gives some of these:

Table 4.2 A selection of possible base operating point control equations

Control Type	Variable	Mismatch Equation
Current Controllers	α_0	$M = Id_{set} - Id_{calculated}$
Extinction angles	α_0	$M = \gamma_{set} - \gamma_{average}$
	α_0	$M = \gamma_{set} - \gamma_{minimum}$
Slack bus power	P_{gen}	$M = \theta_{set} - \angle V_+$
On-load tap changers	Tap(a)	$M = \alpha_{set} - \alpha_{average}$
	Tap(a)	$M = Vd_{set} - Vd_0$
	Tap(a)	$M = \lvert Vac_{set}\rvert - \lvert Vac_+\rvert$
Converter dc current	I_{dc}	$M = I_{dc} - Id_{calculated}$
HVdc link power	I_{set}	$M = P_{set} - Vd_{calc}Id_{calc}$

4.6.2 Base operating point and harmonic information

The current controller shown in Figure 4.8 is typical of controlled rectification. It measures the dc current and compares it to a set point, the difference being applied to a Proportional Integer (PI) controller which produces the alpha order ripple used to generate the converter firing pulses. The corresponding transfer function is:

$$\alpha_{ripple}(k) = \frac{G_t}{1 + jkT_t}\left(T_P + \frac{1}{jkT_I}\right) Id_k \tag{4.51}$$

The HVdc link power controller does not directly affect a system variable, its purpose being to adjust the set point of another controller. In this case, the controller is used to specify the power transfer of an HVdc link by adjusting the dc current controller setpoint as shown in Figure 4.9. This requires the use of an extra control equation to be used as the current controller must be specified. By having the equation set as

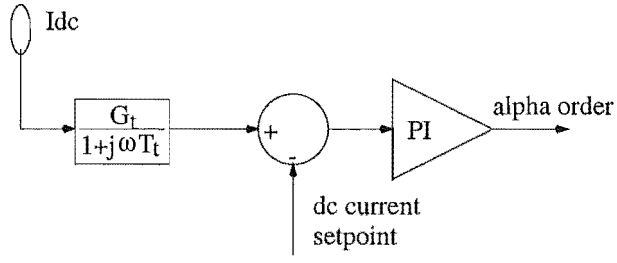

Figure 4.8 Block diagram of the current controller.

slightly larger than is minimally required, realistic controls can be easily implemented. To simplify the algorithm formation at present, a power controller is specified as two separate controllers. However, it is more desirable that the controller be specified as a single unit with two control equations and two control variables.

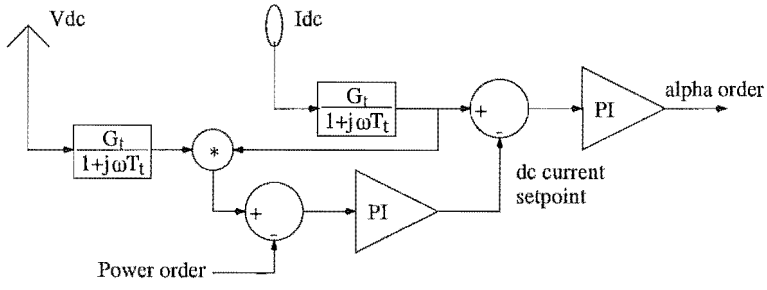

Figure 4.9 Block diagram of a power controller for an HVdc link.

Care must be taken to maintain a full Newton solution structure when modelling a controller such as in Figure 4.9. The dc voltage harmonics (V_{dc}) cannot be those obtained from the converter model harmonic transfers, but rather from nodal analysis of the dc system using the dc current harmonics, which are solution variables. In this way, the alpha order which is used to calculate the firing instants depends directly on the solution variables. No history terms are used which would be the case if the transferred voltage harmonics were used instead.

4.6.3 Discrete decision making within controllers

Often it is necessary to use hysteresis or memory from a previous iteration when it is not possible or too complex, to linearise the controller operation. A classical style of controller in which it is necessary to implement a hysteresis effect, is the minimum gamma controller of an HVdc inverter. During a distorted steady-state, the switching with the minimum extinction angle remains the same. However, without significant prior knowledge of the solution, the switching with the minimum gamma cannot be deduced. This results in the switching, used to specify the average firing angle, being changed during the solution as the switching with the minimum gamma changes. This controller is implemented as follows.

All of the extinction angles of the controlled converter(s) are calculated and the minimum of these determined. If the gamma is *significantly* less than the previous minimum, that switching becomes the new controlled angle. This tolerance is a hysteresis introduced to the decision process to avoid the solution hopping between two very similar angles. This control strategy is discrete and non-linearisable, but has been shown to be robust [Bathurst *et al.* 1997]. While there is a possible way to provide a linearised controller that simulates a minimum gamma controller, it would be significantly more complicated than this.

A divergence case has been noticed using the pure minimum gamma controller with an ac system under unbalanced conditions. After the positive sequence loadflow, the controller needs to be initialised with regards to which switching the average firing angle is controlling. If the wrong switching is chosen, then the variable update pushes the converter into an invalid area of operation with $\gamma < 0$. This divergence can be avoided by using an average gamma controller for the first iteration, after the first update the switching with the minimum gamma becomes apparent.

Another use for memory and hysteresis within a controller is when multiple controls are used. Such a case is again for an HVdc inverter where the inverter is nominally in minimum gamma but, if certain conditions dictate, it may switch to proportional control or even maintain link dc current control. In order to prevent the solution jumping from control to control, a threshold must be in place so that the solution is definitely in the new region of control before the control type changes.

4.7 FORMATION OF SOLUTION JACOBIAN

Formation of an analytic Jacobian for a general system is not immediately straight forward due to the interconnection that exists between the system variables. However, it will be shown that it is not particularly difficult either.

4.7.1 Numerical Derivation

The full numerical Jacobian is the simplest and generally most fool-proof method for obtaining the Jacobian of a desired system. To calculate a column of the Jacobian, the corresponding solution variable is perturbed from a base case and all of the harmonic transfers re-calculated. The solution mismatch equations are evaluated and the difference between these and the mismatches evaluated at the base case is obtained. This difference is then divided by the perturbation magnitude to give the elements for one column of the Jacobian. The full Jacobian is obtained by sequentially perturbing all of the solution variables and calculating the individual columns. For the linearisation to be valid, the perturbation must be small enough so that the system remains in a linear

state around the base point.

$$J = \frac{\delta F}{\delta x} \simeq \frac{F(x+\Delta x)-F(x)}{\Delta x} \tag{4.52}$$

While this method is extremely useful for proofing mismatch equations, new system configurations and new component models, it requires $n+1$ effective iterations where n is the number of solution variables. With a model such as the converter, which uses convolutions in its transfer calculations, this can be very slow and computationally expensive.

With the mismatch function evaluation of the positive sequence loadflow being very fast, due to its simple analytic form, the Jacobian is calculated numerically. This minimises the effort required when investigating new system configurations and models.

4.7.2 Analytic Derivation

To form a general analytic Jacobian, information is required about the structure and inter-connectivity of the system being modelled. For the loadflow part of the system, the nodal matrix of the system provides sufficient information. However when non-linear devices couple between frequencies and busbars are being modelled, more information about their internal action is required.

The formation of the full Jacobian is broken down into stages. Each non-linear device calculates its contribution to the main Jacobian and stores it in ordered sparse lists. These lists are then passed to the main Jacobian formation block which combines them with the rest of the system to form the full Jacobian. The full Jacobian for the system shown in Figure 4.10 is displayed in Figure 4.11 for the first 13 harmonics.

Figure 4.11 illustrates the structure of the Jacobian for a system containing three non-linear devices, one is a salient pole generator attached to the Manapouri-1014 busbar (A1) and the other two are 6-pulse converters attached in parallel at the Tiwai-220 (B2) busbar. The generator is a shunt device and so will only contribute one block to the Jacobian. The converters are series devices which link the ac and dc systems.

As the converters are modelled as two separate devices, their individual Jacobian blocks will have to be added together in all the shunt and linking blocks. While this is slightly less efficient than the single calculation of the Jacobian for a 12-pulse converter, it is more modular and general. It does however require the addition of two sparse matrices. This addition in itself is non-trivial for efficient computation, particularly when multiple devices are present. As the Jacobian blocks can be calculated in an ordered form, an efficient method (as shown in Appendix D) can be used [Pissanetsky 1984].

The ac and dc self blocks of the non-linear devices are placed first (A1, B2 and C3). Then any linear linkages between these busbars and the rest of the system are placed, both harmonic (A2 and B1) and loadflow (A4 and B4). These linear terms are simply part of the system admittance matrix. After this, the Jacobian terms for the

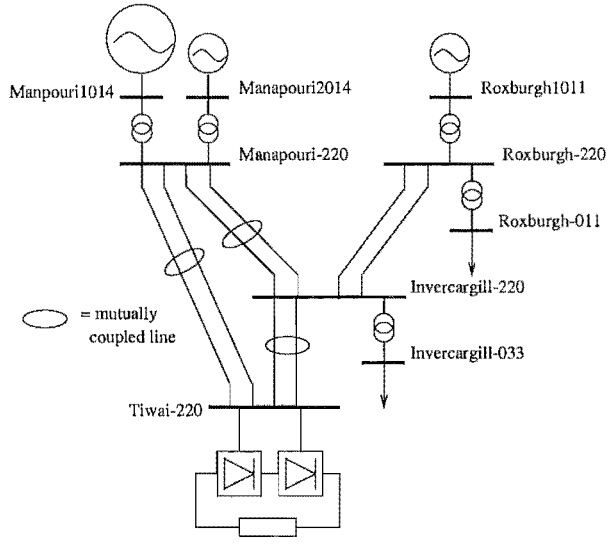

Figure 4.10 Lower South Island testsystem with three non-linear devices

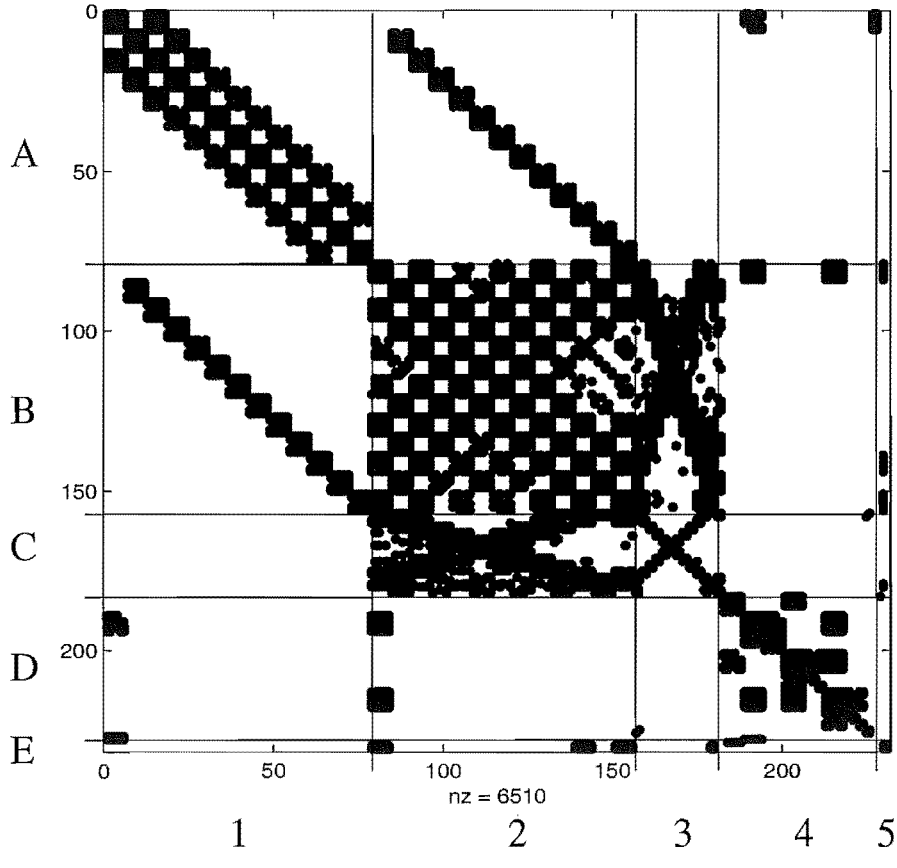

Figure 4.11 13 harmonic Jacobian for Figure 4.10.

ordinary loadflow are placed (row D) in the same way as for an ordinary loadflow. Next the blocks that link two busbars through a harmonic device are placed (B3 and C2). These often couple frequencies and are stored as ordered sparse lists. Placement of these is achieved by moving individually through all the non-linear devices and adding the contributions from the devices that link between the same busbars. The control rows and columns of the Jacobian are the last to be calculated and placed (row E and column 5).

The ability to form the Jacobian in this manner somewhat relies on the linear equation solver's ability to use a general sparse input. As the Y12M linear equation solver re-orders the data as part of its solution, then this is an ideal package for the solution [NEUJW@vm.uni-c.dk].

4.7.3 Hybrid Derivation

The hybrid method uses the best of both the analytic and numerical calculations of the system Jacobian. The analytic Jacobian is ideal for fast calculation but requires a significant amount of knowledge of system behaviour and connection. The numerical Jacobian requires no more knowledge of the system than is required for the nodal analysis and mismatch calculation, but is very slow by comparison and requires significant computational effort.

The hybrid method is used to reduce the calculation complexity of the analytic Jacobian and, in the cases of new model development, remove the immediate need for analytic expressions. This approach uses the analytic formulation for combining the main Jacobian blocks and calculation of the control equation mismatch dependence upon electrical variables. The columns for the control variable effects on the system mismatches are then calculated numerically. Often the interconnection between the control equations is difficult to pre-determine and consequently analytic expressions are difficult to write. Other times the expressions are simply very laborious to calculate and so using a numerical perturbation is actually not that much longer in computational time. Such a case for the latter example is when automatic tap-changer controls are utilised for HVdc converters. The dependence of ac phase currents and dc voltage on the tap variable requires a significant and complex calculation block and so is vastly simpler to do numerically. This approach for the control columns means that a large variety of control variables can be used, which do not have an obvious effect on the controlled device.

Another part of the hybrid Jacobian is the calculation of the block contributions of the individual devices. Provided that the block storage format is identical, then the Jacobian formation can be formed using the analytic approach. This decoupling allows the blocks to be calculated either analytically or numerically. This partial numerical calculation allows a new model to be easily integrated with other existing models with-

out requiring an immediate analytic Jacobian block, and without having to calculate the entire Jacobian numerically.

The above method also allows the potential use of a generic Jacobian block for a new device model. For example, a more accurate ac-dc converter model maybe developed, but the Jacobian could use the existing Jacobian of the simplified converter.

4.8 CONCLUSIONS

An algorithm capable of representing the majority of transmission systems containing non-linear devices has been presented. The solution iteration technique is that of a full Newton method. Positive sequence and three phase loadflows, which incorporate the full control structure, are used for the harmonic system initialisation. The linear busbars then are reduced to only the non-linear busbars at harmonic frequencies, with the loadflow left in full at the power frequency. The solution variables can be a hybrid phase and sequence components to minimise the number of Jacobian elements. Also, a variety of dc system configurations can be used to suit the different types of ac-dc non-linear device. A method was shown that simplifies the formation of the analytic Jacobian to allow fast computation, the resultant solution is fast and robust.

Chapter 5

APPLICATION OF THE HARMONIC DOMAIN ALGORITHM TO HVDC TRANSMISSION

5.1 INTRODUCTION

The contribution of HVdc links to steady-state system distortion is significant due to their non-linearity and high power transfer capability. For this reason it is important to accurately represent the harmonic generation of these installations. This chapter looks at the representation of HVdc links in the general harmonic solution.

5.2 BASIC STRUCTURE OF HVDC INTERCONNECTION

The following is a brief description of typical HVdc configurations and their control strategies. A more in depth description of HVdc transmission can be found in the book "High Voltage Direct Current Transmission" [Arrillaga 1998].

5.2.1 Different configurations

Four basic HVdc link configurations that are found in practice, i.e. monopole, bipole, back to back and multi-terminal. Mono-polar links typically have a single conductor line with the return path using the earth or sea via large electrodes. Bipolar links are typically designed as two independent parallel mono-polar links of opposite polarity with a master control that balances the dc currents. This can virtually eliminate ground return currents during normal operation, but still allows monopolar operation if one pole is removed from service. With back-to-back interconnections both converters are on the same site and the only dc side impedance is a smoothing reactor. This is often small for a variety of reasons, resulting in high harmonic interaction between the two ac systems. The final type of HVdc link involves multiple connection points of either rectifiers or inverters. There are a variety of reasons for using this style of link, both practical and economic.

Documents such as the "Guide for planning dc links terminating at ac systems locations having low short-circuit capacities" [CIGRE 14.07 1992] have tried to provide

a basis for the design of HVdc installations. However, the wide variation of ac systems and loading requirements result in each HVdc installation being unique. Many existing HVdc schemes have also been upgraded to meet new loading requirements, like the New Zealand hybrid upgrade [Gleadow *et al.* 1993]. This combines old existing technology with modern state of the art equipment, the result often being an interesting mix (Figure 5.1). To minimise the number of approximations that need to be made when modelling HVdc schemes in harmonic analysis, a general algorithm should be able to represent the installation complexity as completely as possible, rather than modelling the converters purely as a harmonic current source.

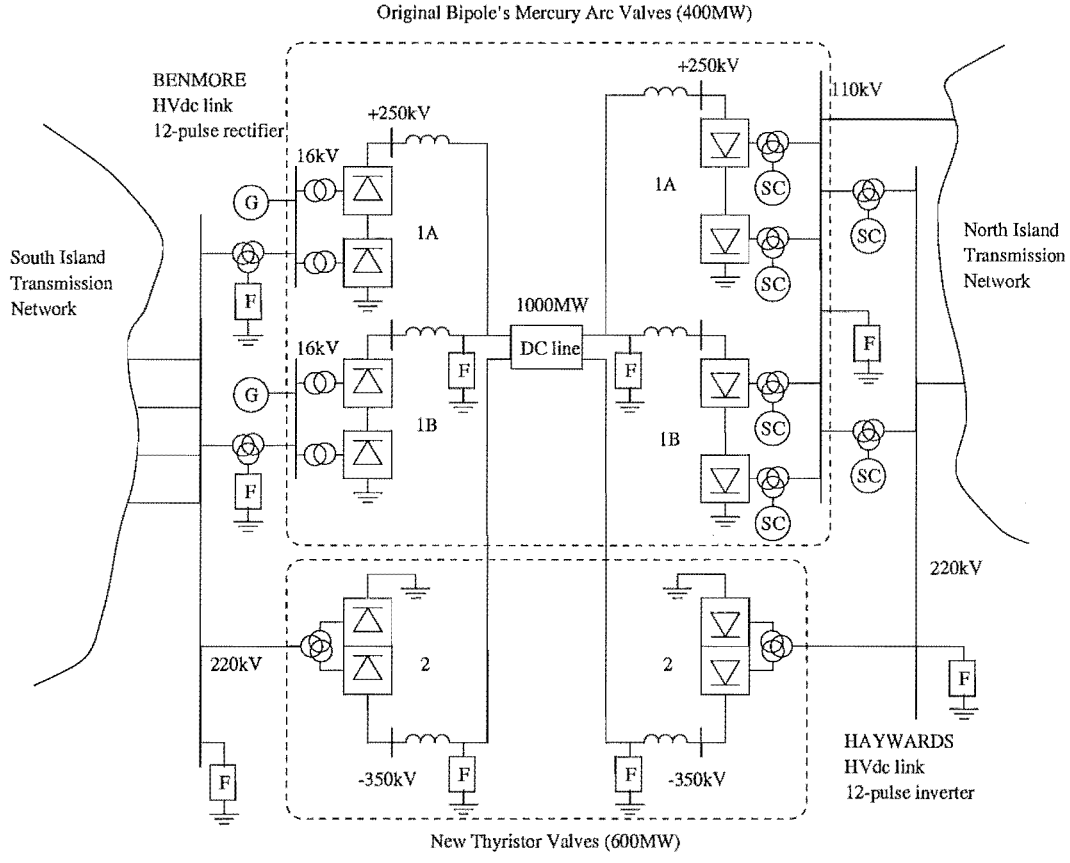

Figure 5.1 New Zealand HVdc link after the hybrid upgrade

Solution considerations for HVdc

When a simple two bus dc system is used, with no dc current leakage, the inverter and rectifier dc current is exactly the same. Moreover, if the rectifier is under constant current control, the dc current is not required as a variable in the solution. However in the New Zealand HVdc link (Figure 5.1), the dc current of the inverters of pole 1 are dependent upon the constant current injections of the rectifiers, the network impedance, and the voltage differential between them. As the dc voltages of the inverters are not known beforehand, the dc currents of the inverters must be represented as solution

variables. In this way, the solution of a multi-terminal HVdc link is structurally similar to the solution of an ac loadflow.

5.2.2 Basic HVdc controls

The full control structure of an HVdc link is very complicated due to the interconnection of steady-state, transient and protection strategies. It is generally sufficient for steady-state representation to simplify this structure down to the basic philosophy of the link operation, while maintaining the aspects important to steady-state analysis.

Typically an HVdc link is under some form of current control, usually specified by the rectifier. This controller will have some form of integral action so that the specified setpoint is reached and can usually be approximated by a simple PI (Proportional Integral) controller. The inverter maintains the link voltage by minimising its extinction angles, i.e. the time remaining after the end of commutation. This also has the effect of minimising the reactive power consumption of the inverter. While under ideal conditions it would be possible to minimise the extinction angle to virtually zero, this would make the inverter very vulnerable to any disturbance on the inverter or rectifier ac systems, thus resulting in a commutation failure. Most inverter controls specify a minimum angle of extinction that should be maintained during normal operation to minimise this risk. This control strategy is referred to as constant commutation margin control or minimum gamma control, where gamma is the angle of extinction.

These two controls represent the basic operation of an HVdc link where the inverter acts as a voltage source and the rectifier as a current source. This form of control is illustrated by the static characteristic shown in Figure 5.2. This characteristic has been modified to improve the dynamic performance by specifying non-optimal inverter firing angles. The characteristic shows the inverter operating nominally under constant dc voltage control, but can move into either minimum gamma or proportional current control if operating conditions require [CIGRE 14.07 1992]. The steady-state operation can be in any of these three conditions during non-ideal system conditions, and so the full control should be represented.

Improved representation can be achieved by the addition of further control blocks which specify various operating conditions for optimum or more realistic performance. The current control can be represented by a PI control loop where the firing angles are modulated by the dc current harmonics. Other extended controls such as the converter transformer tap-changer should also be modelled. The rectifier tap-changer is used to minimise the average firing angle of the converter to reduce its reactive power consumption while still maintaining sufficient voltage to ensure firing [Arrillaga 1998]. The inverter tap-changer controller is used to maximise the dc voltage which in turn, for a specified dc power transfer, will reduce the dc current and hence the real power losses. Finally a dc power controller can be used which adjusts the dc current setpoint

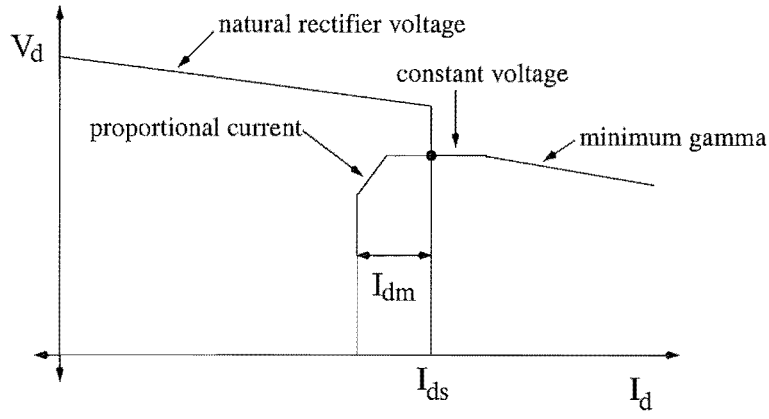

Figure 5.2 Three stage static control characteristic for an HVdc link

of the current controller to obtain a specified power transfer.

The back to back HVdc link at Chandrapur, India is operated under non-optimal minimum gamma to maintain a delicate reactive power balance in the inverter ac system. This critical control is partially achieved by means of a constant dc voltage control at the inverter end of the link [Andersen *et al.* 1998]. Therefore a variety of control strategies are required for realistic system simulation.

Figure 5.3 shows an HVdc link where the operating point is specified by four main parameters; power transfer, dc voltage, minimum gamma and average alpha. Five control equations are used to represent this comprehensive control.

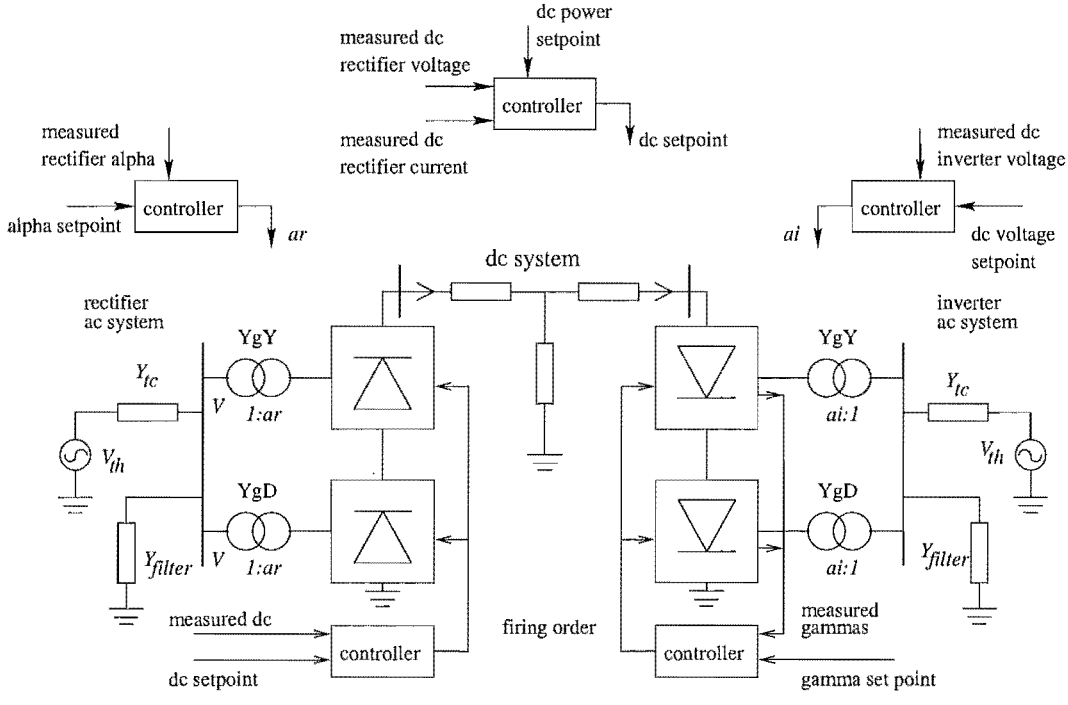

Figure 5.3 Block diagram of full control for an HVdc link.

5.3 HVDC LINK VALIDATION AND ALGORITHM PERFORMANCE

The CIGRE benchmark HVdc link test system [Szechtmann *et al.* 1991] is used to validate the HVdc link representation and demonstrate the performance of the Harmonic Domain algorithm. The system is simple, but operationally difficult due to the presence of strong resonances in the ac and dc systems. It consists of a two terminal 12-pulse monopolar HVdc scheme with thevenin equivalents of the ac systems and filters represented. The rectifier system with SCR=2.5 is used and full system details are shown in Appendix B.

The solution structure can be best explained with reference to the system Jacobian shown in Figure 5.4 and the description in Table 5.1. The converter busbars are expressed in sequence components which reduces the number of Jacobian elements significantly. While the sequence transformation of the Jacobian does require extra computation, the smaller number of elements reduces the computation required for the solution.

Table 5.1 Grid reference for Figure 5.4

Variables	Mismatches	Description
1	A	Rectifier AC busbar
2	B	Inverter AC busbar
3	C	Rectifier DC busbar
4	D	Inverter DC busbar
5	E	AC voltage source busbars
6	F	System control variables

The two ac systems are not synchronously connected and so there is no direct coupling between the two ac busbars represented by numbers 1 and 2. This is shown by the presence of two zero blocks in A2 and B1. The two dc busbars at 3 and 4 are directly coupled through the nodal analysis of the dc system and blocks C4 and D3 are the diagonal linear linking elements.

5.3.1 Algorithm convergence

The robust convergence of the Newton solution with independent rectifier and inverter systems has been previously reported [Smith *et al.* 1996] [Bathurst *et al.* 1996]. To illustrate the convergence properties of the algorithm when representing the full interconnected system, a variety of test cases as shown in Table 5.2, were performed. The results in Table 5.3 indicate that the method is robust and fast.

The three columns of Table 5.3 show the number of solution iterations, Jacobian updates required, and solution times for each of the cases. Each of the cases has three main stages, the positive sequence power-flow (PPF), the three phase power-flow (3PF)

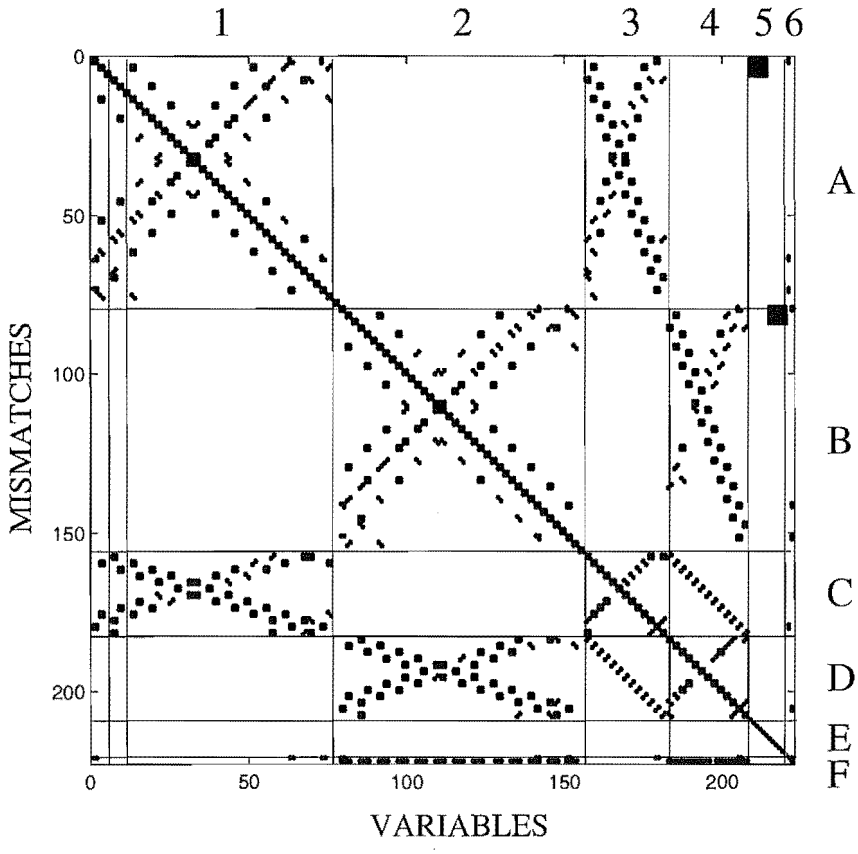

Figure 5.4 Jacobian of an HVdc link for 13 harmonics

Table 5.2 Cases used for convergence testing

Test Cases	
1	Balanced CIGRE basic control
2	Balanced CIGRE full control
3	5% of 2^{nd} harmonic
4	5% Inverter system imbalance
5	Rectifier and Inverter filters removed

and the full harmonic power-flow (HPF). The solution times are for a Sun SPARC-5 workstation with a 160MHz CPU.

5.3.2 Validation with time domain simulation

The time domain simulation package PSCAD/EMTDC [Woodford *et al.* 1983] has been used for validation of the harmonic domain model. The simulation used a time step of $10\mu s$ in double precision for 1.5 seconds and took approximately 30 minutes on the same machine. A window with a duration of one fundamental cycle was applied to the desired waveforms once the simulation had reached steady state. Using a custom component, the system information was written out to a file in full precision to avoid aliasing and discretisation problems.

Table 5.3 Comparisons of test systems

Test case	Solution iterations (PPF,3PF,HPF)	Jacobian updates (PPF,3PF,HPF)	Solution times
1	5,2,5	1,2,1	4.47s
2	8,3,6	4,2,1	6.56s
3	5,2,6	1,2,2	7.60s
4	6,5,6	2,4,1	4.91s
5	6,2,7	3,2,3	11.76s

The comparison is made using case 4 of Table 5.2, where a 5% phase imbalance is present in the inverter ac system. This results in significant non-characteristic harmonic generation by the inverter as shown in Figure 5.5. Figure 5.6 illustrates the effect of this imbalance on the rectifier ac system due to the interconnection of the two converters by the linear dc system.

The harmonic spectra rather than waveforms was used as, in the latter case, the precise harmonic magnitude and phase angle information is swamped by the dominant fundamental values. It should also be noted that the time domain simulation uses significant snubbers to minimise numerical oscillations. The excellent comparison shown illustrates the minimal effect that the snubbers have on the low order harmonics and so justifies the simplification of not including them within the harmonic domain analysis.

5.4 HARMONIC PERFORMANCE

5.4.1 Harmonic transfer through a back to back link

When the HVdc link is significantly long or has a large line impedance, the two ac systems can often be considered as harmonically independent. However, when the link impedance is very low as in the case of back to back installations, harmonics produced by one end directly affect the other. The representation of a back to back link can be achieved in one of two ways. A conventional nodal analysis can be used with numerical shunt resistors on the converter dc terminal busbars so that the system is non-singular. This however may lead to numerical problems due to the ill-conditioned nature of such a system, especially when the series impedance term is small. This can be avoided by the use of the hybrid dc analysis described in Section 4.4.2, when the system is being formed. One of the dc busbars is specified as a voltage harmonic busbar, the dc current harmonics of this busbar becoming the negative of the harmonic currents of the other dc busbar. The solution then continues as normal with the specified busbar using voltage harmonics as its solution variables instead of current harmonics.

To demonstrate the effect that the size of the smoothing reactor of a back to back link has on the harmonic transfer, the reactor is reduced by factors of 10 from 100H

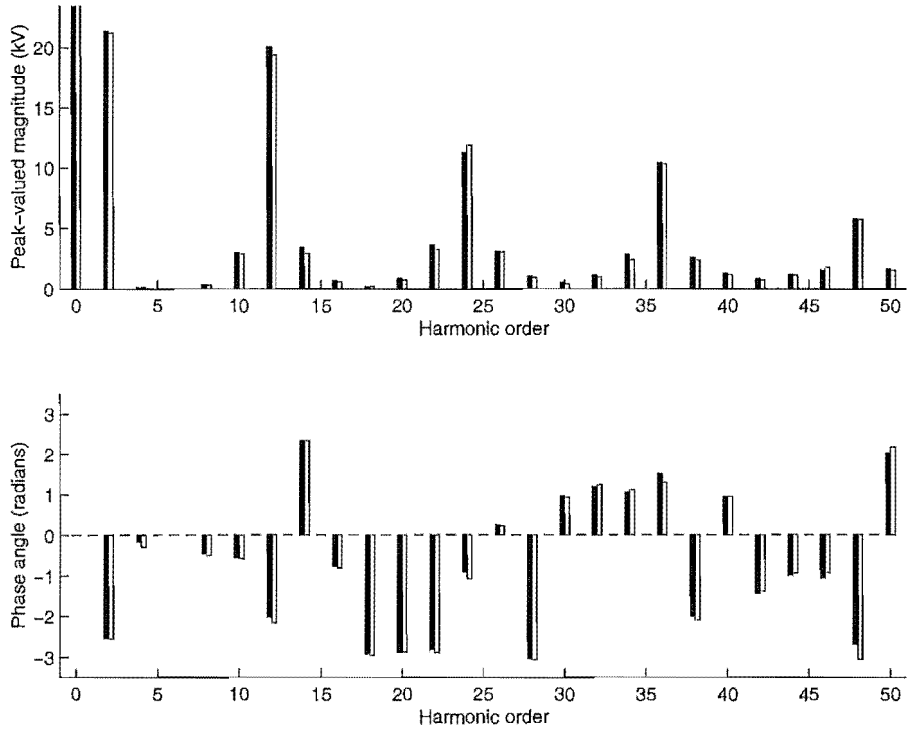

Figure 5.5 Inverter dc voltage harmonics for test case 4, (filled = EMTDC, empty = Harmonic Domain)

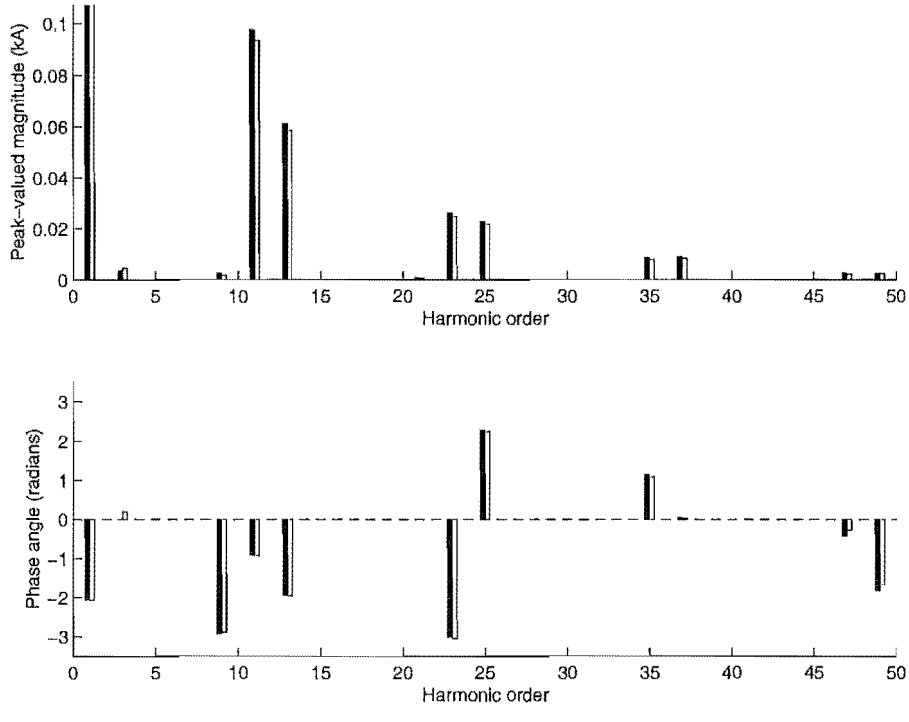

Figure 5.6 Rectifier phase A currents for test case 4, (filled = EMTDC, empty = Harmonic Domain)

to 1μH. For a balanced and undistorted case, this will have little effect as no uncharacteristic harmonics are generated. Figure 5.7 shows the characteristic harmonics of the rectifier ac system under ideal conditions. The test system used is again the CIGRE benchmark model but with the dc line replaced by a smoothing reactor.

With a small imbalance in one ac system, the other ac system also exhibits non-characteristic behaviour due to the harmonic transfer across the link. The two Thevenin voltage sources are controlled to maintain the converter terminal voltages at 1.0 pu positive sequence. An extra control equation is specified to vary the negative sequence component of the inverter source so that 0.02 pu negative sequence voltage is maintained at the inverter terminal busbar. This ensures the same converter operating points so that any changes in the levels of generated harmonics are due solely to the dc smoothing reactor change. The smoothing reactor is again reduced from 100H to 1μH and the results are shown in Figure 5.8.

The harmonic transfer through the link is dominated by a combination of the smoothing reactor and the transformer leakage reactances. With the smoothing reactor reduced to near zero, the dc harmonic currents are limited by the transformer leakage reactances and reach their maximum values.

5.4.2 Harmonic variation with operating point

The variation of harmonic generation comes from two main sources, the first is due to the changes in non-linear device operating points and the second from changes in the system impedances. An HVdc link is affected by a combination of the two sources simultaneously. As the specified dc power of the HVdc link increases, the operating point of the ac system changes, which can result in a change of the ac system impedance. Assuming for the moment that the ac load impedances have a negligible effect on the converter terminal busbar, Figure 5.9 illustrates the change in harmonic generation with power setting.

The link operating point is specified and maintained by seven control equations. These controls adjust firing angles to meet a specified minimum gamma and dc current, two tap changer controls to ensure efficient operation and two voltage source controls to maintain 1.0 pu terminal voltages. Finally, a link power controller is used to specify the dc current setpoint in the rectifier controller. The harmonic information is obtained by performing multiple harmonic solutions automatically with the dc power setpoint being reduced at each run. As the ac and dc systems are not changing between simulations, the system reduction is only performed once and each new iteration uses the previous solution as a starting point.

HVdc converters have reactive power support in the form of capacitor and filter banks. As the link power reduces, these components generate more reactive power than the converters are absorbing. Some filter banks are usually then disconnected, thus

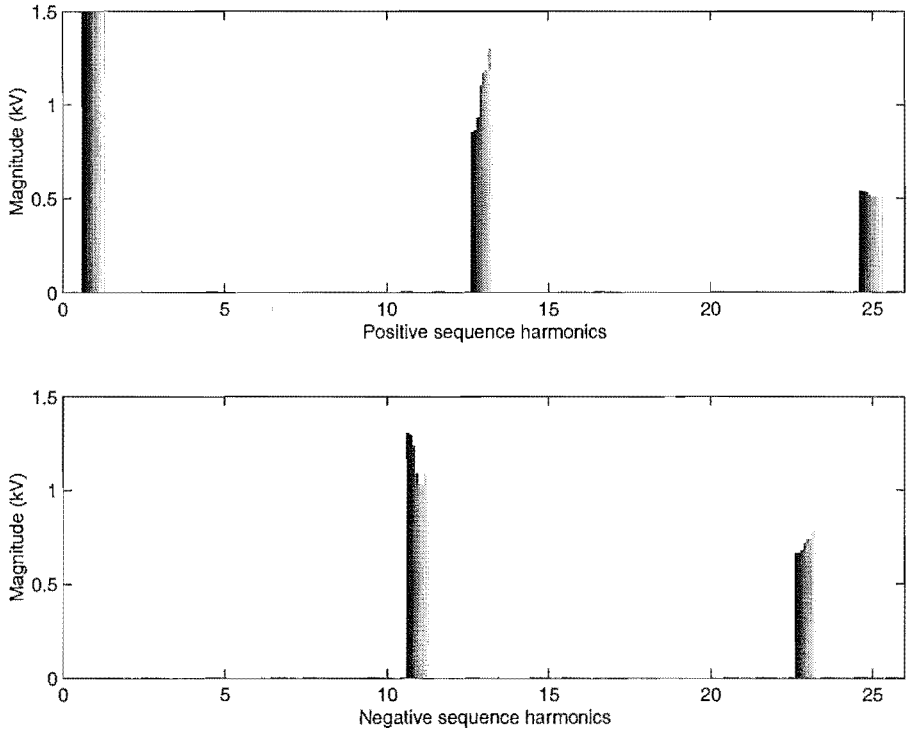

Figure 5.7 CIGRE back to back link rectifier ac voltage harmonics under balanced conditions with dc smoothing reactor reduced from 100H to 1μH

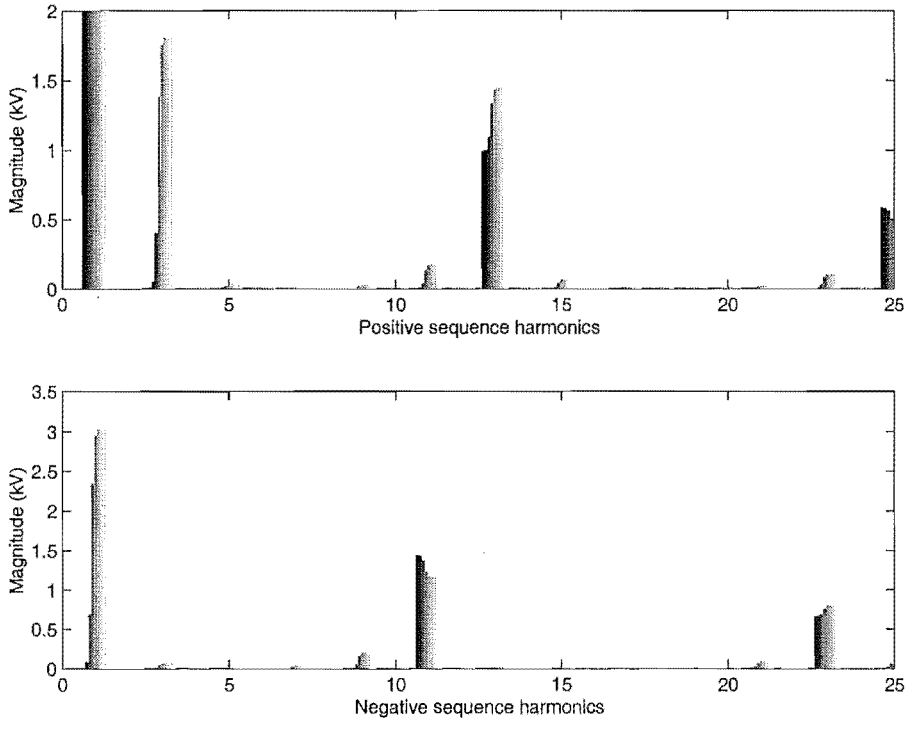

Figure 5.8 CIGRE back to back link rectifier ac voltage harmonics due to inverter negative sequence distortion with dc smoothing reactor reduced from 100H to 1μH

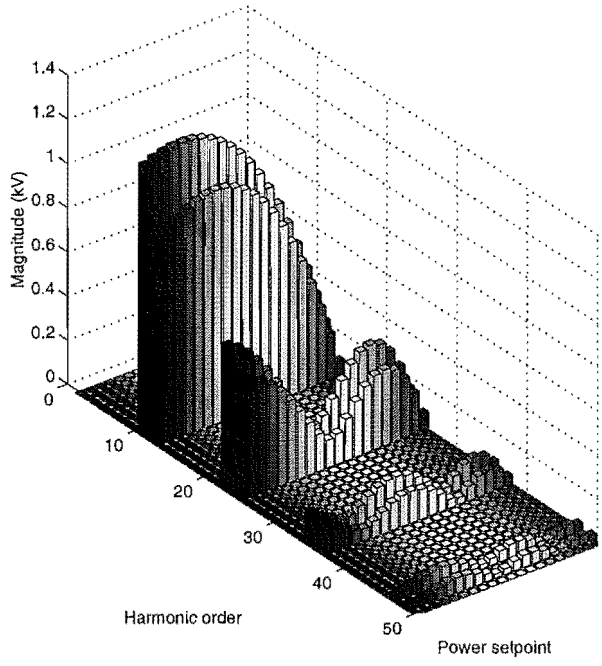

Figure 5.9 CIGRE rectifier ac voltage harmonics due to loading change

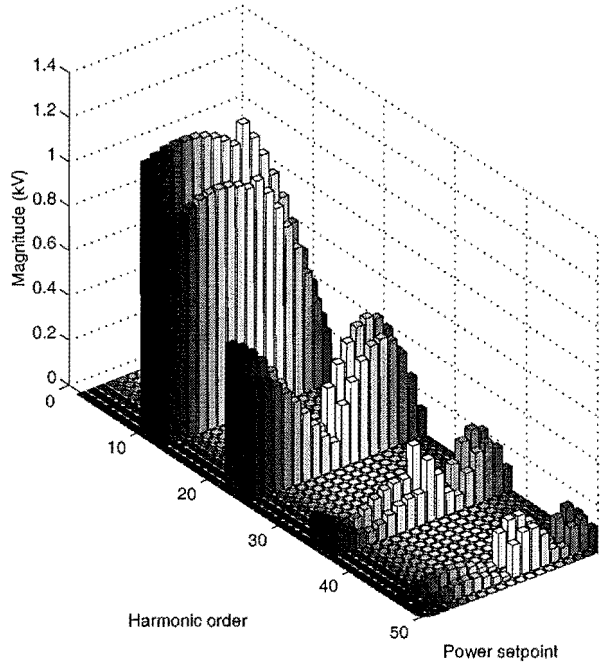

Figure 5.10 CIGRE rectifier ac voltage harmonics due to loading change, with only the type-3 filter in at half dc power

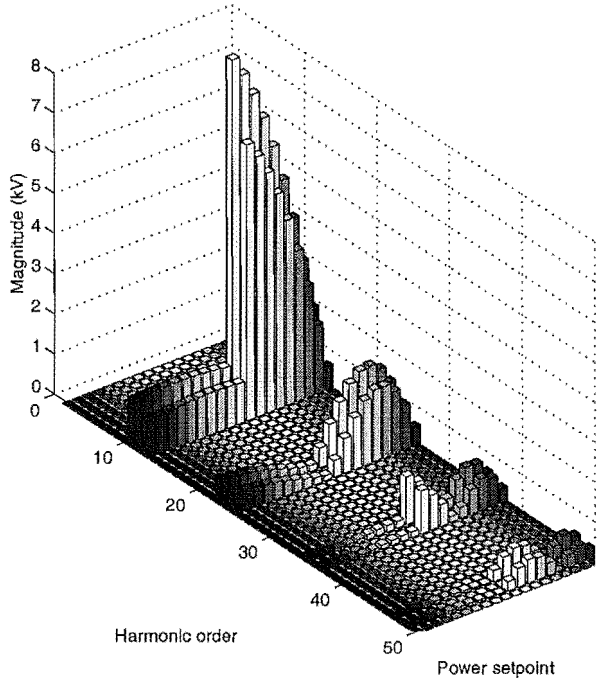

Figure 5.11 CIGRE rectifier ac voltage harmonics due to loading change, with only the type-7 filter in at half dc power

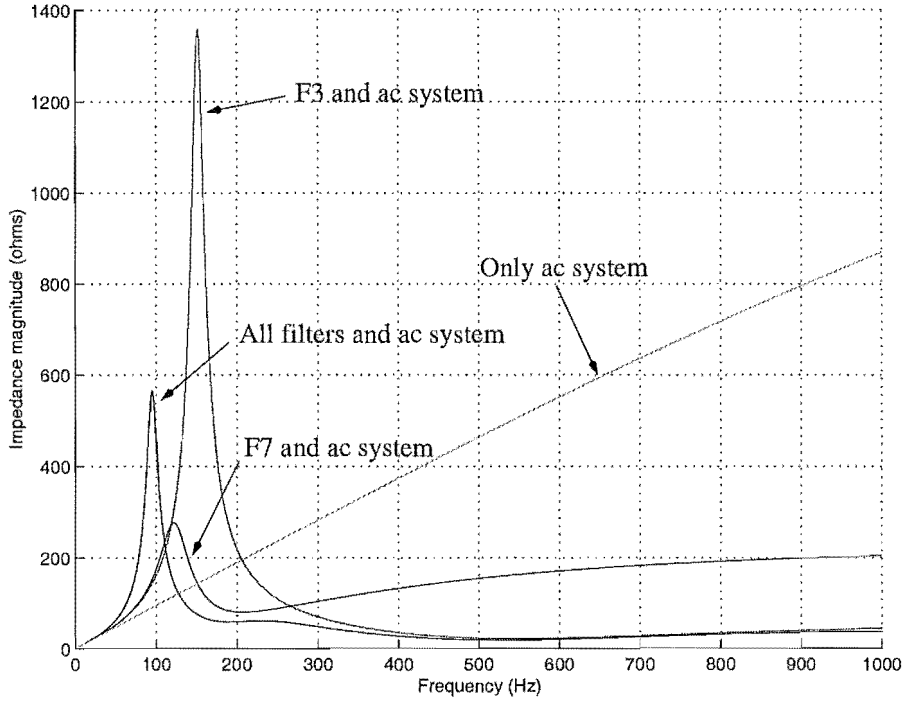

Figure 5.12 CIGRE rectifier ac system impedance variation with filter switching

altering the ac system impedance (Figure 5.12). The previous simulation is repeated but with the filters, as defined in Appendix B, being switched out at half dc power. As Figures 5.10 and 5.11 show, this results in an abrupt change in the voltage harmonic levels at the rectifier terminal. The low order parallel resonance in the ac system is also affected by the combination of filters that are in service. When only the type-3 filter is left in service, the parallel resonance is very close to the third harmonic. Any small amount of fundamental frequency imbalance will result in a significant level of third harmonic voltage. This filter switching combination should therefore be avoided.

5.4.3 Harmonic variation with system frequency

Frequency shifts are not significant for the vast majority of power systems. In special cases, like a remote or islanded generation connected to the system via an HVdc link, it may be desirable to allow the generator frequency to shift to allow optimum turbine operation. Such a case has been proposed for the unit connection of a generator directly to an HVdc converter without filters. As the impedance of this system is very inductive, a wide range of harmonic voltages should be apparent under different operating speeds.

To demonstrate the effects of fundamental frequency variation, two different test systems based upon simplified versions of the CIGRE benchmark system are used. The first system represents the rectifier system in full, but approximates the inverter end of the link by a constant dc voltage source. The second is similar but replaces the rectifier ac system completely with a unit connected salient pole generator. In both cases the ac system frequency is varied from 45Hz to 55Hz and the terminal voltage harmonics are shown in Figures 5.13 and 5.14 respectively. The ac voltage source is controlled in both cases to keep the converter terminal voltage at 1.0 pu.

The changes in the harmonic voltages are mainly due to the varying commutation angle as the commutating reactance increases with the fundamental frequency. Other influencing factors are the frequency dependent admittances and harmonic filters detuning (Table 5.4). All these effects are inherently included in the solution process. As the algorithm works within a per-unit frequency base, the actual frequencies are only required during the initial impedance/admittance calculations.

Table 5.4 Characteristic frequency deviation

Harmonic	f_{range} (Hz)	Δf (Hz)
1	45-55	10
12	540-660	120
24	1080-1320	240
36	1620-1980	360
48	2160-2640	480

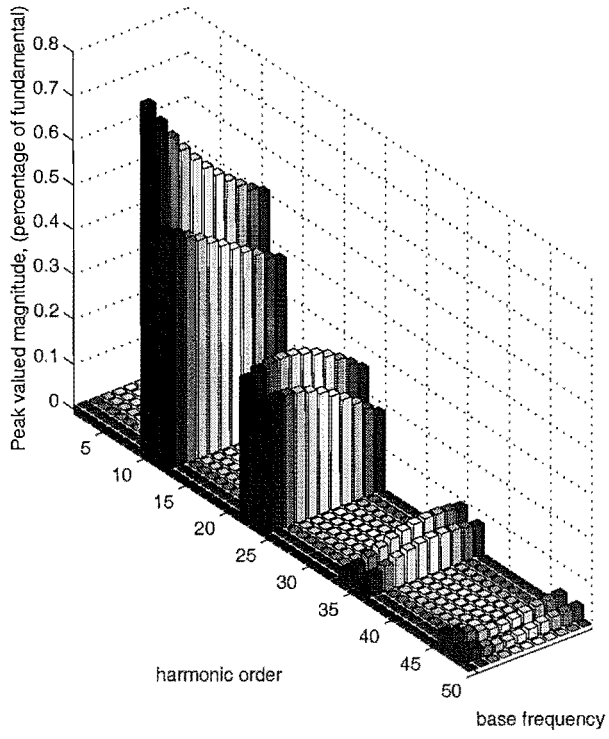

Figure 5.13 CIGRE rectifier ac voltage harmonics with off-nominal base frequency (45-55Hz). Controlled voltage source

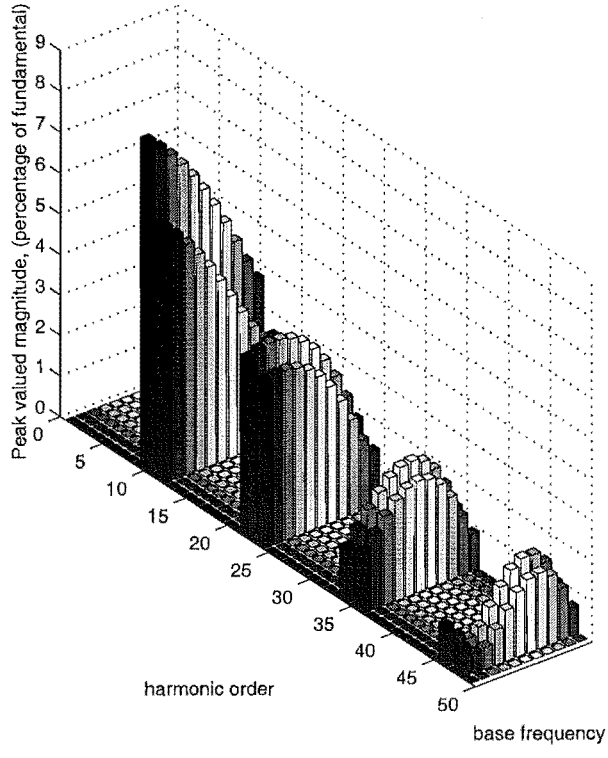

Figure 5.14 Unit connected generator with base frequency variation (45-55Hz)

5.4.4 Harmonic voltage variation with system loading

The changing nature of the power system must be accounted for when performing harmonic studies. As has been previously reported, the harmonic generation of a converter depends on the operating point and on the ac and dc system impedances. The ac system impedance typically changes with time in two major ways. The first is due to changes in the system loading as the active and reactive power drawn usually dictates the harmonic impedance of the load. These changes in the harmonic impedance of the system will affect the harmonic generation of the non-linear devices, and consequently the harmonic profile of the system. The second major source of system impedance variation is topological change which occurs when transmission lines are switched in and out of service. This has an immediate effect on system resonances.

The test system used here is based on the lower South Island power system of New Zealand as shown in Appendix B. It is a useful test system due to its natural imbalance and to the presence of a large power converter situated at the Tiwai-033 busbar. Apart from the converter installation, the system includes two large mixed residential and industrial loads at Invercargill-033 and Roxburgh-011 which vary significantly over the daily period. The harmonic voltages within the system will then be affected by the changes in this loading.

Use is made of the multiple run feature of the algorithm, with the main system data loaded only once. An initial full harmonic solution is obtained, harmonic penetration performed and the resulting harmonic voltages and currents stored. The change in loading information for the new period is read from a data file and a new solution obtained. The process is repeated automatically until all loading cases have been completed. The harmonic voltages for the system were obtained for a 24 hour period and a representative selection of harmonic profiles at four of the system busbars is shown in Figure 5.15. This illustrates the effect of passive system loading changes on the harmonic voltages of a system.

5.5 MODELLING BI-POLAR HVDC LINKS

Most HVdc installations are operated as bi-polar links which minimises the total earth return current. In this configuration, one of the poles has a positive voltage with the dc current flowing from the rectifier to the inverter. The other has a negative voltage with the dc current flowing from the inverter to the rectifier, this results in a nett power transfer from the rectifier ac system to the inverter ac system. The harmonic interaction across the link will be affected by the mutual coupling between the two pole conductors of the transmission line. The need to represent the coupling effect in the harmonic analysis of the HVdc transmission lines is advocated in a recent CIGRE document [Testi 1993], but no indication is given of its relative importance. The effect

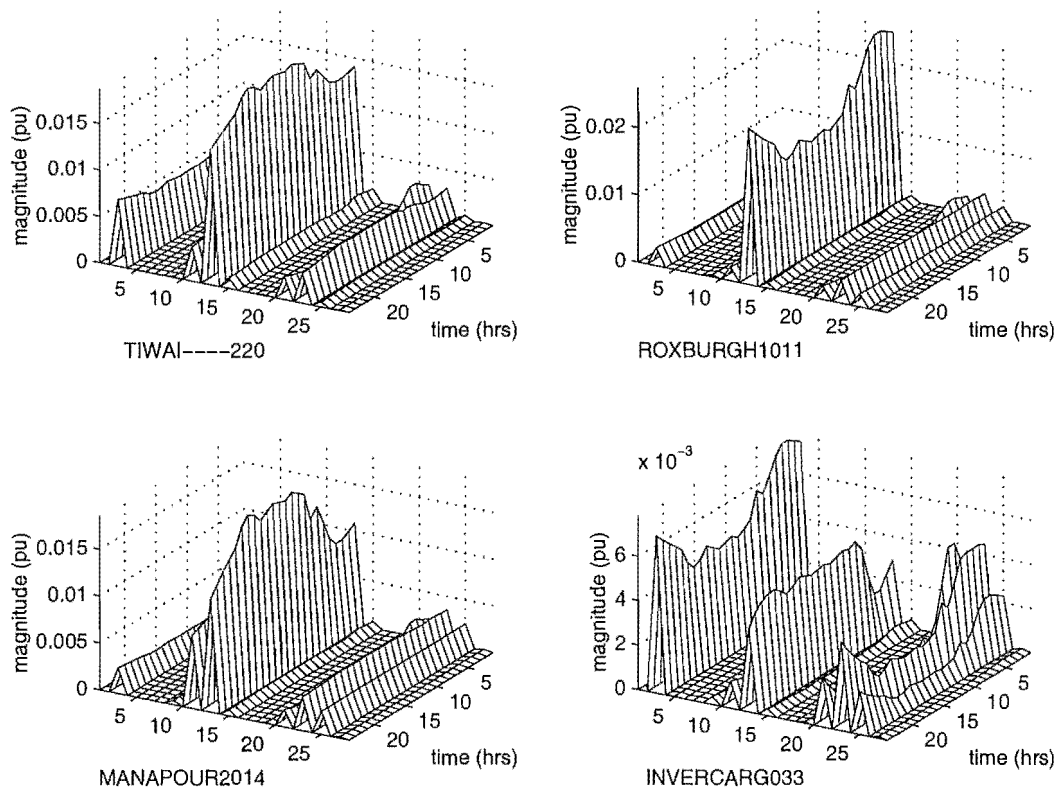

Figure 5.15 Harmonic voltage profile for a 24 hour period

of correct representation of the dc line on the ac-dc system harmonics is investigated by incorporating a frequency domain dc line.

The CIGRE HVdc link test system [Szechtmann *et al.* 1991] has been modified so that a bi-polar operation is achieved. The monopole is split into two poles by reducing the power bases of the converter transformers from 598MVA to 299MVA and the average dc current from 2.0kA to 1.0kA. The dc system power base is halved so that the effective operating point of each pole remains the same. Each pole is individually controlled so that different operating points can be specified. The representation of the bi-polar link has been validated against time domain simulation to a similar degree of accuracy as described earlier for the CIGRE HVdc link. This was done to verify that the dc system handling and converter orientation approach was working correctly (Figures 5.16 and 5.17).

5.5.1 The bi-polar transmission line

The model of a dc transmission line can be simply calculated using conventional multi-conductor transmission line theory [Arrillaga 1997]. Only two conductors are required for a twin circuit line, instead of six for an ac twin circuit line. Little extra effort is required to include the harmonic mutual coupling between the positive and negative

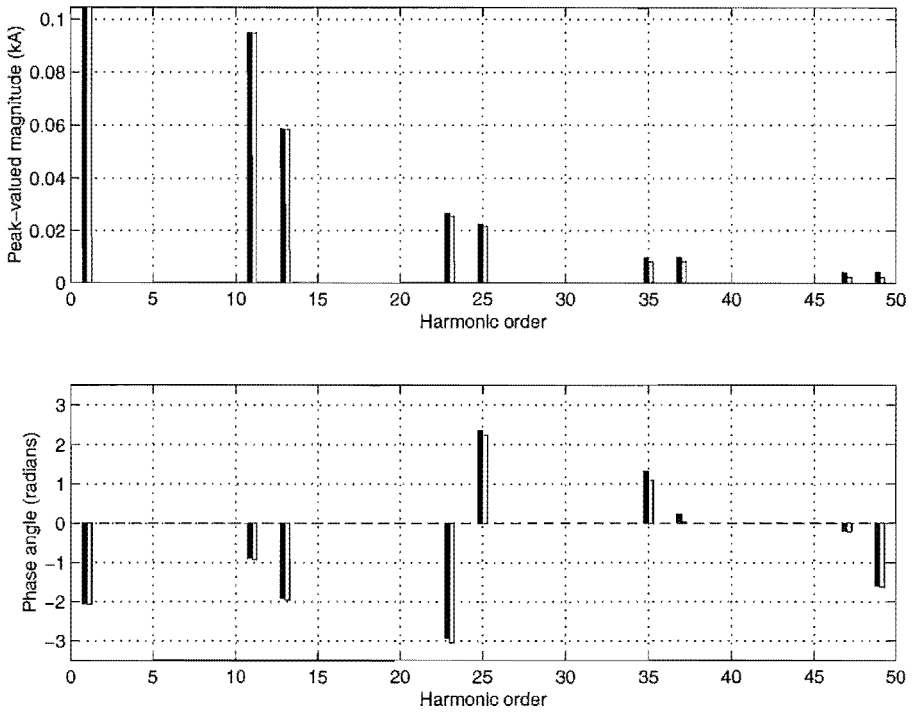

Figure 5.16 Rectifier ac current harmonics using the CIGRE dc systems. (PSCAD=left, HD=right).

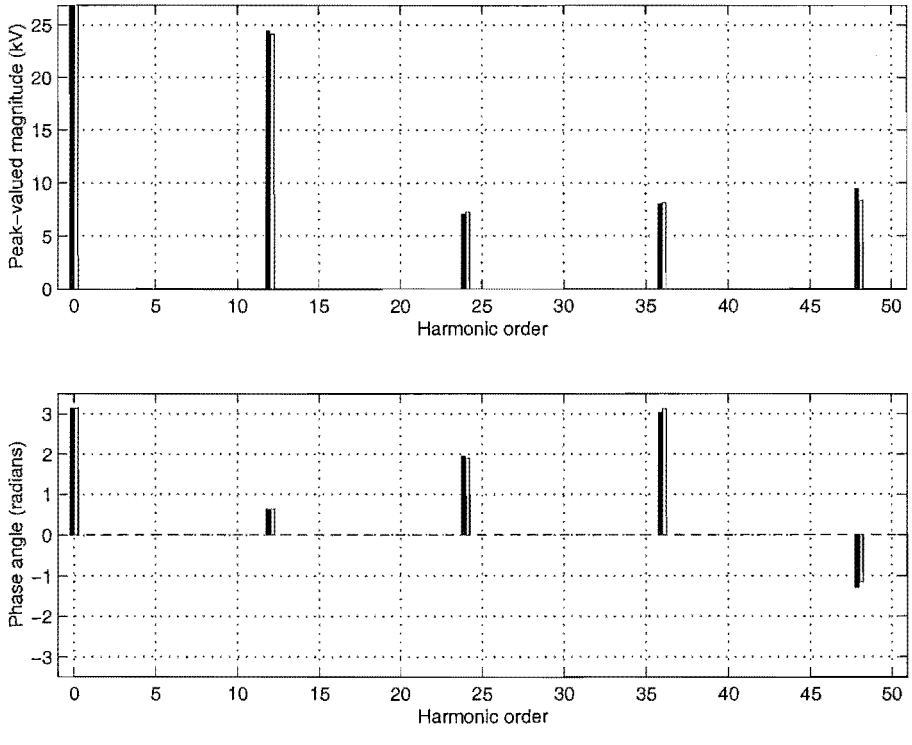

Figure 5.17 Voltage harmonics at the dc terminal of the negative pole inverter using the CIGRE dc systems. (PSCAD=left HD=right)

poles of a bipolar configuration. A section of the New Zealand HVdc line is used for the bipolar test system [Eggleston 1985], with tower and conductor geometry shown in Figure 5.18.

DC resistance	0.0351Ω /km
Diameter	38.4mm
Bundle Spacing	431.8mm
GMR	19.2 mm
Skin ratio	0.3849
Length	200km
Mid span sag	5m
Ground Resistivity	100Ω -m

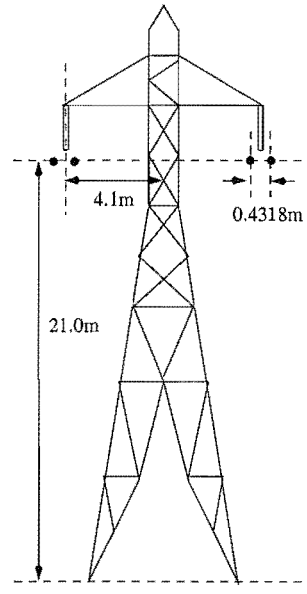

Figure 5.18 Twin circuit DC transmission line

A comparison between time domain and harmonic domain representation is shown here to illustrate the need for a frequency domain model. The comparison is made by shorting the receiving end of the dc line to ground and injecting a one per-unit current into the sending end which is left open circuit. The calculated short circuit impedance is shown by Equation 5.1, where Z_{series} and Y_{shunt} are the series and shunt terms of the bipolar equivalent pi model.

$$Z_{sc} = \frac{1}{(1/Z_{series} + Y_{shunt}),} \tag{5.1}$$

The time domain representation of the frequency dependant transmission line in PSCAD/EMTDC [Manitoba HVdc Research Centre 1988] is achieved by a complicated curve fitting process. As the resulting time domain equivalent is originally derived from frequency domain data, the frequency domain representation can be considered to be the more correct of the two.

The results of Figure 5.19(a) seem to indicate that the time domain model of the transmission line is adequate. The actual error introduced by the time domain curve fitting though, is shown as a percentage difference in Figure 5.19(b). The crosses in Figure 5.19(b) indicate harmonic frequencies and the circles highlight the characteristic 12-pulse harmonic frequencies. As the errors due to the time domain curve fitting are significant, the frequency domain model is preferred for accurate harmonic assessment.

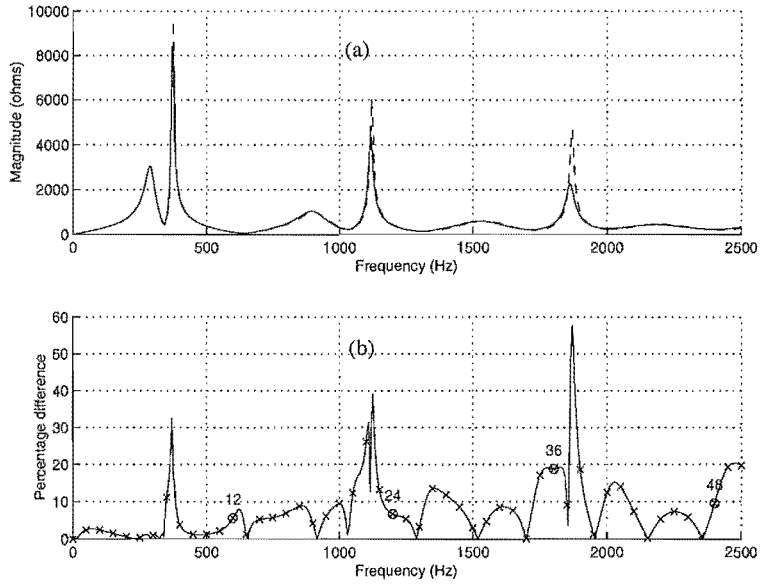

Figure 5.19 Comparison of the direct short circuit impedance of the dc transmission line between time domain and frequency domain representation. (a) Impedance magnitude (dashed=frequency domain, solid=PSCAD/EMTDC), (b) Percentage difference.

5.5.2 Effects of mutual coupling

To assess the effect of representing the mutual coupling between the conductors, the bipolar line described previously is divided into two monopolar lines, each of one conductor placed on separate towers. The bipolar and two monopolar lines replace the dc lines of the modified CIGRE benchmark model used previously.

Transmission line resonance shifts

The dominant effect of the mutual coupling representation is a shift in the resonant frequencies of the line transfer impedances. Figure 5.20 illustrates this shift by comparing the transfer impedances of the monopolar (single circuit) and bipolar (twin circuit) lines.

If a series resonance exists in the transfer impedance at a characteristic harmonic, large harmonic currents will flow between the two HVdc converters. This is very undesirable due to the typically long distances that HVdc lines span. Also, previous experience has shown that the transfer of the dc impedance can significantly effect the nett system impedance at the ac side. Thus an accurate representation of the dc system is important for the full system behaviour.

Effect of dc mutual coupling on harmonics

The representation of the mutual coupling of the dc transmission network produces transfer and shunt impedances different from those of two independent lines. As the

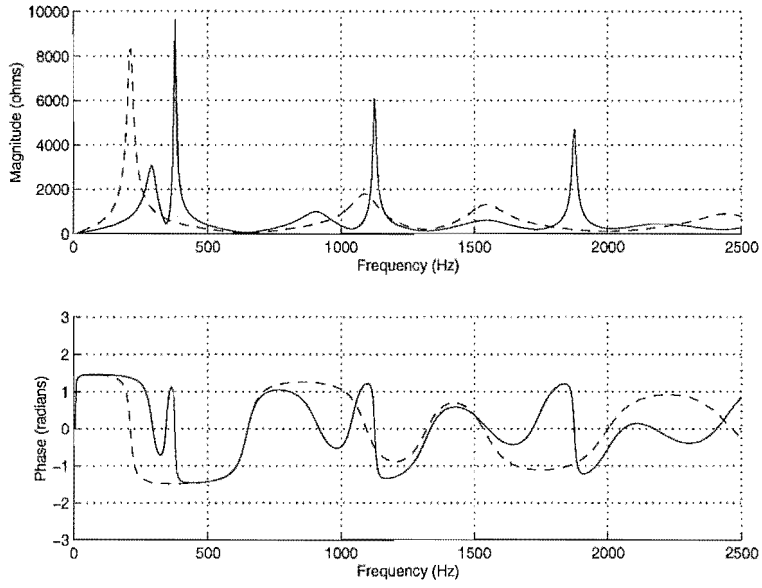

Figure 5.20 Effect of mutual coupling on transfer impedance of a dc transmission line (solid=twin circuit, dashed=single circuit).

resonance points are different, the harmonic interaction between the two ends of the link will also change.

The positive pole rectifier dc voltage harmonics for the two dc systems are shown in Figure 5.21, which shows that mutual coupling has a considerable effect on the dc voltage harmonics. Conversely, the effect of mutual coupling on the ac current harmonics is less significant, even under unbalanced ac system conditions. This is shown in Figure 5.22 for the case of a 5% phase imbalance on the inverter ac system.

Effect of smoothing reactors on link impedance

Most HVdc links use smoothing reactors between the converters and the transmission lines. The main effect of the smoothing reactor is to shift the resonant points as shown in Figure 5.23. As the parallel and series resonances still exist, transmission line coupling should still be represented for accurate harmonic assessment, even if smoothing reactors are present.

5.6 CONCLUSIONS

The representation of common types of HVdc configurations has been shown, using the general harmonic solution algorithm. Both basic and higher levels of control functions can be implemented, so that realistic systems can be modelled. The CIGRE HVdc benchmark system has been used for validation against time domain simulation and excellent solution performance has been demonstrated.

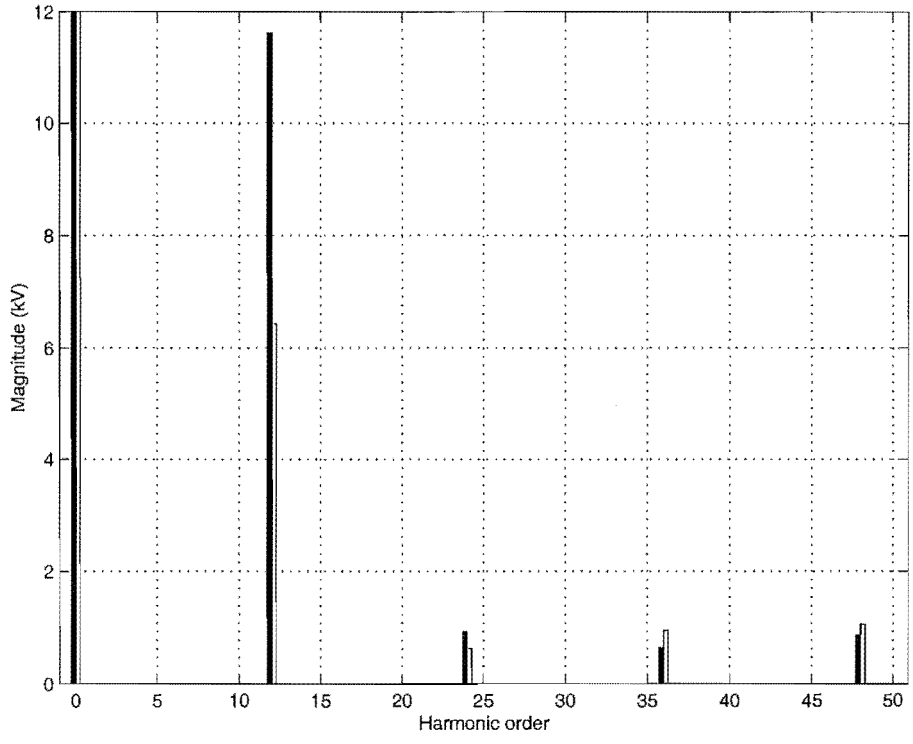

Figure 5.21 Positive pole rectifier dc voltage harmonics for dc line comparisons. (left=single circuit, right=twin circuit)

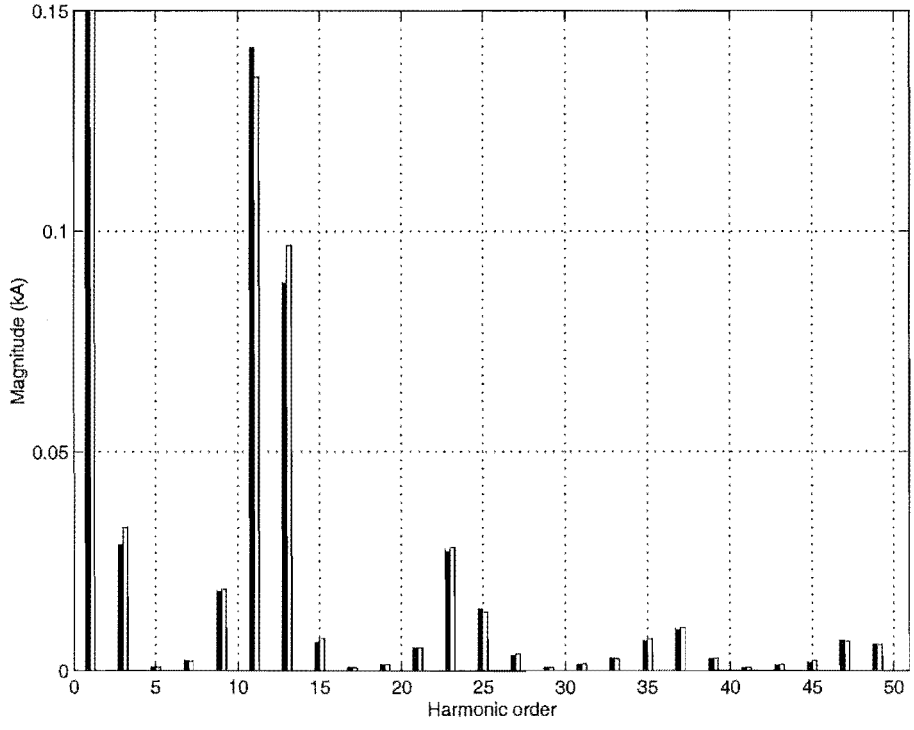

Figure 5.22 Inverter phase A current harmonics; comparison between single and twin circuit representation (left=single circuit, right=twin circuit)

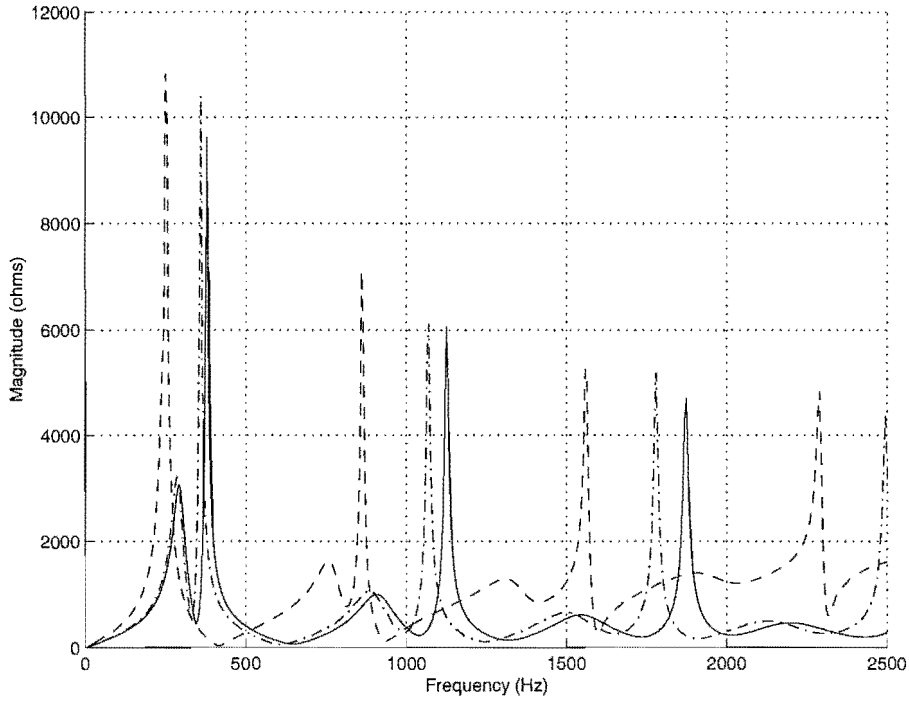

Figure 5.23 Change in self impedance due to smoothing reactors (solid L=0.0H, dash dot L=0.01H, dashed L=0.1H)

The algorithm has also been used to illustrate the variation of harmonic transfer with smoothing reactor size, through a back to back link. With this configuration, maximum harmonic levels are reached which are dictated by the leakage reactances of the converter transformers. The harmonic generation of HVdc links has been shown to be very dependent upon dc power transfer, local filtering conditions, ac system frequency, and the passive ac system loading. These investigations were carried out efficiently using the multiple run feature of the harmonic solution algorithm.

Using the accurate representation of the dc system for bipolar HVdc links has shown that the representation of mutual coupling between the positive and negative poles results in the resonant points of the transmission line being shifted. This coupling has a significant effect on the dc side harmonics and must therefore be taken into account at the design stage. As well as shifting the parallel and series resonances of the dc system, the smoothing reactors increase the impedance magnitude at the series resonant points. This effect will reduce, the harmonic interaction between the two ends of the link, but does not negate the need for accurate dc system representation. The initial results indicate that the dc mutual coupling does not have a major effect on the ac current harmonics of the converters. It may therefore be possible to develop a simplified equivalent of the bipolar link for ac system studies. This would significantly reduce the amount of computation required for the full harmonic solution.

Chapter 6

HIGH PULSE LVDC INSTALLATIONS

6.1 INTRODUCTION

Reduction of harmonic levels is usually achieved by tuned filters or high converter pulse numbers, the latter reduces the harmonic generation of the installation. HVdc installations are limited to 12-pulse configurations as all transformer connections are at high voltage, and so large system harmonic filters are required. For installations such as Aluminium smelters, the transformer secondaries are at sufficiently low voltages to make harmonic elimination by transformer connections a cost effective alternative to ac system filters. In practice however, these configurations produce non-characteristic harmonics due to non-ideal conditions [Yacamini and de Oliveira 1980] [Anderson and Wood 1997].

It has been observed that the characteristic dc current harmonics of an individual 6-pulse converter increase with the pulse number of an installation due to interaction through the dc system. Therefore the calculation of these harmonics requires an accurate representation of the different transformer configurations feeding the parallel connected converter bridges.

This chapter starts by observing the characteristics typical of a parallel connected LVdc installation. It then continues with a method for reducing the pulse number of an installation during outage situations, to minimise low order harmonic generation.

6.2 DEVELOPMENT OF LVDC HIGH CURRENT REPRESENTATIONS

In the parallel configuration of Figure 6.1, the converters are linked via a nodal analysis of the dc system. Previous models have used the dc current harmonics as solution variables, as these are generally the least distorted; this choice also simplified the analytic Jacobian. However, this selection requires inversion of the dc system admittance matrix. With an ideal current source (i.e. $Y_c = 0$), the admittance matrix of the dc system of Figure 6.1 becomes singular, thus requiring the formulation described in Sec-

tion 4.4.2. This formulation does not require matrix inversion and therefore the shunt Y_c can be omitted in the numerical solution.

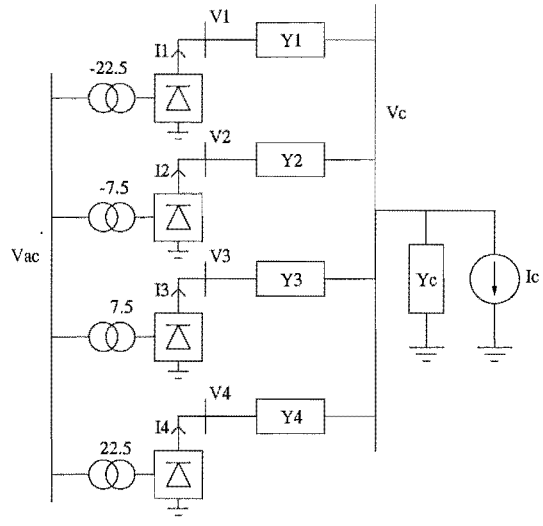

Figure 6.1 24-pulse configuration with parallel dc connection.

The dc current sharing between the uncontrolled converters is determined by the relative dc voltages across the linking impedances. As the dc voltages change during the solution, the dc currents must be used as solution variables.

6.2.1 Validation of the zigzag transformer

The test system, described in Appendix B, involves a single 6-pulse converter with a 15^o phase shift and an inductive ac system containing a 10% positive sequence third harmonic voltage component. This, combined with the significant dc ripple due to the resistive dc system, excites the non-linear transfers of the converter and generates non-characteristic harmonics. The PSCAD/EMTDC and harmonic domain results, shown in Figure 6.2 for the current in phase A of the six-pulse converter, are seen to be practically identical.

6.3 CHARACTERISTICS OF A PARALLEL CONNECTED SYSTEM

With reference to the configuration of Figure 6.1, this section illustrates the operating characteristics of a high pulse installation under ideal and slightly non-ideal conditions. A low impedance ac source is used in most cases to isolate the basic characteristics of the high-pulse parallel installation.

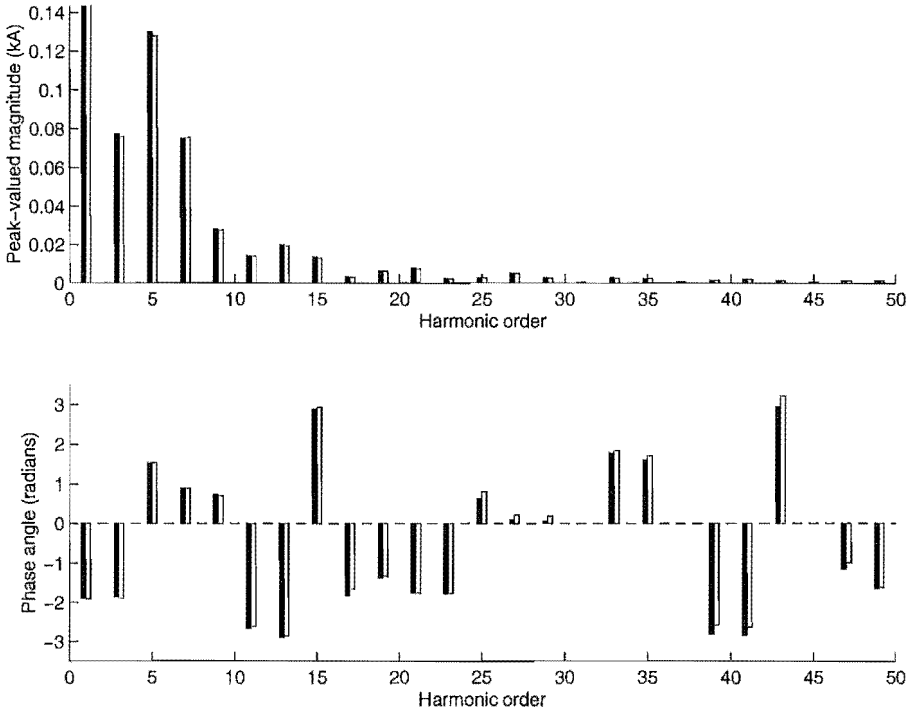

Figure 6.2 AC phase current for 15^o zigzag converter transformer (Black=Time domain, White=Harmonic domain)

6.3.1 Characteristics under ideal conditions

Figure 6.3 shows the primary phase current of a 6-pulse group for the case of a parallel 24-pulse configuration with an ideal dc current source at the common busbar (Appendix B). The dashed waveshape is the phase current for the -22.5^o phase shifted converter when the linking impedance is very large, which results in virtually no dc interaction between the four converters. When the linking impedance is very small (1μH), the different instantaneous dc voltages of the converters cause large circulating currents, which distort the ac current waveshape, as shown by the continuous line.

The left-hand section of Table 6.1 shows the characteristic dc current harmonics of an individual 6-pulse converter as the pulse number of the installation increases. For comparison, the normal pattern associated with series connected converters is also shown in the right-hand section of Table 6.1.

As the series pulse number increases, the number of characteristic current harmonics decreases, leading to a smoother dc current. However in the parallel connection, the phase shift causes a voltage differential across the linking impedance. This results in the number of characteristic dc harmonic currents, in the converter bridges, increasing with the installation pulse number rather than decreasing. This is an important consideration to be taken into account in the design of such installations, as at the least, it will result in increased heating losses.

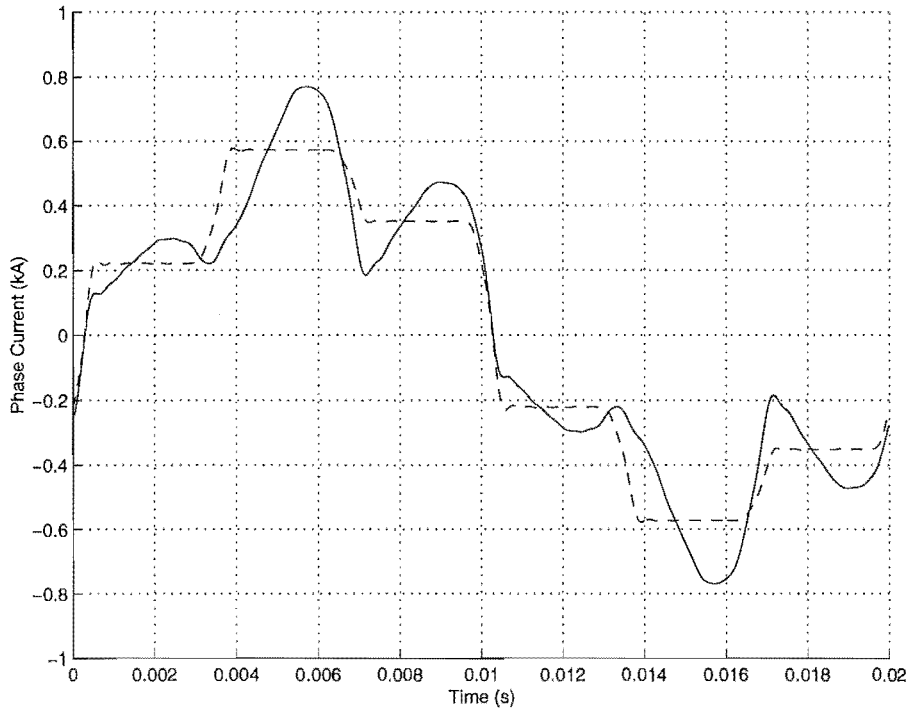

Figure 6.3 AC primary phase current for a -22.5° zigzag connected converter in a 24-pulse parallel installation: Dashed=Large linking impedance, Solid=Small linking impedance.

Table 6.1 Characteristic dc current harmonics of the 6-pulse group in parallel (p) and series (s) connection.

harmonic	12(p)	24(p)	36(p)	48(p)	12(s)	24(s)	36(s)	48(s)
6	0.2326	0.2355	0.2352	0.2352	—	—	—	—
12	—	0.0411	0.0410	0.0410	0.0283	—	—	—
18	0.0129	0.0143	0.0143	0.0143	—	—	—	—
24	—	—	0.0076	0.0077	0.0079	0.0073	—	—
30	0.0055	0.0055	0.0054	0.0055	—	—	—	—
36	—	0.0042	—	0.0042	0.0032	—	0.0028	—
42	0.0028	0.0030	0.0030	0.0031	—	—	—	—
48	—	—	0.0022	—	0.0019	0.0018	—	0.0016
54	0.0016	0.0016	0.0016	0.0017	—	—	—	—
60	—	0.0014	0.0014	0.0014	0.0012	—	—	—
66	0.0012	0.0012	0.0012	0.0012	—	—	—	—
72	—	—	—	0.0010	0.0009	0.0008	0.0008	—
78	0.0009	0.0009	0.0009	0.0009	—	—	—	—
84	—	0.0008	0.0008	0.0008	0.0006	—	—	—
90	0.0007	0.0007	0.0007	0.0007	—	—	—	—
96	—	—	0.0006	—	0.0004	0.0004	—	0.0004
102	0.0005	0.0005	0.0005	0.0005	—	—	—	—

6.3.2 Effect of winding ratio inaccuracies

The effectiveness of harmonic cancellation by transformer phase shifting is dependent upon the accuracy of the actual phase shifting. To illustrate this effect the transformer providing the 22.5^o phase shift for a 24-pulse (4-unit) installation is mis-wound on the n_2 winding by 1%, which causes a 0.4^o change in the angle of shift. As a result significant 6-pulse characteristic harmonics are generated which affect the commutation durations of each 6-pulse group differently. As Table 6.2 shows, this results in different dc currents, and load sharing between the converters.

Table 6.2 Effect of winding ratio differences on a 24-pulse installation.

Group	X_T (pu)	μ (deg)	$I_{dc}(0)$ diff (%)
22.9	0.050	13.645	+0.10
7.5	0.050	13.972	+0.42
-7.5	0.050	13.812	+0.04
-22.5	0.050	13.809	-0.58

6.3.3 Effect of leakage reactance differences

Harmonic cancellation also requires that the operating points of all the converters should be identical. A difference in the transformer leakage reactances will result in different commutation durations and hence operating points. Such a case is illustrated in Table 6.3 where the leakage reactance of the -7.5^o transformer has been increased by 2% with respect to the others. The results show that this asymmetry also upsets the power sharing between the individual converter groups.

Table 6.3 Effect of unequal leakage reactances on a 24-pulse installation.

Group	X_T (pu)	μ (deg)	$I_{dc}(0)$ diff (%)
22.5	0.050	11.446	-1.46
7.5	0.050	11.432	+0.36
-7.5	**0.051**	11.400	-1.54
-22.5	0.050	11.440	+0.66

6.3.4 Effect of fundamental voltage imbalance

Owing to transmission line and loading asymmetry, the fundamental busbar voltages are not perfectly balanced and harmonic currents of non-characteristic orders will be produced. This effect is illustrated in Figure 6.4 for the case of a 2% negative sequence component, where the unbalance causes the converter installation to generate considerable sideband non-characteristic harmonics. In particular, the third harmonic is seen to reach similar levels as the first set of characteristic harmonics (23^{rd} and 25^{th}).

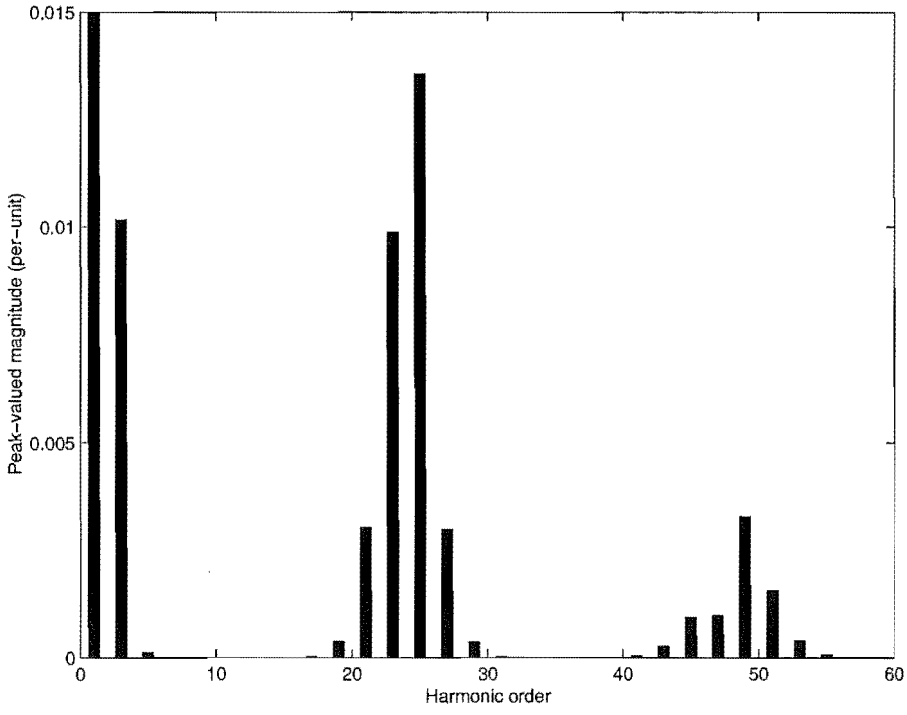

Figure 6.4 Phase current harmonics with a 2% negative sequence fundamental terminal voltage distortion.

As the third harmonic present is generated from the negative sequence fundamental it will be a positive sequence harmonic. This will then not be trapped by delta windings like a zero sequence harmonic and so will be able to propagate though the ac system.

6.4 PULSE REDUCTION OF A HIGH PULSE INSTALLATION

Most low voltage installations such as Aluminium Smelters use on-load tap-changers on the primary sides of the rectifying transformers as a form of coarse dc voltage and hence current control. As the load impedance changes continually during the operation of the potlines, the transformer tap positions move up and down regularly. The wear and tear on the tap changers is considerable, resulting in a group being removed from service for maintenance roughly every six months. When one of these 6-pulse groups is removed from service, the harmonic cancellation is no longer complete as one of the other 6-pulse groups is no longer matched. The installation now appears as a 6-pulse converter and a number of shifted twelve pulse converters, this is referred to as (n-1) operation.

There are typically two ways to deal with this problem in practice. The first is to have a special transformer which can duplicate the phase shift of any of the other transformers, by means of secondary tap changers. When one of the groups is removed, the special transformer is switched in to take its place. This allows the installation to remain at full power without overloading any of the rectiformer units. The other main

approach is to simply accept the 6-pulse harmonic generation and continue to run the plant, with the remaining units sharing the removed converter's load.

The disadvantage of the former approach is the requirement of a complicated, and probably more expensive, spare transformer which can duplicate multiple phase shifts and is only used during maintenance periods. With the latter approach, each unit will be running at only 80 % or so of its design power so that in an (n-1) situation, the installation can still run at full rated power. Also, either extra filtering will be required for the six pulse harmonics generated or higher harmonic penalties will have to be paid.

The effects of (n-1) operation are first illustrated here including the non-equal load sharing of the remaining converters. Then, a possible solution to the (n-1) operation of high-pulse installations is investigated which uses secondary tap-changers to adjust the transformer phase shifts. This will change the installation from its nominal k-pulse operation to (k-6)-pulse operation, thus minimising low order characteristic harmonic generation.

6.4.1 Non-ideal operation

When a single converter is removed from a multi-pulse installation, the ideal harmonic cancellation ceases. The harmonic generation is predominantly 6-pulse with residual 24-pulse operation, as shown by Figure 6.5, for a 24-pulse installation.

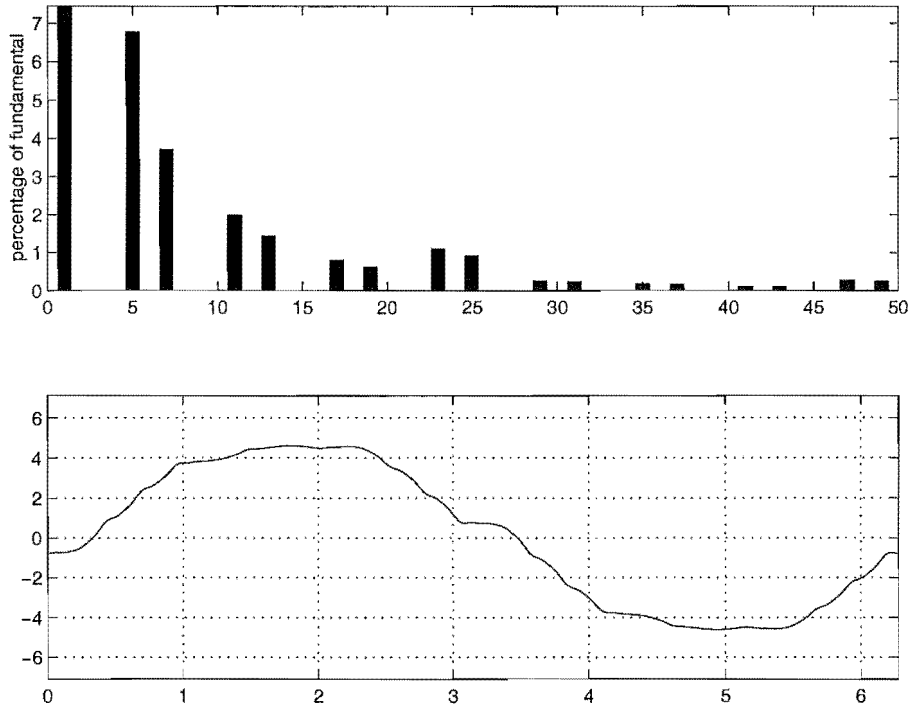

Figure 6.5 Phase A current during n-1 operation of a 24-pulse installation (+7.5 out)

As Table 6.4 illustrates, the remaining converters no longer share the dc load

equally after one has been removed. Even if they did, they would still need to be over-rated by approximately 40% to avoid a nett dc load reduction. The differences in load sharing are caused by the circulating dc currents, not by ac terminal voltage distortion. Cases (1)-(3) illustrate this effect by using a strong ac system and reducing the linking impedances that connect the converters on the dc side. As the linking impedance reduces, the dc current sharing becomes significantly worse. Case (4) shows finally that the load sharing imbalance is due to the dc side current interactions. With virtually no dc side harmonic interaction, the converter loads are balanced even with a relatively weak ac system (high ac harmonic voltage distortion).

Table 6.4 Fractional loadsharing for (n-1) operation of a 24-pulse installation

Case	Shift/Unit out	0	1	2	3	4
(1)	22.5^o	0.250	—	0.331	0.334	0.335
$R_{dc} = 100\mu\Omega$	7.5^o	0.250	0.335	—	0.331	0.334
$L_{dc} = 100\mu$H	-7.5^o	0.250	0.334	0.335	—	0.331
$L_{ac} = 1\mu$H	-22.5^o	0.250	0.331	0.334	0.335	—
(2)	22.5^o	0.250	—	0.319	0.335	0.346
$R_{dc} = 10\mu\Omega$	7.5^o	0.250	0.346	—	0.319	0.335
$L_{dc} = 10\mu$H	-7.5^o	0.250	0.335	0.346	—	0.319
$L_{ac} = 1\mu$H	-22.5^o	0.250	0.319	0.335	0.346	—
(3)	22.5^o	0.250	—	0.298	0.334	0.368
$R_{dc} = 1\mu\Omega$	7.5^o	0.250	0.368	—	0.298	0.334
$L_{dc} = 1\mu$H	-7.5^o	0.250	0.334	0.368	—	0.298
$L_{ac} = 1\mu$H	-22.5^o	0.250	0.298	0.334	0.368	—
(4)	22.5^o	0.250	—	0.334	0.333	0.333
$R_{dc} = 1\Omega$	7.5^o	0.250	0.333	—	0.334	0.333
$L_{dc} = 1$H	-7.5^o	0.250	0.333	0.333	—	0.334
$L_{ac} = 1$mH	-22.5^o	0.250	0.334	0.333	0.333	—

If a further transformer was to be removed, thus causing (n-2) operation, it would be best to remove its matched pair (30^o phase shift difference). This would allow a pseudo 12-pulse operation instead of 6-pulse as shown in Figure 6.6. It is rare that an installation could maintain operation without a load reduction under this configuration as the load on the remaining converters would double. One example though would be for an installation with multiple reduction lines. A scheduled maintenance scheme would remove a pair of matched transformers from different reduction lines to minimise the nett harmonic generation of the installation.

6.4.2 Changing the pulse number of an installation

An appropriate phase shift needed to achieve harmonic cancellation can be determined by the following formulae.

$$\Delta\sigma = \frac{60^o}{\text{number of 6-pulse groups}} \quad , \quad \Delta\sigma = \frac{30^o}{\text{number of 12-pulse groups}} \tag{6.1}$$

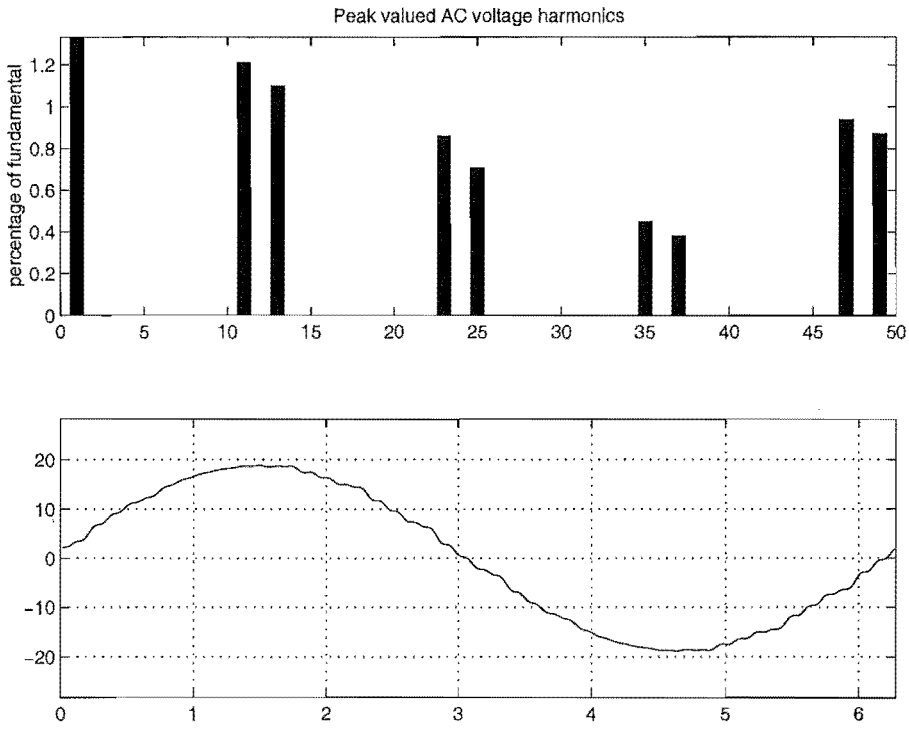

Figure 6.6 Phase A current of a 48-pulse installation operating (n-2) with -7.5^o and 22.5^o units out

For the case of n-1 operation the production of 6-pulse harmonics can be avoided by changing the pulse number of the installation to the ideal number given the number of remaining converter units. For example, when a 24-pulse converter installation loses one 6-pulse group, Table 6.5 shows that, 18-pulse operation can be achieved by adjusting the phasing of the remaining transformer groups in operation to produce 20^o phase shifts.

Table 6.5 Pulse number reduction for a 24-pulse installation to 18-pulse

Shift/Unit out	1	2	3	4
22.5^o	—	10.0^o	30.0^o	30.0^o
7.5^o	10.0^o	—	10.0^o	10.0^o
-7.5^o	-10.0^o	-10.0^o	—	-10.0^o
-22.5^o	-30.0^o	-30.0^o	-10.0^o	—

Similarly, if a 48-pulse converter installation loses one 6-pulse group, Table 6.6 shows that 42-pulse operation can be achieved by adjusting the phasing of the remaining transformer groups to produce 8.572^o phase shifts ($\frac{60}{7}$).

To implement this scheme special, tap-changing windings on the secondary windings of the phase-shifting transformers would be required. These could be installed as off-load tap-changers appropriate to obtain the pre-specified shifts. A pattern emerges for an installation pulse number reduction of one order. To cover for all contingencies, the phase shifting transformers would require a maximum of two off-nominal secondary

Table 6.6 Pulse number reduction for a 48-pulse installation to 42-pulse

Shift	1	2	3	4	5	6	7	8
26.250	—	21.429	21.429	21.429	30.000	30.000	30.000	30.000
18.750	21.429	—	12.857	12.857	21.429	21.429	21.429	21.429
11.250	12.857	12.857	—	4.286	12.857	12.857	12.857	12.857
3.750	4.286	4.286	4.286	—	4.286	4.286	4.286	4.286
−3.750	−4.286	−4.286	−4.286	−4.286	—	−4.286	−4.286	−4.286
−11.250	−12.857	−12.857	−12.857	−12.857	−4.286	—	−12.857	−12.857
−18.750	−21.429	−21.429	−21.429	−21.429	−12.857	−12.857	—	−21.429
−26.250	−30.000	−30.000	−30.000	−30.000	−21.429	−21.429	−21.429	—

tap-settings. However, the two transformers closest to zero shift, would only require one off-nominal secondary tap-setting.

The movement of the secondary tap changers will imbalance the leakage reactances of the remaining converter transformers. The total transformer leakage reactance from the two single phase transformers is given by Equation 6.2. With the off-nominal secondary tap-changer specified as in Equation 6.3, the off-nominal phase shift transformer leakage reactance is as shown in Equation 6.4.

$$X_T = n_2^2 X_2 + n_3^2 X_3 \tag{6.2}$$

$$a_{tap} = \frac{n_{new}}{n_{old}} \tag{6.3}$$

$$\begin{aligned} X_T' &= (a_2 n_2)^2 X_2 + (a_3 n_3)^2 X_3 \\ &= X_T \left(\frac{n_2'^2}{n_2(n_2+n_3)} + \frac{n_3'^2}{n_3(n_2+n_3)} \right) \end{aligned} \tag{6.4}$$

The transformer leakage reactances in the off-nominal secondary tap positions, calculated with Equation 6.4, are shown in Tables 6.7 and 6.8 for a 24-pulse and 48-pulse installations respectively.

Table 6.7 Transformer leakage reactances after off-nominal phase shifting for a 24-pulse installation

Shift/Unit out	X_T%	X_T%	X_T%	X_T%
22.5°	—	10.5176	10.7313	10.7313
7.5°	10.5067	—	10.5067	10.5067
7.5°	10.5067	10.5067	—	10.5067
−22.5°	10.7313	10.7313	10.5176	—

The leakage reactance unbalance between the bridges will result in non-perfect harmonic cancellation. However the low-order harmonic generation is substantially less than in the case of simply having one 6-pulse group out of service. This can be seen in Figure 6.7 for a 24-pulse installation after the −22.5° bridge is removed, when the installation has changed to 18-pulse operation. It is also shown in Figure 6.8 for a 48-pulse installation with the 3.75° bridge removed. The harmonics generated by

Table 6.8 Transformer leakage reactances after off-nominal phase shifting for a 48-pulse installation

Unit out	X_T%	X_T%	X_T%	X_T%	X_T%	X_T%	X_T%	X_T%
26.25°	—	10.0364	10.0364	10.0364	10.1741	10.1741	10.1741	10.1741
18.75°	10.2451	—	9.8803	9.8803	10.2451	10.2451	10.2451	10.2451
11.25°	10.2282	10.2282	—	9.8912	10.2282	10.2282	10.2282	10.2282
3.75°	10.1066	10.1066	10.1066	—	10.1066	10.1066	10.1066	10.1066
−3.75°	10.1066	10.1066	10.1066	10.1066	—	10.1066	10.1066	10.1066
−11.25°	10.2282	10.2282	10.2282	10.2282	9.8912	—	10.2282	10.2282
−18.75°	10.2451	10.2451	10.2451	10.2451	9.8803	9.8803	—	10.2451
−26.25°	10.1741	10.1741	10.1741	10.1741	10.0364	10.0364	10.0364	—

the full installation and reduced pulse number operations are marked in the figures, the remainder are those generated under (n-1) operation. Given that in reality the transformers will not be perfectly balanced under ideal conditions, the residual 6-pulse harmonic generation is not a major concern.

6.5 CONCLUSIONS

The star connected zigzag converter transformer has been validated against time domain simulation with excellent results. A representation of a high pulse installation connected in parallel on the dc side has been developed and used to show the characteristics of such an installation. One of the noticeable differences is that the characteristic dc current harmonics for a parallel connected converter increase with installation pulse number rather than decrease as for a series connection. Also, that any imperfections within the converter transformers result in non-ideal harmonic cancellation which also results in non-equal load sharing between the groups.

When one of the 6-pulse groups is removed from service, (n-1) operation, high levels of 6-pulse harmonic currents are generated. This also results in non-equal load sharing which studies have shown is due to the circulating dc currents, not ac terminal voltage distortion. Proper representation of the dc system is required in order to observe these effects.

A method is shown for reducing the levels of low-order harmonic generation during (n-1) operation by reducing the nominal pulse number. This is achieved by off-nominal secondary tap settings of which a maximum of two is required for the removal of any unit. While the new tap positions result in different leakage reactances between the converter transformers, the low-order harmonic generation is significantly less than normal (n-1) operation.

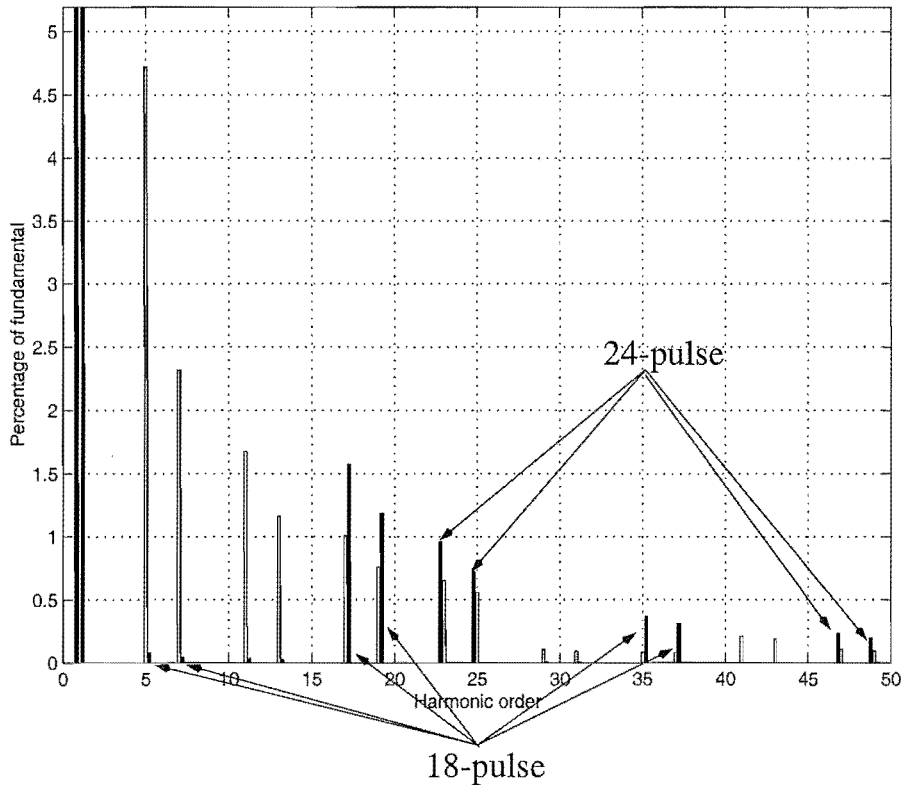

Figure 6.7 Harmonic elimination for n-1 case at a 24-pulse installation (-22.5 out)

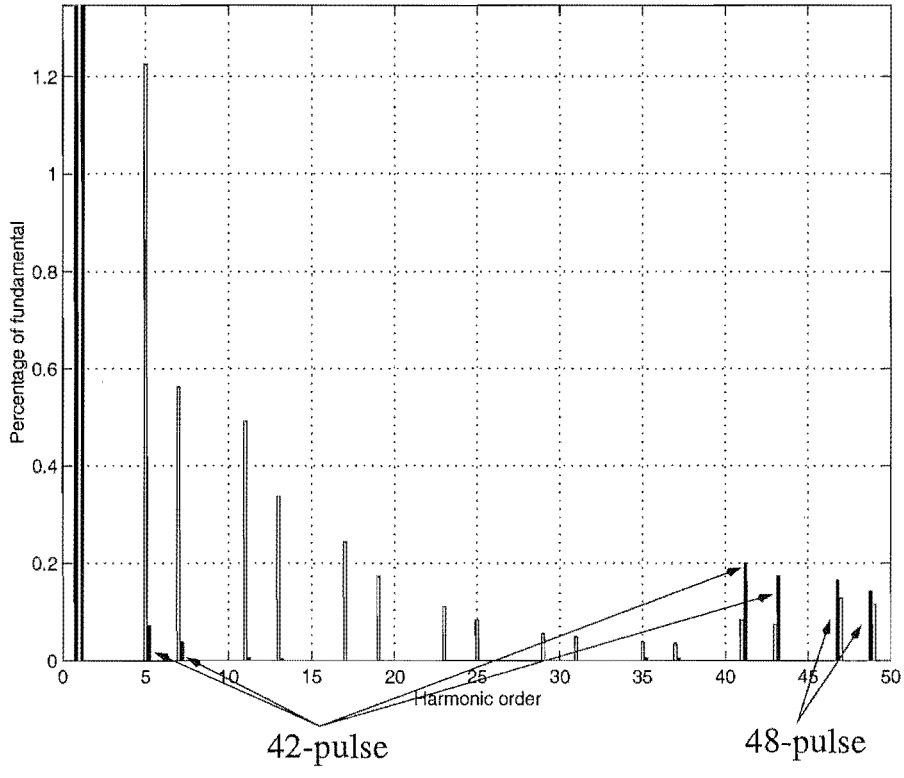

Figure 6.8 Harmonic elimination for n-1 case at a 48-pulse installation (+3.75 out)

Chapter 7

EFFECT OF CONVERTER REPRESENTATION ON SYSTEM IMPEDANCE

7.1 INTRODUCTION

In the calculation of power system harmonic impedances at the point of common coupling, as required for filter design, the contribution of existing converter plants in the system is often ignored on the assumption that the effective converter impedances are too large to be of practical consequence. However, some contributions [Dickmander *et al.* 1994] [Jiang and Gole 1995] have shown that the harmonic impedances of an HVdc converter can affect overall system resonances and should therefore be taken into account in system design and analysis.

A number of techniques for accurate determination of the harmonic impedance of an HVdc converter have been proposed [Dickmander *et al.* 1994] [Wood *et al.* 1995]; two of these are as follows. The first involves a linearised frequency domain transfer function approach, similar in concept to the three port converter model [Larsen *et al.* 1989b]. The second involves the use of a full harmonic domain model of the HVdc converter, using applied harmonic distortions to determine its impedance [Smith *et al.* 1996]. Both of these models provide an insight into, and a method for calculating the effective converter impedance.

This chapter is structured as follows. A fast numerical technique for the calculation of the converter harmonic impedance is shown. Then a study into the dependence of the converter impedance on its operating point is carried out. Finally the effect of the converter on the ac system impedance is investigated using the full harmonic model and some simplified converter representations.

7.2 CONVERTER IMPEDANCE BY NUMERICAL LINEARISATION

The converter impedance at any frequency can be described by four real values in the form of a tensor [Smith 1996], i.e.

$$\begin{bmatrix} V_r \\ V_i \end{bmatrix} = \begin{bmatrix} z_{11} & z_{12} \\ z_{21} & z_{22} \end{bmatrix} \begin{bmatrix} I_r \\ I_i \end{bmatrix} \tag{7.1}$$

The derivation of these frequency dependent impedances required either large numbers of perturbations or a numerical reduction of the analytic Jacobian matrix, both of these methods being computationally intensive.

The four unknowns $(z_{11}, z_{12}, z_{21}, z_{22})$ in Equation 7.1 require four simultaneous equations for their solution, some re-arrangement results in Equation 7.2. Working on the premise that for a small change in the terminal distortion the converter is linear, each impedance tensor can be derived using two sequential perturbations from a base case. At each perturbation, the changes in terminal voltage and converter current at that frequency are noted after re-converging the full harmonic solution. By re-converging the system with the perturbation, the effect of the ac and dc system impedance at other frequencies is incorporated. Equation 7.2 will be relatively well conditioned if the perturbations are in quadrature.

$$\begin{bmatrix} \Delta V_{r1} \\ \Delta V_{i1} \\ \Delta V_{r2} \\ \Delta V_{i2} \end{bmatrix} = \begin{bmatrix} \Delta I_{r1} & \Delta I_{i1} & 0 & 0 \\ 0 & 0 & \Delta I_{r1} & \Delta I_{i1} \\ \Delta I_{r2} & \Delta I_{i2} & 0 & 0 \\ 0 & 0 & \Delta I_{r2} & \Delta I_{i2} \end{bmatrix} \begin{bmatrix} z_{11} \\ z_{12} \\ z_{21} \\ z_{22} \end{bmatrix} \tag{7.2}$$

If the impedance is not phase dependent, it can be represented in complex form and so $z_{11} = z_{22}$ and $z_{12} = -z_{21}$. When the impedance is phase dependent, the tensor describes a circular locus around a complex impedance point. The complex centroid and radius of the locus are be described by the following equations [Smith 1996]:

$$Z_{centre} = \frac{1}{2}(z_{11} + z_{22}) + i\frac{1}{2}(z_{21} - z_{12}) \tag{7.3}$$

$$radius = \frac{1}{2}\sqrt{(z_{11} + z_{22})^2 + (z_{12} + z_{12})^2} \tag{7.4}$$

This twin perturbation approach is only valid when the converter impedance at the perturbation frequency is linear. If the impedance is non-linear then the tensor representation is invalid and the twin perturbation approach will result in an incorrect solution. A possible method for checking the accuracy of the twin perturbation approach is to make another perturbation and calculate the impedance at that point.

Then, using the previously calculated tensor impedance, a check is made to see whether that point is on the locus.

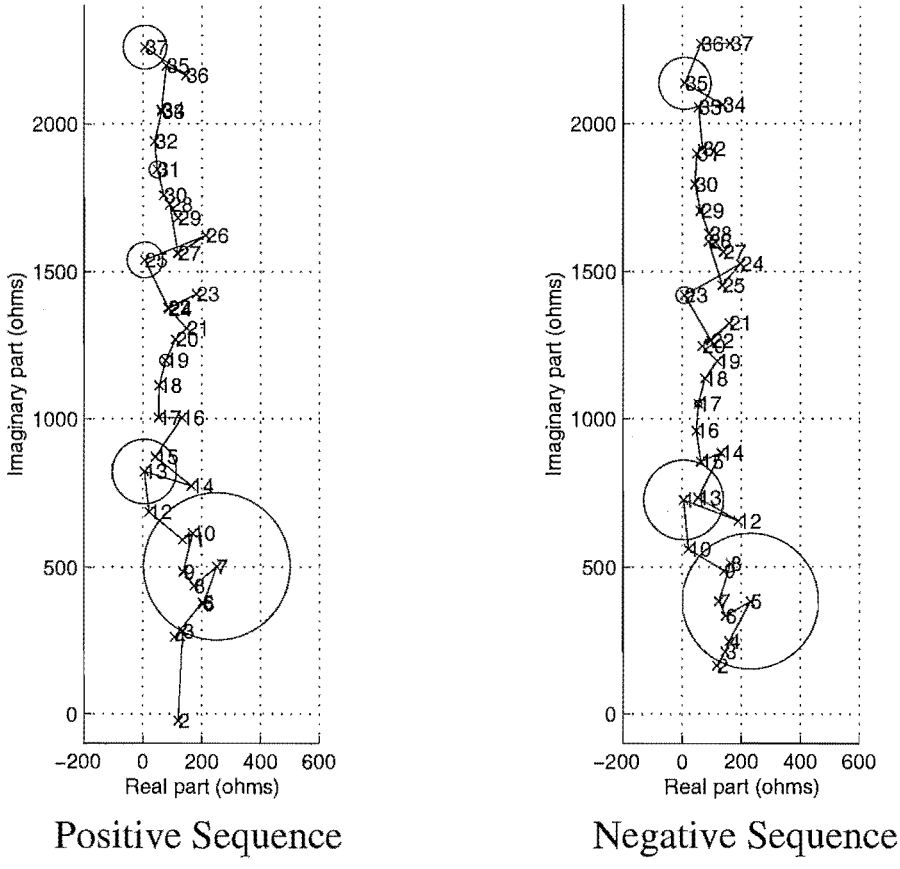

Figure 7.1 Tensor impedance of the CIGRE HVdc rectifier at the nominal operating point

Figure 7.1 shows the positive (left) and negative (right) sequence impedances of the CIGRE rectifier as viewed from the ac system. The 6-pulse characteristic frequencies are phase dependent while the non-characteristic frequencies can be represented as complex impedances. The converter impedance is predominantly inductive but the dc system does influence this.

7.3 CONVERTER IMPEDANCE DEPENDENCE ON OPERATING POINT

The six pulse ac-dc converter is often described as a non-linear device. The description relates to the frequency conversion process. Preliminary investigations have also been carried out [Smith 1996] on the effect that the magnitude of a single harmonic frequency has on the converter impedance. It was found that for a given operating point, the impedance did not change significantly for distortion levels of up to 12% of the fundamental.

Another effect investigated was the dependence of the impedance on the operating point. For this, the dc current setpoint was reduced from 2000A to 200A in 100 steps. The impedance was found to vary significantly; although no useful relationships could be derived as the terminal voltage went from 1.0pu to 1.2pu, the firing angle from 14^o to 50^o and the commutation period from 23^o to 0.7^o. The following section investigates the potential source of this variation.

7.3.1 Dependence on commutation period

The commutation period variation has been highlighted as the major source of non-linearity [Wood 1993] [Todd 1998]. The switching instances can be easily modulated by the harmonics on either side of the converter and therefore accurate resolution of these instants is important for accurate results. From the classical converter equations, it can be seen that the commutation period, μ, is affected by all the other variables determining the operating point.

$$\mu = \cos^{-1}\left(\cos(\alpha) - \frac{\sqrt{2}X_T I_d}{\sqrt{3}|V_+|}\right) - \alpha \tag{7.5}$$

The effect of the commutation period on the ac side impedance is investigated by a type of control that monitors the average commutation period and adjusts the firing angle to achieve the specified commutation period with a constant dc current. Once the initial harmonic solution has converged, the firing angle is locked to remove any effect of this control and the impedance calculated by the twin perturbation method. A new dc current level is set, the solution re-converged with the firing angle unlocked, and the next impedance calculation performed. The result is the relationship between converter impedance and average dc current, for a specified average commutation period.

For the following three cases, the dc current was reduced from the initial starting current (Table 7.1) until the firing angle reached zero. The resulting positive sequence impedance magnitudes are shown in Figure 7.2. Only the centroids of any phase dependent impedances have been plotted to simplify the illustration. The ac system was represented by an ideal voltage source and the dc current was ripple free.

Table 7.1 Initial conditions for the different operating points

μ	I_{do}	α_o
10^o	1.2kA	72.9^o
15^o	1.5kA	47.1^o
20^o	2.0kA	44.8^o

The non-characteristic harmonic impedances did not change with the variation of firing angle and dc current, only when the commutation period was varied did they change. Of the phase dependent impedances (6-pulse characteristics), only the 12-pulse

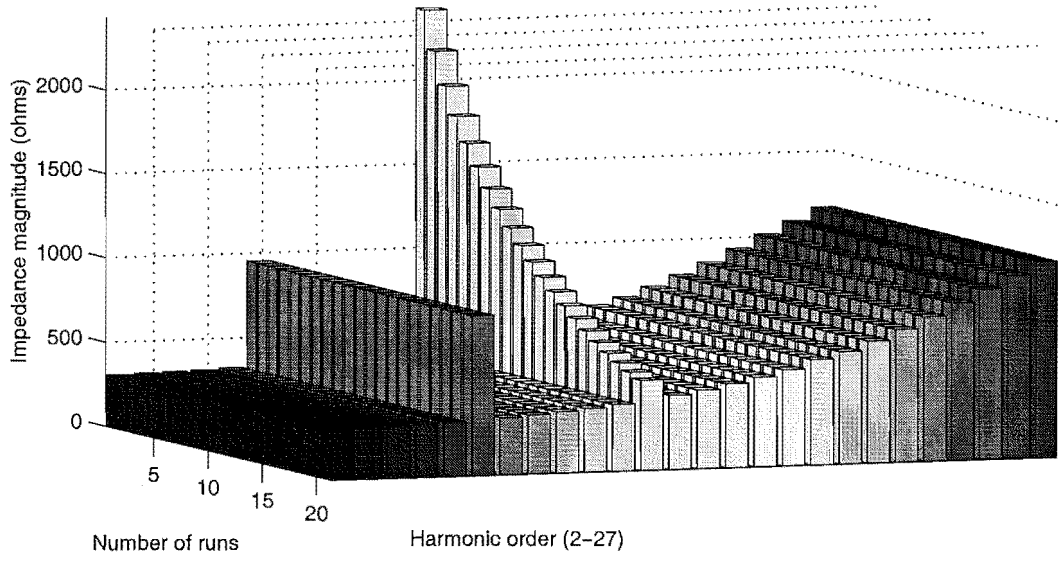

(a) Impedance variation for $\mu = 15^o$

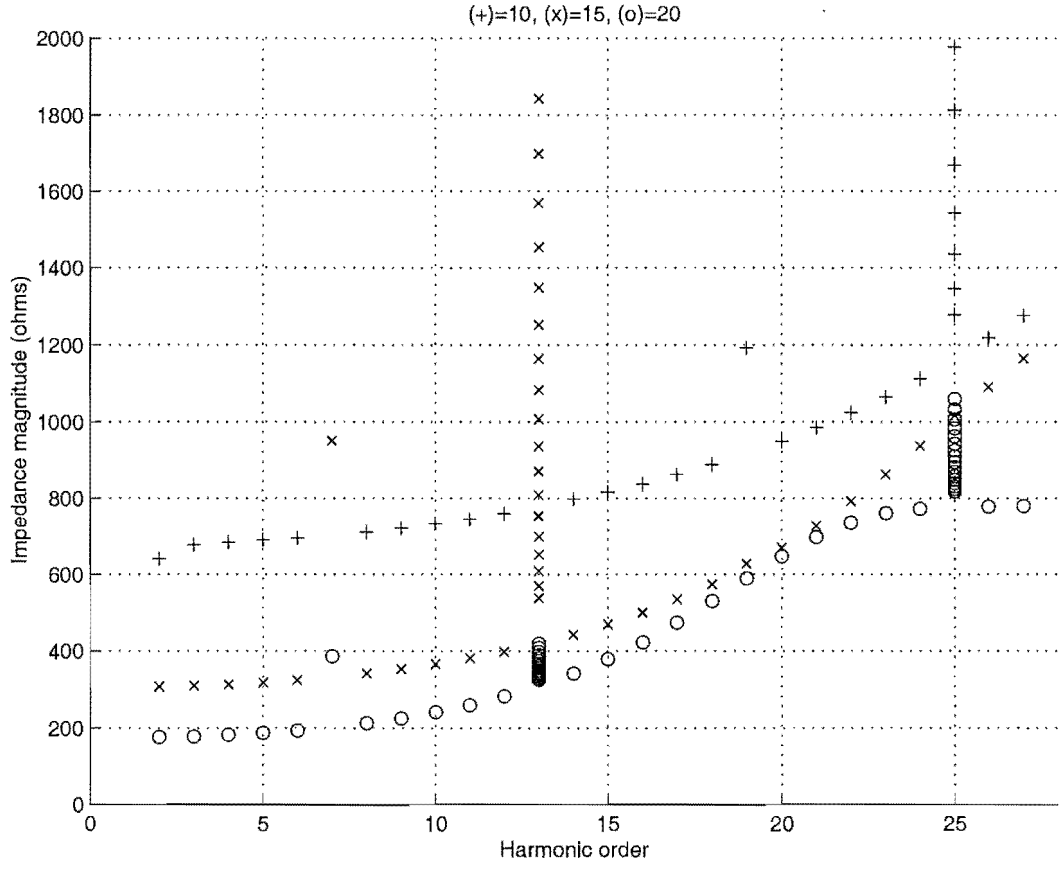

(b) Impedance change with different commutation angles $(10^o, 15^o, 20^o)$

Figure 7.2 Tensor impedance magnitude variation with commutation angle

characteristic impedances varied with firing angle. The variation of one of these tensors is shown for the positive sequence 13^{th} harmonic in Figure 7.3 for a commutation angle of 15^o. The variation itself indicates a direct relationship with the average dc current, which is being reduced in a linear fashion.

This infers that the non-characteristic harmonic impedance for a given converter is predominantly dependent upon the commutation period. A simplified model of the harmonic impedance of a converter should include this variation with the commutation period.

7.3.2 Dependence on terminal voltage imbalance

The most common non-ideal condition within a large transmission system is fundamental voltage imbalance, typically due to the transmission line asymmetry. This effect will result in the converter generating non-characteristic harmonics, most strongly the positive sequence third harmonic. Figure 7.4 shows the impedance plot for the first 7 positive sequence harmonics of the 12-pulse converter with negative sequence voltage variation. As the voltage imbalance increases from 0% to 5%, the non-characteristic harmonics become phase dependent and grow slightly with the distortion. These results apply to an operating point of $\alpha = 15^o$ $I_{do} = 1.0$ kA and an approximate commutation period of 20^o for a strong ac system and smooth dc current.

The phase dependence of all the harmonic frequencies increases with fundamental frequency imbalance. As the changes are small for low levels of distortion, an impedance representation based on balanced conditions will be reasonable.

7.4 EFFECT OF CONVERTER MODELLING ON REDUCED SYSTEM IMPEDANCES

An important consideration in the design of a new installation or power system component, such as a capacitor bank or system filters, is the effect of that component has on ac system resonances. To estimate this, the passive ac system is reduced to a shunt equivalent at the respective busbar and a range of system impedances is then produced. However, the reduction process assumes that the ac impedance of all system components can be accurately represented. Until recently there was no method to accurately represent the non-linear devices in the frequency domain and consequently approximations had to be made. This section investigates the effect that the non-linear devices have on the linearised system impedance in order to assess the validity of some of the approximations that are made.

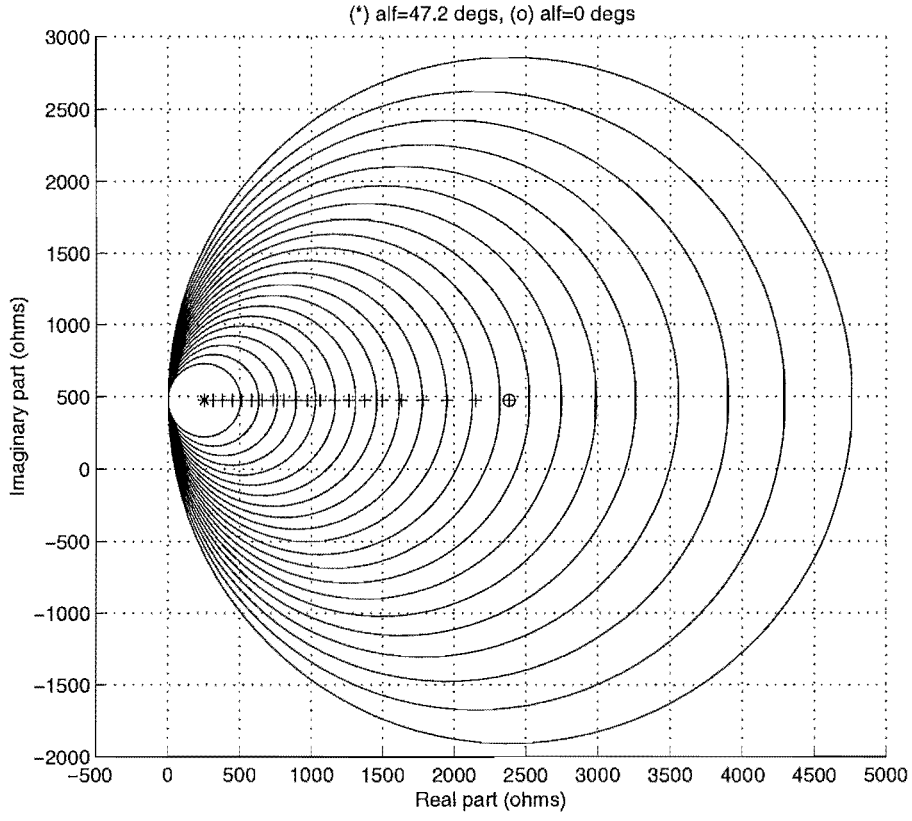

Figure 7.3 Positive sequence 13^{th} harmonic impedance variation with dc current

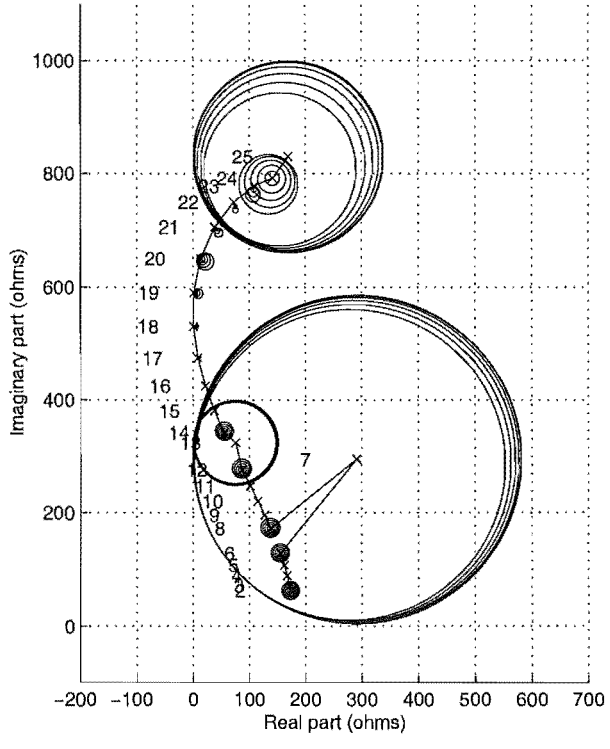

Figure 7.4 Positive sequence harmonic impedance variation with increasing fundamental voltage imbalance

7.4.1 Converter representation

As the majority of harmonic analysis programs cannot represent the harmonic interaction behaviour of non-linear devices, a variety of approximations need to be made with regards to converter representation. As illustrated in Section 7.2, the converter impedance is relatively inductive and increases with frequency.

The first two approaches use conventional passive system reduction methods with different converter representations. The third approach is new and is the most accurate as the full system with all non-linearities are represented.

Ideal current source

This solution works on the assumption that the converter impedance is very large compared to the ac system impedance. Therefore, this approach assumes that the converter impedance does not significantly affect the frequency response of the system, and the contribution of the converter to the ac system impedance is ignored. This assumption is considered realistic especially in the presence of ac system filters.

Simple Norton equivalent

The converter is represented as a Norton equivalent with the impedance calculated by a predetermined equation. Harmonic current injections are also specified to complete the equivalent representation, these are obtained from a loadflow solution using either classical analysis or a simplified harmonic model.

One such predetermined equation was proposed by Dickmander [1994] to solve the Geomagnetic Induced Current (GIC) problem observed during commissioning tests of the Quebec-New England Phase II HVdc transmission system. The initial design had neglected the effect of the converter ac side impedance. Using the following equations, the effect was noted and design adjustments made to counter the adverse resonances, i.e.

$$Z_{ac(+)}(f) = Z_{dc}(f - f_{power})K_s + jX_T^+(f) \tag{7.6}$$

$$Z_{ac(-)}(f) = Z_{dc}(f + f_{power})K_s + jX_T^-(f) \tag{7.7}$$

$$K_s = \frac{1}{2}.\frac{\pi^2}{9}.\left(\frac{a_{pri}}{a_{sec}}\right)^2.\frac{1}{n_b} \tag{7.8}$$

where f_{power} is the power frequency, $\left(\frac{a_{pri}}{a_{sec}}\right)$ is the converter transformer turns ratio and n_b is the number of bridges ($n_b = 2$ for monopolar operation). The above equations described a worst case scenario for interaction between the ac and dc systems as the commutation period is zero and there is the least damping of the dc side impedance,

when reflected through to the ac side. Also the authors noted that an approximation is made by neglecting the ac impedance reflected from the opposite ac sideband frequency.

The effect of the commutation period variation with voltage harmonic distortion can be incorporated into the harmonic ac impedance. In this form the converter is represented by Equation 7.9, where the elemental blocks are given by a describing function analysis [Wood *et al.* 1995].

$$\begin{bmatrix} V_{dc} \\ I_{ac(+)} \\ I_{ac(-)} \end{bmatrix} = \begin{bmatrix} a & b & c \\ d & e & f \\ g & h & i \end{bmatrix} \begin{bmatrix} V_{ac(p)} \\ V_{ac(-)} \\ I_{dc} \end{bmatrix} \tag{7.9}$$

For simplicity, the reflected ac system impedance can be neglected as the transformer impedance will probably be larger than that of the ac system. With this simplification, the converter ac impedances can be written as Equations 7.10 and 7.11.

$$Z_{ac}^{+} = \frac{Z_{dc} - c}{dZ_{dc} - dc + fa}, \ (V_{ac(-)} = 0) \tag{7.10}$$

$$Z_{ac}^{-} = \frac{Z_{dc} - c}{hZ_{dc} - hc + ib}, \ (V_{ac(+)} = 0) \tag{7.11}$$

Full converter representation

Based upon the linearisation method discussed in Section 7.2, this method obtains the network impedance as seen from a remote busbar taking into consideration all the interaction that occurs between the non-linear devices. The linearised representation is obtained by perturbing the specified busbar with small current injections, converging to the full harmonic solution and observing the changes in the harmonic voltages. The impedance obtained from this method is a function of the linear system impedance and the impedance of all the non-linear devices within the system. When comparing this accurate representation with the simplified models, any phase dependencies from non-linear devices are approximated by their complex impedance centroid (Equation 7.3).

Comparison of converter modelling methods

Since Equation 7.6 ignores the effects of the steady-state commutation period and the commutation period variation, this method will result in the least realistic damping for the ac system impedance. Figure 7.5(a) shows that this impedance, the dashed line, can be significantly different from the true impedance and so the results will be overly pessimistic.

In the test system the ac system voltage source was controlled so that the rectifier terminal voltage remained at 1.0 pu. To equate the models, commutation circuit

resistance is neglected and the inverter is represented as a constant dc voltage source (495 kV). The first case analysed the base operating point of $I_d = 2.0$ kA, $\alpha = 14.946^o$ and $\mu = 23.201^o$. This gave rise to the lower impedance curves shown by an (x). In the second case, the dc current was reduced to $I_d = 1.0$ kA which required the converter operating conditions to be changed to, $\alpha = 14.508^o$ and $\mu = 14.426^o$; the results are shown by the upper impedance curves marked with a (+). The Wood approach is shown by the solid lines and appears to be reasonable when compared with the harmonic impedances calculated by the full representation.

For the frequency range shown in Figures 7.5(a) and 7.5(b), the describing function approach provides a good representation of the true converter impedance. However, when the frequency range is extended for the $I_d = 2.0$ kA case, the linearisations made in Wood's analysis produce significant error (Figures 7.5(c) and 7.5(d)) [Wood 1993]. This method was originally developed to describe the HVdc converter for control analysis which generally only requires frequencies $f < 500$ Hz. The majority of the frequency couplings occur below this frequency and so it may be sufficient to approximate the converter by a simple RL equivalent which continues the inductive trend above 500 Hz.

7.4.2 Test systems and results

Effect of CIGRE rectifier on ac system impedance

To assess the effect of the CIGRE rectifier on its ac system, a small hypothetical measurement transformer was attached to the rectifier busbar. This results in a nett ac system impedance with the converter in parallel with the linear ac system. The three impedances shown in Figure 7.6 were obtained through numerical frequency scans of the different representations.

For the majority of the frequencies, the converter impedance can be assumed to have a negligible effect on the ac system impedance. However the ideal source approach indicates a large parallel resonance around the second harmonic (100Hz) where the more accurate methods all indicate a much greater damping. Dickmander's simple expression results in over damping of this resonance as it predicts a much lower converter ac side impedance. The full harmonic solution and the describing function approach both accurately represent the damping. The full harmonic solution approach also has the inverter installation represented in full and so it can be assumed that, for this system, the inverter has negligible influence on the rectifier ac system impedance.

Effect of remote converter representation on the ac system impedance

The first test looks at the required level of converter representation when performing an analysis on the remainder of the ac system. Using the Lower South Island test system

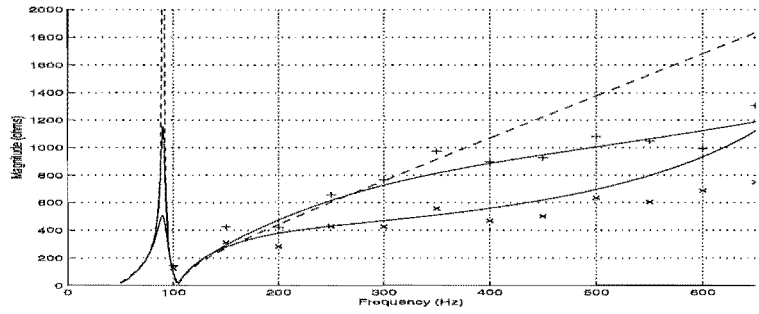

(a) Impedance magnitude (0-650Hz)

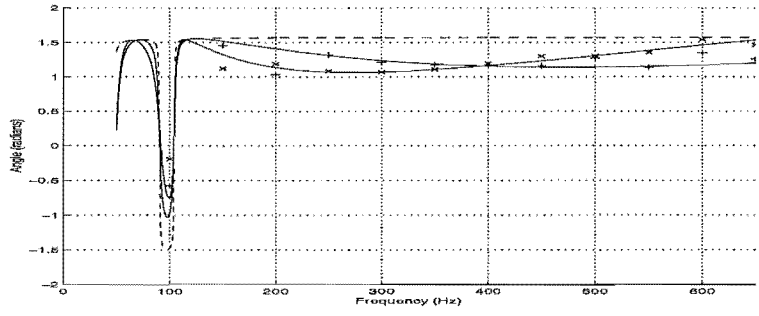

(b) Impedance angle (0-650Hz)

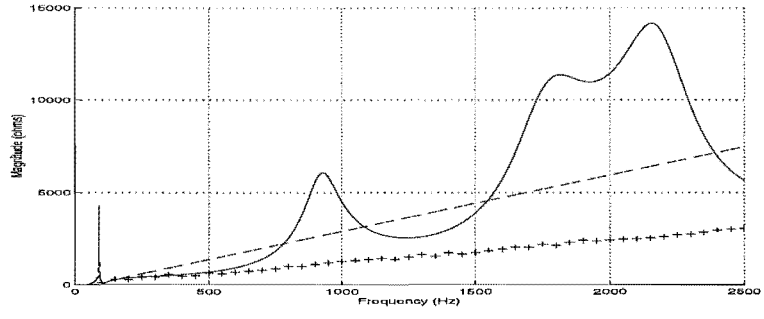

(c) Impedance magnitude (0-2500Hz)

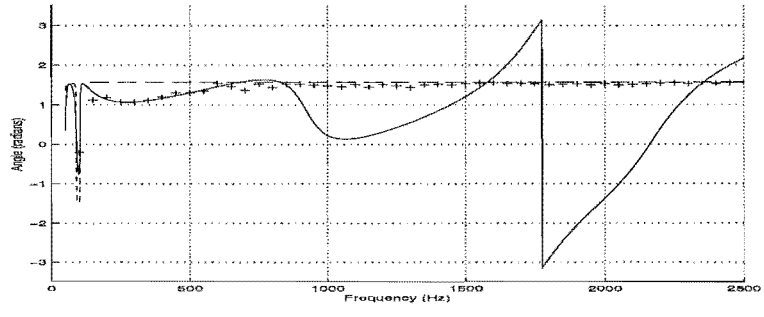

(d) Impedance angle (0-2500Hz)

Figure 7.5 Comparison of the positive sequence ac CIGRE rectifier impedance calculations (Full representation, +=1kA, x=2kA) (Solid=Wood approach) (Dashed=Dickmander)

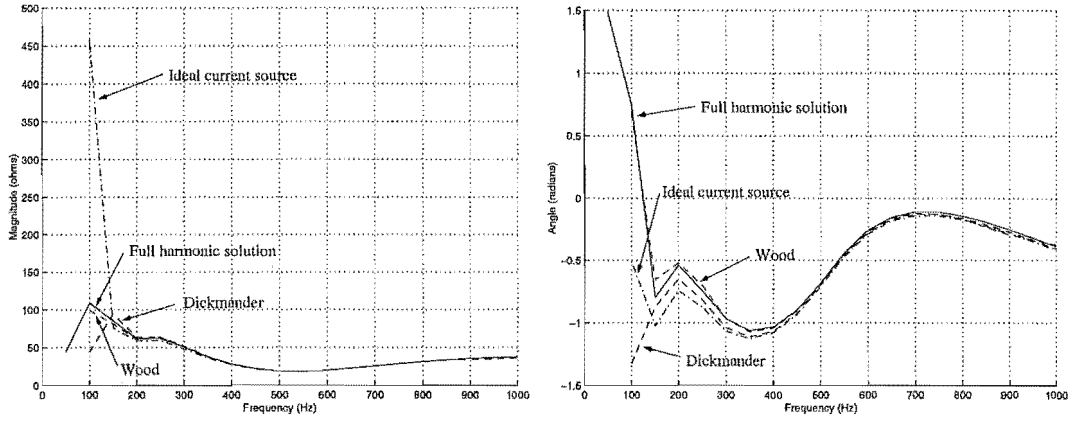

(a) Impedance magnitude

(b) Impedance angle

Figure 7.6 Comparison of the positive sequence CIGRE ac system impedance with the converters represented

of Appendix B, the Tiwai-033 converters are represented in the same three ways; ideal source, simple Norton equivalents, and the full harmonic approach.

There is some difficulty in the appropriate representation of the parallel connected installation at the Tiwai-033 busbar. With the dc load as an ideal dc current source, the dc harmonic impedance is infinite. The simple expression by Dickmander assumes that the converter impedance is only a scaled form of the dc side impedance. With the dc system as an ideal current source, the Dickmander representation will be the same for the ideal source.

Using the describing function approach with the ideal dc current source, Equation 7.9 can be simplified as for the positive sequence, $V_{ac(-)} = 0$ and $I_{dc} = 0$, similarly for the negative sequence. This then allows the positive and negative sequence impedances to be as shown in Equations 7.12 and 7.13.

$$Z_{ac(+)} = \frac{1}{d}\ , (V_{ac(-)} = 0 \text{ and } I_{dc} = 0) \tag{7.12}$$

$$Z_{ac(-)} = \frac{1}{h}\ , (V_{ac(+)} = 0 \text{ and } I_{dc} = 0) \tag{7.13}$$

This is the contribution of the commutation period variation due to ac terminal harmonic voltage distortion. An integer scaling factor is also applied to reflect the number of bridges in parallel on the ac side. The results for this installation are shown in Figure 7.7.

Again, the Wood describing function approach is the closest to the full representation, although it does diverge at the two higher parallel resonances due to the approximations made. However, it would be possible to switch to a simpler model at this point for the higher frequencies based upon the inductive trend of the converter

impedance.

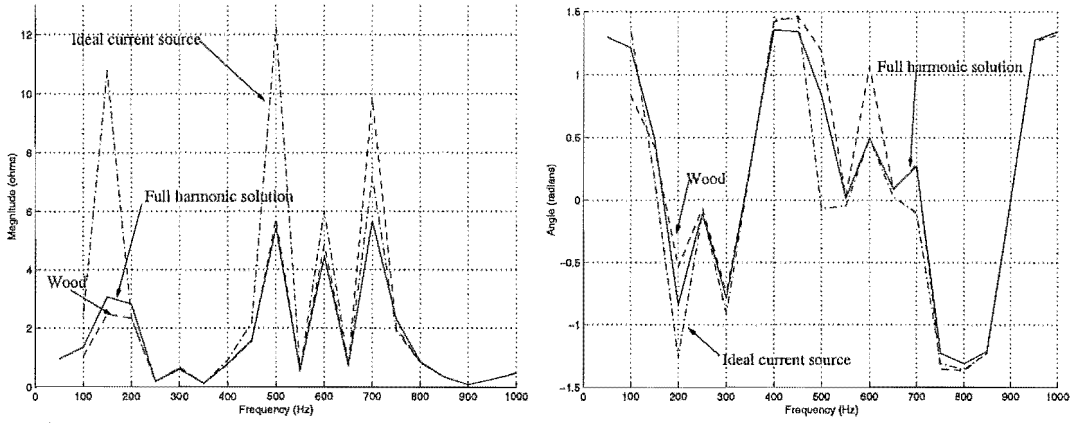

(a) Tiwai-033 impedance magnitude

(b) Tiwai-033 impedance angle

Figure 7.7 Comparison of the positive sequence ac converter impedance calculations

The effect of the converter modelling on the extended transmission system is shown in Figure 7.8, where a comparison is made between the ideal source representation and the full harmonic representation. As can be seen, the converter modelling still has a considerable effect on the damping of low frequency parallel resonances, quite dominantly at the Manapouri-220 busbar. This is interesting as that busbar is some 170 km distant from the converter installation.

Effect of the Tiwai-033 installation, (n-1) operation

As explained in Chapter 6 the high pulse operation of an installation, such as the Aluminium Smelter at Tiwai-033, is achieved by means of zig-zag wound transformers with auto-winding transformers which require a significant amount of maintenance. Consequently, the installation is often run with imperfect harmonic cancellation in the (n-1) mode of operation.

Figure 7.9 shows that this mode of operation does not significantly affect the ac system impedance, even though one converter is out of service. This is due in part to the installation maintaining constant dc power by increasing the dc currents in the remaining converters. This has the effect of increasing the average commutation periods of the converters, which in turn lowers their ac side impedance. The lower impedance of the three converters in parallel is similar to the original impedance of the four nominally loaded converters, thus causing no significant change in the ac system impedance.

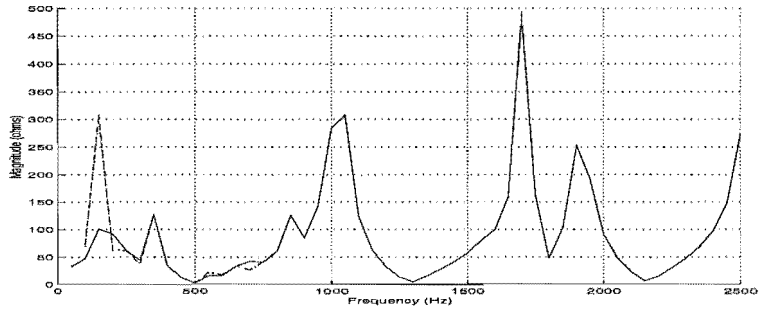

(a) Tiwai-220 mag

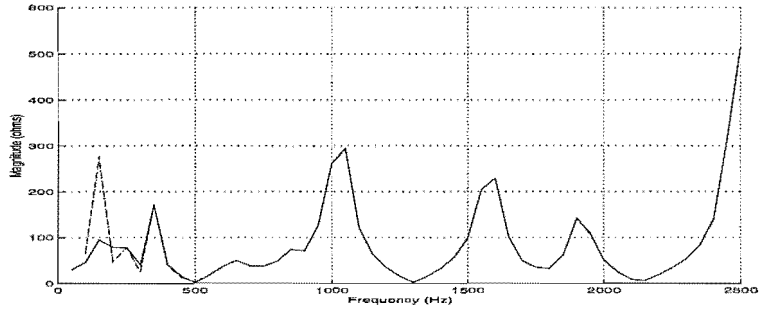

(b) Invercargill-220 mag

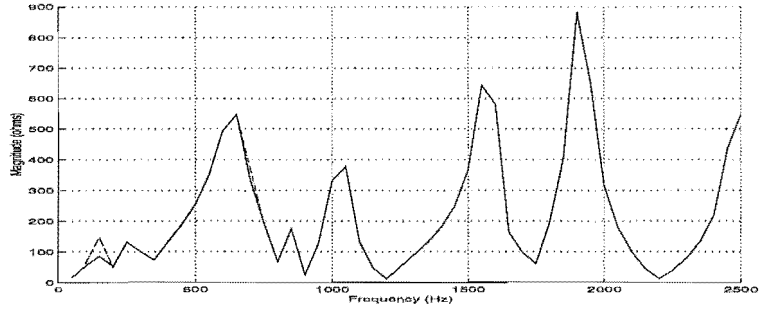

(c) Roxburgh-220 mag

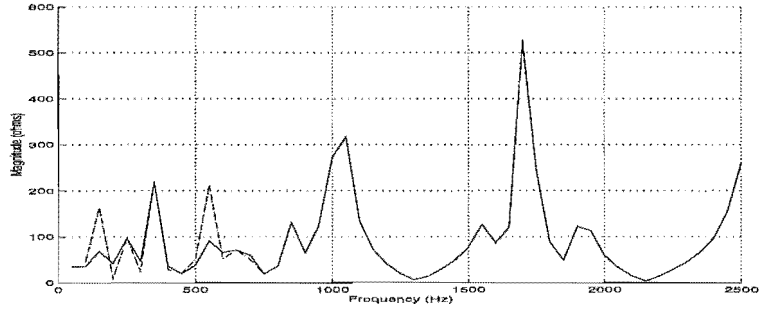

(d) Manapouri-220 mag

Figure 7.8 Effect of Tiwai Aluminium smelter rectifiers on ac system impedance (solid=full, dashed=ideal source)

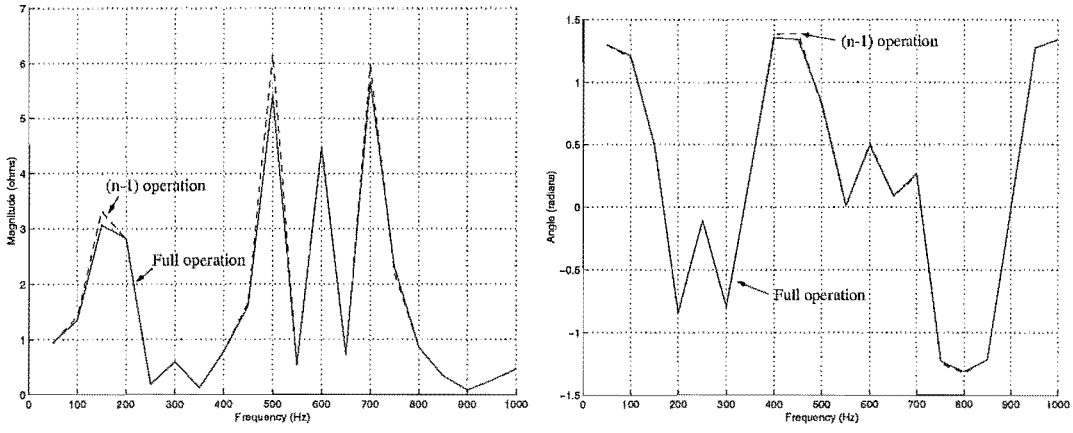

(a) Tiwai-220 magnitude

(b) Tiwai-220 angle

Figure 7.9 Comparison of ac system impedance during (n-1) operation

7.5 CONCLUSIONS

A fast numerical technique for obtaining accurate converter harmonic impedances, called the twin perturbation, has been shown. It inherently incorporates the full effects of the connected ac and dc systems and represented the linear phase dependency of the converter. Using this method, it was shown that the ac impedance for a given converter is governed solely by the commutation period for non-characteristic harmonics. The characteristic impedances were phase dependent and exhibited a strong linearity with the dc current.

The effect of the converter impedance on the ac system impedance was investigated using the twin perturbation and a number of other approximate methods. These studies showed that it is important to represent the converter impedance accurately at frequencies below 500 Hz, as the converter impedance can have a major damping effect on parallel resonances.

The attractions of the simple converter ac impedance expression derived by Dickmander are due to its relative simplicity. However, most of the analysis is now performed by computer simulation and so the simplicity of the formulation is secondary to the simplicity of the interface and input requirements. For approximate but relatively accurate ac system impedance analysis, a hybrid approach between the describing function analysis and a simple RL equivalent for high frequencies should be developed. This method would then be a reasonable approximation at all frequencies and be fast compared to the full harmonic approach. The only extra input requirements would be some basic converter operating point information.

Chapter 8

A CRITICAL ASSESSMENT OF POWER SYSTEM HARMONIC ANALYSIS

8.1 INTRODUCTION

Direct solution methods are most commonly used by the industry to obtain information of harmonic flows. The non-linear device harmonic current injections are based upon either predicted terminal voltages, or loadflow solutions. In practice such approaches can lead to incorrect levels of harmonic distortion and uncharacteristic behaviour.

Sophisticated models of the static converter are now becoming available to analyse their response in the presence of ac voltage and dc current distortions. In combination with harmonic penetration studies, these models require an iterative process and result in accurate solutions. The development of the iterative solution has followed a progression from early models employing a simple fixed point iteration, to recent models utilising Newton's method. The move toward the more complicated Newton's method was prompted by convergence difficulties often associated with fixed point iterations.

Complicating the development has been a reliance on the formation of electrical equivalents at every stage of the solution process, with a particular implication being the representation of all quantities by complex numbers. In recent years there has been a clear trend away from the use of electrical equivalents to a more sophisticated representation of a system by means of steady-state equations, much like the load flow formulation. This allows electrical circuit constraints, control and switching functions to be incorporated in a unified way, which in turn permits more robust iterative techniques, such as Newton's method to be used.

A recent paper [Smith *et al.* 1998] has made a qualitative comparison of the accuracy of Iterative Harmonic Analysis (IHA) methods with reference to 12-pulse ac-dc converters embedded in ac power systems. While there is no doubt that the iterative methods can provide very accurate solutions, there is no quantitative information on the relative accuracy of simple and complex techniques.

If the system is very strong and well balanced then obviously a simple approach such as a direct positive sequence analysis is all that is required. The presence of a highly

resonant weak system and high imbalance requires a more detailed harmonic analysis. Some other factors such as site history or knowledge of imbalanced transformers may also affect the analysis decisions. All of these are relatively obvious when it comes to choosing a solution method. For the majority of cases though, there may not be indications such as these to suggest a course of action; for these therefore some other form of indicator is necessary.

The other major issue is with regards to the extent and method of system representation which is often overlooked during modelling decisions. This is discussed in the following sections.

8.2 COMPARISONS OF PASSIVE SYSTEM REPRESENTATIONS

8.2.1 The different modelling approaches

There are basically three different methods for harmonic representation of the ac transmission system; positive sequence frequency domain, three-phase frequency domain and three-phase time domain. The key difference between these three methods is the representation of system imbalance and complex frequency dependencies such as skin effect. Normally most of these complex frequency dependencies relate to the modelling of transmission lines. By ignoring such things as skin effect and system imbalance, the three different modelling methods will yield the same results.

The positive sequence solutions are based on the fundamental frequency loadflow information. This approach is very useful as it enables a simple frequency analysis based on the typically most available information. The transmission line is assumed to be an equivalent π-model with long line effects fitted to each frequency term.

The three phase frequency domain transmission lines are built up from a geometric analysis using Carson's Equations [Carson 1926] and modelled as equivalent π-models. This is the most accurate method of representing the transmission lines, as the components can be unbalanced and contain specified levels of frequency dependency. The main difficulty with frequency domain methods has always been the representation of time dependant effects such as magnetic saturation and switching.

Time domain modelling has no difficulty in the representation of system imbalance but, the more complex frequency dependencies provide more of a problem. The transmission lines are the most important frequency dependent components and a significant amount of work has gone into their accurate representation. PSCAD/EMTDC uses Norton equivalents derived from curve fitting to frequency domain data which provide reasonable results [Manitoba HVdc Research Centre 1988].

The major limitation with the last two techniques is the level of system information required, such as the physical geometry and conductor properties of the individual

transmission lines. For full system studies this information may be available but for the fast studies required during tendering, there may only be basic loadflow information available which severely limits the choices.

8.2.2 Comparison of modelled impedances

For the average transmission system, the positive and negative sequence harmonic impedances are very similar, it is only the zero sequence impedance that is significantly different. Figure 8.1 shows a comparison of the positive sequence impedance derived from a single phase penetration program with the positive and zero sequence impedances from a full three phase analysis. As the single phase harmonic penetration typically treats the all sequences as the same, no significant differences will be noticed with the characteristic harmonics. However, if any zero-sequence harmonics are being modelled (transformer saturation, etc) errors will result from the significant differences in the impedances. Another major problem with single phase analysis that is not normally well accounted for are the differences in phase shifting between positive and negative harmonics across phase shifting transformers. Delta or ungrounded star connections will also result in in-correct representation of zero-sequence harmonic flows if not properly accounted for.

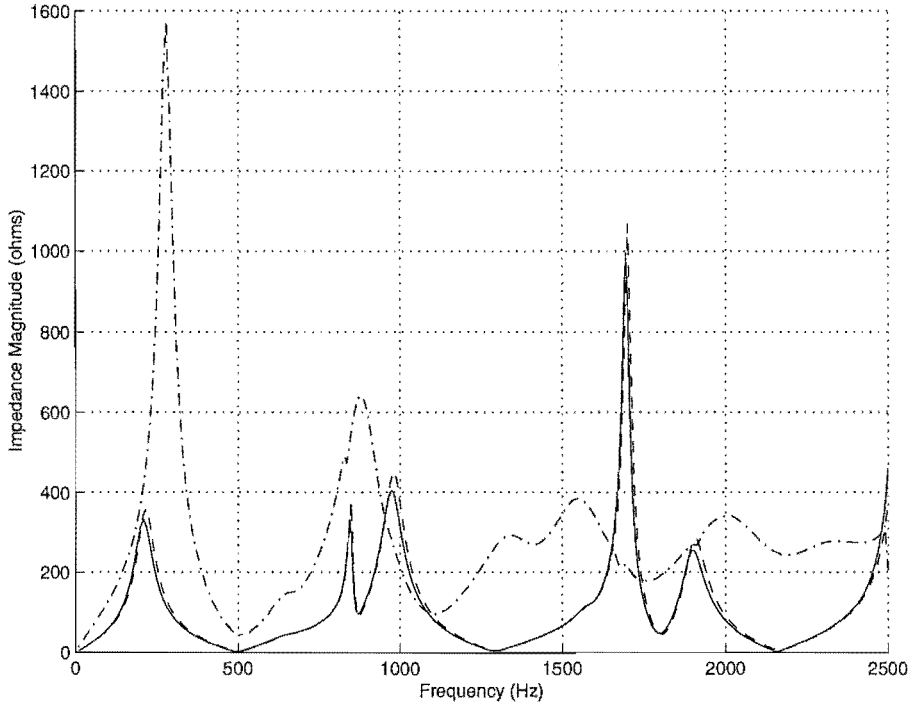

Figure 8.1 Comparison of impedances of a single phase penetration program with a full three phase analysis (solid=Positive Sequence (3 phase), dashed=Positive Sequence (Single phase), dash dot= (Zero Sequence (3 phase))

Besides the incorrect representation of the zero sequence impedance, single phase

analysis ignores the coupling effect that exists between sequences. Figure 8.2 shows this for the upper triangle elements of the sequence impedance matrix. The figure also shows a comparison between the time domain and frequency domain representations. While for the most part the time domain results appear to be reasonable, there is significant error in the coupling terms and zero sequence representations.

8.2.3 Extent of system representation

The depth of system modelling is an important aspect for consideration. From a system stability point of view the Short Circuit Ratio and its associated indices provide a useful measure of where on the load curve the operating point is. However, the Short Circuit MVA rating of a busbar from which the SCR is derived, provides no real frequency information about the system, as Figure 8.3 shows for the positive sequence scan for the Tiwai-220 busbar of the New Zealand South Island power system. The busbar has a Short Circuit rating of 1925 MVA at an angle of -82 degrees. For comparison the frequency scan of the simple RL equivalent, derived from this information, is shown as a dotted line on the same plot. Any harmonic analysis decision based on the SCR will provide meaningless results, as none of the resonances or frequency dependency of the system are represented.

A paper from the IEEE "Task force on harmonics modelling and simulation" [1996] indicates that it is common to represent the network to at least five busbars or two transformations. Also that all busbars with significant capacitive compensation should be explicitly represented.

Figure 8.4 gives some indication of the changes that are evident by the extent in which the transmission system is modelled. The solid line indicates a representation of the entire 110 busbar transmission system (11 kV and above) of the South Island of New Zealand. The dashdotted line is with the system reduced down to the local 220 kV network and only significant loads and generators represented (Lower South Island test system). The dashed line refers to the 220 kV transmission network represented with no generators, transformers or loads.

8.2.4 Frequency resolution for ac system studies

Another key part to harmonic studies of ac and dc systems is the frequency resolution required to ensure that no significant information is missed. Figure 8.5 illustrates for a typical system that a resolution of 10 Hz will accurately represent the transmission system impedance. There is some deviation around the sharp parallel resonances as shown by the 5 Hz resolution plot but the difference is not significant. The 50 Hz representation however is reasonable but could hide important information as a large frequency increment could miss a parallel resonance. Thus for investigative studies to observe the effect of new passive components, a 10 Hz resolution should be adequate.

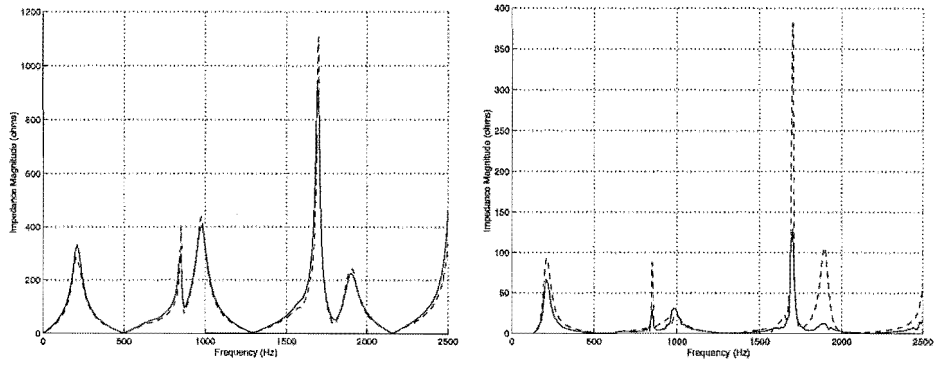

(a) Zac(+,+) (b) Zac(+,-)

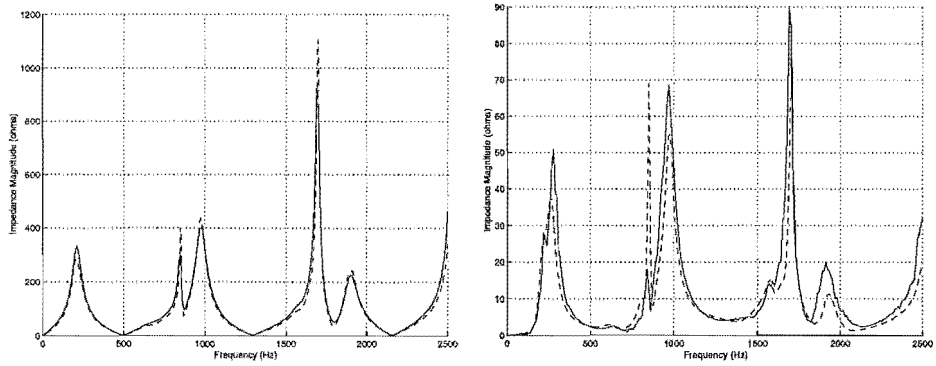

(c) Zac(-,-) (d) Zac(-,0)

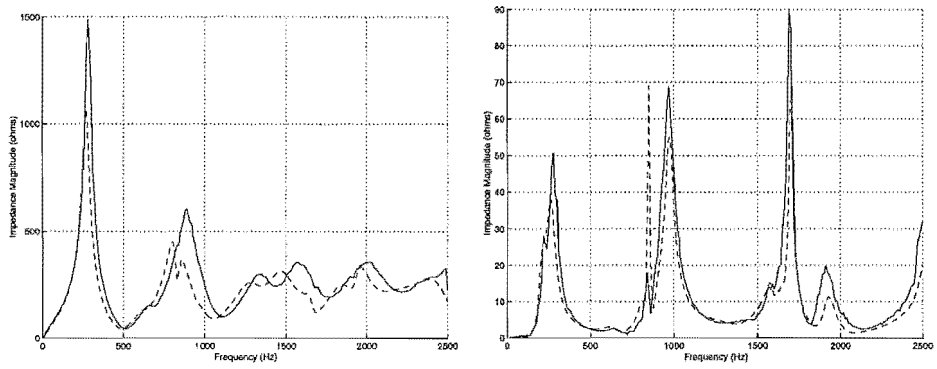

(e) Zac(0,0) (f) Zac(+,0)

Figure 8.2 Reduced impedance at Tiwai-220 (solid=Frequency domain, dashed=Time domain), Frequency resolution = 10 Hz

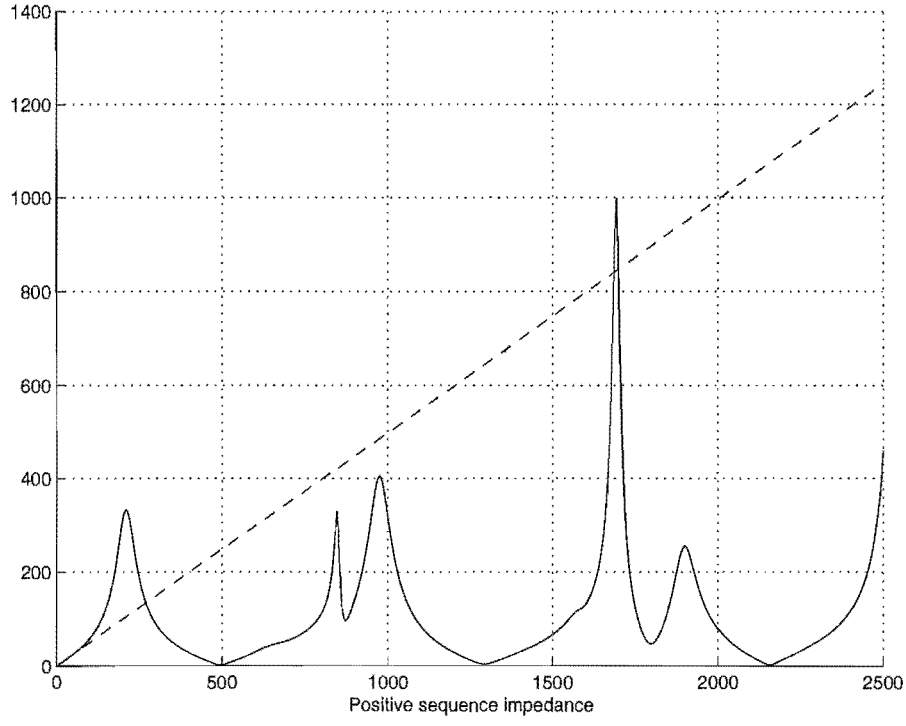

Figure 8.3 Comparison of three phase frequency domain impedance (solid) with a simple SC MVA representation (dashed)

8.3 MECHANISM FOR HARMONIC INTERACTION

The main effect of non-linear device *interaction* through the ac system is the generation of harmonic voltages due to each device's harmonic current injections. If a harmonic device is relatively insensitive to harmonic voltages at its terminal busbar, then it will require a significant harmonic voltage distortion before any *interaction* will occur.

8.3.1 Interaction assessment

When considering the effect of a remote harmonic injection, two things must be taken into consideration. The first is the harmonic impedance of the ac system reduced to the specific busbar, and the second is the current gain matrix of the remote injection. The latter is the amplification, or more typically reduction, that occurs to any current injected at a remote busbar to the equivalent current injection at the specified busbar.

$$\begin{bmatrix} I_{local} \\ \hline I_{remote} \end{bmatrix} = \left[\begin{array}{c|c} A & B \\ \hline C & D \end{array}\right] \begin{bmatrix} V_{local} \\ \hline V_{remote} \end{bmatrix} \tag{8.1}$$

During the system reduction the current gain can be calculated by using a 1.0 pu current injection at all harmonics and equating $(BD^{-1}I_{remote})$, where the shunt admittance is $(A - BD^{-1}C)$. The result is a Norton equivalent of the ac system which

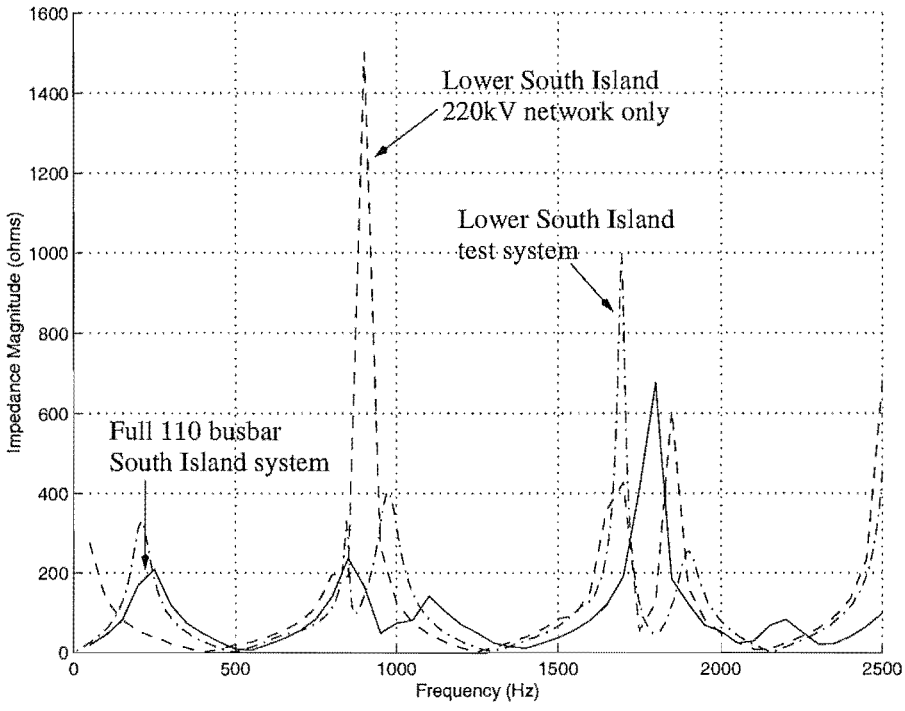

Figure 8.4 Comparison of depth of ac system representation

can be used to determine the degree of interaction between the harmonic generation sources.

The example used here is the interaction potential within the power system of the South Island of New Zealand. There is a large HVdc rectifier installation (1000MW) situated at the Benmore-220 busbar and another multi-pulse installation at Tiwai-033 (480MW). These two busbars are separated by approximately 400km of transmission lines, the reduced impedances and current gains are shown in Figure 8.6.

As the current gain from the Benmore converter busbar is relatively small, and none of the characteristic harmonics generated by the HVdc rectifier terminal lie on a parallel resonance, the harmonic voltages at Tiwai-033 due to the Benmore injections are likely to be minimal. As these are minimal, the Benmore rectifier is not likely to have a significant effect on Tiwai under this operating condition. From Tiwai to Benmore the current gain is higher, but the impedance is lower resulting in a minimal effect except at the third harmonic. Thus a conclusion on this information is that there is minimal interaction between Tiwai and Benmore.

To illustrate this two brief tests are performed with the results shown in Figures 8.7 and 8.8. The first is looking at the harmonic voltages at Benmore-220 with and without Tiwai-033 represented, the second is the same but at Tiwai-033 with and without Benmore represented.

The actual harmonic voltage results indicate that the initial estimation of minimal interaction is correct. Care must be taken though to note that the representation of the

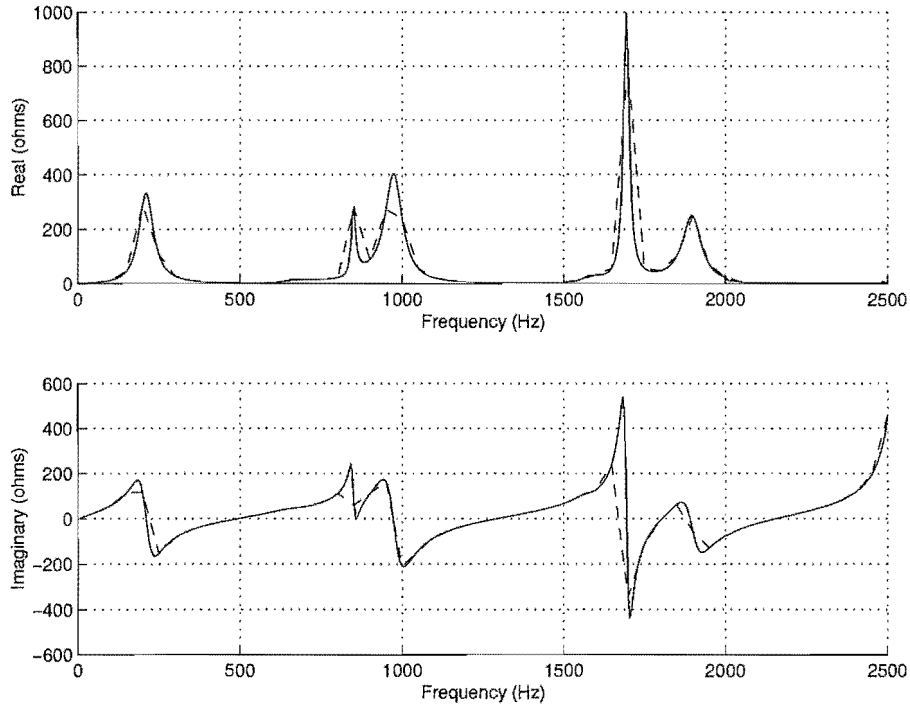

Figure 8.5 Comparison of ac system frequency resolution for the LSI impedance at the Tiwai-220 busbar (solid=5 Hz, dash-dot=10 Hz, dashed=50 Hz)

converters is sufficient. As the previous chapter has shown, the low-order resonances can be significantly affected by this. In this case, the converters were represented as ideal sources to replicate the results available with typical commercial packages.

Tiwai (n-1) operation

A worse case is when one of the six pulse rectifiers at Tiwai is removed from service for maintenance. This removes the ideal harmonic cancellation and the system reverts to 6-pulse generation. As can be seen in Figure 8.9, this results in an increased level of harmonic absorption at the Benmore-220 busbar at the 5^{th} and 7^{th} harmonics. This would not be shown by an isolated converter study and so both devices should be represented during the system analysis.

8.3.2 Historical case

Prior to 1983 there were no filters installed at the Tiwai-033 busbar. Also, as the HVdc link was only upgraded in 1989, the 220kV HVdc rectifiers and filters at Benmore-220 did not exist. The system is reassessed under this original operating condition and shown in Figure 8.10.

The initial indication is that the rectifiers at Benmore should have a negligible effect on the Tiwai-033 installation. However, there is a significant unbalanced current

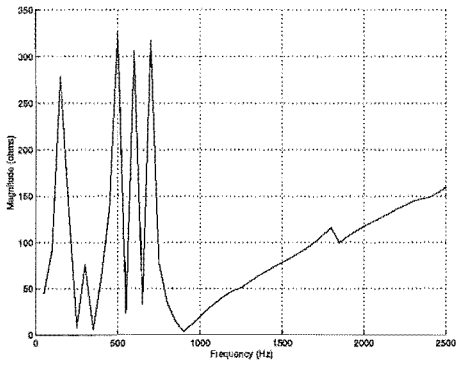

(a) Reduced impedance at Tiwai-033

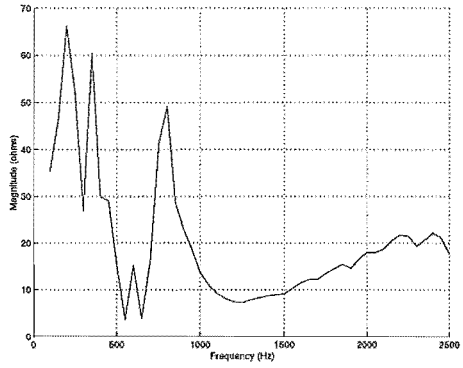

(b) Reduced impedance at Benmore-220

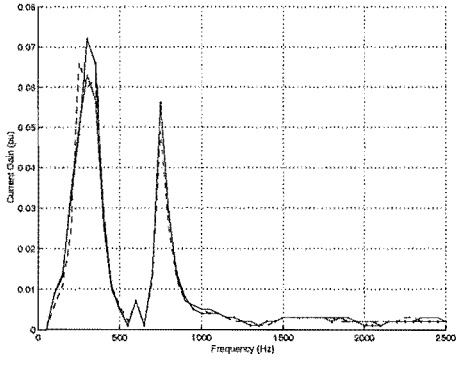

(c) Current gain from Benmore-220 to Tiwai-033 (3 phase)

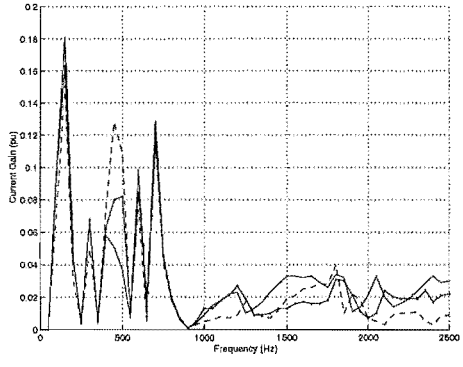

(d) Current gain from Tiwai-033 to Benmore-220 (3 phase)

Figure 8.6 Effect of Benmore-220 on Tiwai-033 (a),(c), and Benmore-220 on Tiwai-033 (b),(d)

gain from Tiwai-033 to Benmore-220 terminating in a high Norton impedance. This would result in reasonable levels of harmonic voltage distortion.

This is by no means a conclusive study as an exhaustive investigation of multiple heavy and lightly loaded system studies is required for this. Rather, this is an indication of an approach that can be used for early assessment of non-linear device harmonic interaction.

8.4 COMPARISON OF DIRECT ANALYSIS WITH IHA

As stated previously, the positive sequence approach will work sufficiently well for characteristic harmonics. However, as it assumes completely balanced systems, it will not be able to accurately analyse non-characteristic behaviour. For this end, three phase analysis programs can more accurately predict the imbalanced nature of harmonic flows. They most often use constant harmonic current or voltage injections which

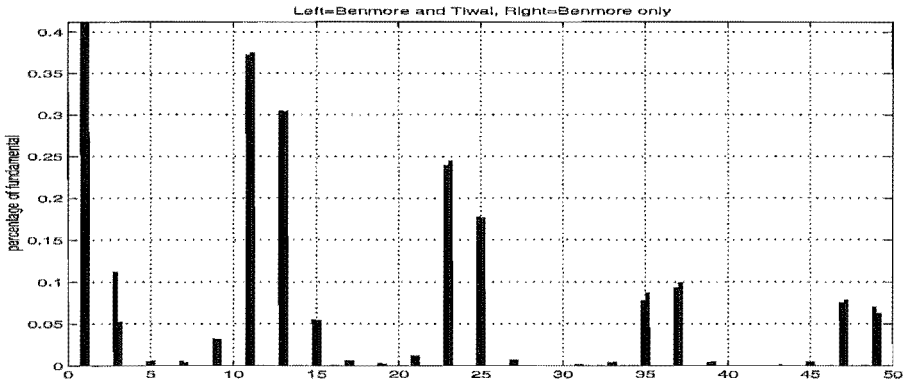

Figure 8.7 Effect of Tiwai-033 on Benmore-220 voltage harmonics

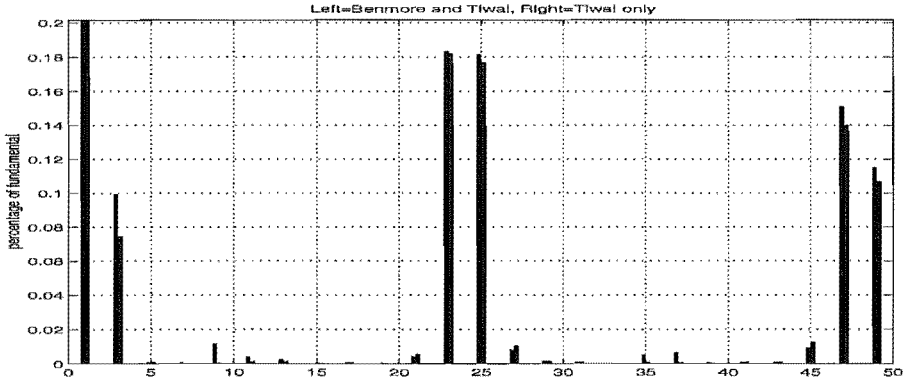

Figure 8.8 Effect of Benmore-220 on Tiwai-033 voltage harmonics

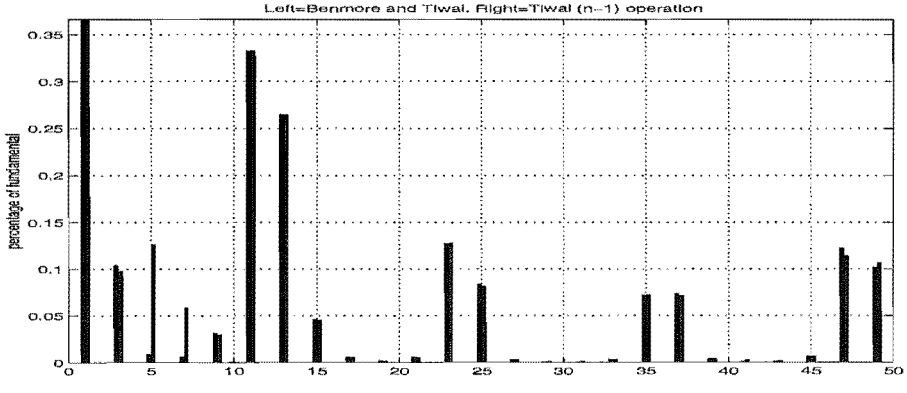

Figure 8.9 Effect of (n-1) at Tiwai-033 on Benmore-220 voltage harmonics

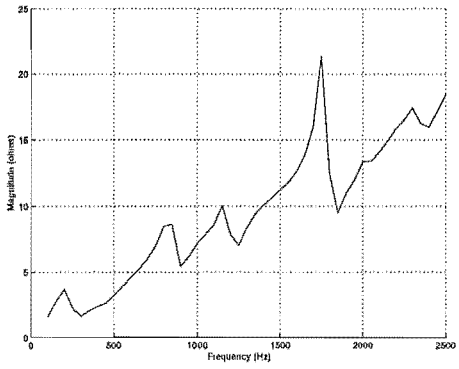

(a) Reduced impedance at Tiwai-033

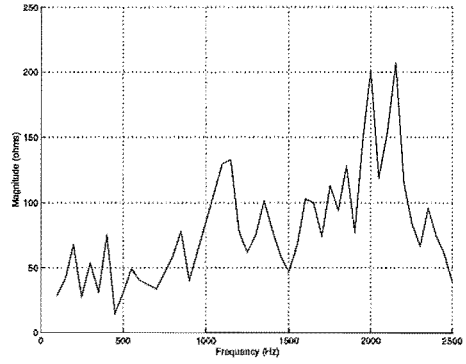

(b) Reduced impedance at Benmore-220

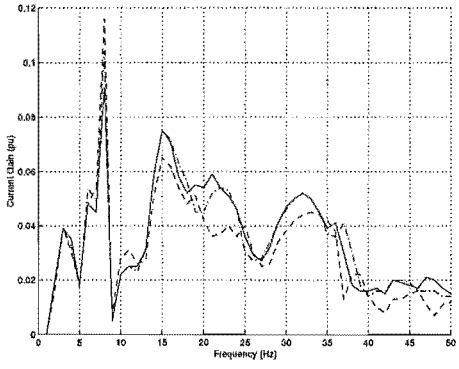

(c) Current gain from Benmore-220 to Tiwai-033 (3 phase)

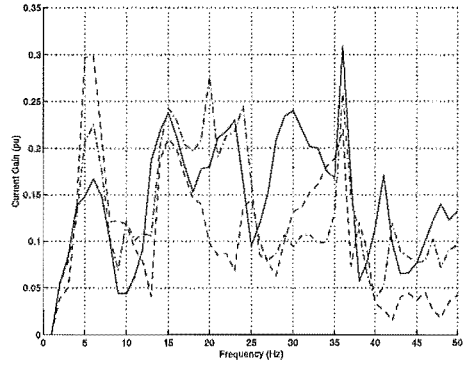

(d) Current gain from Tiwai-033 to Benmore-220 (3 phase)

Figure 8.10 Effect of Benmore-220 on Tiwai-033 (a),(c), and Benmore-220 on Tiwai-033 (b),(d) for the pre-1983 case

assumes the injections are independent of system operating conditions and harmonic levels throughout the system. While this constant source representation does allow system measurements to be used directly within the analysis, they do not represent the true nature of non-linear loads. Thunberg [1998] showed that a Norton representation of system loads yielded better results than use of constant injections; a method for the calculation of the Norton equivalents from measurements was also shown. As most non-linear devices are not ideal current sources, their effective impedances should be represented for accurate results.

The ac side harmonic current injections for the direct solution are calculated using a three phase power frequency voltage, i.e. assuming that there is no ac or dc harmonic distortion. These harmonic currents are injected into the system impedance matrix to calculate the harmonic voltages throughout the ac system. Without performing the three phase loadflow, the terminal voltage imbalance would have to be estimated and will only provide approximate non-characteristic harmonic levels. An extension to this

simple approach is to include the Norton impedance of the non-linear devices in the Direct Norton Analysis (DNA). This is done here using the impedances derived in Chapter 7 for the converter installations. This will result in a closer representation of the non-linear device to that of the full harmonic solution.

8.4.1 Comparison using the Lower South Island test system

The first case is for the nominally operated Lower South Island test system as shown in Appendix B. The first three columns of Table 8.1 show the harmonic currents calculated by the Direct Analysis (DA), Direct Norton Analysis (DNA) and the full Iterative Harmonic Analysis. The last three columns show the harmonic voltages that result from the three different representations. The harmonic current injections for both direct analysis methods are calculated from the same loadflow information.

These comparisons in Table 8.1 show that the ideal current source approach predicts high levels of third harmonic voltage and some other non-characteristic harmonics. With the converter impedance represented, the third harmonic is reduced substantially and provides a better agreement with that of the full harmonic solution. The full harmonic solution also shows the remainder of the non-characteristic harmonics reducing significantly from even those given by DNA approach.

Table 8.1 Comparison of direct solution methods, Tiwai-033 busbar

h	I_{DA}	I_{DNA}	I_{IHA}	$\|V_{DA}\|\%$	$\|V_{DNA}\|\%$	$\|V_{IHA}\|\%$
1	100.000	100.000	100.000	100.000	100.000	100.000
3	0.410	0.410	0.116	2.329	0.512	0.659
5	0.003	0.003	0.006	0.000	0.000	0.001
19	0.004	0.004	0.001	0.001	0.001	0.000
21	0.091	0.091	0.028	0.026	0.025	0.008
23	0.930	0.930	0.844	0.412	0.393	0.375
25	0.850	0.850	0.767	0.495	0.461	0.447
27	0.088	0.088	0.023	0.062	0.058	0.016
29	0.005	0.005	0.001	0.004	0.004	0.001
43	0.005	0.005	0.000	0.007	0.006	0.000
45	0.049	0.049	0.014	0.075	0.070	0.022
47	0.229	0.229	0.198	0.379	0.366	0.328
49	0.201	0.201	0.175	0.365	0.369	0.317

8.4.2 Comparison using the CIGRE test system

Another case where the full harmonic solution is required is the inverter end of the CIGRE HVdc link. A 5% phase imbalance in the inverter ac system impedance produces 3.7% negative sequence distortion at the inverter terminal busbar. Table 8.2 shows the same solution comparisons as above for this case.

Table 8.2 Comparison of direct solution methods, CIGRE inverter busbar

h	I_{DA}	I_{DNA}	I_{IHA}	$\|V_{DA}\|\%$	$\|V_{DNA}\|\%$	$\|V_{IHA}\|\%$
1	100.000	100.000	100.000	100.000	100.000	100.000
3	0.787	0.787	1.476	0.530	0.616	0.989
5	0.054	0.054	0.048	0.030	0.031	0.026
7	0.053	0.053	0.056	0.018	0.019	0.019
9	0.579	0.579	0.557	0.118	0.120	0.113
11	4.649	4.649	4.434	0.805	0.807	0.765
13	2.857	2.857	2.933	0.606	0.604	0.620
15	0.365	0.365	0.318	0.098	0.098	0.085
17	0.053	0.053	0.045	0.017	0.017	0.014
19	0.049	0.049	0.047	0.017	0.017	0.016
21	0.166	0.166	0.164	0.060	0.060	0.059
23	0.758	0.758	0.848	0.270	0.270	0.301
25	0.766	0.766	0.757	0.264	0.264	0.260
27	0.148	0.147	0.132	0.048	0.048	0.043

Due in part to the relatively high impedance dc system, the representation of the converter impedance is not very significant for the majority of the harmonics. However, for the low order and characteristic harmonics, the effect of the dc current ripple is significant, as illustrated by the differences even with the Norton equivalent. In particular, not performing a full harmonic solution for this system will predict lower levels of third harmonic than are actually present.

8.5 ASSESSMENT CRITERIA

As the differences that have been observed between the direct solutions and the full harmonic solution are sometimes significant, it would be desirable to decide in advance the necessity of a full solution. To achieve this aim, some form of assessment criteria or indicator is required; preferably an automatic one. The criteria should give an indication of the degree of change to be expected between the initial current calculations and the final solution, without actually performing the full solution.

8.5.1 Harmonic voltage distortion

A direct solution is performed to obtain the harmonic voltages at all the non-linear device busbars. Then using knowledge of the non-linear device sensitivities, a decision can be made as to whether the direct method is sufficient or a full IHA is to be used.

The problem with this approach is that there is no immediate feedback with regards to interaction between two non-linear devices as the harmonic currents are calculated independently of the rest of the system. However, the harmonic voltages at one busbar may be affected significantly by harmonic current injections from another busbar. In

this case it is likely that different harmonic interaction will be observed with a full harmonic solution. A slightly different approach would be to use superposition and independently evaluate the harmonic injections from each device. Then, by inspecting the sets of harmonic voltages, a decision could be made as to the best method of analysis to pursue.

8.5.2 Harmonic current re-evaluation

The injection of a harmonic current into a system busbar produces a voltage of the same frequency. This new voltage may then affect the harmonic currents generated by the non-linear device, which in turn affects the voltage and so forth. The sensitivity of the non-linear device to voltage distortion somewhat dictates the number of iterations required, and similarly the system impedance at that busbar determines the amount of distortion that is caused by the current injection. By observing the change in the harmonic currents that are generated by the device, the sensitivity of the non-linear device to voltage distortion is revealed. This may provide some indication of the potential degree of change that is to be expected from the full solution.

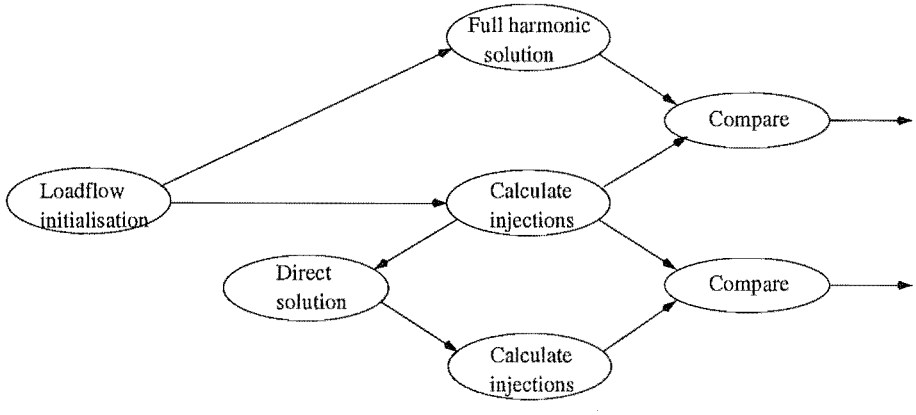

Figure 8.11 Illustration of method of harmonic current re-evaluation

Figure 8.11 illustrates this criterion based on an initial three phase loadflow solution. From this point the initial set of full harmonic currents are calculated; these are then injected into the ac system to return harmonic voltages, the new harmonic current injections are re-evaluated from these distorted voltages. This is essentially the first step in a Gauss-Seidel style IHA. The change in the harmonic currents following the first iteration evaluation are compared with those after the full harmonic solution to decide whether they can provide a useful indication. A large current change between the initial direct penetration and the re-evaluation may then be a indication of the need for a full harmonic solution.

8.6 TESTING THE PROPOSED IHA INDICATORS

In order to gauge the usefulness of the aforementioned indicators, several tests are performed with the indicators. In the following cases, three sets of harmonic currents are shown. The first uses only the distorted fundamental derived from the initial three phase loadflow, the second includes the harmonic distortion from the first iteration of the Gauss-Seidel step, and the third is from the complete harmonic solution.

8.6.1 Indicator test with the Lower South Island test system

Using the New Zealand Lower South Island test system, a test study is carried out to observe what the indicators show. The dc system at the Tiwai-033 24-pulse installation is such that there is minimal dc current ripple in the converters. The results for this study are shown in Table 8.3.

As the magnitude of relative change, $|\Delta I_{re-eval}\%|$ and $|\Delta I_{IHA}\%|$, is roughly the same, the re-evaluation method will possibly yield some information; even though $I_{re-eval}$ increased while I_{IHA} decreased. This indicator suggests that the levels of the third and characteristic harmonics will change significantly from the initial direct penetration levels. By observing the harmonic voltages, the full solution harmonics are relatively low. The voltages obtained from the Direct Analysis are similar apart from the third harmonic. However, as Section 8.4 showed, better agreement can be obtained by representing the Norton impedance of the converters.

Table 8.3 Testing indicators with the LSI test system

h	$I_{DA}\%$	$I_{re-eval}$	I_{IHA}	$\|\Delta I_{re-eval}\%\|$	$\|\Delta I_{IHA}\%\|$	$\|V_{DA}\|\%$	$\|V_{IHA}\|\%$
1	100.000	100.002	100.040	0.002	0.040	100.111	100.000
3	0.410	0.770	0.116	0.360	0.294	2.332	0.659
5	0.003	0.070	0.006	0.067	0.003	0.000	0.001
19	0.004	0.008	0.001	0.004	0.003	0.001	0.000
21	0.091	0.163	0.028	0.071	0.063	0.026	0.008
23	0.930	0.827	0.844	0.103	0.086	0.413	0.375
25	0.850	0.748	0.767	0.102	0.083	0.495	0.447
27	0.088	0.164	0.023	0.077	0.065	0.062	0.016
29	0.005	0.025	0.001	0.021	0.003	0.004	0.001
43	0.005	0.008	0.000	0.003	0.005	0.007	0.000
45	0.049	0.085	0.014	0.037	0.034	0.075	0.022
47	0.229	0.173	0.198	0.056	0.031	0.379	0.328
49	0.201	0.159	0.175	0.042	0.027	0.365	0.317

8.6.2 Indicator test with the CIGRE HVdc test system

A similar test is performed on the CIGRE HVdc test system with a 5% imbalance in the inverter ac system impedance. This imbalance generates non-characteristic ac and

dc harmonics which propagate through both systems. The results of the indicators for the inverter ac system, shown in Table 8.4, illustrate the need for more detailed analysis to assess the third and characteristic harmonics.

Table 8.4 Testing indicators with the CIGRE HVdc test system

h	$I_{DA}\%$	$I_{re-eval}$	I_{IHA}	$\lvert\Delta I_{re-eval}\%\rvert$	$\lvert\Delta I_{IHA}\%\rvert$	$\lvert V_{DA}\rvert\%$	$\lvert V_{IHA}\rvert\%$
1	100.000	100.040	100.029	0.040	0.029	99.614	100.000
3	0.787	2.247	1.476	1.459	0.689	0.528	0.989
5	0.054	0.114	0.048	0.060	0.006	0.030	0.026
7	0.053	0.118	0.056	0.065	0.003	0.018	0.019
9	0.579	0.783	0.557	0.204	0.022	0.117	0.113
11	4.649	4.441	4.436	0.208	0.213	0.802	0.765
13	2.857	3.053	2.934	0.196	0.077	0.604	0.620
15	0.365	0.483	0.318	0.118	0.047	0.098	0.085
17	0.053	0.099	0.045	0.046	0.008	0.017	0.014
19	0.049	0.095	0.047	0.045	0.002	0.017	0.016
21	0.166	0.206	0.164	0.039	0.002	0.059	0.059
23	0.758	0.781	0.848	0.023	0.090	0.269	0.301
25	0.766	0.659	0.758	0.107	0.009	0.263	0.260
27	0.148	0.169	0.132	0.022	0.016	0.048	0.043

The rectifier ac system also has non-characteristic harmonics due to the imbalance in the inverter ac system. As Table 8.5 shows, the ordinary direct analysis will not show this, as current harmonics are calculated assuming no harmonic distortion. The current re-evaluation does show the presence of non-characteristic harmonics, thus indicating the need for a full IHA solution.

Table 8.5 Testing indicators with the CIGRE HVdc test system

h	$I_{DA}\%$	$I_{re-eval}$	I_{IHA}	$\lvert\Delta I_{re-eval}\%\rvert$	$\lvert\Delta I_{IHA}\%\rvert$	$\lvert V_{DA}\rvert\%$	$\lvert V_{IHA}\rvert\%$
1	100.000	99.999	99.988	0.000	0.012	99.613	100.000
3	0.000	0.316	0.165	0.316	0.165	0.000	0.122
5	0.000	0.001	0.000	0.001	0.000	0.000	0.000
7	0.000	0.002	0.001	0.002	0.000	0.000	0.000
9	0.000	0.115	0.066	0.115	0.066	0.000	0.014
11	3.769	3.485	3.492	0.284	0.276	0.667	0.618
13	2.018	2.285	2.153	0.267	0.135	0.438	0.468
15	0.000	0.042	0.003	0.042	0.003	0.000	0.001
17	0.000	0.001	0.000	0.000	0.000	0.000	0.000
19	0.000	0.001	0.000	0.001	0.000	0.000	0.000
21	0.000	0.051	0.019	0.051	0.019	0.000	0.007
23	0.936	0.935	0.935	0.001	0.001	0.338	0.338
25	0.789	0.810	0.789	0.021	0.000	0.276	0.276
27	0.000	0.040	0.009	0.040	0.009	0.000	0.003

One of the other major reasons for using an iterative harmonic solution is the presence of two or more non-linear devices coupled through the ac system. In such cases,

the devices cannot be considered in isolation from one another as the harmonic voltages produced by one will affect the harmonic generation of the other. Consequently, a unified solution approach is most likely to be necessary, although the importance of the unified representation depends on the degree of coupling between the systems.

8.7 CONCLUSIONS

The three phase frequency domain model provides the most accurate system representation for harmonic analysis. Care must be taken when reducing a system to include relevant local loads, generators and transmission lines; an automated scheme could be used to evaluate the change in system impedance as each component is removed. This would allow the specification of the degree of error acceptable when reducing a system to an equivalent.

The current re-evaluation method is not an overly useful indicator of the need to perform IHA. It has some use in assessing the sensitivity of a non-linear device to determine whether it should be included in the system model. However, it may be more beneficial for this purpose to assess the degree of non-linear device interaction by calculating the reduced impedance and current gain matrix of Section 8.3.

The best alternative is to perform an IHA and a Direct Norton Analysis for a number of different cases and obtain a degree of confidence in the DNA method. This should provide a real indication and a measure of the inaccuracies inherent within the DNA study. However to do this, a general harmonic solution algorithm that can represent multiple non-linear devices is required. Also for harmonic transfer across HVdc links, a DNA solution will require some thought in order to represent the harmonic transfer between the ac and dc systems.

Chapter 9

CONCLUSIONS AND FUTURE WORK

9.1 CONCLUSIONS

Based on a review of techniques used for power system harmonic modelling, a specification for a general harmonic solution algorithm has been proposed. The algorithm allows simultaneous solution of multiple interconnected non-linear devices with realistic controls, using a full Newton method. A minimal solution set is obtained by reducing the linear system to the non-linear device busbars at harmonic frequencies. Maintaining the three phase loadflow during the harmonic solution eliminates any requirements for a loadflow equivalent. The full harmonic solution is initialised with a three phase loadflow which allows a fast and robust solution. A number of validations have been performed using conventional time domain simulation; excellent comparisons were obtained.

The harmonic domain solution of the 6-pulse converter has been extended to include most transformer configurations. The converter model has been made more modular with the switching instants solved explicitly as internal variables, and the Jacobian block has been modified to account for their modulation effects.

The multiple run feature of the algorithm has been used to illustrate the harmonic transfer and behaviour of HVdc links, under a range of operating conditions. It was also shown that the accurate representation of the mutual coupling of the dc transmission line is important, when representing bipolar HVdc links.

High-pulse installations with converters connected in parallel on the dc side were modelled. In such a configuration, the number of characteristic dc current harmonics of a single converter increase with the installation pulse number. During outage conditions, the effective pulse number of an installation is reduced to the pulse number of the basic phase-shifting unit, i.e. 6 or 12-pulse. A method was shown to increase the installation's effective pulse number by using secondary tap-changers to change the transformer phase shifts. This resulted in minimal low order harmonic generation during outage conditions. The harmonic impedance of the converter was calculated by a fast numerical technique and used to show that, for a given converter, the commuta-

tion period is the major source of impedance variation. This method was also used to compare a variety of simplified converter impedance models, and assess the effect of the converter impedance on the nett ac system impedance. Accurate converter impedance representation is important for low frequencies, and one of the simplified models provided satisfactory results. The inclusion of the converter impedance in a direct solution gives more accurate results than a conventional current source representation. A degree of confidence can be obtained in the direct solutions of a system, by comparison with Iterative Harmonic Analysis.

9.2 FUTURE WORK

9.2.1 Representation of other non-linear devices

FACTS devices

The representation of Flexible AC Transmission System (FACTS) devices is very important for future harmonic analysis, as these will soon become common within transmission networks. The Thyristor Controlled Reactor (TCR), Static Var Compensator (SVC) and the Thyristor Controlled Series Capacitor (TCSC) devices have the TCR branch in common. It should therefore be relatively easy to develop a common module for the analysis of these devices, based upon the basic nodal analysis and convolution approach described in this thesis.

The modelling of a static compensator (STATCOM) would be similar to that of the 6-pulse converter. As it is a voltage sourced converter, the input parameters would be the ac voltage and dc voltage though, instead of the ac voltage and dc current. As STATCOMs use forced turn off devices such as GTOs, the switching instants are pre-defined by the controller. The same convolution analysis could be used to build a piece-wise equivalent of the ac-dc and dc-ac transfers.

Non-linear transformer

The representation of non-linear transformers within the Harmonic Domain has already been done. While these models were developed using the complex conjugate solution, it is relatively simple to convert them to a real valued positive frequency solution as shown in Chapter 2. These models would be a very valuable addition and there is the possibility of representing the converter transformer in this fashion as well. This should be investigated as a means of representing converter transformer saturation.

Constant power variable frequency drive

Another potentially interesting device to be included in the harmonic solution, is the variable frequency motor drive. These typically use a three phase rectifier feeding a

high frequency PWM inverter directly connected to the motor. Because of the control action of the inverter, the device appears as a constant dc power load, irrespective of the dc voltage. The inverter then draws a dc current that is dependent upon the dc voltage to provide the specified dc power. In the presence of dc voltage ripple, the inverter draws ripple current to maintain constant power, which has the effect of amplifying the original dc voltage ripple. This is a problem ideally suited to Iterative Harmonic Analysis.

The inverter, assumed initially as an ideal dc power source, would be represented within the solution as a current dependent voltage source. The voltage would be calculated by a time domain division, which is analogous to the frequency domain deconvolution. The advantage of this representation is that it uses conventional dc system analysis. Two FFT functions would be required for the harmonic transfer and it is believed that the analytic Jacobian of the deconvolution would be relatively straight forward to obtain.

Series capacitor commutated converter

While no series compensated HVdc transmission scheme exist, the concept is being taken seriously at the moment. A harmonic model of a series compensated converters will be required, when such installations are designed. The implementation of the series compensated converter in the harmonic domain involves a second-order commutation circuit. This will require two initial conditions, i.e. the dc current and the dc voltage across the commutating capacitance. These will have to be solved for in terms of the solution variables and switching instances.

Active filters

An active filter is used to cancel harmonic currents by injecting anti-phase currents into the supply. Typically these devices use high frequency switching and the characteristic harmonics that they generate are not an immediate concern. The device could thus be represented by a transfer function in series with a control loop transfer function. This would allow designers to accurately determine the performance and requirements of the device ratings within a system during the initial design stages.

Comparison of star-g/delta zigzag and star-g/star zigzag transformers

As Figure 9.1 shows, there are two main ways of connecting a transformer in zigzag to achieve arbitrary phase shifts; they are referred to as star and delta zigzags respectively. While the characteristics of the star zigzag have been explored within this thesis, it would be worthwhile doing a similar study on the delta zigzag. The latter can be constructed from only three secondary windings as opposed to six for the star

zigzag. It maybe more or less sensitive to winding inaccuracies and leakage reactance imbalances. The presence of a delta winding inherent within the delta will trap any triplen harmonics generated from the magnetisation as well. The performance of delta zigzags for pulse reduction should also be investigated.

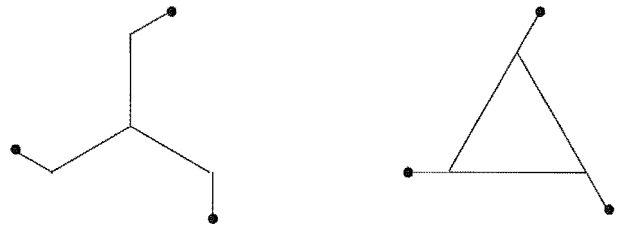

Figure 9.1 Different zigzag transformer connections

9.2.2 Extension of the algorithm to interharmonics

The logical extension of the algorithm to represent interharmonics is to reduce the base frequency to the highest common multiple of the system frequencies. However for a 50 Hz to 60 Hz link this would require a base frequency of 10 Hz and a solution of 300 frequencies per system, for the first 50 integer harmonics. The solution size, and consequently the solution time, will grow by a factor somewhere between 5 and 25. Thus, to make such a solution practical, the following refinements are suggested.

Modifications to the solution structure

For a standard 50 integer harmonic solution it can be noticed that less than half of the frequencies are non-zero, or that a large number of them are below a certain threshold. A balanced 50 harmonic solution of a 12-pulse converter has only 9 ac system harmonics and 4 dc system harmonics. If some imbalance is introduced, then this may grow to may be 15-20 harmonics. By representing only the significant frequencies within the solution, it is possible to shrink the overall size of the system Jacobian. A far more dramatic reduction would take place if this were done for a 10 Hz base system. However, the frequencies of significance are not known in advance and therefore the solution arrays would have to be adjusted adaptively at every iteration. A new routine would calculate the nodal contributions from all of the non-linear devices at all frequencies, and then select only the frequencies that are greater than a specified threshold. Most of this frequency selection is inherent in the general harmonic algorithm, i.e. it can solve only the first 13 harmonics from the full 50 harmonic data set. It would not require major changes to the algorithm to implement such a method. The major drawback is that the Jacobian would have to be updated multiple times. However, by initially estimating the frequencies present, this could be minimised.

Modifications to the linear system

A problem arising from the reduction of the effective base frequency is the amount of information storage required for the linear system. A base frequency reduction from 50 Hz to 10 Hz results in a factor of 5 increase while a reduction to 1 Hz results in a factor of 50. It has been shown in the thesis that a resolution of 10 Hz represents the frequency dependency of the linear system reasonably accurately. For an analysis of the interaction between 50 Hz and 51 Hz systems, it should be reasonable to store the system information at 10 Hz intervals. If a frequency of 663 Hz is required, the 13^{th} harmonic of the 51 Hz system, the parameters are calculated from an interpolation between the 660 Hz and 670 Hz frequencies.

Modifications to the converter

The converter model itself can have its computational burden reduced by carefully observing the operating conditions. If only a fraction of the full voltage harmonic array is represented within the solution, only these frequencies will be required within the convolution. This can significantly reduce the amount of computation required for the convolutions. A further improvement is to use converter theory to predict what frequencies are going to be generated, and consequently only do the convolution for those frequencies. However, this approximation may introduce error into the converter analysis and should be used with caution. A further suggestion is to use half-wave symmetry to minimise the number of switching angle calculations required.

9.2.3 Improvements to direct analysis methods

The representation of converter impedances within a direct harmonic solution resulted in improved solution accuracy. This method was termed a Direct Norton Analysis (DNA). A hybrid approach between the Wood's describing function analysis and a simple R-L equivalent for high frequencies should be developed. This method would then be a reasonable approximation at all frequencies and be fast compared to the full harmonic approach. A three phase ac-dc loadflow would be required for accurate prediction of the terminal voltage distortion and consequently the non-characteristic harmonic generation.

For harmonic interaction between ac systems through an HVdc link, a sequential solution of the systems should be used starting with the most imbalanced system first. This would give some indication to the degree of harmonic transfer through the systems. For further detailed analysis, this method should be run in conjunction with the full harmonic approach so as to ensure the solution validity.

Appendix A

CONVERTER TRANSFORMER SAMPLE FORMULATION

A.1 EXPRESSIONS FOR YG-Y AND YG-D TRANSFORMERS

The following are the expressions derived by Smith [1996] for the star-ground/star and star-ground/delta transformers, based on the definitions in Chapter 3.

$$I_{comm} = [P_{comm\_V}] \begin{bmatrix} V_B \\ V_E \\ V_O \end{bmatrix} + [P_{comm\_I}] [I_{dc}] \tag{A.1}$$

$$V_d = [P_{volt\_V}] \begin{bmatrix} V_B \\ V_E \\ V_O \end{bmatrix} + [P_{volt\_I}] [I_{dc}] \tag{A.2}$$

A.1.1 Star-g/star

Commutation current sample

$$P_{comm\_V} = \frac{1}{jk} \begin{bmatrix} \frac{1}{X_B+X_E} & \frac{-1}{X_B+X_E} & 0 \end{bmatrix} \tag{A.3}$$

$$P_{comm\_I} = \frac{X_E}{X_B + X_E} \tag{A.4}$$

Voltage sample during a commutation period

$$P_{volt\_V} = \begin{bmatrix} \frac{X_E}{X_B+X_E} & \frac{X_B}{X_B+X_E} & -1 \end{bmatrix} \tag{A.5}$$

$$P_{volt\_I} = -jk \left(\frac{X_E}{X_B + X_E} + X_O \right) \tag{A.6}$$

Voltage sample during a normal conduction

$$P_{volt\_V} = \begin{bmatrix} 1 & 0 & -1 \end{bmatrix} \tag{A.7}$$

$$P_{volt\_I} = -jk\left(X_B + X_O\right) \tag{A.8}$$

Transformer transfer matrix

$$\begin{bmatrix} I_a \\ I_b \\ I_c \end{bmatrix} = \begin{bmatrix} 1 & 0 \\ 0 & 1 \\ -1 & -1 \end{bmatrix} \begin{bmatrix} I_A \\ I_B \end{bmatrix} \tag{A.9}$$

A.1.2 Star-g/delta

Commutation current sample

$$P_{comm\_V} = \frac{1}{j\sqrt{3}k} \begin{bmatrix} \frac{1}{X_B} & \frac{-1}{(X_O+X_E)} & \frac{-1}{(X_O+X_E)} \end{bmatrix} \tag{A.10}$$

$$P_{comm\_I} = \frac{X_E}{X_O + X_E} \tag{A.11}$$

Voltage sample during a commutation period

$$P_{volt\_V} = \sqrt{3} \begin{bmatrix} 0 & \frac{X_O}{X_O+X_E} & \frac{-X_E}{X_O+X_E} \end{bmatrix} \tag{A.12}$$

$$P_{volt\_I} = \frac{-j3kX_OX_E}{X_O + X_E} \tag{A.13}$$

Voltage sample during a normal conduction

$$P_{volt\_V} = \sqrt{3} \begin{bmatrix} \frac{(X_O+X_E)}{X_B+X_O+X_E} & \frac{-X_B}{X_B+X_O+X_E} & \frac{-X_B}{X_B+X_O+X_E} \end{bmatrix} \tag{A.14}$$

$$P_{volt\_I} = \frac{-j3kX_B\left(X_O + X_E\right)}{X_B + X_O + X_E} \tag{A.15}$$

Transformer transfer matrix

Using the nodal admittance matrix of the transformer defined in the following form:

$$\left[\begin{array}{c} I_a \\ I_b \\ I_c \\ \hline I_A \\ I_B \end{array}\right] = \left[\begin{array}{cc|c} & & \\ A & B & \\ & & \\ \hline & & \\ C & D & \\ & & \end{array}\right] \left[\begin{array}{c} V_a \\ V_b \\ V_c \\ \hline V_A \\ V_B \end{array}\right] \tag{A.16}$$

The three primary phase currents can be obtained in terms of the primary voltages and two of the secondary phase currents.

$$\left[\begin{array}{c} I_a \\ I_b \\ I_c \end{array}\right] = \Big([A] - [B][D]^{-1}[C]\Big) \left[\begin{array}{c} V_a \\ V_b \\ V_c \end{array}\right] - [B][D]^{-1} \left[\begin{array}{c} I_A \\ I_B \end{array}\right] \tag{A.17}$$

A.2 DERIVATION OF THE GENERAL CONVERTER TRANSFORMER FORMULATION

A linear transformer can be represented by the admittance matrix of the form given by Equation A.18. Based upon the analysis of Chapter 3, the general sample expressions of Equations A.19 and A.20 can be formed.

$$\left[\begin{array}{c} I_P \\ I_S \end{array}\right] = \left[\begin{array}{cc} A & B \\ C & D \end{array}\right] \left[\begin{array}{c} V_P \\ V_S \end{array}\right] \tag{A.18}$$

$$V_d = \left[\begin{array}{cc} p_B & p_O \end{array}\right] \left(\left[\begin{array}{c} I_B \\ I_O \end{array}\right] - \left[\begin{array}{ccc} c_{Ba} & c_{Bb} & c_{Bc} \\ c_{Oa} & c_{Ob} & c_{Oc} \end{array}\right] \left[\begin{array}{c} V_A \\ V_B \\ V_C \end{array}\right] \right) \tag{A.19}$$

$$I_c = \frac{1}{p_B - p_E} \left(\left[\begin{array}{cc} p_B & p_E \end{array}\right] \left[\begin{array}{ccc} c_{Ba} & c_{Bb} & c_{Bc} \\ c_{Ea} & c_{Eb} & c_{Ec} \end{array}\right] \left[\begin{array}{c} V_A \\ V_B \\ V_C \end{array}\right] - p_{(E)} I_d \right) \tag{A.20}$$

where,

$$\begin{aligned} \left[\begin{array}{cc} p_{Be} & p_{Eb} \end{array}\right] &= \left[\begin{array}{cc} Di_{BB} & Di_{BE} \end{array}\right] - \left[\begin{array}{cc} Di_{EB} & Di_{EE} \end{array}\right] \\ \left[\begin{array}{cc} p_{Bo} & p_{Ob} \end{array}\right] &= \left[\begin{array}{cc} Di_{BB} & Di_{BO} \end{array}\right] - \left[\begin{array}{cc} Di_{OB} & Di_{OO} \end{array}\right] \end{aligned} \tag{A.21}$$

The reduced D matrix can be analytically inverted which allows the expressions of p_B, p_O and p_E to be expressed analytically.

$$D = \begin{bmatrix} D_{11} & D_{12} \\ D_{21} & D_{22} \end{bmatrix} \quad , \quad D^{-1} = \begin{bmatrix} Di_{11} & Di_{12} \\ Di_{21} & Di_{22} \end{bmatrix} \tag{A.22}$$

therefore,

$$\begin{aligned} Di_{11} &= \frac{D_{22}}{D_{11}D_{22} - D_{12}D_{21}} \quad , \quad Di_{12} = \frac{-D_{12}}{D_{11}D_{22} - D_{12}D_{21}} \\ Di_{21} &= \frac{-D_{21}}{D_{11}D_{22} - D_{12}D_{21}} \quad , \quad Di_{22} = \frac{D_{11}}{D_{11}D_{22} - D_{12}D_{21}} \end{aligned} \tag{A.23}$$

From Equations A.21 and A.23, the p terms can be expressed directly in terms of the original D matrix elements.

$$\begin{aligned} p_{Be} &= \frac{D_{EE} + D_{EB}}{D_{BB}D_{EE} - D_{BE}D_{EB}} \quad , \quad p_{Eb} = \frac{-D_{BE} - D_{BB}}{D_{BB}D_{EE} - D_{BE}D_{EB}} \\ p_{Bo} &= \frac{D_{OO} + D_{OB}}{D_{BB}D_{OO} - D_{BO}D_{OB}} \quad , \quad p_{Ob} = \frac{-D_{BO} - D_{BB}}{D_{BB}D_{OO} - D_{BO}D_{OB}} \\ (p_{Be} - p_{Eb}) &= \frac{D_{BB} + D_{BE} + D_{EB} + D_{EE}}{D_{BB}D_{EE} - D_{BE}D_{EB}} \end{aligned} \tag{A.24}$$

A.2.1 Commutation current sample

Using Equation A.20, the commutation current samples can be formed. First, a simplification is made:

$$\begin{bmatrix} h_B & h_E \end{bmatrix} = \frac{\begin{bmatrix} p_{Be} & p_{Eb} \end{bmatrix}}{(p_{Be} - p_{Eb})} = \frac{\begin{bmatrix} (D_{EB} + D_{EE}) & -(D_{BB} + D_{BE}) \end{bmatrix}}{D_{BB} + D_{BE} + D_{EB} + D_{EE}} \tag{A.25}$$

Substituting this simplification in the commutation current equation and removing the frequency dependency as in Section 3.2.3, the following is obtained:

$$P_{comm\_V} = \frac{1}{jk} \begin{bmatrix} h_B & h_E \end{bmatrix} \begin{bmatrix} C_{Ba} & C_{Bb} & C_{Bc} \\ C_{Ea} & C_{Eb} & C_{Ec} \end{bmatrix} \tag{A.26}$$

$$P_{comm\_I} = -h_E \tag{A.27}$$

A.2.2 Voltage sample during a commutation period

The dc voltage samples are given by Equation A.19, with the secondary phase currents defined in terms of the dc current and commutation current given in Equation A.25. For the voltage sample during a commutation, the expression obtained in the previous

section is substituted in and then simplified. This is as follows:

$$P_{volt\_V} = \left([p_{Bo}]\,[P_{comm\_V}] - \begin{bmatrix} p_{Bo} & p_{Ob} \end{bmatrix} \begin{bmatrix} C_{Ba} & C_{Bb} & C_{Bc} \\ C_{Oa} & C_{Ob} & C_{Oc} \end{bmatrix} \right) \quad \text{(A.28)}$$

$$P_{volt\_I} = jk\,(p_{Bo}P_{comm\_I} - p_{Ob}) \quad \text{(A.29)}$$

A.2.3 Voltage sample during a normal conduction

The dc voltage samples for a normal conduction period are much simpler as the secondary phase currents are only that of the dc current.

$$P_{volt\_V} = -\begin{bmatrix} p_{Bo} & p_{Ob} \end{bmatrix} \begin{bmatrix} C_{Ba} & C_{Bb} & C_{Bc} \\ C_{Oa} & C_{Ob} & C_{Oc} \end{bmatrix} \quad \text{(A.30)}$$

$$P_{volt\_I} = jk\,(p_{Bo} - p_{Ob}) \quad \text{(A.31)}$$

This expression is the same as for a commutation period except that $P_{comm\_V} = 0$ and $P_{comm\_I} = 1$.

A.3 PROOF OF SAMPLES FOR A YG-D TRANSFORMER

In order to briefly demonstrate that this approach provides the same results as the detailed analysis, the nodal admittance matrix for a star-ground/star transformer, as shown in Section 3.2.4, is used with the mutual coupling terms set to zero. This is then verified by comparison with the original results as derived by Smith [1996]. The derivations here use the two switching periods of Table A.1. Note, the derivations here refer to the specific phases (a/b/c) whereas the general expressions earlier refer to the general nodes (B/E/O).

Table A.1 Switching periods used for validation

p	B	E	O
1	a	c	b
2	a	c	b

$$Y_{(s-g/d)} = \left[\begin{array}{ccc|ccc} y_a & 0 & 0 & -\frac{1}{\sqrt{3}}y_a & 0 & \frac{1}{\sqrt{3}}y_a \\ 0 & y_b & 0 & \frac{1}{\sqrt{3}}y_b & -\frac{1}{\sqrt{3}}y_b & 0 \\ 0 & 0 & y_c & 0 & \frac{1}{\sqrt{3}}y_c & -\frac{1}{\sqrt{3}}y_c \\ \hline -\frac{1}{\sqrt{3}}y_a & \frac{1}{\sqrt{3}}y_b & 0 & \frac{1}{3}(y_a+y_b) & -\frac{1}{3}y_b & -\frac{1}{3}y_a \\ 0 & -\frac{1}{\sqrt{3}}y_b & \frac{1}{\sqrt{3}}y_c & -\frac{1}{3}y_b & \frac{1}{3}(y_b+y_c) & -\frac{1}{3}y_c \\ \frac{1}{\sqrt{3}}y_a & 0 & -\frac{1}{\sqrt{3}}y_c & -\frac{1}{3}y_a & -\frac{1}{3}y_c & \frac{1}{3}(y_a+y_c) \end{array}\right] \quad \text{(A.32)}$$

The p terms are expressed directly in terms of the original D matrix elements using the analytic inverse of Equation A.24:

$$\begin{aligned} p_{Be} &= \frac{3y_c}{y_ay_b + y_ay_c + y_by_c} \quad , \quad p_{Eb} = \frac{-3y_b}{y_ay_b + y_ay_c + y_by_c} \\ p_{Bo} &= \frac{3y_c}{y_ay_b + y_ay_c + y_by_c} \quad , \quad p_{Ob} = \frac{-3y_a}{y_ay_b + y_ay_c + y_by_c} \\ (p_{Be} - p_{Eb}) &= \frac{3(y_c + y_b)}{y_ay_b + y_ay_c + y_by_c} \end{aligned} \tag{A.33}$$

Similarly for the h_B and h_E terms:

$$\begin{bmatrix} h_B & h_E \end{bmatrix} = \begin{bmatrix} \left(\frac{y_c}{y_b+y_c}\right) & \left(\frac{-y_b}{y_b+y_c}\right) \end{bmatrix} \tag{A.34}$$

A.3.1 Commutation current sample

$$\begin{aligned} P_{comm\_V} &= \frac{1}{j\sqrt{3}k} \begin{bmatrix} \frac{y_c}{y_b+y_c} & \frac{-y_b}{y_b+y_c} \end{bmatrix} \begin{bmatrix} -y_a & y_b & 0 \\ y_a & 0 & -y_c \end{bmatrix} \\ &= \frac{1}{j\sqrt{3}k} \begin{bmatrix} \frac{-y_ay_c - y_ay_b}{y_b+y_c} & \frac{y_by_c}{y_b+y_c} & \frac{y_by_c}{y_b+y_c} \end{bmatrix} \\ &= \frac{1}{j\sqrt{3}k} \begin{bmatrix} \frac{-1}{X_a} & \frac{1}{X_b+X_c} & \frac{1}{X_b+X_c} \end{bmatrix} \end{aligned} \tag{A.35}$$

$$\begin{aligned} P_{comm\_I} &= \frac{y_b}{y_b + y_c} \\ &= \frac{X_c}{X_b + X_c} \end{aligned} \tag{A.36}$$

A.3.2 Voltage sample during a commutation period

$$\begin{aligned} P_{volt\_V} &= \sqrt{(3)} \left(\left[\frac{y_c}{y_ay_b + y_ay_c + y_by_c} \right] \begin{bmatrix} \frac{-y_ay_c - y_ay_b}{y_b+y_c} & \frac{y_by_c}{y_b+y_c} & \frac{y_by_c)}{y_b+y_c} \end{bmatrix} \right. \\ &\quad \left. - \begin{bmatrix} \frac{y_c}{y_ay_b+y_ay_c+y_by_c} & \frac{-y_a}{y_ay_b+y_ay_c+y_by_c} \end{bmatrix} \begin{bmatrix} -y_a & y_b & 0 \\ 0 & -y_b & y_c \end{bmatrix} \right) \\ &= \frac{\sqrt{3} \begin{bmatrix} \left(\frac{y_ay_cy_c+y_ay_by_c}{y_b+y_c} - y_ay_c\right) & \left(\frac{-y_by_cy_c}{y_b+y_c} + y_ay_b + y_by_c\right) & \left(\frac{-y_by_cy_c}{y_b+y_c} - y_ay_c\right) \end{bmatrix}}{y_ay_b + y_ay_c + y_by_c} \\ &= \sqrt{3} \begin{bmatrix} 0 & \frac{y_b}{y_b+y_c} & \frac{-y_c}{y_b+y_c} \end{bmatrix} \\ &= \sqrt{3} \begin{bmatrix} 0 & \frac{X_c}{X_b+X_c} & \frac{-X_b}{X_b+X_c} \end{bmatrix} \end{aligned} \tag{A.37}$$

$$\begin{aligned} P_{volt\_I} &= j3k \left(\left(\frac{y_c}{y_ay_b + y_ay_c + y_by_c} \right) \left(\frac{y_b}{y_b + y_c} \right) - \left(\frac{-y_a}{y_ay_b + y_ay_c + y_by_c} \right) \right) \\ &= j3k \frac{\left(\frac{1}{X_c} \cdot \frac{X_c}{X_b+X_c} + \frac{1}{X_a} \right) X_aX_bX_c}{X_a + X_b + X_c} \end{aligned}$$

$$= \left(\frac{j3kX_bX_c}{X_b + X_c}\right) \tag{A.38}$$

A.3.3 Voltage sample during a normal conduction

$$\begin{aligned} P_{volt\_V} &= \sqrt{(3)}\left(-\begin{bmatrix} \frac{y_c}{y_ay_b+y_ay_c+y_by_c} & \frac{-y_a}{y_ay_b+y_ay_c+y_by_c} \end{bmatrix}\begin{bmatrix} -y_a & y_b & 0 \\ 0 & -y_b & y_c \end{bmatrix}\right) \\ &= \sqrt{3}\begin{bmatrix} \frac{-y_ay_c}{y_ay_b+y_ay_c+y_by_c} & \frac{y_ay_b+y_by_c}{y_ay_b+y_ay_c+y_by_c} & \frac{-y_ay_c}{y_ay_b+y_ay_c+y_by_c} \end{bmatrix} \\ &= \sqrt{3}\begin{bmatrix} \frac{-X_b}{X_a+X_b+X_c} & \frac{X_a+X_b}{X_a+X_b+X_c} & \frac{-X_b}{X_a+X_b+X_c} \end{bmatrix} \end{aligned} \tag{A.39}$$

$$\begin{aligned} P_{volt\_I} &= j3k\left(\left(\frac{y_c}{y_ay_b + y_ay_c + y_by_c}\right) - \left(\frac{-y_a}{y_ay_b + y_ay_c + y_by_c}\right)\right) \\ &= \frac{j3kX_b\left(X_a + X_c\right)}{X_a + X_b + X_c} \end{aligned} \tag{A.40}$$

A.4 AN EXAMPLE OF A COUPLED INDUCTANCE MATRIX

The following is an example of a coupled inductance matrix of a multi-limb delta/star-ground transformer, calculated using the Unified Magnetic Equivalent Circuit formulation [Enright 1996]. It is assumed linear and is based on the parameters of three-phase five-limb hydro-electric power station transformer operating within the New Zealand ac system [Enright *et al.* 1999]. The required parameters are only the name-plate data and the core-aspect ratios. The three inductance matrices given here are for the same name plate data but different core configurations. The data is in henries and for a three phase bank of single phase transformers, a three-phase three-limb transformer and a three-phase five limb transformer. Many thanks to Dr. Wade Enright for this data.

Table A.2 Name-plate data of the transformer

Nominal power rating	61MVA
Primary winding voltage	11kV
Secondary winding voltage	220kV
Base frequency	50Hz
Leakage reactance	10.27%

$$L_{bank} = \left[\begin{array}{ccc|ccc} 0.359 & 0.000 & 0.000 & 7.173 & 0.000 & 0.000 \\ 0.000 & 0.359 & 0.000 & 0.000 & 7.173 & 0.000 \\ 0.000 & 0.000 & 0.359 & 0.000 & 0.000 & 7.173 \\ \hline 7.173 & 0.000 & 0.000 & 143.580 & 0.000 & 0.000 \\ 0.000 & 7.173 & 0.000 & 0.000 & 143.580 & 0.000 \\ 0.000 & 0.000 & 7.173 & 0.000 & 0.000 & 143.580 \end{array}\right] \tag{A.41}$$

$$L_{3\_limb} = \left[\begin{array}{ccc|ccc} 0.393 & -0.056 & -0.014 & 7.845 & -1.129 & -0.277 \\ -0.056 & 0.322 & -0.056 & -1.129 & 6.440 & -1.129 \\ -0.014 & -0.056 & 0.393 & -0.277 & -1.129 & 7.845 \\ \hline 7.845 & -1.129 & -0.277 & 157.040 & -22.573 & -5.531 \\ -1.129 & 6.440 & -1.129 & -22.573 & 128.940 & -22.573 \\ -0.277 & -1.129 & 7.845 & -5.531 & -22.573 & 157.040 \end{array}\right] \quad \text{(A.42)}$$

$$L_{5\_limb} = \left[\begin{array}{ccc|ccc} 0.271 & -0.183 & -0.088 & 5.418 & -3.655 & -1.757 \\ -0.183 & 0.366 & -0.183 & -3.655 & 7.316 & -3.655 \\ -0.088 & -0.183 & 0.271 & -1.757 & -3.655 & 5.418 \\ \hline 5.418 & -3.655 & -1.757 & 108.490 & -73.097 & -35.131 \\ -3.655 & 7.316 & -3.655 & -73.097 & 146.450 & -73.097 \\ -1.757 & -3.655 & 5.418 & -35.131 & -73.097 & 108.490 \end{array}\right] \quad \text{(A.43)}$$

The transfer matrix that connects nodal quantities to primitive quantities for a delta/star-grounded transformer is:

$$C^T_{(d/s-g)} = \left[\begin{array}{ccc|ccc} 1 & -1 & 0 & 0 & 0 & 0 \\ 0 & 1 & -1 & 0 & 0 & 0 \\ -1 & 0 & 1 & 0 & 0 & 0 \\ \hline 0 & 0 & 0 & 1 & 0 & 0 \\ 0 & 0 & 0 & 0 & 1 & 0 \\ 0 & 0 & 0 & 0 & 0 & 1 \end{array}\right] \quad \text{(A.44)}$$

where, the nodal admittance matrix is given by:

$$\left[\begin{array}{c} I_a \\ I_b \\ I_c \\ \hline I_A \\ I_B \\ I_C \end{array}\right] = \left[C_{(d/s-g)}\right]\left[j\omega L_{prim}\right]^{-1}\left[C_{(d/s-g)}\right]^T \left[\begin{array}{c} V_a \\ V_b \\ V_c \\ \hline V_A \\ V_B \\ V_C \end{array}\right] \quad \text{(A.45)}$$

Appendix B

TEST SYSTEMS

B.1 CIGRE HVDC TEST SYSTEM

The CIGRE benchmark model [Szechtmann *et al.* 1991] consists of weak rectifier and inverter ac systems resonant at the second harmonic and a dc system resonant at the fundamental frequency. Both ac systems are balanced and connected in star-ground, the system is shown in Figure B.1 with additional information in Table B.1. The HVdc link is a 12-pulse monopolar configuration with the converter transformers connected star-ground/star and star-ground/delta. Figures B.2 to B.4 show the impedance scans of the ac and dc systems. The phase imbalance for the inverter ac system is typically a 5.0% resistance inserted into one phase in series with the ac system.

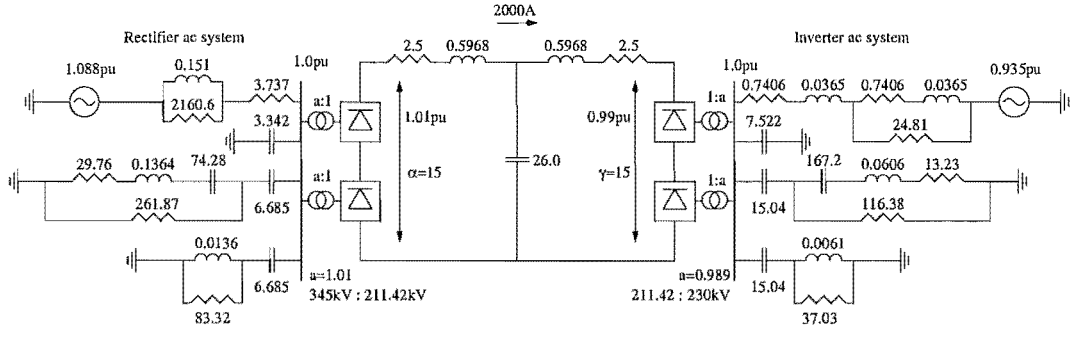

Figure B.1 CIGRE HVdc benchmark test system. (All components in Ω, H and μF)

B.2 LOWER SOUTH ISLAND TEST SYSTEM

This test system is based on the lower South Island power system of New Zealand. It is a useful test system due to its naturally imbalanced form and to the presence of a large power converter situated at the Tiwai-033 busbar. Apart from the converter installation, the system includes two major city loads that vary significantly over the daily period. The 220kV transmission lines are all specified by their geometry and conductor specifications, and consequently are unbalanced and couple between sequences. An example of the impedance scans are available in Chapter 8. The original system, as

Rectifier ac voltage base	345.0kV
Inverter ac voltage base	230kV
Rectifier voltage source	$1.088\ \angle 22.18^o$
Inverter voltage source	$0.935\ \angle -23.14^o$
Nominal dc voltage	500kV
Transformer power base	598MVA
Transformer leakage reactance	0.18 pu
Transformer secondary voltage	211.42kV
Nominal Rectifier firing angle	15.0^o
Nominal Inverter extinction angle	15.0^o
Thyristor forward voltage drop	0.001kV
Thyristor onstate resistance	0.01 Ω
Snubber resistance	5000 Ω
Snubber capacitance	0.05 μF
dc current transducer gain	0.5
dc current transducer time constant	0.001s
PI controller proportional gain	1.0989
PI controller time constant	0.0091s
Type-1 filter	shunt capacitor
Type-2 filter	single tuned filter
Type-3 filter	special CIGRE filter

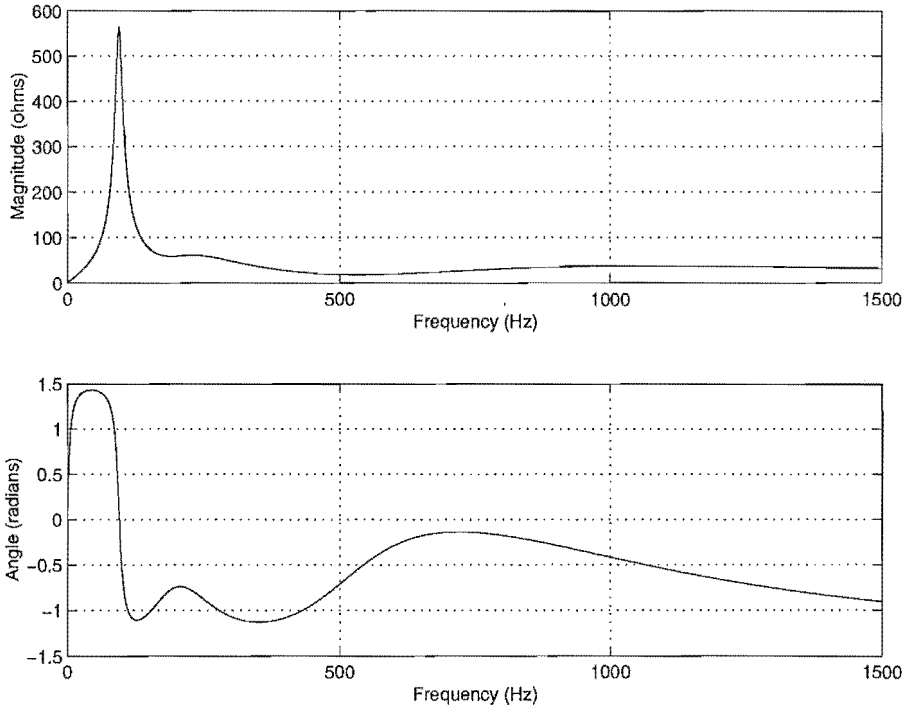

Figure B.2 Frequency scan of the CIGRE rectifier ac system impedance

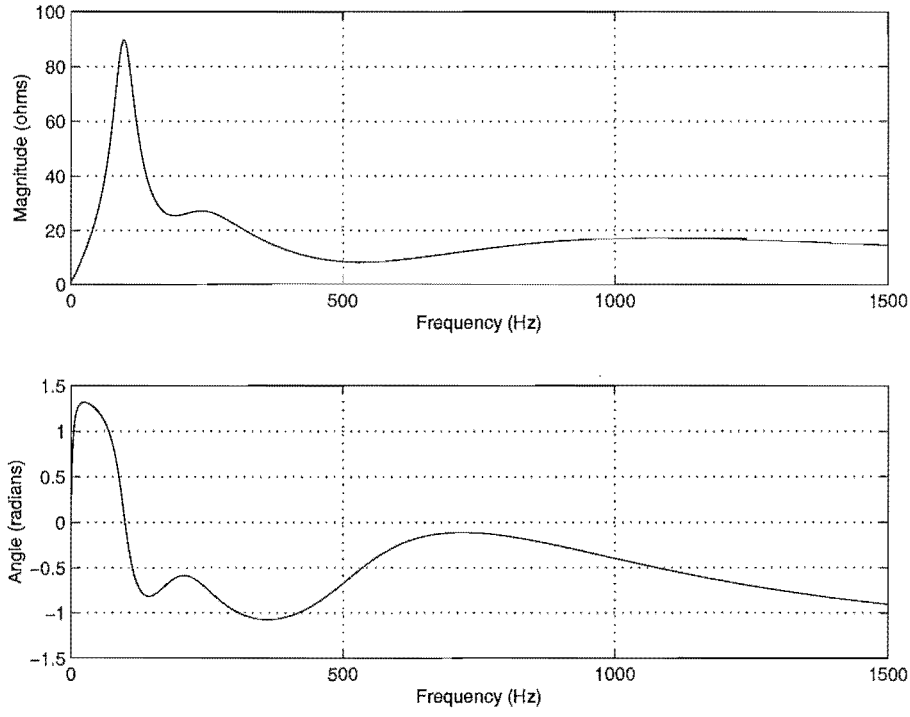

Figure B.3 Frequency scan of the CIGRE inverter ac system impedance

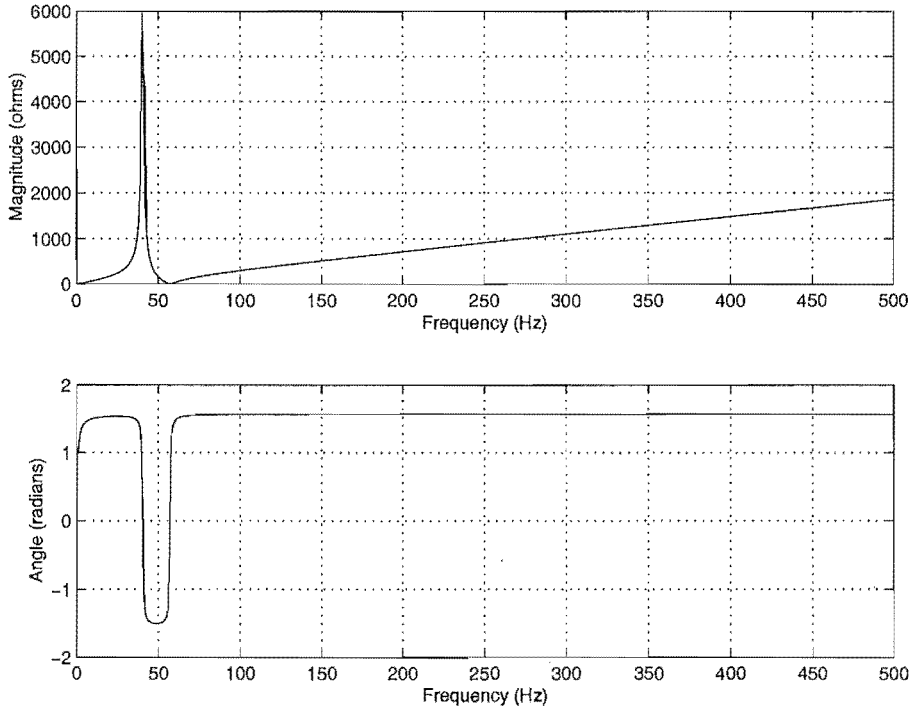

Figure B.4 Frequency scan of the CIGRE dc system impedance

widely published, did not represent the Tiwai-033 busbar, but rather connected directly to the Tiwai-220 busbar. Tables B.2 to B.8 show all of the necessary information, the three phase loadflow results are shown in Table B.9.

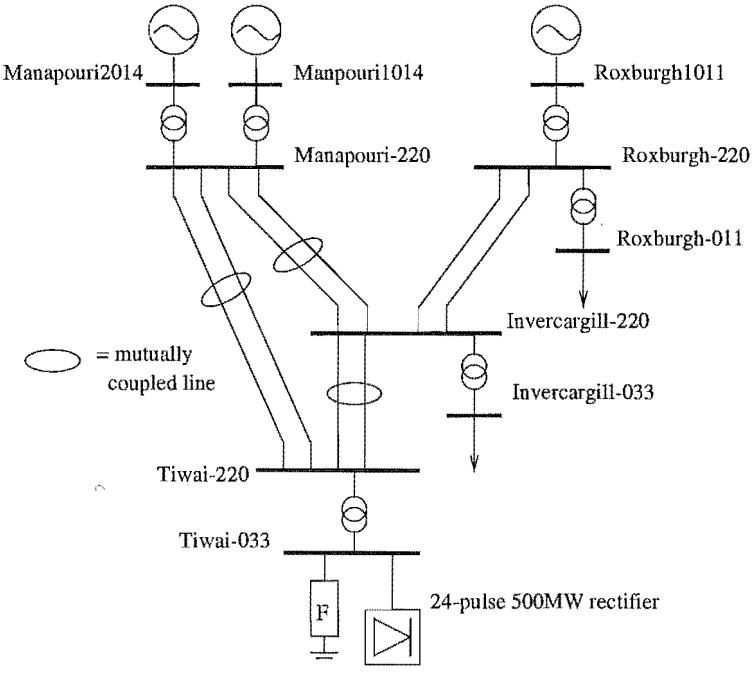

Figure B.5 Lower South Island of New Zealand test system

The number of circuits is given by (Nc) with the conductor dimensions by (Cx) and (Cy), the number of earth-wires by (Ne) with dimensions by (Ex) and (Ey). The line to line busbar voltage is given in kV by the last three digits of its name. The power base is 100 MVA and the system frequency is 50 Hz. The filters at the Tiwai-033 busbar consist of three banks of series RLC branches connected in star-ground. The rectifier installation at the Tiwai-033 busbar is approximately 480MW and 130MVar. The rectifier has been represented by a 24-pulse installation connected in parallel on the dc side, by small linking reactors (R=1$\mu\Omega$, L=1μH) to an ideal current source (80 kA). The converters are diode rectifiers with transformer specifications as given in Table B.1.

Table B.1 Converter information for the Lower South Island test system

	Phase shift	X_l	V_{pri}	V_{sec}	P_{base}
Converter 1	22.5^o	0.05 pu	33.0 kV	5.0 kV	100 MVA
Converter 2	7.5^o	0.05 pu	33.0 kV	5.0 kV	100 MVA
Converter 3	-7.5^o	0.05 pu	33.0 kV	5.0 kV	100 MVA
Converter 4	-22.5^o	0.05 pu	33.0 kV	5.0 kV	100 MVA

Table B.2 Transmission line parameters for Lower South Island test system

	Busbars	Length	Conductor type	Earth-wire type
1	Manapouri-220 to Invercargill-220	152.90 km	GOAT (30/3.71+7/3.71 ACSR)	(7/3.05 Gehss)
2	Manapouri-220 to Tiwai-220	175.60 km	GOAT (30/3.71+7/3.71 ACSR)	(7/3.05 Gehss)
3	Invercargill-220 to Tiwai-220	24.30 km	GOAT (30/3.71+7/3.71 ACSR)	(7/3.05 Gehss)
4	Invercargill-220 to Roxburgh-220	132.20 km	ZEBRA (42/3.18 7/3.18 ACSR)	(7/3.05 Gehss)
5	Invercargill-220 to Roxburgh-220	129.80 km	ZEBRA (42/3.18 7/3.18 ACSR)	—

Table B.3 Conductor geometry for Lower South Island transmission lines (in metres)

	Cx1	Cx2	Cx3	Cy1	Cy2	Cy3	Ex1	Ey1	Bundle Sep	Nc	Ne
1	4.80	6.34	4.42	12.50	18.00	23.50	0.00	28.94	0.46	2	1
2	4.80	6.34	4.42	12.50	18.00	23.50	0.00	29.00	0.45	2	1
3	4.77	6.29	4.41	12.50	17.95	23.41	1.52	28.26	0.46	2	2
4	0.00	6.47	12.94	12.50	12.50	12.50	4.61	18.41	-	1	2
5	0.00	7.20	14.40	12.50	12.50	12.50	-	-	-	1	0

Table B.4 Positive sequence data for Lower South Island transmission lines

	R_{series}(pu)	X_{series}(pu)	B_{shunt}(pu)
1	0.013213	0.090105	0.289716
2	0.015130	0.103601	0.332103
3	0.002124	0.014353	0.046259
4	0.017947	0.111500	0.178836
5	0.017490	0.111338	0.172195

Table B.5 Generator information for Lower South Island testsystem

Busbar	x_d''	V_{set}	P_{set}
Manapouri-1014	0.037	1.0 pu	200.0 MW
Manapouri-2014	0.074	1.0 pu	200.0 MW
Roxburgh-1011	0.062	1.0 pu	slack

Table B.6 Transformer information for the Lower South Island testsystem

Pri. Busbar	Sec. Busbar	Pri. Con.	Sec. Con.	R_l(pu)	X_l(pu)	Tap
Manapouri-220	Manapouri-1014	Star-g	Delta	0.0006	0.02690	0.025 pri
Manapouri-220	Manapouri-2014	Star-g	Delta	0.0006	0.05360	0.025 pri
Roxburgh-220	Roxburgh-1011	Star-g	Delta	0.0006	0.03816	0.025 pri
Invercargill-033	Invercargill-220	Star-g	Delta	0.0006	0.10290	0.025 pri
Roxburgh-011	Roxburgh-220	Star-g	Delta	0.0006	0.03816	0.025 pri
Tiwai-220	Tiwai-033	Star-g	Star-g	0.0006	0.02083	—

Table B.7 System loads for Lower South Island test system (MW, MVar)

Busbar	P_a	Q_a	P_b	Q_b	P_c	Q_c
Invercargill-033	45.00	12.00	45.00	12.00	45.00	12.00
Roxburgh-011	30.00	18.00	30.00	18.00	30.00	18.00

Table B.8 Filters at the Tiwai-033 busbar

Connection	R (Ω)	L (mH)	C (μF)
Star-g	0.606	19.30	21.00
Star-g	0.424	9.63	21.50
Star-g	2.340	17.20	3.49
Star-g	1.660	14.40	5.80

Table B.9 Sample three phase loadflow results

Sequence voltages

$\|V_+\|$	$\angle V_+$	$\|V_-\|$	$\angle V_-$	$\|V_0\|$	$\angle V_0$	Busbar
0.93732	13.04	0.00830	-170.82	0.00562	134.15	TIWAI—-033
0.95732	19.54	0.00816	-169.83	0.00553	134.15	TIWAI—-220
1.00000	0.00	0.00192	173.75	0.00000	90.00	ROXBURGH1011
1.00595	26.69	0.00331	148.27	0.00052	81.22	MANAPOURI220
1.00000	0.62	0.00187	178.27	0.00000	0.00	MANAPOUR1014
1.00000	4.54	0.00187	178.27	0.00000	-45.00	MANAPOUR2014
0.99164	24.91	0.00318	143.75	0.00061	105.97	ROXBURGH-220
0.99400	52.86	0.00326	113.75	0.00014	51.00	ROXBURGH-011
0.96364	20.55	0.00742	-172.40	0.00465	131.10	INVERCARG220
0.93359	41.44	0.00784	157.51	0.00136	0.44	INVERCARG033

Sequence currents

$\|I_+\|$	$\angle I_+$	$\|I_-\|$	$\angle I_-$	$\|I_0\|$	$\angle I_0$	Busbar
5.38105	177.94	0.00674	11.88	0.00000	80.11	TIWAI—-033
0.00000	13.87	0.00000	34.57	0.00000	-101.31	TIWAI—-220
2.44350	-22.95	0.03096	-96.25	0.00000	88.57	ROXBURGH1011
0.00000	122.34	0.00000	-24.64	0.00000	-69.15	MANAPOURI220
2.61783	-16.64	0.05059	-91.73	0.00000	80.54	MANAPOUR1014
2.55313	-7.17	0.02534	-91.73	0.00000	75.96	MANAPOUR2014
0.00000	132.34	0.00000	-131.49	0.00000	5.71	ROXBURGH-220
1.05590	-158.10	0.00015	27.28	0.00347	-39.00	ROXBURGH-011
0.00000	163.18	0.00000	115.35	0.00000	-1.15	INVERCARG220
1.49658	-153.49	0.00218	64.73	0.01258	-89.56	INVERCARG033

Phase powers

P_a	Q_a	P_b	Q_b	P_c	Q_c	Busbar
-159.93	-44.19	-162.67	-44.04	-164.38	-43.13	TIWAI—-033
0.00	0.00	0.00	0.00	0.00	0.00	TIWAI—-220
74.74	32.74	74.21	31.30	76.06	31.24	ROXBURGH1011
0.00	0.00	0.00	0.00	0.00	0.00	MANAPOURI220
83.11	27.52	81.95	25.14	84.94	24.98	MANAPOUR1014
83.08	18.09	82.72	16.92	84.20	16.80	MANAPOUR2014
0.00	0.00	0.00	0.00	0.00	0.00	ROXBURGH-220
-30.00	-18.00	-30.00	-18.00	-30.00	-18.00	ROXBURGH-011
0.00	0.00	0.00	0.00	0.00	0.00	INVERCARG220
-45.00	-12.00	-45.00	-12.00	-45.00	-12.00	INVERCARG033

B.3 ZIGZAG TRANSFORMER VALIDATION

The test system used for validation of the zig-zag converter transformer was a single unit attached to a highly inductive ac system and resistive dc system as shown by Figure B.6. The resistive dc system and inductive ac system provide high levels of harmonic distortion which will excite all the non-linear transfers. The system information is given in Table B.10.

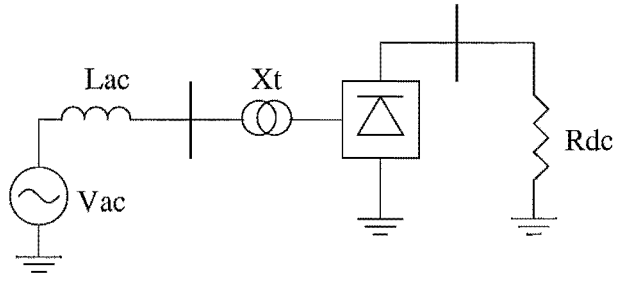

Figure B.6 Test system used for zigzag transformer validation

Table B.10 System information for zigzag transformer validation

Base frequency	50 Hz
$V_{ac}(50Hz)$	1.0 pu (+ve seq)
$V_{ac}(150Hz)$	0.1 pu (+ve seq)
L_{ac}	100.0 mH
R_{dc}	200.0 Ω
X_T	0.10 pu
Phase shift	15.0^o
P_{base}	100 MVA
V_{base}	100 kV
T_{ratio}	1:1

B.4 TEST SYSTEM FOR MULTIPULSE INSTALLATION CHARACTERISTICS

The following is the test system used for the investigations into the characteristics of multi-pulse parallel connected installations. Figure B.7 shows the system configuration and Table B.11 provides the system parameters used.

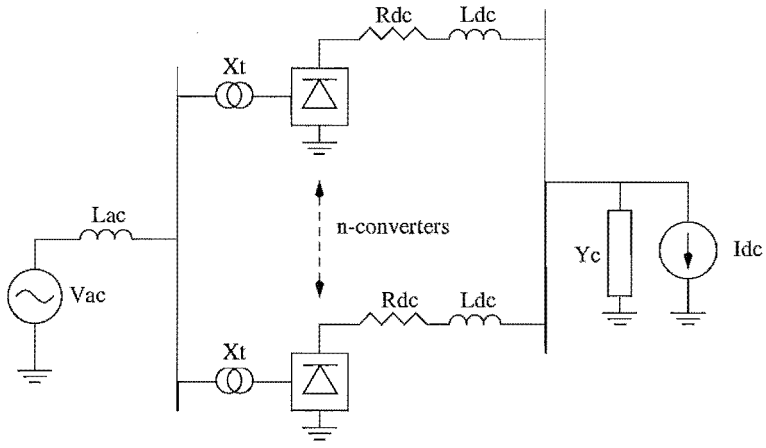

Figure B.7 Test system used for multi-pulse characteristics

Table B.11 System information for multi-pulse characteristics

Base frequency	50 Hz
P_{base}	100 MVA
$V_{ac}(50Hz)$	1.0 pu (+ve seq)
$I_{dc}(0Hz)$	10 kA/converter
L_{ac}	1.0 mH
R_{dc}	$1.0\mu\Omega$
L_{dc}	1.0μH
Y_c	0.0 pu
X_T	0.05 pu or 0.10 pu
V_{pri}	33.0 kV
V_{sec}	5.0 kV
Phase shift (24-pulse)	$+22.5^o$, $+7.5^o$, -7.5^o, -22.5^o
Phase shift (48-pulse)	$+26.25^o$, $+18.75^o$, $+11.25^o$, $+3.75^o$, -26.25^o, -18.75^o, -11.25^o, -3.75^o

Appendix C

DERIVATION OF JACOBIAN BLOCKS

C.1 6-PULSE CONVERTER

C.1.1 Initial breakdown of the partial derivatives

Using knowledge of the harmonic transfer calculations of the converter, the partial derivatives can be expanded as shown in Chapter 3. A slightly simplified version is shown below for the main electrical transfers. A large number of common blocks can be seen from these equations which are derived in the following sections. When using the chain rule to combine these expressions, care must be used as the expressions are not complex but real-valued tensors. Thus the multiplications must be as 2*2 matrices, not complex multiplication. As the convolution is expressed as an analytic function, the frequency coupling of the partial derivatives can be easily obtained. Simplifications can be made by observing the relative effects of the individual terms to the nett derivatives. Such as the effect of commutation angle modulation on the ac phase currents is minimal and so the exclusion of this term is not noticed.

$$\frac{\partial I_{ac}}{\partial V_{ac}} = \frac{\partial I_{comm}}{\partial V_{ac}} \otimes \psi + \left(I_{comm} \otimes \frac{\partial \psi}{\partial \theta}\right) \frac{\partial \theta}{\partial V_{ac}} + \left(I_{comm} \otimes \frac{\partial \psi}{\partial \phi}\right) \frac{\partial \phi}{\partial V_{ac}} + \left(I_{dc} \otimes \frac{\partial \psi}{\partial \theta}\right) \frac{\partial \theta}{\partial V_{ac}} + \left(I_{dc} \otimes \frac{\partial \psi}{\partial \phi}\right) \frac{\partial \phi}{\partial V_{ac}} \tag{C.1}$$

$$\frac{\partial I_{ac}}{\partial I_{dc}} = \frac{\partial I_{comm}}{\partial I_{dc}} \otimes \psi + \left(I_{comm} \otimes \frac{\partial \psi}{\partial \theta}\right) \frac{\partial \theta}{\partial I_{dc}} + \left(I_{comm} \otimes \frac{\partial \psi}{\partial \phi}\right) \frac{\partial \phi}{\partial I_{dc}} + \frac{\partial I_{dc}}{\partial I_{dc}} \otimes \psi + \left(I_{dc} \otimes \frac{\partial \psi}{\partial \theta}\right) \frac{\partial \theta}{\partial I_{dc}} + \left(I_{dc} \otimes \frac{\partial \psi}{\partial \phi}\right) \frac{\partial \phi}{\partial I_{dc}} \tag{C.2}$$

$$\frac{\partial V_{dc}}{\partial V_{ac}} = \frac{\partial V_{volt}}{\partial V_{ac}} \otimes \psi + \left(V_{volt} \otimes \frac{\partial \psi}{\partial \theta}\right) \frac{\partial \theta}{\partial V_{ac}} + \left(V_{volt} \otimes \frac{\partial \psi}{\partial \phi}\right) \frac{\partial \phi}{\partial V_{ac}} \tag{C.3}$$

$$\frac{\partial V_{dc}}{\partial I_{dc}} = \frac{\partial V_{volt}}{\partial I_{dc}} \otimes \psi + \left(V_{volt} \otimes \frac{\partial \psi}{\partial \theta}\right) \frac{\partial \theta}{\partial I_{dc}} + \left(V_{volt} \otimes \frac{\partial \psi}{\partial \phi}\right) \frac{\partial \phi}{\partial I_{dc}} \tag{C.4}$$

C.1.2 Effect of electrical variables on samples

The effect of the electrical variables on the steady-state samples are just the transfer matrices. With the phase currents, only four of the commutation currents affect each phase and so only those four will contribute to the Jacobian term. For the dc voltage all 12 samples affect the voltage and so all 12 get included.

$$\frac{\partial I_{comm}(l)}{\partial V_{ac}(k)} = \sum \frac{1}{jk} P_{comm\_V} \tag{C.5}$$

$$\frac{\partial I_{comm}(l)}{\partial I_{dc}(k)} = \sum P_{comm\_I} \tag{C.6}$$

$$\frac{\partial V_{volt}(l)}{\partial V_{ac}(k)} = \sum P_{volt\_V} \tag{C.7}$$

$$\frac{\partial V_{volt}(l)}{\partial I_{dc}(k)} = \sum jk P_{volt\_I} \tag{C.8}$$

C.1.3 Effect of electrical variables on switchings

Firing angles

The partial derivatives of the firing angles with respect to the electrical variables are formed from the following expressions. The final expression depends upon the firing strategy used, which dictates the mismatch F_θ.

$$\frac{\partial \theta_p}{\partial V_{ac}} = \frac{\partial \theta_p}{F_{\theta_p}} \frac{F_{\theta_p}}{\partial V_{ac}} \tag{C.9}$$

$$\frac{\partial \theta_p}{\partial I_{dc}} = \frac{\partial \theta_p}{F_{\theta_p}} \frac{F_{\theta_p}}{\partial I_{dc}} \tag{C.10}$$

For the un-controlled converter, the firing angles are defined by the positive going commutation voltage zero-crossing.

$$F_{\theta_p} = Imag\left\{\sum_{k=1}^{nh} \left(V_{volt}(2p-1)_k - V_{volt}(2p-2)_k\right) \exp^{jk\theta_p}\right\} \tag{C.11}$$

$$\frac{\partial F_{\theta_p}}{\partial \theta_p} = Imag\left\{\sum_{k=1}^{nh} jk \left(V_{volt}(2p-1)_k - V_{volt}(2p-2)_k\right) \exp^{jk\theta_p}\right\} \tag{C.12}$$

$$\frac{\partial F_{\theta_p}}{\partial V_{ac}(k)} = Imag\left\{\left(P_{volt\_V}(2p-1)_k - P_{volt\_V}(2p-2)_k\right) \exp^{jk\theta_p}\right\} \tag{C.13}$$

$$\frac{\partial F_{\theta_p}}{\partial I_{dc}(k)} = Imag\left\{jk \left(P_{volt\_I}(2p-1)_k - P_{volt\_I}(2p-2)_k\right) \exp^{jk\theta_p}\right\} \tag{C.14}$$

For the current-controlled converter, the firing angles are defined by the intersection of the equidistant firing pulses with the alpha-order ripple from the dc current.

$$F_{\theta_p} = Imag\left\{ j\left(\alpha_{ripple}(0) + \beta_p - \theta_p\right) + \sum_{k=1}^{nh} \alpha_{ripple}(k) \exp^{jk\theta_p} \right\} \quad \text{(C.15)}$$

$$\frac{\partial F_{\theta_p}}{\partial \theta_p} = Imag\left\{ -j + \sum_{k=1}^{nh} jk\alpha_{ripple}(k) \exp^{jk\theta_p} \right\} \quad \text{(C.16)}$$

$$\frac{\partial F_{\theta_p}}{\partial V_{ac}(k)} = 0 \quad \text{(C.17)}$$

$$\frac{\partial F_{\theta_p}}{\partial I_{dc}(k)} = Imag\left\{ \frac{\partial \alpha_{ripple}(k)}{\partial I_{dc}(k)} \exp^{jk\theta_p} \right\} \quad \text{(C.18)}$$

End of commutation angles

The end of commutation angle sensitivity to the electrical variables comes from two locations. The first is the direct effect on the end of commutation angle mismatch equation, the other is from the modulation of the firing instant which depends upon the control strategy.

$$\frac{\partial \phi_p}{\partial V_{ac}} = \frac{\partial \phi_p}{\partial F_{\phi_p}} \left(\frac{\partial F_{\phi_p}}{\partial V_{ac}} + \frac{\partial F_{\phi_p}}{\partial \theta_p} \frac{\partial \theta_p}{\partial V_{ac}} \right) \quad \text{(C.19)}$$

$$\frac{\partial \phi_p}{\partial I_{dc}} = \frac{\partial \phi_p}{\partial F_{\phi_p}} \left(\frac{\partial F_{\phi_p}}{\partial V_{ac}} + \frac{\partial F_{\phi_p}}{\partial \theta_p} \frac{\partial \theta_p}{\partial V_{ac}} \right) \quad \text{(C.20)}$$

The mismatch for the end of commutation is shown next.

$$F_{\phi_p} = \left(I_{dc}(0) - D\right) + Imag\left\{ \sum_{k=1}^{nh} \left(I_{dc}(k) - I_{comm}(p)_k\right) \exp^{jk\phi_p} \right\} \quad \text{(C.21)}$$

$$D = Imag\left\{ \sum_{k=1}^{nh} I_{comm}(p)_k \exp^{jk\theta_p} \right\} \quad \text{(C.22)}$$

$$\frac{\partial F_{\phi_p}}{\partial \phi_p} = Imag\left\{ \sum_{k=1}^{nh} jk \left(I_{dc}(k) - I_{comm}(p)_k\right) \exp^{jk\phi_p} \right\} \quad \text{(C.23)}$$

$$\frac{\partial F_{\phi_p}}{\partial V_{ac}(k)} = Imag\left\{ \left(\frac{1}{jk}\right) P_{comm\_V}(p)_k \left(\exp^{jk\theta_p} - \exp^{jk\phi_p} \right) \right\} \quad \text{(C.24)}$$

$$\frac{\partial F_{\phi_p}}{\partial I_{dc}(k)} = Imag\left\{ \exp^{jk\phi_p} + \left(\frac{1}{jk}\right) P_{comm\_I}(p)_k \left(\exp^{jk\theta_p} - \exp^{jk\phi_p} \right) \right\} \quad \text{(C.25)}$$

$$\frac{\partial F_{\phi_p}}{\partial \theta_p} = Imag\left\{ \sum_{k=1}^{nh} jk I_{comm}(p)_k \exp^{jk\theta_p} \right\} \quad \text{(C.26)}$$

C.1.4 Effect of switchings on sampling function

The sign of the partial derivative of the sampling function with respect to a switching instant, is dependent upon whether the switching instant is the beginning or ending instant that defines the period.

$$\psi(k) = \frac{1}{k\pi}(\exp^{jka} - \exp^{jkb})^* \tag{C.27}$$

$$\frac{\partial\psi(k)}{\partial\theta} = \pm\frac{1}{\pi}\left(j\exp^{jk\theta}\right)^* \tag{C.28}$$

$$\frac{\partial\psi(k)}{\partial\phi} = \pm\frac{1}{\pi}\left(j\exp^{jk\phi}\right)^* \tag{C.29}$$

C.2 LOADFLOW BUSBAR BLOCKS

C.2.1 Star-ground PQ load

The phase mismatch is written in real and imaginary parts, the following simplifications can be made:

$$M_{Pa} = P_a + V_{ra}I_{ra} + V_{i(a)}I_{ia} \tag{C.30}$$

$$M_{Qa} = Q_a + V_{ia}I_{ra} - V_{r(a)}I_{ia} \tag{C.31}$$

$$I_{ra} = \sum_{p=1}^{nb}(V_{r(p)}Y_{r(a,p)} - V_{i(p)}Y_{i(a,p)}) \tag{C.32}$$

$$I_{ia} = \sum_{p=1}^{nb}(V_{r(p)}Y_{i(a,p)} + V_{i(p)}Y_{r(a,p)}) \tag{C.33}$$

Using the chain rule, the partial derivative of M_{Pa} with respect to the real part of the voltage V_{rp} can be written as:

$$\frac{\partial M_{Pa}}{\partial V_{rp}} = \frac{\partial V_{ra}}{\partial V_{rp}}I_{ra} + V_{ra}\frac{\partial I_{ra}}{\partial V_{rp}} + \frac{\partial V_{ia}}{\partial V_{rp}}I_{ia} + V_{ia}\frac{\partial I_{ia}}{\partial V_{rp}} \tag{C.34}$$

The derivatives of the nodal current at bus a with respect to the nodal voltage at bus p are:

$$\begin{bmatrix} \partial I_{ra} \\ \partial I_{ia} \end{bmatrix} = \begin{bmatrix} Y_{r(a,p)} & -Y_{i(a,p)} \\ Y_{i(a,p)} & Y_{r(a,p)} \end{bmatrix} \begin{bmatrix} \partial V_{rp} \\ \partial V_{ip} \end{bmatrix} \tag{C.35}$$

Using this and the expanded power mismatch derivative, the full expression is shown below, where $I_{rp} = I_{ip} = 0$ for $p \neq a$.

$$\begin{bmatrix} \dfrac{\partial M_{Pa}}{\partial M_{Qa}} \end{bmatrix} = \left[\begin{array}{c|c} I_{rp} + V_{ra}Y_{r(a,p)} + V_{ia}Y_{i(a,p)} & I_{ip} - V_{ra}Y_{i(a,p)} + V_{ia}Y_{r(a,p)} \\ \hline -I_{ip} - V_{ra}Y_{i(a,p)} + V_{ia}Y_{r(a,p)} & I_{rp} - V_{ra}Y_{r(a,p)} - V_{ia}Y_{i(a,p)} \end{array}\right] \begin{bmatrix} \dfrac{\partial V_{rp}}{\partial V_{ip}} \end{bmatrix}$$

(C.36)

The partial derivatives for ungrounded star and delta load connections can be obtained by a similar analysis.

C.2.2 PV Generator busbar

The PV controlled generator busbar mismatches are slightly more difficult as they are of mixed types. The mismatches are also formed in terms of sequence components, while the voltage variables are in phase components.

$$M_{P_+} = P_{set} - Real(V_+ I_+^*) \tag{C.37}$$
$$M_{V_+} = V_{set}^2 - V_+ V_+^* \tag{C.38}$$
$$M_{I_-} = V_- Y_{gen_-} + I_- \tag{C.39}$$
$$M_{I_0} = V_0 Y_{gen_0} + I_0 \tag{C.40}$$

The mismatches are expanded out as follows for the self Jacobian block, i.e. at this busbar. For other busbars, the expressions simplify somewhat.

$$\frac{\partial M_{P_+}}{\partial V_p} = Real\left(\frac{\partial V_{r_+}}{\partial V_p} I_{r_+} - \frac{\partial V_{i_+}}{\partial V_p} I_{i_+} + V_{r_+} \frac{\partial I_{r_+}}{\partial V_p} - V_{i_+} \frac{\partial I_{i_+}}{\partial V_p}\right) \tag{C.41}$$
$$\frac{\partial M_{V_+}}{\partial V_p} = Real\left(2\frac{\partial V_{r_+}}{\partial V_p} + 2\frac{\partial V_{i_+}}{\partial V_p}\right) \tag{C.42}$$
$$\frac{\partial M_{I_-}}{\partial V_p} = \frac{\partial V_-}{\partial V_p} Y_{gen_-} + \frac{\partial I_-}{\partial I_p}\frac{\partial I_p}{\partial V_p} \tag{C.43}$$
$$\frac{\partial M_{I_0}}{\partial V_p} = \frac{\partial V_0}{\partial V_p} Y_{gen_0} + \frac{\partial I_0}{\partial I_p}\frac{\partial I_p}{\partial V_p} \tag{C.44}$$

The sequence transform from phase quantities to sequence quantities in real valued form is as follows, where $a = \exp^{j2\pi/3}$:

$$\begin{bmatrix} \partial V_{r_+} \\ \partial V_{i_+} \\ \hline \partial V_{r_-} \\ \partial V_{i_-} \\ \hline \partial V_{r_0} \\ \partial V_{i_0} \end{bmatrix} = \frac{1}{3} \left[\begin{array}{cc|cc|cc} 1 & 0 & a_r & -a_i & a_r^2 & -a_i^2 \\ 0 & 1 & a_i & a_r & a_i^2 & a_r^2 \\ \hline 1 & 0 & a_r^2 & -a_i^2 & a_r & -a_i \\ 0 & 1 & a_i^2 & a_r^2 & a_i & a_r \\ \hline 1 & 0 & 1 & 0 & 1 & 0 \\ 0 & 1 & 0 & 1 & 0 & 1 \end{array}\right] \begin{bmatrix} \partial V_{r_a} \\ \partial V_{i_a} \\ \hline \partial V_{r_b} \\ \partial V_{i_b} \\ \hline \partial V_{r_c} \\ \partial V_{i_c} \end{bmatrix} \tag{C.45}$$

and the transform from nodal voltage to nodal current is the system admittance.

$$\begin{bmatrix} \partial I_{ra} \\ \partial I_{ia} \end{bmatrix} = \begin{bmatrix} Y_{r(a,p)} & -Y_{i(a,p)} \\ Y_{i(a,p)} & Y_{r(a,p)} \end{bmatrix} \begin{bmatrix} \partial V_{rp} \\ \partial V_{ip} \end{bmatrix} \tag{C.46}$$

C.3 CONTROL EQUATION ROWS

The following are the Jacobian blocks for a sample of control equations. Often there is similarity between the control equations which allows the same Jacobian block to be used. There maybe some subtle differences within the controllers which, while the mismatches appear the same, the variable linkages are different.

C.3.1 Converter controls

dc current based controls

If a converter is under current control or that its dc current is a system variable, the following mismatches are required.

$$M_{Id} = Y_{dc}V_{dc}(0) - I_{set} \tag{C.47}$$

$$M_{Id} = Y_{dc}V_{dc}(0) - I_{var} \tag{C.48}$$

These have the same Jacobian blocks which are:

$$\frac{\partial V_{dc}(0)}{\partial V_{ac}(k)} = \frac{\partial V_{dc}(0)}{\partial V_{ac}(k)} \otimes \psi + V_{dc}(0) \otimes \left(\frac{\partial \psi}{\partial \phi} \frac{\partial \phi}{\partial V_{ac}(k)} + \frac{\partial \psi}{\partial \theta} \frac{\partial \theta}{\partial V_{ac}(k)} \right) \tag{C.49}$$

$$\frac{\partial V_{dc}(0)}{\partial I_{dc}(k)} = \frac{\partial V_{dc}(0)}{\partial V_{ac}(k)} \otimes \psi + V_{dc}(0) \otimes \left(\frac{\partial \psi}{\partial \phi} \frac{\partial \phi}{\partial I_{dc}(k)} + \frac{\partial \psi}{\partial \theta} \frac{\partial \theta}{\partial I_{dc}(k)} \right) \tag{C.50}$$

switching angle based controls

Often the controller uses the converter switching angles to define the operating point. These controllers are such as the minimum or average gamma and average commutation period controls.

$$M_{\gamma\_min} = (\delta_p - \phi_p) - \gamma_{set} \tag{C.51}$$

$$M_{\gamma\_avg} = \frac{1}{6}\sum_{p=1}^{6} (\delta_p - \phi_p) - \gamma_{set} \tag{C.52}$$

$$M_{\mu\_avg} = \frac{1}{6}\sum_{p=1}^{6} (\phi_p - \theta_p) - \mu_{set} \tag{C.53}$$

Most of the blocks required have been derived earlier, the new Jacobian blocks are:

$$\frac{\partial \delta_p}{\partial V_{ac}} = \frac{\partial \delta_p}{F_{\delta_p}} \frac{F_{\delta_p}}{\partial V_{ac}} \tag{C.54}$$

$$\frac{\partial \delta_p}{\partial V_{ac}} = \frac{\partial \delta_p}{F_{\delta_p}} \frac{F_{\delta_p}}{\partial I_{dc}} \tag{C.55}$$

where,

$$F_{\delta_p} = Imag\left\{\sum_{k=1}^{nh}\left(V_{samp}(2p-1)_k - V_{samp}(2p)_k\right)\exp^{jk\delta_p}\right\} \quad \text{(C.56)}$$

$$\frac{\partial F_{\delta_p}}{\partial \delta_p} = Imag\left\{\sum_{k=1}^{nh} jk\left(V_{samp}(2p-1)_k - V_{samp}(2p)_k\right)\exp^{jk\delta_p}\right\} \quad \text{(C.57)}$$

$$\frac{\partial F_{\delta_p}}{\partial V_{ac}(k)} = Imag\left\{\left(P_{samp\_V}(2p-1)_k - P_{samp\_V}(2p)_k\right)\exp^{jk\delta_p}\right\} \quad \text{(C.58)}$$

$$\frac{\partial F_{\delta_p}}{\partial I_{dc}(k)} = Imag\left\{jk\left(P_{samp\_I}(2p-1)_k - P_{samp\_I}(2p)_k\right)\exp^{jk\delta_p}\right\} \quad \text{(C.59)}$$

C.3.2 Loadflow controls

Slack generator control

The slack generator power setpoint is maintained within the solution as a control variable. This allows the flexibility to use any device as the slack busbar. The slack busbar constraint is as follows, where α_{set} is the ac system angle reference.

$$M_{slack} = \arctan\left(\frac{Imag\{V_+\}}{Real\{V_+\}}\right) - \alpha_{set} \quad \text{(C.60)}$$

The control equation row only has terms at the slack busbar, although, the ac system reference busbar does not have to be the slack generator busbar. The Jacobian terms are as follows:

$$\frac{\partial M_{slack}}{\partial V_{ac}} = \frac{1}{V_+}\frac{\partial V_+}{V_{ac}} \quad \text{(C.61)}$$

Controlled voltage source

Another frequently used control strategy is the controlled ac voltage source. The voltage source is specified in terms of sequence components and these are controlled to give a specified voltage at a busbar. The specified voltage can be balanced or distorted and the busbar can be the voltage source busbar or a different one.

$$M_{vs} = V_+V_+^* - V_{set} \quad \text{(C.62)}$$

The partial derivatives are:

$$\frac{\partial M_{vs}}{\partial V_{ac}} = \frac{\partial V_+}{V_{ac}}V_{ac}^* + V_{ac}\frac{\partial V_+^*}{V_{ac}} \quad \text{(C.63)}$$

Appendix D

SPARSE HANDLING ROUTINES

The use of sparse techniques can significantly reduce the amount of storage required for non-full matrices. A dynamic technique allows the structure of the matrix to be changed after formation, while a static technique allows only the element values to be changed. A simple dynamic technique is not structurally ordered, which means there is no simple method for locating specific elements. Static techniques are usually optimised for specified matrix manipulations.

D.1 STORAGE TECHNIQUES USED

Two techniques are used by the algorithm for storage of the system admittance matrix. The initial storage is a partially ordered dynamic technique that is used for forming the main admittance matrix. The complex storage array is N elements long and has the busbar shunt admittance terms stored first in a sequential order. This makes it simple to locate these terms for modification, and for use in the analytic Jacobian calculation. The busbar linking terms are stored randomly after these terms. Three integer arrays of size N are used for referencing the main array. Two store the row and column indices and the third is a reference to the complex admittance storage array.

The second storage method is a static technique is a row-ordered method, optimised for fast matrix multiplications and matrix additions [Press *et al.* 1992] [Pissanetsky 1984]. The following section is verbatim from "Numerical Recipes in FORTRAN" [Press *et al.* 1992]. For use within the algorithm, instead of containing the actual elements, the defined array sa is an integer array that stores the index into the complex storage array previously mentioned.

D.1.1 Row-indexed sparse storage mode

To represent a matrix A of logical size $N * N$, the row-indexed scheme sets up two one-dimensional arrays, call them sa and ija. The first of these stores matrix element values in single or double precision as desired; the second stores integer values. The storage rules are:

- The first N locations of *sa* store A's diagonal matrix elements, in order. (Note that diagonal elements are stored even if they are zero; this is at most a slight storage inefficiency, since diagonal elements are nonzero in most realistic applications.)

- Each of the first N locations of *ija* stores the index of the array *sa* that contains the first *off-diagonal* elements of the corresponding row of the matrix. (If there are no off-diagonal elements for that row, it is one greater than the index in *sa* of the most recently stored element of a previous row.)

- Location 1 of *ija* is always equal to N+2. (It can be read to determine N.)

- Location N+1 of *ija* is one greater than the index in sa of the last off-diagonal element of the last row. (It can be read to determine the number of nonzero elements in the matrix, or the logical length of the arrays *sa* and *ija*.) Location N+1 of *sa* is not used and can be set arbitrarily.

- Entries in *sa* at locations ≥N+2 contain A's off-diagonal values, ordered by rows and, within each row, ordered by columns.

- Entries in *ija* at locations ≥N+2 contain the column number of the corresponding element in *sa*

While these rules seem arbitrary at first sight, they result in a rather elegant storage scheme. As an example, consider the matrix

$$A = \begin{bmatrix} 3 & 0 & 1 & 0 & 0 \\ 0 & 4 & 0 & 0 & 0 \\ 0 & 7 & 5 & 9 & 0 \\ 0 & 0 & 0 & 0 & 2 \\ 0 & 0 & 0 & 6 & 5 \end{bmatrix} \tag{D.1}$$

In row-indexed compact storage, matrix D.1 is represented by the two arrays of length 11, as follows

index k	1	2	3	4	5	6	7	8	9	10	11
ija(k)	7	8	8	10	11	12	3	2	4	5	4
sa(k)	3	4	5	0	5	-	1	7	9	2	6

Notice that according to the storage rules, the value of N (namely 5) is $ija(1) - 2$, and the length of each array is $ija(ija(1) - 1) - 1$, namely 11. The diagonal element in row i is $sa(i)$, and the off-diagonal elements in that row are in $sa(k)$ where k loops from $ija(i)$ to $ija(i) - 1$, if the upper limit is greater or equal to the lower one.

D.2 SPARSE MATRIX MULTIPLICATION

The multiplication of a square sparse matrix of size N, stored using the aforementioned row-indexed sparse storage mode (ija, sa and Y), by a column vector (V) of size N is as follows:

```
do v=1,N
 I(v)=Y(sa(v))*V(v)
 do k=ija(v),ija(v+1)-1
  I(v)=I(v)+Y(sa(k))*V(ija(k))
 end do
end do
```

D.3 SPARSE MATRIX ADDITION

The same static storage technique can be used for adding two sparse matrices together. There are two stages to the addition, the first is a symbolic addition followed by the element addition. The result is a row-ordered matrix but it is no-longer column ordered. A minor modification to the diagonal storage in aforementioned rules allows the addition of non-square matrices. The requirements of this process are two integer arrays (*Switch* and *Sum_ija*) and an integer/real/complex summand array (*Sum*) both of size N.

The *Switch* array identifies the presence of an off-diagonal element at this column by storing the current row number in that column number. The location of the matrix element in the *sa* array, given by *ija(J)*, is stored in *Sum_ija* (step 1). A similar thing is done for the second matrix, but care is taken that no duplicate off-diagonals are stored in *Sum_ija* (step 2). A full length one-dimensional vector of the appropriate *type* is zeroed at the appropriate indices (step 3). The diagonal elements of both the matrices are added together and stored in this full array (step 4). The elements of the first matrix are placed into the full array (step 5). The second array elements are then added to the *sum* array, thus adding any elements that are in the same locations (step 6). The full row array *sum* is then transferred into the general sparse storage arrays. A more detailed description of this process can be found in reference [Pissanetsky 1984].

```
C ** initialise the switching array, Switch (Ix)
      index=N+1 ! indexing element for the summand array
      full_index=1 ! indexing element for final array
      DO row=1,N+1
       Switch(row)=0
      END DO
C ** perform symbolic addition of all blocks at this busbar
      DO row=1,N
       Dnum=Dnum1
       Sum_ija(row)=index
       Switch(row)=row
```

```
C ** fill in the switch array for the first matrix (step 1)
       DO J=ija_1(row),ija_1(row+1)-1
        Switch(ija_1(J))=row
        Sum_ija(index)=ija_1(J)
        index=index+1
       END DO
C ** fill in the switch array for the second matrix (step 2)
       DO J=ija_2(row),ija_2(row+1)-1
        IF (Switch(ija_2(J)).NE.row) THEN
         Switch(ija_2(J))=row
         Sum_index(index)=ija_2(J)
         index=index+1
        END IF
       END DO
      END DO ! row
      Sum_ija(N+1)=index
C ** perform the numerical addition of the matrices
      DO row=1,N
C ** initialising the full sum array "Sum(size N*1)" (step 3)
       DO index=Sum_ija(row),Sum_ija(row+1)-1
        Sum(Sum_ija(index))=0.0
       END DO
       Sum(row)=sa_1(row)+sa_2(row) ! diagonal terms (step 4)
C ** place the first sparse matrix (step 5)
       DO index=ija_1(row),ija_1(row+1)-1
        Sum(ija_1(index))=sa_1(index)
       END DO
C ** add the second sparse matrix (step 6)
       DO index=ija_2(row),ija_2(row+1)-1
        Sum(ija_2(index))=Sum(ija_2(index))+sa_2(index)
       END DO
C ** transfering full sum array to a general sparse storage array (step 7)
       Row_store(full_index)=row
       Col_store(full_index)=row
       Ele_store(full_index)=Sum(row)
       full_index=full_index+1
       DO index=Sum_ija(row),Sum_ija(row+1)-1
        Row_store(full_index)=row
        Col_store(full_index)=Sum_ija(index)
        Ele_store(full_index)=Sum(Sum_ija(index))
        full_index=full_index+1
       END DO
      END DO ! row
```

Appendix E

PUBLISHED PAPERS

The following papers have been published in conjunction with this research:

1. G.N. Bathurst, N.R. Watson, and J. Arrillaga, 'Modelling of bipolar HVdc links in the Harmonic Domain', *IEEE Transactions (submitted), 1998*

2. G.N. Bathurst, B.C. Smith, N.R. Watson, and J. Arrillaga, 'Harmonic Domain modelling of high pulse converters', *IEE Transactions on Electric Power Applications (accepted for publication), 1998*

3. G.N. Bathurst, B.C. Smith, N.R. Watson, and J. Arrillaga, 'Modelling of HVdc transmission systems in the Harmonic Domain', *IEEE Transactions on Power Delivery (accepted for publication), 1998*

4. N.R. Watson, J. Arrillaga, B.C. Smith, and G.N. Bathurst, 'A Graphical Interface for Interactive AC/DC System Harmonic Analysis', *Proceedings of the 8th ICHQP Conference, 1998, Vol. 1, pp 407-411.*

5. G.N. Bathurst, B.C. Smith, N.R. Watson, and J. Arrillaga, 'A modular approach to the solution of the three-phase harmonic power-flow', *Proceedings of the 8th ICHQP Conference, 1998, Vol. 2, pp 653-659.*

6. G.N. Bathurst, B.C. Smith, N.R. Watson, and J. Arrillaga, 'Analysis of the HVdc inverter in the harmonic domain', *Proceedings of the 7th European Power Electronics conference, EPE'97, Oct. 1997, Norway, Vol. 1, pp 1.260-1.265*

7. G.N. Bathurst, B.C. Smith and N.R. Watson, 'Newton solution of a generic minimum gamma controlled HVdc inverter in the harmonic domain', *Proceedings of the 3rd New Zealand Conference of Postgraduate Students in Engineering and Technology, Christchurch, July 1-2, 1996, p-52-57*

REFERENCES

[Acha 1988]

Enrique Acha. *Modelling of power system transformers in the complex conjugate harmonic space.* PhD thesis, Department of Electrical and Electronic Engineering, University of Canterbury, Christchurch, New Zealand, 1988.

[Andersen *et al.* 1998]

B.R. Andersen, D.R. Monkhouse, R.S. Whitehouse, J.D.G. Williams, V.K. Prasher, and Devinder Kumar. Commisioning the 1000MW back to back HVdc link at chandrapur, india. *CIGRE*, vol. 1, 1998.

[Anderson and Wood 1997]

G.W.J. Anderson and A.R. Wood. Harmonic modelling of a 540MW LVdc rectifier terminal. *Proceedings of IPEC 1997*, volume 2, pp. 798–803, Singapore, 1997.

[Aprille and Trick 1972]

T.J. Aprille and T.N. Trick. Steady-state analysis of non-linear circuits with periodic inputs. *Proceedings of the IEEE*, volume 60(1), pp. 108–114, January 1972.

[Arrillaga *et al.* 1983]

J. Arrillaga, C.P. Arnold, and B.J. Harker. *Computer Modelling of Electrical Power Systems.* John Wiley and Sons, 1983.

[Arrillaga *et al.* 1987]

J. Arrillaga, N.R. Watson, J.F. Eggleston, and C.D. Callaghan. Comparison of steady-state and dynamic models for the calculation of AC/DC system harmonics. *IEE Proceedings Part C*, volume 134(1), pp. 31–37, January 1987.

[Arrillaga *et al.* 1995]

J. Arrillaga, A. Medina, M.L.V. Lisboa, M.A. Cavia, and P. Sànchez. The harmonic domain. a frame of reference for power system harmonic analysis. *IEEE Transactions on Power Systems*, volume 10(1), pp. 433–440, February 1995.

[Arrillaga 1983]

J. Arrillaga. *High Voltage Direct Current Transmission.* Peter Peregrinus Ltd, London, U.K., 1983.

[Arrillaga 1997]
J. Arrillaga. *Power System Harmonic Analysis.* J. Wiley and Sons, London, 1997.

[Arrillaga 1998]
J. Arrillaga. *High voltage direct current transmission.* The Institution of Electrical Engineers, London, United Kingdom, 2 edition, 1998.

[Asensi *et al.* 1998]
R. Asensi, J.G. Mayordomo, F. Orzáez, and L.F. Beites. Iterative harmonic analysis for controlled and uncontrolled ac-dc converters under unbalanced conditions: a compromise between model accuracy and flexibility. *Proceedings of the 8th ICHQP conference*, volume 1, pp. 412–418, October 1998.

[Bathurst *et al.* 1996]
G.N. Bathurst, B.C. Smith, and N.R. Watson. Newton solution of a generic minimum gamma controlled HVdc inverter in the harmonic domain. *Proceedings of the third New Zealand conference of postgraduate students in Engineering and Technology*, volume 1, pp. 52–57, July 1996.

[Bathurst *et al.* 1997]
G.N. Bathurst, B.C. Smith, N.R. Watson, and J. Arrillaga. Analysis of the HVdc inverter in the harmonic domain. *Proceedings of the 7-th EPE–Conference*, volume 1, pp. 1.260–1.265, 1997.

[Bathurst *et al.* 1998a]
G.N. Bathurst, B.C. Smith, N.R. Watson, and J. Arrillaga. A modular approach to the solution of the three-phase harmonic power-flow. *Proceedings of the 8th ICHQP conference*, volume 1, pp. 407–411, October 1998.

[Bathurst *et al.* 1998b]
G.N. Bathurst, B.C. Smith, N.R. Watson, and J. Arrillaga. Harmonic domain modelling of high pulse converters. *IEE Proceedings (accepted for publication)*, 1998.

[Callaghan and Arrillaga 1989]
C.D. Callaghan and J. Arrillaga. Double-iterative algorithm for the analysis of power and harmonic flows at AC/DC converter terminals. *IEE Proceedings Part C*, volume 136(6), pp. 319–324, November 1989.

[Callaghan 1989]
C.D. Callaghan. *Three phase integrated load and harmonic flows.* PhD thesis, Department of Electrical and Electronic Engineering, University of Canterbury, Christchurch, New Zealand, August 1989.

[Carbone *et al.* 1992]

R. Carbone, M. Fantauzzi, F. Gagliardi, and A. Testa. Some considerations on the iterative harmonic analysis convergence. *Proceedings of ICHPS V*, 1992.

[Carpinelli *et al.* 1994]

G. Carpinelli, F. Gagliardi, M. Russo, and D. Villacci. Generalised converter models for iterative harmonic analysis in power systems. *IEE Generation, Transmission and Distribution*, volume 141(5), September 1994.

[Carson 1926]

J.R. Carson. Wave propagation in overhead wires with ground reutrn. *Bell System Technical Journal*, vol. 1, pp. 539–554, October 1926.

[Chen *et al.* 1996]

S. Chen, A.R. Wood, and J. Arrillaga. HVdc converter transformer core saturation instability - a frequency domain analysis. *IEE Proceedings of Generation, Transmission and Distribution*, volume 143(1), pp. 75–81, January 1996.

[Densem *et al.* 1984]

T.J. Densem, P.S. Bodger, and J. Arrillaga. Three phase transmission system modelling for harmonic penetration. *IEEE Transactions on Power Apparatus and Systems*, volume 103, pp. 310–317, February 1984.

[Densem 1983]

T.J. Densem. *Three phase power system harmonic penetration.* PhD thesis, Department of Electrical and Electronic Engineering, University of Canterbury, Christchurch, New Zealand, 1983.

[Dickmander *et al.* 1994]

D.L. Dickmander, S.Y. Lee, G.L. Desilets, and M. Granger. AC/DC harmonic interactions in the presence of GIC for the Quebec-New England phase II HVdc transmission. *IEEE Transactions on Power Delivery*, volume 9(1), pp. 68–78, January 1994.

[Dinh *et al.* 1997]

N.Q. Dinh, J. Arrillaga, A.R. Wood, S. Chen, W. Enright, B.C. Smith, and Z. Du. Harmonic evaluation of benmore converter station when operated as a group connected unit. *IEEE Transactions on power delivery*, volume 12(4), pp. 1730–1735, October 1997.

[Dinh *et al.* 1998]

N.Q. Dinh, J. Arrillaga, and B.C. Smith. A steady-state model of direct connected generator-HVdc converter units in the harmonic domain. *IEE Generation, Transmission and Distribution*, 1998.

[Dommel 1969]

H.W. Dommel. Digital computer simulation of electromagnetic transients in single and multiphase networks. *IEEE Transactions on Power Apparatus and Systems*, volume 88(4), pp. 388–399, April 1969.

[Eggleston 1985]

J.F. Eggleston. *Harmonic modelling of transmission systems containing synchronous machines and static converters.* PhD thesis, Electrical and Electronic Engineering, University of Canterbury, New Zealand, 1985.

[Enright *et al.* 1999]

W. Enright, N. Watson, and O. Nayak. Three-phase five-limb unified magnetic equivalent circuit transformer models for PSCAD V3. *Proceedings of IPST'99 (submitted)*, 1999.

[Enright 1996]

W.G. Enright. *Transformer models for electromagnetic transient studies with particular reference to HVdc transmission.* PhD thesis, Department of Electrical and Electronic Engineering, University of Canterbury, New Zealand, February 1996.

[Gleadow *et al.* 1993]

J. Gleadow, M.T. O'Brien, and J.E. Flectcher. Principle features of the dc hybrid link. *International colluquium on HVdc and flexible ac power transmission systems*, volume 1.3, Wellington, New Zealand, 1993.

[Heydt and Xia 1982]

G.T. Heydt and D. Xia. Harmonic power flow studies parts 1 and 2. *IEEE Transactions on Power Apparatus and Systems*, volume 101(6), pp. 1257–1265, June 1982.

[Hu and Yacamini 1993]

L. Hu and R. Yacamini. Calculation of harmonics and interharmonics in HVdc schemes with low dc side impedance. *IEEE Proceedings -C*, volume 140(6), pp. 469–476, November 1993.

[Jiang and Gole 1995]

X. Jiang and A.M. Gole. A frequency scanning technique for the indentification of harmonic instabilities in HVdc systems. *IEEE Transactions on Power Delivery*, volume 10(4), pp. 1875–1881, October 1995.

[Kimbark 1971]

E.W. Kimbark. *Direct current transmission.* Wiley Interscience, New York, 1971.

[Larsen *et al.* 1989a]

E.V. Larsen, D.H. Baker, and J.C. McIver. Low-order harmonic interaction on

AC/DC systems. *IEEE Transactions on Power Delivery*, volume 4(1), January 1989.

[Larsen *et al.* 1989b]
E.V. Larsen, M. Sublich, and S.C. Kapoor. Impact of stray capacitance on HVdc harmonics. *IEEE Transactions on Power Delivery*, volume 4(1), pp. 637–645, January 1989.

[Lisboa 1996]
Maria Luiza Viana Lisboa. *Three-phase three-limb transformer models in the Harmonic Domain.* PhD thesis, Department of Electrical and Electronic Engineering, University of Canterbury, Christchurch, New Zealand, August 1996.

[Mayordomo *et al.* 1997]
J.G. Mayordomo, L.F. Beites, R. Asensi, and M. Izzeddine. A new frequency domain arc furnace model for iterative harmonic analysis. *IEEE Transactions on Power Delivery*, volume 12(4), pp. 1771–1778, October 1997.

[CIGRE 14.07 1992]
CIGRE 14.07. Guide for planning DC links terminating at ac systems locations having low short-circuit capacities. *CIGRE Journal*, vol. 1, June 1992.

[IEEE Task Force 1996]
IEEE Task Force. Modeling and simulation of the propagation of harmonics in electric power networks. *IEEE Transactions on Power Delivery*, volume 11(1), pp. 466–474, January 1996.

[IEEE Taskforce 1996]
IEEE Taskforce. Modeling and simulation of the propagation of harmonics in electric power networks. *IEEE Transactions on Power Delivery*, volume 11(1), pp. 452–465, January 1996.

[Manitoba HVdc Research Centre 1988]
Manitoba HVdc Research Centre. PSCAD/EMTDC V3 users manual. Manitoba HVdc Research Center, Winnipeg, Canada, 1988.

[NEUJW@vm.uni-c.dk]
NEUJW@vm.uni-c.dk. Y12M linear equation solver in Fortran 77 and documentation. www.netlib.org/y12m/.

[Medina and Arrillaga 1994]
A. Medina and J. Arrillaga. Analysis of transformer-generator interaction in the harmonic domain. *IEE Proceedings on Generations, Transmission and Distribution*, volume 141(1), pp. 38–46, May 1994.

[Nguyen 1997]
H.L. Nguyen. Newton-raphson method in complex form. *IEEE Transactions on Power Systems*, volume 12(3), pp. 1355–1359, 1997.

[Nhut-Quang 1998]
Dinh Nhut-Quang. *Harmonic Domain modelling of direct connected generator and HVdc converter units.* PhD thesis, Department of Electrical and Electronic Engineering, University of Canterbury, Christchurch, New Zealand, January 1998.

[Pissanetsky 1984]
Sergio Pissanetsky. *Sparse Matrix Technology.* Academic Press Inc. London, ISBN 0-12-557580-7, 1984.

[Press *et al.* 1992]
W.H. Press, S.A. Teukolsky, W.T. Vetterling, and B.P. Flannery. *Numerical Recipes in FORTRAN.* Cambridge University Press, 2 edition, 1992.

[Reeve and Baron 1971]
J. Reeve and J.A. Baron. Harmonic interaction between hvdc converters and ac power systems. *IEEE Transactions on Power Apparatus and Systems*, volume 90(6), pp. 2785–2793, 1971.

[Rico *et al.* 1996]
J.J. Rico, E. Acha, and T.J.E. Miller. Harmonic domain modelling of three-phase thyristor-controlled reactors by means of switching vectors and discrete convolutions. *IEEE Transactions on Power Delivery*, volume 11(3), pp. 1678–1684, July 1996.

[Sadek *et al.* 1992]
K. Sadek, N. Christl, and P. Lüzelberger. AC/DC harmonic interaction in HVdc systems. *IEEE International conference on harmonics in power systems*, pp. 196–201, 1992.

[Semlyen *et al.* 1987]
A. Semlyen, E. Acha, and J. Arrillaga. Harmonic norton equivalent for the magnetising branch of a transformer. *IEE Part C*, volume 143(2), pp. 162–169, March 1987.

[Shore *et al.* 1989]
N.L. Shore, G. Anderssen, A.P. Canelhas, and G. Asplund. A three-pulse model of D.C. side harmonic flow in HVdc systems. *IEEE Transactions on Power Delivery*, volume 4(3), pp. 1945–1954, July 1989.

[Smith and Arrillaga 1997]
B.C. Smith and J. Arrillaga. Improved three-phase load flow using phase and sequence components. *IEE (accepted for publication)*, 1997.

[Smith and Arrillaga 1998]
B.C. Smith and J. Arrillaga. Power flow constrained harmonic analysis in ac-dc power systems. *IEEE Transactions on Power Systems*, 1998.

[Smith *et al.* 1996]
B.C. Smith, N.R. Watson, A.R. Wood, and J. Arrillaga. Newton solution for the steady-state interaction of AC/DC systems. *IEE Proceedings for Generation, Transmission and Distribution*, volume 143(2), pp. 200–207, March 1996.

[Smith *et al.* 1998]
B.C. Smith, J. Arrillaga, A.R. Wood, and N.R. Watson. A review of iterative harmonic analysis for AC-DC power systems. *IEEE*, volume 11(2), pp. 180–185, January 1998.

[Smith 1996]
B.C. Smith. *A harmonic domain model for the interaction of the HVdc convertor with ac and dc systems.* PhD thesis, Department of Electrical and Electronic Engineering, University of Canterbury, Christchurch, New Zealand, February 1996.

[Szechtmann *et al.* 1991]
M. Szechtmann, T. Weiss, and C.V. Thio. First benchmark model for HVdc control studies. *Electra*, vol. 1, no. 135, pp. 55–57, April 1991.

[Testi 1993]
G. Testi. Dc side harmonics and metering in HVdc transmission systems. *CIGRE SC-14, Task Force 2, WG 14.03*, vol. 1, 1993.

[Thunberg and Söder 1998]
E. Thunberg and L. Söder. A harmonic norton model of a real distribution network. 8^{th} *International Conference on Harmonics and Quality of Power*, volume 1, pp. 279–284, October 1998.

[Todd 1998]
S. Todd. *s-domain modelling for HVdc converter installation transient control design.* PhD thesis, Department of Electrical and Electronic Engineering, University of Canterbury, Christchurch, New Zealand, February 1998.

[Valcárcel and Mayadomo 1993]
M. Valcárcel and J.G. Mayadomo. Harmonic power flow for unbalanced systems. *IEEE Transactions on Power Delivery*, volume 8(4), pp. 2052–2059, October 1993.

[Watson 1987]
N.R. Watson. *Frequency dependent ac system equivalents for harmonic studies and transient converter simulation.* PhD thesis, Department of Electrical and Electronic Engineering, University of Canterbury, Christchurch, New Zealand, 1987.

[Wood and Arrillaga 1995]
A.R. Wood and J. Arrillaga. Composite resonance; a circuit approach to the waveform distortion dynamics of an HVdc converter. *IEEE Transactions on Power Delivery*, 1995.

[Wood *et al.* 1995]
A.R. Wood, B.C. Smith, and J. Arrillaga. The harmonic impedance of an HVdc converter. *European Power Electronic Conference, EPE'95*, September 1995.

[Wood 1993]
A.R. Wood. *An analysis of non-ideal HVdc converter behaviour in the frequency domain, and a new control proposal.* PhD thesis, Department of Electrical and Electronic Engineering, University of Canterbury, Christchurch, New Zealand, November 1993.

[Woodford *et al.* 1983]
D. Woodford, A. Gole, and R. Menzies. Digital simulation of dc links and ac machines. *IEEE Transactions on Power Apparatus and Systems*, volume 102(6), pp. 1616–1623, June 1983.

[Xu *et al.* 1991a]
W. Xu, J.R. Marti, and H.W. Dommel. Harmonic analysis of systems with static compensators. *IEEE Transactions on Power Systems*, volume 6(1), pp. 183–190, February 1991.

[Xu *et al.* 1991b]
W. Xu, J.R. Marti, and H.W. Dommel. A multiphase harmonic loadflow solution technique. *IEEE Transactions on Power Systems*, volume 6(1), pp. 174–182, February 1991.

[Xu *et al.* 1994]
W. Xu, J.E. Drakos, Y.M. Mansour, and A. Chang. A three-phase converter model for harmonic analysis of HVdc systems. *IEEE Transactions on Power Delivery*, volume 9(3), pp. 1724–1731, July 1994.

[Yacamini and de Oliveira 1980]
R. Yacamini and J.C. de Oliveira. Harmonics in multiple converter systems: a generalised approach. *IEE Proceedings Pt. B*, volume 127, pp. 96–106, March 1980.